Queen Mary University of London

Barts and the London School of Medicine and Dentistry

Department of Clinical and Diagnostic Oral Science

Extracellular Citrate as a Novel Biomarker of Senescence; Insights from Metabolomic Profiling

Author:
Emma L.N. James

Supervisors:
Prof. E. Kenneth Parkinson
and
Dr. Hong Wan

Thesis submitted for the partial fulfillment of the degree of

Doctor of Philosophy

October 2016

0.1 Author's Declaration

I, Emma Louise Naomi James, confirm that the research included within this thesis is my own work or that where it has been carried out in collaboration with, or supported by others, that this is duly acknowledged and my contribution indicated.

I attest that I have exercised reasonable care to ensure that the work is original, and does not to the best of my knowledge break any UK law, infringe any third party's copyright or other Intellectual Property Right, or contain any confidential material.

I accept that the College has the right to use plagiarism detection software to check the electronic version of the thesis.

I confirm that this thesis has not been previously submitted for the award of a degree by this or any other university.

The copyright of this thesis rests with the author and no quotation from it or information derived from it may be published without the prior written consent of the author.

Details of previously published data: James, Emma L; Michalek, Ryan D; Pitiyage, Gayani N; de Castro, Alice M; Vignola, Katie S; Jones, Janice; Mohney, Robert P; Karoly, Edward D; Prime, Stephen S. & Parkinson, Eric Kenneth. 2015. **Senescent Human Fibroblasts Show Increased Glycolysis and Redox Homeostasis with Extracellular Metabolomes That Overlap with Those of Irreparable DNA Damage, Aging, and Disease**. *Journal of Proteome Research*, 14(4), 1854-1871.

Signature: Emma James

Date: October 2016

0.2 Abstract

Senescent cells play an important role in normal biological processes such as wound healing and cancer prevention. If not effectively cleared by the immune system however, senescent cells can accumulate and have been linked to negative events; most notably fibrosis and ageing.

To understand more about the molecular mechanisms underpinning senescence as well as the effects senescent cells have on surrounding cells, the organism as a whole and why some cells evade the immune system, it is necessary to study and manipulate senescent cells *in vitro* and *in vivo*. In order to do this, accurate identification of senescent cells is required, something which can currently only be achieved by staining for multiple markers, a process that requires invasive tissue sampling when using *in vivo* models, and is a limitation in human studies in particular. A secreted biomarker that is detectable in bio-fluids such as blood would facilitate more informative human and animal studies.

In this thesis un-targeted metabolomic screens were performed using fibroblasts from multiple tissue types and two well characterised models of senescence: replicative senescence and irreparable DNA double strand break induced senescence. Controls for transient growth arrest and repairable DNA damage were also included and all groups were compared to young dividing cells. These investigations not only give insight into the metabolic changes occurring in senescence but also provided candidate biomarkers that were then more closely studied using targeted techniques. Extracellular citrate was identified as the most robust candidate, and its regulation was investigated at the molecular level.

The work presented in this thesis represents a novel contribution to the field of senescence both in terms of the metabolic profiles of senescent and quiescent fibroblasts and the strong candidate biomarker, citrate, which has the potential to broaden studies of senescence in humans *in vivo*.

0.3 Acknowledgements

There are many people who contributed to my PhD in many different ways, and to all those people I feel indebted. To begin with, the funding for my project and hence the opportunity for me to work on it came from both Queen Mary University of London and a James Paget Award, so to those organisations I am extremely grateful. Professor Ken Parkinson has of course been fundamental to the success of the project; I could not have asked for a better supervisor. His encyclopedic knowledge, enthusiasm and tireless curiosity have inspired me throughout my time here and I have tried my best to learn from his example. Under his guidance I have been encouraged to try new things, test crazy hypotheses, reach out to other scientists but above all practice the scientific method with a genuine desire to reach the truth.

I would also like to thank the many people who have offered technical assistance throughout the project, including Jan and Belen for their help with imaging and Gary for help with flow cytometry. In particular I would like to thank the people that helped with the analytical chemistry techniques: Harold Toms for his time and patience with the NMR, and Jake Bundy, Sarah Davies and Mark Bennett from Imperial for the huge amount of help, time and resource they gave for targeted GCMS, without which the project would have stalled.

While there have been many periods of intense stress over the last few years, I have always found happiness and compassion in my colleagues the Blizard: Kaveh, Karen, Ngoc, Kasia, Debbie, Fatima, Anke, Hannah, Fiona, Hong, Simon and Eleni who have helped me stay sane, but especially Steve Cannon, who is ever sympathetic to my hanger and has saved the day on numerous occasions when things in the lab haven't gone to plan. His kindness and sense of humour have given me perspective and helped me carry on when I've felt defeated. I am also grateful to Ryan Salucideen, my desk buddy (and main source of procrastination) for the first two years, for all the philosophical discussions and lessons in logic, which have come in useful many times!

I owe a huge amount to the patience and understanding of my friends and family;

in particular my mum and dad, my sister Katie, my grannies, my best friend Sophie, Jackie and Phil, Sue and Neil, who have been very supportive of me even though I have not been able to be there for them as much as I would have liked over the last few years. I am so grateful for their love and belief in me (not to mention the financial help!) and I hope I have made them proud. Finally I would like to give my heartfelt thanks to Steve West, my soulmate, whose constant love and support has kept me going through the hardest times and whose passion for science inspires me every day. His advice and insight has helped me on numerous occasions, including technical advice on image processing and figure presentation, but most of all I would like to thank him for always showing me kindness and love even when I was irritable and generally not fun to be around (which has been quite a few times over the last few years).

Contents

List of Figures

List of Tables

Table of abbreviations

Table 1: **Table of abbreviations**

°C	Degrees Centigrade
µl	Microlitre
µm	Micrometre
^{13}C	Carbon 13, heavy carbon, a stable isotope of carbon
^{1}H	Protium, a stable isotope of Hydrogen
3OHB	3-hydroxybutyrate
4HNE	4-hydroxynonenal
5'/3'	5 prime/3 prime
53BP1	p53-binding protein 1
9-1-1 complex	RAD9-RAD1-HUS1

Abbreviation	Full title
Acetyl-CoA	Acetyl-coenzyme A
ACLY	ATP citrate lyase
ACO1	Aconitase 1 (cytoplasmic)
ACO2	Aconitase 2 (mitochondrial)
ADP	Adenosine di-phosphate
AKT	Cellular homologue of murine thymoma virus Akt8 oncoprotein
ALT	Alternative lengthening of telomeres
AMP	Adenosine mono-phosphate
AMPK	5' AMP- activated protein kinase
ANOVA	Analysis of variance
ARF	Alternative reading frame
ATCC	American Type Culture Collection
ATM	Ataxia telangiectasia mutated
ATP	Adenosine triphosphate
ATR	Ataxia telangiectasia and Rad3 related
ATRIP	ATR-interacting protein
BCAA	Branched chain amino acids
BRAF	Murine Sarcoma Viral (V-Raf) Oncogene Homolog B1
BRCA1	Breast cancer susceptibility 1
BrdU	Synthetic analogue of thymidine containing Bromine
BSA	Bovine serum albumin
C/EBPβ	CCAAT/enhancer-binding protein beta
CDC25	Cell division cycle 25
CDK	Cyclin dependent kinase
cDNA	Complimentary DNA

Abbreviation	Full title
CDOS	Clinical and Diagnostic Oral Sciences
CHK1/2	Checkpoint kinase 1/2
CI	Chemical impact ionisation
Cmpds	Cumulative mean population doublings
Con	Confluent
CREB	cAMP-response element binding protein
CS	Citrate synthase
CT	Threshold crossing
CXCL/CCL	Chemokine
D2O	Deuterium oxide
DAPI	4',6-diamidino-2-phenylindole
DCF	2', 7' -dichlorofluorescein
DCI	Desorption chemical ionisation
DDR	DNA damage response
DMEM	Dulbecco's Modified Eagle Medium
DNA	Deoxyribonucleic acid
DNA-SCARS	DNA segments with chromatin alterations reinforcing senescence
DSB	Double strand break
DSS	4,4-dimethyl-4-silapentane-1-sulfonic acid
ECM	Extracellular matrix
EDTA	Ethylenediaminetetraacetic acid
EGF	Endothelial growth factor
EI	Electron impact ionisation
ELISA	Enzyme linked immunosorbent assay
ESI	Electron spray ionisation

Abbreviation	Full title
ETC	Electron transport chain
EtOH	Ethanol
EZH2	Histone H3 lysine 27 methyl transferase
FACS	Flow assisted cell sorting
FAD+	Flavin adenine dinucleotide (oxidised)
$FADH_2$	Flavin adenine dinucleotide (reduced)
FCS	Foetal calf serum
FOXO	Forkhead Box O
g	Gram
g/L	Grams/Litre
G1/2/0	Gap phase 1/2/0
GAPDH	Glyceraldehyde-3-phosphate dehydrogenase
GC	Gas chromatography
ɣH2AX	Histone variant H2AX phosphorylated on serine 139
GLUT1/4	Glucose transporter 1/4
GPC	Glycerophoshorylcholine
GPI	Glucose phosphate isomerase
Gr	Growing
GSH	Reduced glutathione
Gy	Gray
H_2DCFDA	2',7'-dichlorofluoroscindiacetate
H_2O_2	Hydrogen peroxide
H3K9me3	Trimethylated lysine 9 histone H3
HA	Haemaglutanin tag
HAT	Histone acetyl transferase
HCl	Hydrochloric acid

Abbreviation	Full title
HDAC	Histone deactylase
HDACI	Histone deactylase inhibitor
HDF	Human diploid fibroblast
HFF	Human foreskin fibroblasts
HK2	Hexokinase 2
HMDB	Human metabolome database
HP1ɣ	Heterochromatin protein 1 gamma
HPLC	High performance liquid chromatography
HRP	Horse radish peroxidase
HuR	Human antigen R
I value	Spin value
IDH1	Isocitrate dehydrogenase 1
IL	Interleukin
IrrDSB	Irreparable DNA double strand break
IrrDSBsen	Irreparable DNA double strand break induced senescence
kB	Kilobase
KDa	Kilo Dalton
KLF	Krupel-like transcription factor
LC	Liquid chromatography
LS	Serum starved
Luperox TBHP	Tert-butylhydroperoxide
M	Mitosis
MALDI	Matrix assisted laser desorption ionisation
MCM	Mini chromosome maintenance protein
MDA	Mean decrease accuracy

Abbreviation	Full title
MDH1	Malate dehydrogenase 1
MDM2	Mouse double minute 2 homolog (or E3 ubiquitin-protein ligase)
ME2	Malic enzyme 2
mg	Milligram
miR34A	Micro-RNA 34A
mL	Millilitre
MLL	Lysine N-Methyltransferase 2A
mM	Milli Molar
mm	Millimetre
MMP	Matrix metallo proteinase
MnSOD	Manganese superoxide dismutase
mpd	Mean population doubling
MRE1	Meiotic recombination 11
MRN complex	Meiotic recombination 11 (MRE1), RAD50 and Nibrin (NBS1) complex
mRNA	Messenger RNA
MS	Mass spectrometry
ms	Millisecond
MS/MS	Tandem mass spectrometry
MSTFA	n-methyl-n-(trimethylsilyl) trifluoroacetamide
mTOR	Mammalian/mechanistic target of rapamycin
MTT	4,5-dimethylthiazol-2-yl)-2,5-diphenyltetrazolium bromide
NAD+	Nicotinamide adenine dinucleotide (oxidised)
NADH	Nicotinamide adenine dinucleotide (reduced)

Abbreviation	Full title
NADP+	Nicotinamide adenine dinucleotide phosphate (oxidised)
NADPH	Nicotinamide adenine dinucleotide phosphate (reduced)
NBS1	Nibrin
NFkB	Nuclear factor kappa light chain enhancer of activated B cells
NHOF1/5	Normal human oral fibroblast1/5
NI	Nanospray ionisation
nm	Nanometre
NMR	Nuclear magnetic resonance
NRAS	Neuroblastoma RAS Viral (V-Ras) Oncogene Homolog
NS	Not significant
OIS	Oncogene induced senescence
OOB	Out of bag
OTSU	Otsu's thresholding algorithm
OXPHOS	Oxidative phosphorylation
$p16^{INK4A}$	Cyclin dependent kinase inhibitor 2A
$p21^{WAF1}$	Cyclin dependent kinase inhibitor 1A
P38 MAPK	Mitogen activated protein kinase 38
p53	Tumour suppressor protein 53
PBN	N-tert-butyl-a-phenylnitrone
PBS	Phosphate buffered saline
PCA	Principal components analysis
PcG	Polycomb group protein
PCK2	Phosphoenolpyruvate carboxykinase 2
PCNA	Proliferating cell nuclear antigen

Abbreviation	Full title
PCR	Polymerase chain reaction
PDH	Pyruvate dehydrogenase complex
PDK1/2/4	Pyruvate dehydrogenase kinase 1/2/4
PEsen	Proliferative exhaustion induced senescence
PFK1	Phosphofructokinase
PGE2	Prostaglandin E2
PGM	Phosphoglycerate mutase
pH	Logarithmic measure of hydrogen ion concentration
PI3K	Phosphoinositide 3-kinase
PKM1/2	Pyruvate kinase isoform M1/2
PML	Promyelocytic leukemia
$ppCO_2$	Partial pressure of carbon dioxide
PPP	Pentose phosphate pathway
PRPS1	Phosphoribosyl Pyrophosphate Synthetase 1
QC	Quality control
QMUL	Queen Mary University of London
qPCR	Quantitative polymerase chain reaction
Qui	Serum starved quiescent
Rb	Retinoblastoma protein
Redox	Reduction-oxidation
RIPA	Radioimmunoprecipitation assay buffer
RNA	Ribonucleic acid
ROI	Region of interest
ROS	Reactive oxygen species
RPA	Replication protein A
Rpm	Rotations per minute

Abbreviation	Full title
S	Synthesis phase
SAHF	Senescence associated heterochromatic foci
SASP	Senescence associated secretory phenotype
SAβ-gal	Senescence associated beta galactosidase
SCID	Severe combined immunodeficiency
SCO2	Synthesis of cytochrome oxidase 2
SDS	Sodium dodecyl sulphate
SDS-PAGE	Sodium dodecyl sulphate poly acrylamide gel electrophoresis
Sen	Senescent
SIM	Selective ion monitoring mode
SIRT1	Silent information regulator 2 homologue 1
SMAD2	Similar to Mothers Against Decapentaplegic 2
Suv39h	Suppressor of variegation 3-9 homolog 1
T0	Time zero
TBS-T	Tris buffered saline containing 0.1% vol/vol Tween 20
TCA	Tricarboxylic acid
TE	Tris-EDTA
TERC	Telomerase RNA component
TERT	Telomerase reverse transcriptase
TGF-β	Transforming growth factor beta
TIGAR	TP53 induced glycolysis and apoptosis regulator
TIMP	MMP inhibitor
TOF	Time of flight
TOPB1	Topoisomerase (DNA) II Binding Protein 1
TRF1/2	Telomere repeat binding factors 1/2

Abbreviation	Full title
U	Units
UHPLC	Ultra-high performance liquid chromatography
UV	Ultraviolet
V	Volt
vol/vol	Volume/volume
weight/vol	Weight/volume
xg	Relative centrifugal force measured in multiples of the standard acceleration due to gravity at the Earth's surface
X-Gal	5-bromo-4-chloro-3-indolyl-b-Dgalactopyranoside

Chapter 1

An introduction to the use of metabolic biomarkers of senescence

1.1 Cellular senescence

Senescence, defined as a state of irreversible growth arrest, has been observed since biologists first succeeded in culturing explanted cells *in vitro,* and attempts to explain the phenomenon are still being refined to this day. In 1921 the Nobel laureate Alexis Carrel published his observations that the growth rate and *in vitro* lifespan of chicken fibroblasts cultured in serum was related to the age of the animal the serum was derived from, and suggested that cells did not suffer loss of an "accelerating factor" but stopped multiplying only because of an *external* inhibiting factor (Carrel, 1921). This idea was contradicted 40 years later when Leonard Hayflick and Paul Moorhead famously observed that one population of human embryonic fibroblasts had a cumulative population doubling limit *in vitro* of between 40 and 60 doublings before proliferation eventually stopped, but cells from older individuals had a lower replication limit. Hayflick and Moorhead made the link that each cell can only go through a finite number of divisions, which the cell can keep count of (hence why the cells from older individuals went through less divisions *in vitro*, because they had already been through more divisions *in vivo*), before an *internal* blocking mechanism comes into effect (Hayflick and

Moorhead, 1961). This became known as the Hayflick Limit.

Hayflick is the one most often remembered, as he correctly identified that cells contain an internal mechanism that stops proliferation, however it is now clear that the internal mechanism which brings about senescence can be activated independently of the Hayflick Limit. For example, external factors that stress the cell can induce senescence, and could explain Carrel's findings (why such factors were present in the serum of Carrel's aged chickens will be discussed later). Furthermore, it is now apparent that senescence entails much more than just growth arrest and this introduction will give an overview of what we know of the mechanisms underpinning senescence, the resulting phenotype and its importance in biological processes and pathologies *in vivo*.

1.1.1 Senescence requires irreversible cell cycle arrest

A permanent growth arrest requires exit from the cell cycle (see figure 1.1). The cell cycle is a sequence of phases during which the integrity of the cell's genetic material is checked, DNA is duplicated and finally the cell divides. Each phase is tightly regulated by two groups of proteins: cyclins and cyclin dependent kinases (CDKs), which work together to ensure that relevant transcription factors are active at each stage of the cell cycle. The most important of these transcription factors when considering senescence is E2F, a family of 5 transcription factors that target nucleotide sequences present in the promoter regions of several genes essential for cell growth control, including c-myc, CDK1 and E2F-1 itself.[1] E2F is prevented from acting as a transcription factor by the Retinoblastoma protein (Rb) (Hiebert et al., 1992). The Rb family of proteins are the products of the Retinoblastoma gene originally identified in the eye and they act

[1]Three of the members of the E2F family, namely E2F1-3, are known as 'activators' because they are potent activators of transcription of cyclins that promote S phase entry. Inactivation of these three transcription factors results in a complete failure to proliferate, as shown by the use of conditional mutant E2F1-3 by Wu et al (Wu et al., 2001)(however, it is also known that E2F1, which is stabilised by the DNA damage response proteins ATM and ATR (Lin et al., 2001), also promotes apoptosis if expressed at high enough levels). In contrast E2F4 and E2F5 repress the E2F response genes by recruiting pocket proteins (Rb and its family members p107 and p130), and histone modifying enzymes. E2F6, the final family member, is also a repressor but through a pocket protein independent mechanism.

as 'gatekeepers', controlling whether the cell cycle continues through from G1 phase to S phase via their interactions with certain transcription factors and promoter regions. When in a de-phosphorylated state, Rb binds E2F in the trans-activation domain, so the E2F-Rb complex is still able to bind to the promoter regions of the E2F target genes, but E2F's ability to recruit transcriptional machinery is disabled. Instead of recruiting transcriptional machinery, the complex recruits factors that enhance transcriptional repression such as histone deacetylase enzymes (HDACs) and the histone methyl-transferase SUV39H1. This inhibition is stopped at the G1/S checkpoint by CDK4/6 and cyclin D combined with CDK2 and cyclin E, which phosphorylate Rb. Phosphorylation of Rb causes it to release E2F, facilitating transcription of S phase genes and the continuation of the cell cycle (Zhang et al., 2000). During S phase multivulval class B (MuvB) complexes with the transcription factor BMYB to control gene expression, while gene expression in late G2 and M phase is controlled by the MuvB core binding to the transcription factors BMYB and FOXM1 (reviewed in Sadasivam and DeCaprio (2013)). During G0 MuvB binds to p130-E2F dimerisation partner (DP), forming the DP, Rb-like, E2F and MuvB (DREAM) complex which represses all cell cycle dependent gene expression (Litovchick et al., 2007).

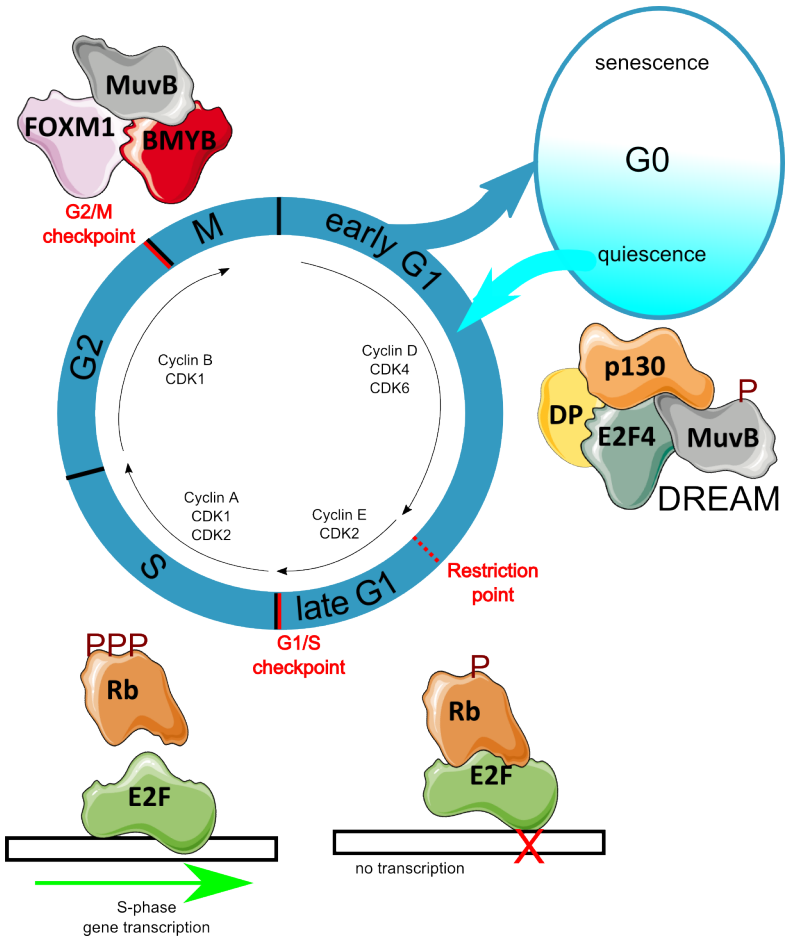

Figure 1.1: **Schematic showing the stages of the cell cycle**. The early part of the first gap phase (G1) is mitogen dependent and driven forward by the action of cyclin D in combination with CDKs 4 and 6, however once past the G1 restriction point progression no longer requires mitogens to be present. The late stage of G1 is driven by cyclin E and CDK2. The G1/S checkpoint is the point at which the cell commits to synthesising duplicate copies of its DNA ready for cell division. If there are are no inhibitory signals then the actions of CDK4/6 with cyclin D combined with CDK2 and cyclin E phosphorylate Rb, which throughout G1 had been hypo-phosphorylated allowing it to remain bound to the transcription factor E2F. Once hyper-phosphorylated, Rb dissociates from E2F and the transcription of proteins required for S phase can begin. Following S phase the cell enters a second gap phase (G2) and the cell prepares for division by synthesising the necessary proteins. A final checkpoint (G2/M) must then be passed before mitosis can begin, the cell will not be able to proceed if DNA damage response pathways are active. Late G2-M gene expression is controlled by multi-vulval class B (MuvB) binding the transcription factors BMYB and FOXM1. G0 is a resting phase entered into by cells which are not preparing to divide, such as terminally differentiated cells (which may only re-enter the cell cycle under specific circumstances), quiescent cells (which will re-enter the cell cycle once stimulated to do so), and senescent cells (which have permanently exited the cell cycle and cannot re-enter, but remain metabolically active). Cell cycle dependent gene expression is repressed during G0 by the p130-E2F4 dimerisation partner (DP), Rb-like, E2F and MuvB (DREAM) complex.

1.1.2 Quiescence and geroconversion

As already mentioned, cells in G0 that are not in a permanent or stable state of arrest are known as quiescent, and can remain quiescent indefinitely. The transition from this reversible growth arrest to senescence is known as 'geroconversion' and there is evidence to suggest it is caused by continued signals to divide, in particular from the target of rapamycin (TOR) pathway, while the cell cycle is still arrested (Demidenko and Blagosklonny, 2008; Blagosklonny, 2012).

1.1.3 Key senescence effector proteins

Although senescence is induced and maintained by a host of complex pathways and processes, there are some key proteins that play particularly important roles. These are p53, its downstream effector CDK inhibitor $p21^{WAF1}$, and the CDK inhibitor $p16^{INK4A}$.

1.1.3.1 p53

At the time of writing, a Pub Med search for 'p53' returned 128045 articles. It is one of the most studied proteins, which is not surprising because p53 and its family members are involved in numerous cellular functions; development (Gannon and Jones, 2012), metabolic regulation (Gottlieb and Vousden, 2010) and apoptosis (Giorgi et al., 2015) to name just a few. p53 is most famous for its role as the 'guardian of the genome', because of its involvement in maintaining the integrity of the germ line (Muller et al., 2000) and its role as a tumour suppressor protein (Olivier et al., 2010), which is ironic because when it was first discovered it was believed to be an oncoprotein; many groups had identified p53 cooperating with oncogenic Ras in several forms of cancer, but it was later discovered that all of these oncogenic examples of p53 were actually mutant p53; wild type p53 prevents oncogenic transformation in many cases (reviewed in Lane and Levine, 2010). As we shall see, p53's role in maintaining genomic integrity and preventing neoplastic transformation involves the regulation of senescence, via several mechanisms. p53 is known to be activated by various post translational

modifications, and in 2000 Karen Webley and co-workers published a detailed account of the different phosphorylation states of p53 at the N and C termini in response to different senescence inducing stimuli. They demonstrated, using antibodies specific to particular phosphorylated amino acid residues, that cells which had senesced due to reaching the Hayflick limit had p53 phosphorylated on different residues to cells treated with the DNA damaging agent bleomycin, ultraviolet (UV) radiation, and ionising radiation, although all of these conditions had the phosphorylation of serine 15 on p53 in common. This lead to the hypothesis that different kinases were involved in the regulation each of these mechanisms leading to activation of p53 (Webley et al., 2000).

1.1.3.2 $p21^{WAF1}$

$p21^{WAF1}$(also known as $p21^{CIP1}$, and referred to in some papers as senescent cell derived inhibitor 1) is a member of the Cip and Kip family of CDK inhibitors that also includes p27 and p57, encoded by the gene *CDKN1A* (reviewed in Abbas and Dutta, 2009). $p21^{WAF1}$ is best known for functions in cell cycle inhibition; this role was discovered when immunoprecipitation experiments showed the 21 KDa protein to be interacting with and inhibiting cell cycle regulating proteins (Harper et al., 1993) and it was found to be elevated in senescent cells (Noda et al., 1994), but it can also protect against apoptosis (Sheikh et al., 1995). The activity of $p21^{WAF1}$ in response to DNA damage is dependent on transcriptional activation by p53, and p53 can also activate 21 transcription in response to Ras activation (Macleod et al., 1995), although it can also be transcriptionally regulated independently of p53 by Ras and Raf and by other stimuli such as nuclear receptors, vitamin D receptors and androgens via the transcription factor E2F1. Alternatively the Krüppel-like transcription factor (Klf) family member KLF6 can co-operate with p300-CREB binding protein (a transcriptional co-activator) to activate *CDKN1A* transcription (reviewed in Abbas and Dutta, 2009).

In addition, $p21^{WAF1}$ regulation by post translational modifications is very important as it is a highly unstable protein that is targeted for ubiquitination or proteolysis unless

it is protected by chaperone proteins, which are recruited following binding of adaptor proteins to $p21^{WAF1}$ (Jascur et al., 2005). Furthermore, post-translational modifications such as phosphorylation facilitate the transport of $p21^{WAF1}$ to different cell compartments, where its function is different. For example nuclear $p21^{WAF1}$ acts as a cell cycle inhibitor whereas the anti-apoptotic functions require the protein to be localised to the cytoplasm, which occurs following phosphorylation by the serine threonine protein kinase AKT1 (Ping et al., 2006).

1.1.3.3 $p16^{INK4A}$

The only known function of $p16^{INK4A}$ is the inhibition of CDK4 and CDK6. It has been shown to accumulate in senescence (Hara et al., 1996) and is also a functional marker of ageing (Krishnamurthy et al., 2004; Liu et al., 2009; Baker et al., 2016). Since its discovery in 1993 (Serrano et al., 1993) mutations in or loss of the gene have been associated with several cancers (Li et al., 2011). $p16^{INK4A}$ is encoded by the gene CDKN2A, which also includes an alternative reading frame (ARF) that encodes $p14^{ARF}$. Activation of these genes is independent of p53 and is regulated by polycomb group proteins (PcG) (Bracken et al., 2007).

1.1.3.4 Inhibition of the cell cycle by senescence effector proteins

Activation of p53 in response to DNA damage, oncogenic signalling or other cellular stress results in the transcription of several downstream targets, which have both direct and indirect effects on the senescence growth arrest (although the relationship between senescence and p53 is complex and in some contexts p53 can inhibit senescence induction (Salama et al., 2014)). One such downstream target is micro RNA 34A (miR34A) (He et al., 2007), which negatively regulates the expression of Sirtuin 1 (SIRT1) (Yamakuchi et al., 2008). SIRT1 itself is capable of negatively regulating p53 by deacetylating lysine 382, which disables p53 transcriptional activity (Langley et al., 2002), so p53 dependent transcription of miR34A results in a positive feedback loop, stabilising p53

and therefore promoting the induction of senescence. In addition, SIRT1 also negatively regulates nuclear factor kappa light chain enhancer of activated B cells (NFkB) which is activated in response to senescence inducing stimuli such as DNA double strand breaks (DSB) and has important but incompletely understood roles in senescence; silencing of NFkB has been shown to result in senescence bypass, suggesting it could be necessary for growth arrest in some contexts (Rovillain et al., 2011), however it has also been demonstrated that non-canonical activities of NFkB can suppress senescence by directly modulating the CDKs and even $p21^{WAF1}$ (Iannetti et al., 2014).

Another downstream transcriptional target of p53 is $p21^{WAF1}$ Qian and Chen, 2013). $p21^{WAF1}$ is a potent inhibitor of CDKs and can inhibit the phosphorylation of Rb by cyclin A-CDK2, cyclin E-CDK2, cyclin Dl-CDK4, and cyclin D2-CDK4 complexes (Harper et al., 1993). In addition, $p21^{WAF1}$ influences the cell cycle by binding to proliferating cell nuclear antigen (PCNA), preventing access by Cyclin D, which is required for cell cycle progression (Stein et al., 1999).

Increased expression of $p16^{INK4A}$ following PcG protein regulation (due to DNA damage or oncogenic signalling) specifically inhibits CDK4 and CDK6 via stearic hindrance (Alcorta et al., 1996; Stein et al., 1999; Brookes et al., 2004).

In karatinocytes it has been shown that p53 levels decline in established senescence (Kim et al., 2015) and in human diploid fibroblast (HDF) cells undergoing senescence it has been observed that $p21^{WAF1}$ is elevated in the early stages of growth arrest and $p16^{INK4A}$ gradually increases so that in late senescence $p21^{WAF1}$ levels (and also presumably activated p53) are low and $p16^{INK4A}$ levels are high (Stein et al., 1999) however neither protein is essential to all modes of senescence (Stein et al., 1999; Prieur et al., 2011).

The summary diagram in figure 1.2 shows how cell cycle arrest can be brought about through a variety of pathways initiated by either proliferative exhaustion, genotoxic stress, or oncogene expression. These routes to senescence will be discussed in the following subsections.

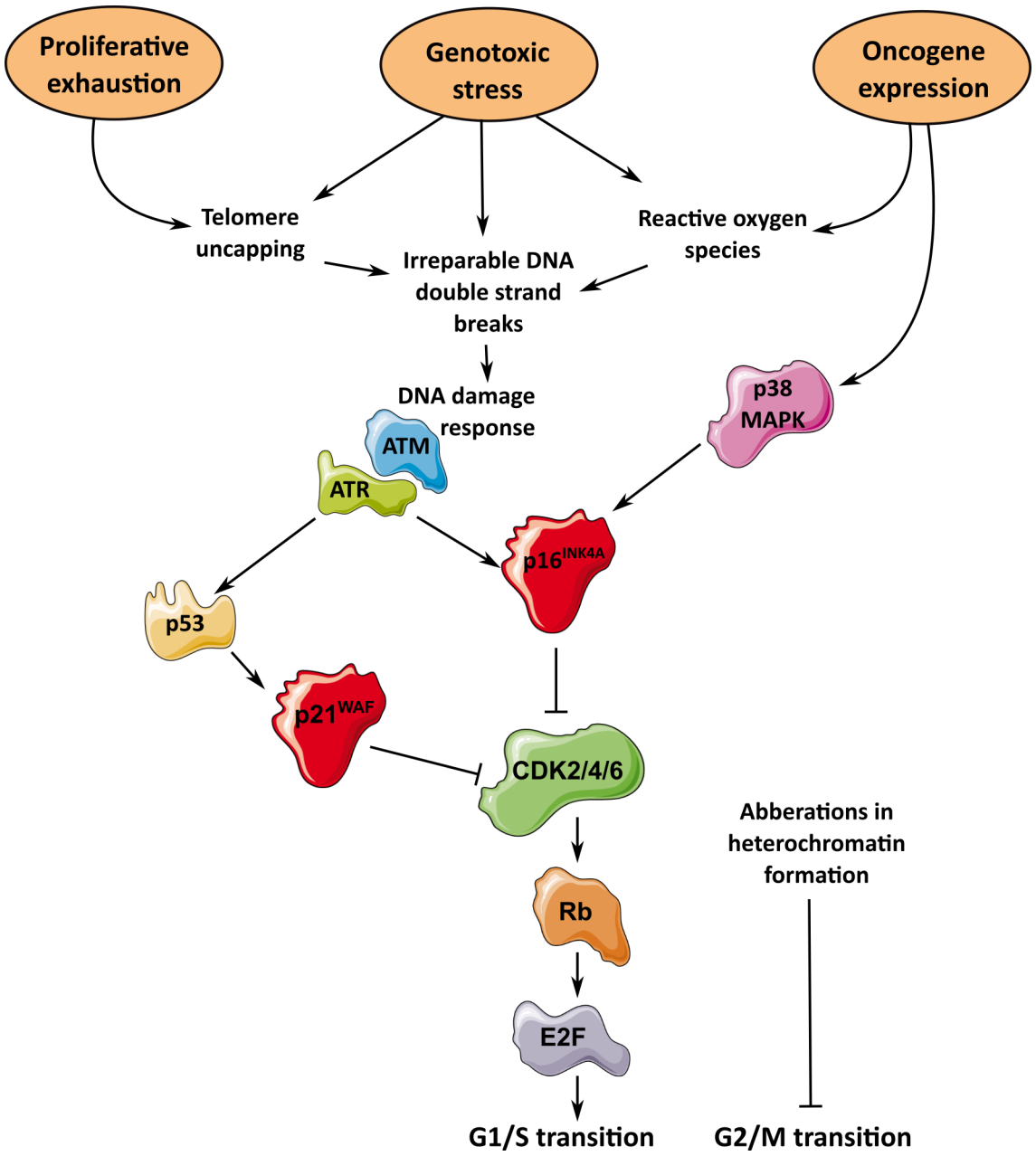

Figure 1.2: **Simplified overview of senescence induction** showing the three general senescence inducing stimuli; proliferative exhaustion, genotoxic stress and oncogene expression. These modes of induction often converge on DNA damage signalling which is regulated by proteins such as ataxia telangiectasia mutated (ATM) and ataxia telangiectasia and Rad3-related (ATR) which induce $p16^{INK4A}$. Activation of p53 results in the transcription $p21^{WAF1}$, and these CDK inhibitors prevent CDKs from phosphorylating Rb. Phosphorylation of Rb is required for it to release the transcription factor E2F which is responsible for transcription of genes needed for synthesis (S) phase, so inhibition of E2F leads to cell cycle arrest in G1. Oncogene expression activates the mitogen activated protein kinase 38 (p38 MAPK) pathway, also resulting in CDK inhibition. Cell cycle arrest can occur in G2 via a separate route involving alterations in heterochromatin structure.

1.1.4 Proliferative exhaustion induces senescence via telomere shortening

Hayflick and Moorhead observed that somatic cells can only go through a finite number of divisions and cells are able to keep track of how many they have already been through, as evidenced by the observation that cells from older individuals have less capacity to proliferate once explanted to culture than cells from a young individual, even when given the same culturing conditions (Hayflick and Moorhead, 1961). Subsequent research has identified the mechanism that keeps track of the number of cell divisions as telomere erosion via end-replication inhibition (Olovnikov, 1971). These multifunctional heterochromatin structures, made from up to 15kB of DNA 5'-TTAGGG-3' repeats (Moyzis et al., 1988) bound to associated proteins (including the shelterin complex), are found at the ends of all linear eukaryotic chromosomes. Telomeres form loops, called 'T Loops', that act as a cap; stabilising the end of the telomere (Griffith et al., 1999), protecting the ends of DNA from being recognised as a DNA double strand break and getting degraded as part of a DNA damage response (DDR), also preventing end fusion events and helping to position the chromosomes within the nucleus. The basic structure of a telomere is shown in figure 1.3.

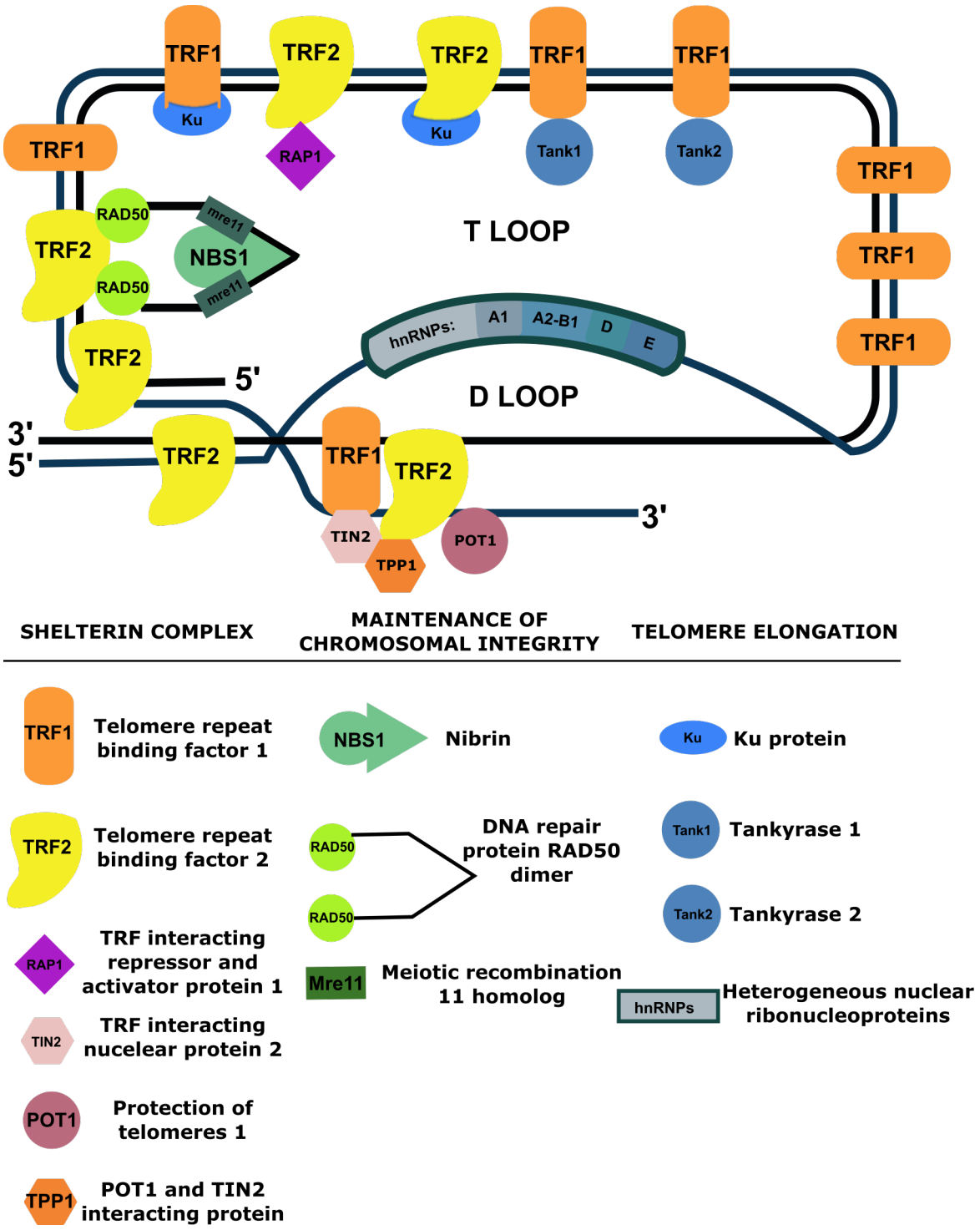

Figure 1.3: **The simplified structure of a telomere**. Telomeres are structures of heterochromatin that form 'caps' in concert with various proteins (which form the shelterin complex) on the ends of linear DNA of eukaryotic chromosomes, preventing recognition as a strand break and also protecting coding DNA from sequence loss due to the end replication problem. The cap structure contains a T Loop, which houses proteins involved in maintenance of chromosomal integrity and telomere elongation, as well as a smaller D loop. Schematic made with help from Katie R. James.

Another function of telomeres is to facilitate the complete replication of entire chromosomes, although at the cost of the telomere sequence itself. With each cell division some of the telomere sequence is lost during S phase due to the 'end replication problem' which occurs as an inevitable result of DNA polymerase working to replicate DNA in the 5'→3' direction, and exonuclease digestion of the C tail (Olovnikov, 1971). By sacrificing some of the telomere sequence, the DNA that encodes the genome is spared. Furthermore, the structure of the telomere prevents the repair of DNA double strand breaks by non-homologous end joining, which could explain the build up of DNA double strand breaks in post mitotic tissues, such as brain and liver, with age (Muraki et al., 2013). Once a critical telomere length is reached disruption in the proteins associated with the telomere allows it to be recognised as dysfunctional and a DDR is launched, resulting in senescence (d'Adda di Fagagna et al., 2003; Takai et al., 2003). Senescence induced via proliferative exhaustion will henceforth be referred to as PEsen.

1.1.4.1 Telomerase prevents PEsen

Germ line cells and embryonic stem cells do not encounter the problem of telomere erosion because they are able to replenish their telomeres using a ribonucleoprotein enzyme called telomerase. The enzyme contains a telomerase reverse transcriptase enzymatic sub unit (TERT) and an RNA template (*TERC*) (Kim et al., 1994), and works by copying the repeating sequence directly onto the end of the chromosome (Feng et al., 1995). Although telomerase is not expressed in most somatic cells, some cancer cells are able to switch on telomerase and can become immortal (Kim et al., 1994; Killela et al., 2013).

1.1.4.2 Non canonical functions of telomerase

Telomerase is also known to have functions other than lengthening telomeres, some of which require both the TERT and *TERC* components (non-canonical I functions) and some which only require the TERT component (non-canonical II functions). Non-

canonical I functions are associated with neoplasia formation and an insensitivity to transforming growth factor beta (TGF-β) and epidermal growth factor whereas non-canonical II functions are involved in apoptosis resistance and the activation of WNT and MYC signalling (reviewed in Parkinson et al., 2008).

1.1.4.3 Alternative lengthening of telomeres (ALT) can also prevent PEsen

Cancer cells that do not express telomerase can also lengthen telomeres using an alternative lengthening of telomeres (ALT); a mechanism that is not completely understood. The evidence suggests that ALT occurs via recombination using proteins that are present in all normal somatic cells such as the members of the MRN complex (meiotic recombination 11 (MRE1), RAD50 and Nibrin (NBS1)), and it is suggested that some proteins, such as telomere repeat binding factors 1 and 2 (TRF1 and TRF2), which can be lost in cancer, are usually preventing ALT (reviewed in Cesare and Reddel, 2010).

1.1.5 Premature senescence in the absence of telomere attrition

In the absence of shortened telomeres cells can still enter senescence via other routes if necessary. The expression of oncogenes, certain histone modifications and genotoxic stress can all lead to senescence, and can occur independently of each other, although sometimes the pathways overlap. Oncogene expression and genotoxic stress, along with telomere attrition, are all thought to illicit senescence ultimately via a DNA damage response (DDR).

1.1.5.1 Oncogene induced senescence (OIS)

A key role of senescence *in vivo* is thought to be tumour suppression, so it is no surprise that genes coding for p53, Rb and $p16^{INK4A}$ are among the top 10 most commonly mutated genes in cancer (Atlas, 2015). It was initially demonstrated *in vitro* that oncogenic *Ras* expression in the presence of functional p53 or $p16^{INK4A}$ leads to a short

period of hyper-proliferation that then triggers a permanent cell cycle arrest in G1 (Serrano et al., 1997) and subsequent work showed that a downstream effector of Ras signalling; the Raf/MEK/MAP Kinase signalling cascade, is also capable of causing senescence (Zhu et al., 1998; Lin et al., 1998). These signalling cascades are now known to bring about a growth arrest via p38 MAP Kinase driven histone modifications (more detail on this is given in subsection 1.1.5.2) leading to elevation of $p16^{INK4A}$ (Wang et al., 2002; Deng, 2003) .The mechanism was observed not to be overcome by TERT in early studies (Wei S.; Sedivy, J. M., 1999) suggesting a mechanism independent of telomere shortening but more recent work suggests that stochastic damage at telomeres following oncogene expression can also contribute to the senescence induction in some cases (Suram et al., 2012).

In addition to expression of oncogenes, loss of tumour suppressor genes can also trigger of OIS and evidence of this occurring *in vivo* came in 2005 from murine models of cancer which showed p53 mediated senescence in response to loss of the tumour suppressor protein Pten prevented tumour formation (Chen et al., 2005). Loss of Pten (as well as over-expression/activating mutation of cellular homologue of murine thymoma virus Akt8 oncoprotein (AKT) or phosphoinositide 3-kinase (PI3K)) causes senescence via activation of the PI3K/AKT/mammalian target of rapamycin (mTOR) pathway: AKT inhibits forkhead transcription factor FOXO3, a transcription factor for radical scavenger manganese superoxide dismutase (MnSOD), resulting in lower MnSOD levels and therefore increased radicals and reactive oxygen species (ROS) which activates p53 and leads to $p21^{WAF1}$induced senescence (reviewed in Xu et al., 2014).

1.1.5.2 Histone modifications can lead to premature senescence

Changes in chromatin structure, i.e. the ways in which DNA is organised around histone protein octamers, are seen in senescence in the form of senescence associated heterochromatic foci (SAHFS) (Narita et al., 2003a). These foci are the result of large scale chromatin condensation (Funayama et al., 2006), facilitated by histone chaperone

proteins such as HIRA, ASF1a and UBN1 (Zhang et al., 2005; Banumathy et al., 2008).

The two main modifications that occur in chromatin are acetylation/de-acetylation and methylation/de-methylation of histones, which are the main proteins in chromatin. Acetylation, by histone acetyl transferases (HATs), adds an acetyl group from a donor such as acetyl Co A, to the N terminal of the histone protein, removing the positive charge and allowing the chromatin to de-compact. De-acetylation by histone deacetylase enzymes (HDACs) restores a positive charge on the histone N terminus, and thereby attracts the negative phosphate groups of DNA, causing the DNA to wrap more tightly around the histone proteins, and preventing transcription factors from interacting with the DNA (reviewed in de Ruijter et al., 2003).

Methylation of histones by methyl-transferases can either activate or repress transcription, depending on the level of methylation and the amino acid being methylated. For example the tri-methylation of an amino acid might activate transcription, but di-methylation of the same amino acid may cause silencing, again by regulating the access transcription factors have to the DNA (reviewed in Greer and Shi, 2012). These events are regulated by a complex web of pathways; of particular relevance here are the polycomb group complexes, or 'PcG's. These multi-subunit transcriptional repressor complexes are comprised of, among other things, a histone H3 lysine 27 methyl transferase (EZH2) and a RING finger protein (BMI1). In proliferating cells a PcG complex binds to a non coding antisense RNA known as ANRIL (Pasmant et al., 2007; Yap et al., 2010) and to the CDKN2a locus, which is the locus of the $p16^{INK4A}$ protein and the indirect activator of p53 ARF, and BMI1 represses expression of both genes. However, under senescence inducing conditions, such as oncogenic Ras activity, de-methylation of lysine 27 on histone H3 by histone demethylase JMJD3 (Barradas et al., 2009), and lower expression of EZH2 results in loss of binding and therefore loss of repression by PcG, contributing to the increased expression of $p16^{INK4A}$ (Bracken et al., 2007). Also contributing to the up-regulation of $p16^{INK4A}$ in senescence is another methyl-transferase; MLL1, which methylates H3 on lysine 4, activating transcription

(Kia et al., 2008). In addition, it is possible to induce senescence using HDAC inhibitors (HDACIs), predominantly through a $p16^{INK4A}$ dependent mechanism that has not yet been fully defined (Munro et al., 2004).

Further studies into the links between OIS and histone modifications show that PcGs are also involved in the up-regulation of $p16^{INK4A}$ via p38MAP Kinase (Deng, 2003) because the p38MAP Kinase target MAPKAPK3 phosphorylates PcG proteins, causing dissociation of PcG from chromatin and preventing the repression of CDKN2a (Voncken et al., 2004).

1.1.5.3 Genotoxic stress induces premature senescence

In this thesis genotoxic stress is considered as a condition that results in the generation of DNA double strand breaks, the best characterised of which are ionising radiation and ROS.

Ionising radiation refers to high energy particles or waves that are capable of removing an electron from atoms or molecules. X rays, gamma rays, beta particles (high-speed electrons), alpha particles (the nucleus of the helium atom), neutrons, protons, and other heavy ions such as the nuclei of elements are all forms of ionising radiation, and when they pass through a cell the energy released is absorbed by nearby atoms, causing either the gain of an electron, i.e. excitation, or the loss of an electron, i.e. ionisation, from any orbital (not necessarily the outer orbital). The removal of electrons from inner orbitals creates highly unstable radicals that quickly react with nearby atoms to replace the electron, causing the breakage of chemical bonds and oxidation of molecules. This damage can occur directly to the DNA, causing base lesions such as oxidation of deoxyribose, the formation of adducts and cross-links as well as both single and double strand breaks (reviewed in O'Neill and Fielden, 2013) however, because cells are approximately 70% water the majority of the DNA damage induced by ionising radiation is thought to occur through an indirect route, whereby cellular components, for example water and proteins, form free radicals (predominantly HO•

and RO2•) which then in turn react with DNA. Defining the damage inflicted on DNA by radicals generated from the ionisation of water as "indirect" has been called into question by O'Neill et al (O'Neill and Fielden, 2013), who have pointed out that close interaction with water is important for the secondary and tertiary structures of DNA, with approximately 20 water molecules being required per nucleotide.

ROS, released as a by-product of oxidative metabolism (reviewed in Murphy, 2009), also cause DNA damage by forming radicals predominantly from water. The most common species are the hydroxyl radical HO• and also the non radical H_2O_2. The mechanisms of lesion formation are the same as those which occur when ionising radiation hits the water associated with DNA; HO• can force its way into a double bond in a heterocyclic DNA base (this is known as addition) and remove a H atom from the methyl group on thymine or any of the C-H bonds on 2-deoxyribose (this is known as abstraction) to form C- or N- centred radicals of DNA bases as well as radicals of the sugar backbone of DNA, which continue to react with neighbouring molecules to form a variety of products (explained in detail in von Sonntag, 2006). The overall result is disruption in the structure of the DNA double helix so that single and double strand breaks can form.

Genotoxic stress is not only acquired following a large insult such as ionising radiation, it can occur following a gradual built up of radicals, for example due to excessive electron leakage from the mitochondrial electron transport chain. Elevated ROS level is a common effect of mitochondrial damage and forms the basis of the 'free radical theory of ageing' (Harman, 1992). This theory states that ageing occurs because of accumulated molecular damage, however there is compelling evidence that the inevitable accumulation of molecular damage over time is correlated with, but not a cause of, physiological ageing (reviewed in Speakman and Selman, 2011). The link between senescence, ROS and physiological ageing will be discussed further in section 1.3.4 on page 68.

1.1.5.4 Non-cell autonomous senescence

It is possible for senescent cells to induce senescence in neighbouring cells via soluble factors released as part of the senescence associated secretory phenotype (SASP, described in more detail later in section 1.2.3), as demonstrated by Juan Carlos Acosta and colleagues, who showed that co-culture of OIS senescent cells with non- senescent cells, distinguished using the fluorescent marker mCherry which was only expressed in the non-senescent cells, resulted in a stable growth arrest in the mCherry positive cells after just a few days. The authors identified members of the TGF-β family and VEGF as key mediators in this effect (Acosta et al., 2013).

1.1.6 The DNA damage response (DDR) plays a key role in initiating senescence induction pathways

Although senescence can be induced by a variety of events, a common factor in the induction and maintenance of the senescence phenotype in many cases is activation of the DDR signaling pathway. As we have seen in the previous sections of this introduction, DNA integrity is compromised once a telomere becomes critically short and the shelterin complex protecting the end of the linear DNA becomes disrupted (subsection 1.1.4 on page 37), when radical scavenger levels are transcriptionally repressed (subsection 1.1.5.1 on page 40) and also when excessive numbers of radicals are produced, for example following radiation or mitochondrial dysfunction (subsection 1.1.5.3). Cells are adept at dealing with various types of DNA damage including single and double strand breaks; often the damage can be repaired but if it cannot the cell must undergo either apoptosis or senescence to prevent passing mutated DNA on to daughter cells. Below is an outline of the key processes involved in the DDR and resulting repair or senescence/apoptosis induction.

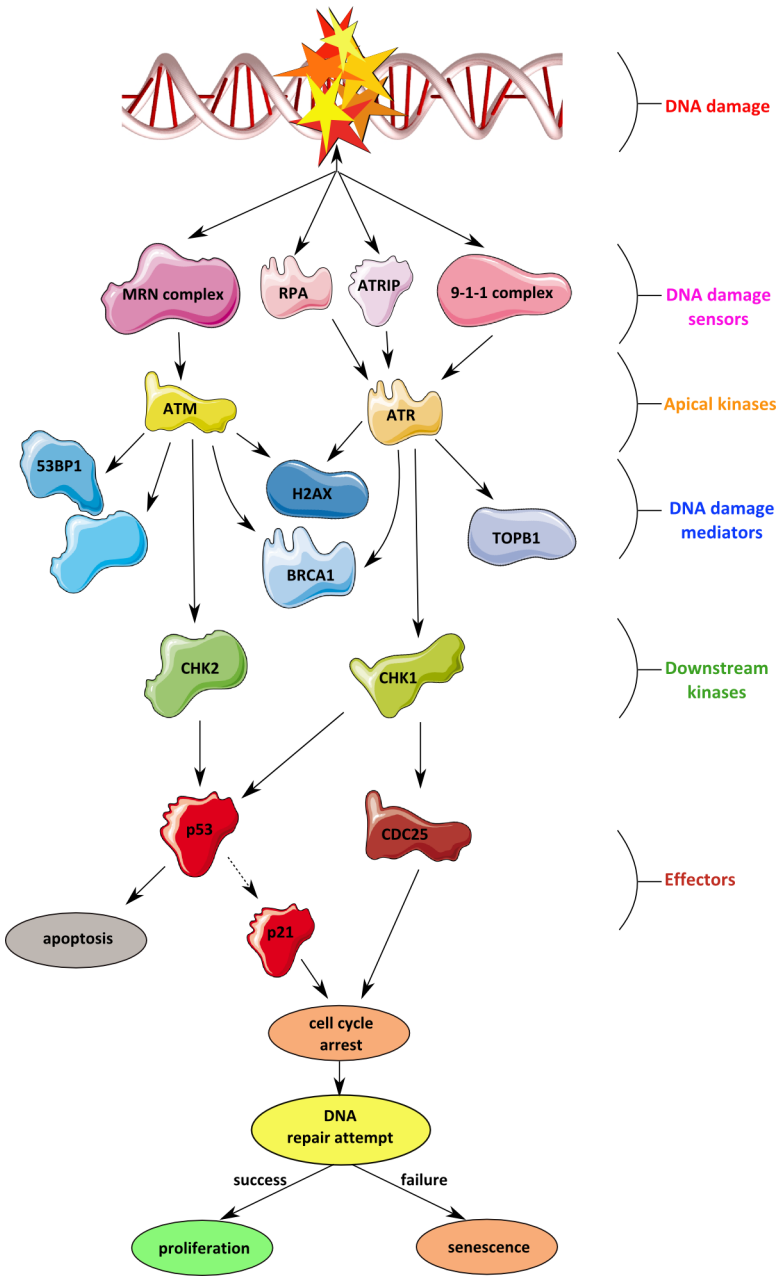

Figure 1.4: **Main components of the DNA damage response (DDR) pathway** (adapted from Sulli et al., 2012). MRN complex binds to RPA and 9-1-1 complex and is stabilised by ATRIP. These sensors recruit ATM and ATR, which recruit DNA damage mediators. Phosphorylation of H2AX facilitates recruitment of MDC1, amplifying DDR signalling with activation of ATM. 53BP1 sustains DDR signalling via ATM activation, and TOPB1 further reinforces the DDR by activating ATR (Kumagai et al., 2006). BRCA1 is also recruited by ATM and ATR and is involved in coordinating DNA repair (Cortez et al., 1999; Huen et al., 2010). CHK1 and CHK2 are also recruited. Negative regulation of CDC25 by CHK1 can lead to cell cycle arrest in G2, and the activation of p53 by CHK2 can result in apoptosis or senescence via $p21^{WAF1}$.

DNA damage 'sensors' such as the MRE11-RAD50-NBS1 (MRN) complex, which

detects DNA double strand breaks, and replication protein A (RPA) and the RAD9-RAD1-HUS1 (9-9-1) complex which detect exposed single stranded DNA, recruit the protein kinases ataxia telangiectasia and Rad3-related (ATR) and ataxia telangiectasia mutated (ATM) to the site of damage. The two kinases respond to specific kinds of DNA damage; ATM is predominantly activated by double strand breaks (DSBs) whereas ATR responds to the type of genotoxic stress that is caused by DNA replication stress, which is also caused by oncogenes. Once at the site of damage ATM and ATR phosphorylate proteins such as breast cancer susceptibility 1 (BRCA1) and p53 (Banin et al., 1998), as well as provoking a second wave of phosphorylation by activating the kinase checkpoint kinase 2 (CHK2). CHK2 is then able to phosphorylate p53 on serine 20, which lies in the p53 binding site for E3 ubiquitin-protein ligase (MDM2) (Chehab et al., 1999). MDM2 is a protein that marks p53 for proteolysis, so blocking its binding acts to increase p53 activity. Furthermore, phosphorylation of the histone H2AX, to form ɣH2AX, causes recruitment of more ATM in a positive feedback loop facilitated by p53-binding protein 1 (53BP1) and mediator of DNA-damage checkpoint 1 (reviewed in Marechal and Zou, 2013). Furthermore, phosphorylation of cell division cycle 25 (CDC25) on serine 216 by checkpoint kinase 1 (CHK1) negatively regulates CDC25, which usually facilitates the transition from G2 into M phase resulting in a G2 arrest (Peng et al., 1997). The DDR results in either apoptosis or stalled replication until the DNA can be repaired . In the event that the damage is irreparable, DNA segments with chromatin alterations reinforcing senescence (DNA-SCARS) can form and the cell will never regain the ability to divide, therefore it becomes senescent.

To summarise, senescence is a state of permanent cell cycle arrest that can be induced by proliferative exhaustion, oncogene expression, genotoxic stress or disruption to heterochromatin structure. Most of these routes converge at the DNA damage response and are ultimately enforced by either p53 or $p16^{INK4A}$, although there is a lot of variation in senescence induction and maintenance that we do not yet understand; for example species and tissue specific differences, and what effect the surrounding envir-

onment has. This variation can also be seen in the senescence phenotype, making the identification of senescent cells with certainty quite challenging.

1.2 The cellular senescence phenotype

Observing the senescent phenotype helps us to identify senescent cells and can also give us insights into what effect senescent cells might have *in vivo.* We do not yet understand enough to have a fully defined phenotype of cellular senescence, let alone a single robust marker with which to easily identify them *in vivo*, however we do have some knowledge to work with.

1.2.1 Growth arrest

Although as yet there is not one clear marker of cellular senescence, the definition of cellular senescence as a state of permanent growth arrest does offer some obvious starting points when trying to identify a senescent population *in vitro* (of course this excludes terminally differentiated/post mitotic cells, which will also not be proliferating). Monitoring the rate at which the population doubles when under favourable conditions (sub-confluent distribution on a suitable surface, correct pH media, correct temperature, enough nutrients, mitogens and growth factors, and not infected with mycoplasma or other pathogen) is a good indicator of the replicative potential of the cells. Generally, if the population has not completed one population doubling in one month, it is likely that the population is senescent. Population growth can be monitored in a number of ways, the most straight forward of which is to count the cells and compare to the amount that were seeded originally, to calculate how many time the cells must have divided. The replication of DNA can also be detected by addition of 5-bromo-2'-deoxyuridine, which is de-aminated to BrdU, a synthetic analogue of thymidine which has a Bromine (Br) in the place of a CH_3 group, making it easy to detect. In theory, incorporation of BrdU into DNA only occurs if the cells are in S phase, so if cells do

not incorporate BrdU even after a long exposure it suggests the population is growth arrested (Nowakowski et al., 1989), however active DNA repair would also allow for incorporation of BrdU potentially creating false positives.

Alternatively, it is possible to assess the replicative potential of the cells by looking for the expression of proteins necessary for cell division. One such protein is MCM7 (mini chromosome maintenance protein 7, also known as MCM2) which combines with other MCMs to form a hetero-hexamer helicase complex, crucial for at least two known functions: "licencing" of origins of replication to ensure that DNA is only copied once in every cycle (Chong et al., 1995), and the formation of the DNA replication fork (reviewed in Forsburg, 2004). Additionally, it has been reported that MCM7 interacts with Rb and the possibility that Rb inhibits cell cycle progression by sequestering MCM proteins has been raised (Sterner et al., 1998). Reduced levels of MCM7 therefore indicate the cell is not capable of duplicating its DNA and cannot be dividing. Another protein that signifies whether or not the cell is capable of dividing is Ki67. Although the function of the Ki67 protein is unknown, it is always present in the nuclei of cells in mitosis, G1, S or G2 phase (reviewed in Scholzen and Gerdes, 2000), so absence of Ki67 means the cell is in G0 and cannot divide at that moment. It is possible, when using Ki67 to look for non-dividing cells, to get a false negative result if the cell is growth arrested outside of G0. Growth arrest at the G1/S and G2/M checkpoints is known to occur (see section 1.1.6 on page 45), and cells that become arrested at these points will not affect Ki67 protein levels (Lundblad et al., 1991).

It is worth noting, however, that a non dividing cell, i.e. a cell that is growth arrested, is not necessarily senescent. A transiently growth arrested (quiescent) cell in G0 may re-enter the cell cycle if it is stimulated to do so, and a terminally differentiated cell will also not divide but is not considered senescent, which is why it is important to also consider other aspects of the senescent phenotype when trying to ascertain if a cell is senescent or not.

1.2.2 Morphological changes

It is often reported that cells induced to senescence by strand breaks or cellular stress have an enlarged size and flattened morphology (Angello et al., 1989), and in some cases become multi-nucleated (Kuilman et al., 2010), although these features appear to be cell type specific. The most popular assay for senescence, the senescence associated beta galactosidase (SAβ-gal) assay, capitalises on another morphological change common in senescence; increased lysosome mass (Kurz et al., 2000). Although originally thought to be a form of galactosidase specific to senescence, it has been confirmed that SAβ-gal and lysosomal β-gal are the same protein (Lee et al., 2006). The activity of SAβ-gal is easy to detect by addition of colourless 5-bromo-4-chloro-3-indolyl-β-D-galactopyranoside (X-Gal), which is hydrolysed by SAβ-gal to yield galactose and 5-bromo-4-chloro-3-hydroxyindole. The latter then spontaneously forms a dimer that is oxidized to the insoluble blue precipitate 5,5'-dibromo-4,4'-dichloro-indigo, which can be detected visually (Debacq-Chainiaux et al., 2009). When the assay is performed in atmospheric ppCO_2 the external environment of the cells is around pH 6.0, well above the optimal working pH for the β-gal enzyme (pH 4.6) Under these conditions in growing cells there is no detectable activity however because senescent cells have a large, acidic lysosome compartment the enzyme activity in senescent cells is still enough to create a characteristic blue crescent in the cytoplasm (Yang and Hu, 2005). An image of an SAβ-gal positive fibroblast with a large flat morphology, which is most likely senescent, next to some smaller SAβ-gal negative fibroblasts can be seen in figure 1.5. As increased lysosomal size is not a feature only seen in senescence (it is also a feature of autophagy, for example) the assay is prone to giving false positives. Despite this limitation it is still a useful marker when performed carefully and in conjunction with other markers.

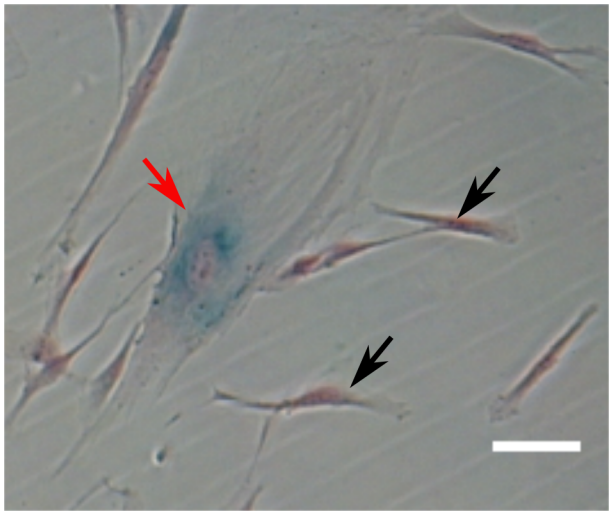

Figure 1.5: **Senescence associated beta galactosidase (SAβ-gal) staining of IMR90 fibroblast cells**. Black arrows point to SAβ-gal negative cells while the red arrow points to an SAβ-gal positive cell. Scale bar represents 25µm.

1.2.3 The Senescence Associated Secretory Phenotype (SASP)

Another aspect of the senescence phenotype, and one which is undoubtedly important in any functions senescent cells may have *in vivo,* is the secretome. It has been recognised for some time that senescent cells have an altered secretome (Rinehart and Torti, 1997), which has become known as the senescence associated secretory phenotype (SASP), although it is yet to be fully characterised. So far a number of cytokines, chemokines, growth factors, shed cell surface receptors and survival factors have been identified through a combination of mRNA screens and ELISA assays (Kuilman et al., 2008; Acosta et al., 2008; Downward et al., 2008). These molecules are are secreted from senescent human cells *in vitro* as part of a cell strain specific secretory phenotype which can also vary depending on senescence induction mechanism. A summary of some of the factors identified as elevated in senescence can be seen in table 1.1.

The variability in the production of these factors is probably due to the fact that many if not all of them are related to an event or process that is intertwined with the processes that underpin senescence, but not directly senescence itself because although the knock down or over-expression of the factor may inhibit or induce senescence in the

given model, there isn't one signature SASP that holds true for all cell types and all induction modes. In support of this idea, Jean-Phillipe Coppé and colleagues demonstrated that ectopic expression of $p16^{INK4A}$ and $p21^{WAF1}$ caused a stable growth arrest but not a detectable SASP, and in addition those growth arrested cells did not have any paracrine effect on epithelial cells (Coppé et al., 2011). Furthermore, the only known function of $p16^{INK4A}$ is to cause cell cycle arrest, whereas other aspects of the senescence induction process, such as DDR or oncogene expression have effects in other areas of the cell biology.

Group	SASP factor name
Interleukins (IL)	IL6; IL7; IL1α and β
Chemokines (CXCL, CCL)	IL8 growth-related oncogene (GRO)-a, b, g; membrane co-factor protein (MPC)-2 and 4; MIP-1α and 3α; HCC-4; Eotaxin-3
Other inflammatory factors	Granulocyte-macrophage colony-stimulating factor (GM-CSE); macrophage migration inhibitory factor (MIF)
Growth factors/ growth regulators	Amphiregulin; epiregulin; heregulin; endothelial growth factor (EGF); basic fibroblast growth factor (bFGF); hepatocyte growth factor (HGF); keratinocyte growth factor (KGF); vascular endothelial growth factor (VEGF); Angiogenin; stem cell factor (SCF); stromal cell derived factor (SDF)1; placental growth factor (PIGF); insulin-like growth factor (IGFBP)-2, 3, 4, 6 and 7
Proteases and regulators	Matrix metalloproteinase (MMP)-1, 3, 10, 12, 13 and 14; tissue inhibitor of metalloproteinases (TIMP)2; plasminogen activator inhibitor (PAI)-1 and 2; Cathepsin B
Shed receptors/ ligands	Intercellular adhesion molecule (ICAM)-1 and 3; osteoprotegerin (OPG); Soluble tumour necrosis factor receptor I (sTNFRI); tumour necrosis factor apoptosis-inducing ligand (TRAIL)-R3; Fas; urokinase-type plasminogen activator receptor (uPAR); EGF-receptor (EGF-R)
Non-protein soluble factors	Prostaglandin E2 (PGE2); nitric oxide (NO)
Insoluble factors	Fibronectin

Table 1.1: **A summary of SASP factors,** shown to be elevated in the secretome of senescent cells. Adapted from Young and Narita, 2009. This list is not exhaustive and factors listed here may not be present in some instances of senescence depending on the cell type and the mode of senescence induction.

1.2.3.1 Regulation of the SASP

Feedback loops and transcriptional regulation of the SASP

The SASP appears to be regulated by a combination of feedback loops and transcriptional modulation. Interleukin 1 (IL1) and TGF-β, which are released by some senes-

cent cells as part of the SASP, are capable of paracrine senescence transfer via oxidative stress signalling as well as forming a positive feedback loop and re-enforcing senescence in the original senescent cell (Hubackova et al., 2012; Acosta et al., 2013; Hassona et al., 2013). Perhaps the presence of such factors in the serum of aged chickens were responsible for the effects seen on young cells by Carrel in 1921 (Carrel, 1921). Furthermore during OIS the transcription factors NFkB and CCAAT/enhancer-binding protein beta (C/EBPβ) are known to regulate inflammatory molecules such as interleukin 6 (IL6) via interactions with chromatin, but IL6 is also itself important for maintaining senescence in the OIS model tested (Kuilman et al., 2008). Similarly, it has been observed that OIS fibroblasts secreting interleukin 8 (IL8, also regulated by NFkB and C/EBPβ), a chemokine that binds to CXCR2 (a chemokine receptor) also up-regulate the expression of CXCR2 to form a feedback loop that reinforces senescence (Acosta et al., 2008). Further evidence of the importance of transcriptional modulation in regulation of the SASP is the observation that histone deacetylase inhibitors (HDACIs) are capable of modulating some components of the the SASP, such as osteopontin. Interestingly, and in support of the idea that the SASP is related to the processes associated with senescence rather than the stable growth arrest itself, this effect was shown to be independent of senescence (Pazolli et al., 2012). The ability to modulate the SASP using HDACIs was also found to be independent of the DDR, although most other factors have been shown to be regulated by some aspect of the DDR (Coppé et al., 2010b).

Regulation of the SASP by p53 Interestingly, although p53 is important for the induction of senescence in most cases, it was discovered by knocking down p53 prior to induction of senescence by either DNA damage (caused by X-ray), proliferative exhaustion or RAS expression, that p53 actually acts to restrain the SASP both in terms of the amount of SASP factors produced and how quickly they are produced, although knock-down of p53 in cells that were already senescent (a state maintained by $p16^{INK4A}$) did not affect the SASP (Downward et al., 2008). This could suggest that a major component of the SASP is driven by the senescence inducing stimulus, such as DDR or

MAP kinase signalling which p53 works to minimise, rather than the ongoing cell cycle arrest itself.

Regulation of the SASP by the DDR

It is acknowledged that for most SASP components, a sustained DDR response is necessary, as it has been shown that ablation of DNA damage response factor ATM results in a reduced secretion of the SASP components IL6 and IL8 in both DDR induced senescence and OIS (Rodier et al., 2009). This effect may be at least partially explained by the observation already mentioned previously; that IL6 and IL8 are regulated by NFkB signalling, which is activated by ATM in response to the DDR (McCool and Miyamoto, 2012). Furthermore, recently a key molecule linking the DDR to the SASP has been identified; the methyl-transferase MLL1 has epigenetic control over pro-proliferative genes that enhance the DDR, and inhibition of MLL1 leads to a repression of the SASP without affecting the stable growth arrest of the cell (Capell et al., 2016).

Metabolic enzymes can regulate the SASP

There is also an accumulating body of evidence that the SASP can be regulated by metabolic enzymes. The protein kinase mechanistic target of rapamycin (mTOR) responds to a wide range of signals, including nutrient levels, by facilitating protein and lipid synthesis (reviewed in Laplante and Sabatini, 2012) and it has been shown that inhibition of mTOR in OIS fibroblasts also represses the SASP, by reducing the transcription of SASP factors again without affecting the senescent growth arrest (Herranz et al., 2015). Furthermore, the induction of several SASP proteins are reportedly mediated by the mitochondrial enzyme carnitine palmitoyl transferase 1 in OIS, but not following PEsen (Quijano et al., 2012). The role of mitochondria in senescence and the SASP has been the subject of several studies (reviewed in (Correia-Melo and Passos, 2015)) and recently it has been demonstrated that deleting mitochondria from senescent cells ablates the inflammatory aspects of the SASP (Correia-Melo et al., 2016), confirm-

ing that key elements of the SASP require mitochondria, although specific mechanisms have not been thoroughly investigated.

Importantly, metabolic enzymes have been reported to affect not only the SASP but also the senescence growth arrest itself. For example, forced expression of the malic enzyme ME2 is sufficient to delay senescence in human fibroblasts (Jiang et al., 2013), and 5' adenosine mono-phosphate (AMP)- activated protein kinase (AMPK) can induce premature senescence **(Wang et al., 2003)**. AMPK is an energy sensor activated by an elevated AMP: adenosine tri-phosphate (ATP) ratio, and usually cooperates with SIRT1 to promote autophagy and survival, both features that are usually associated with inhibition of senescence (Salminen and Kaarniranta, 2012), however it appears that following chronic signalling AMPK promotes senescence via p53 activation, by phosphorylating p53 on serine 15 (Jones et al., 2005) and also by inhibiting the cytoplasmic export of the RNA binding protein HuR, preventing it from regulating the expression of proliferative genes (Wang et al., 2001, 2003).

1.2.4 Senescent cells have an altered metabolism

Given that some metabolic enzymes can regulate aspects of the SASP and even senescence itself, it comes as no surprise that another feature of senescent cells is altered metabolism. Cellular metabolic networks are highly complex, but here we will aim to highlight some examples of alterations that are important in senescence.

1.2.4.1 Carbohydrate metabolism

Under normoxic conditions, the most efficient way to produce energy (stored in ATP) from the carbohydrate glucose is via oxidative phosphorylation which occurs in the mitochondria. This process requires glucose to be broken down to pyruvate in the cytoplasm, a process known as glycolysis, and for the pyruvate to be converted to acetyl-CoA by the pyruvate dehydrogenase complex in the mitochondria. Acetyl CoA then enters the mitochondrial tri-carboxylic acid (TCA) cycle (also known as the citric

acid cycle, or the Krebs cycle after Sir Hans Krebs, the biochemist who identified the TCA cycle at University of Sheffield in 1937, for which he shared the 1953 Nobel Prize for physiology) where it is further broken down in 9 more enzymatic steps to oxaloacetate, producing reduced nicotinamide adenine dinucleotide (NADH) (see figure 1.6). NADH is an electron donor in the electron transport chain (ETC), where 30-36 ATP molecules are produced per glucose molecule via oxidative phosphorylation (OXPHOS), in the inter-membrane space of mitochondria.

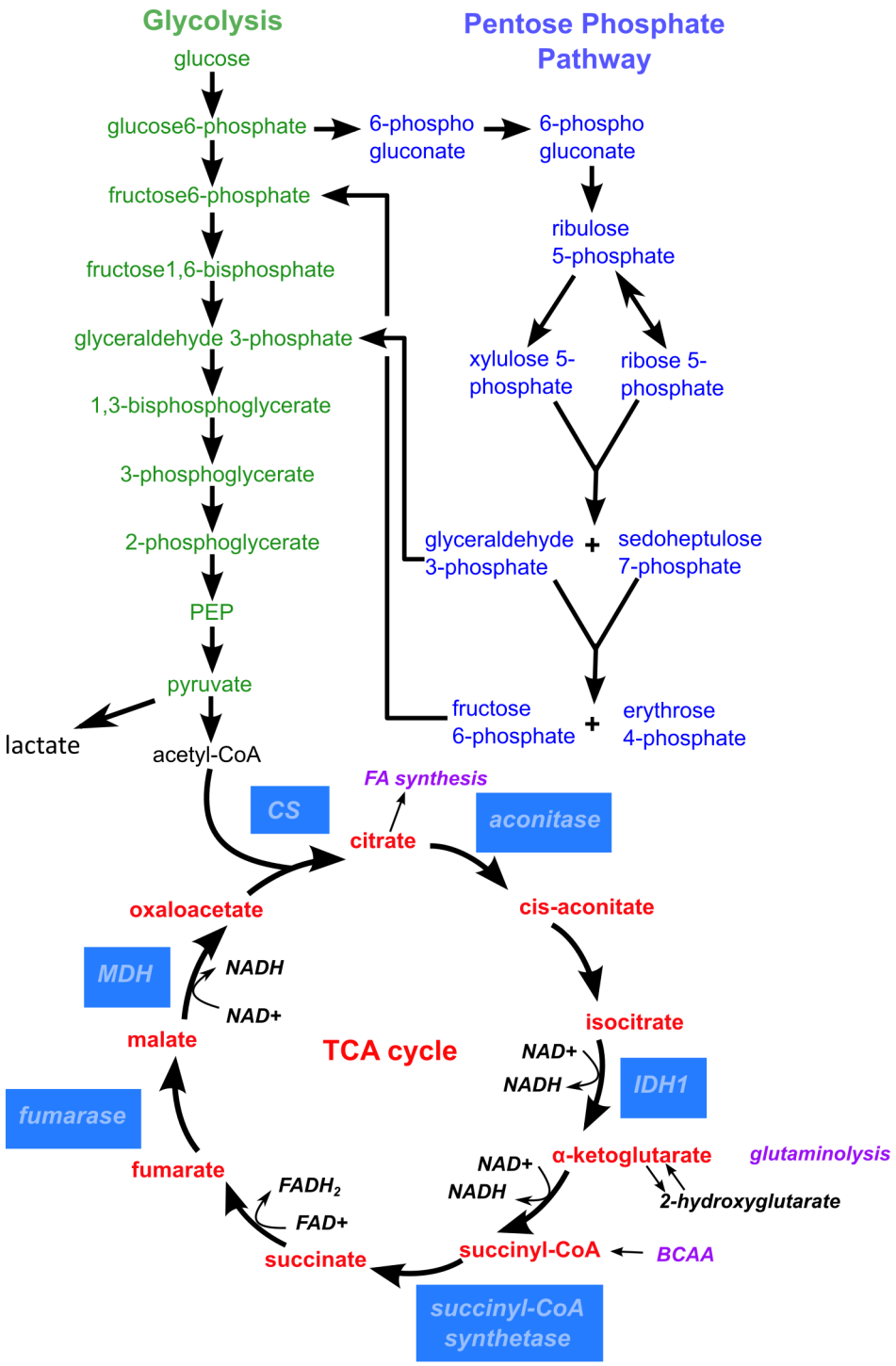

Figure 1.6: **Carbohydrate metabolism pathways glycolysis, the tricarboxylic acid (TCA) cycle and the pentose phosphate pathway (PPP).** The blue boxes represent some key enzymes in the TCA cycle CS: citrate synthase, IDH1: isocitrate dehydrogenase 1, MDH: malate dehydrogenase. BCAA: branched chain amino acids. FA: fatty acid. FAD(H_2/+): flavin adenine dinucleotide (reduced/oxidised). NAD(H/+): nicotinamide adenine dinucleotide (reduced/oxidised).

OXPHOS relies on oxygen as an electron acceptor, so only occurs when oxygen is

available and in functioning mitochondria. In the absence of one or both of these, cells rely mainly on glycolysis, which produces two ATP per glucose molecule, but does not require oxygen or functioning mitochondria. The use of glycolysis rather than OXPHOS under normoxic conditions is a common feature of cancer cells and has been named the Warburg effect, after Otto Warburg, the scientist who discovered the 'oxidative glycolytic' phenotype, characterised by excessive lactate production (Warburg et al., 1924). It has been hypothesised that this metabolic reprogramming confers a survival advantage on the cancer cells which will eventually reside in a hypoxic environment if the tumour outgrows vascularisation. The acidic extracellular environment produced due to the excess lactic acid secretion from glycolytic cells also favours survival of the cancer cells over normal cells, and may promote invasion, as well as preventing apoptosis upon detachment (anoikis) thus facilitating metastasis (Kato et al., 2013). The Warburg effect has also been reported in senescence (Dörr et al., 2013), and several other groups have provided data that supports the theory that senescent cells are glycolytic (Goldstein et al., 1982; James et al., 2015).

However, as would be expected from such a complex state as senescence, there is clearly more to the altered metabolism than the Warburg effect. Jan Dörr and colleagues observed that the Warburg effect they saw in their cells was regulated via the M1 isoform of pyruvate kinase (PKM1), which promotes the breakdown of pyruvate in the TCA cycle, so alongside the Warburg effect they also reported enhanced OXPHOS. The authors named this phenotype 'hyper-metabolism' (Dörr et al., 2013). A similar result was reported by Werner Zwerschke and co-workers, who measured the rate of glucose consumption and lactate production in senescent fibroblasts compared to proliferating fibroblasts and found that while the relationship between glucose consumption and lactate production was linear in proliferating cells, with 90% of the consumed glucose being converted to lactate, the senescent cells were converting a lot less to lactate, suggesting the carbon from glucose is shuttled elsewhere during senescence. This result was unexpected as the authors had demonstrated that there was an up-regulation in

glycolytic protein expression and also much higher catalytic activity of the M2 isoform of pyruvate kinase (PKM2) which is usually associated with cell proliferation (Zwerschke et al., 2003).

To further add to the complexity, a paradox exists between the observed over expression of glycolytic enzymes and the senescent growth arrest. Over-expression of the glycolytic enzymes phosphoglycerate mutase (PGM) and glucose phosphate isomerase (GPI) has been shown by Kondoh et al to facilitate bypass of senescence, while inhibition of those enzymes induced senescence. The authors drew the conclusion that cells which were able to switch to glycolytic metabolism were more protected from oxidative damage, due to a reduction in use of the oxidative mitochondrial pathways that are known to produce large amount of ROS. In the absence of glycolysis the extra ROS generation was enough to cause senescence (Kondoh et al., 2005).

It is possible that in certain contexts, for example depending on the levels of ROS, that there is both repression and promotion of glycolysis in senescence. Supporting the possibility of a heterogeneous, or perhaps temporal, metabolic phenotype in senescence is the fact that the interactions of senescence effector proteins with glycolytic enzymes are complex and sometimes contradictory. This is especially true for p53, which as well as being an important mediator of senescence, also has well established roles in energy homeostasis and response to nutrient deficiency (reviewed in Vousden and Ryan, 2009). In general p53 acts to inhibit glycolysis in favour of oxidative phosphorylation, for example by inducing expression of TP53 induced glycolysis and apoptosis regulator (TIGAR), a phosphatase that degrades fructose-2,6-bisphosphate, preventing activation of phosphofructokinase-1. Reduced activation of this glycolytic enzyme results in a reduced glycolytic metabolism (Bensaad et al., 2006; Li and Jogl, 2008). Additional anti-glycolytic activities of p53 include reduction of glucose intake via down-regulation of glucose transporters GLUT1 and GLUT4 (Schwartzenberg-Bar-Yoseph et al., 2004) and the suppression of pyruvate dehydrogenase kinase 2 (PDK2), therefore preventing inhibition of the pyruvate dehydrogenase complex and facilitating the metabolism of

pyruvate to acetyl CoA rather than lactate (Contractor and Harris, 2011). Although this action does not directly inhibit glycolysis, it reduces the amount of NAD+ immediately available for more glycolysis. PGM is also indirectly negatively regulated by p53 via its downstream effector MDM2 (Mikawa et al., 2014). It may also be the case that promotion of glycolysis by p53 is context specific, for example when oxidative metabolism pathways are compromised. Buzzai et al observed that treatment of $p53^{-/-}$ cells with metformin, which inhibits oxidative mitochondrial metabolism via the electron transport chain, caused cell death following nutrient deprivation but the same treatment in $p53^{+/+}$ cells provoked a switch to glycolysis and cell survival, suggesting p53 is capable of activating glycolysis in the event of compromised mitochondrial metabolism (Buzzai et al., 2007). p53 is also able to down-regulate the malic enzymes ME1 and ME2, which are TCA cycle associated enzymes important for production of the reduced form of nicotinamide adenine dinucleotide phosphate (NADPH), lipogenesis and glutamine metabolism. Repression of these enzymes has been shown to enhance the senescence growth arrest mediated by p53 (Jiang et al., 2013).

There are also conflicting reports on the functionality of the TCA and OXPHOS in senescent cells. Senescence, especially OIS, is associated with increased ROS, as evidenced by addition of hydrogen peroxide causing an increase in expression of senescence effectors and inducing senescence, and the increase in ROS when senescence effector proteins are expressed (Lee et al., 1999). ROS can cause oxidation of lipids in the mitochondrial membrane, which reduces the capacity for the TCA cycle and OXPHOS to occur. Intrinsically there is always some electron leakage from the mitochondrial complex I and III during OXPHOS; these electrons are readily taken by oxygen to form a superoxide ion (one form of ROS), even when mitochondria are healthy (Murphy, 2009). This leads to the hypothesis that glycolytic metabolism, or at least mild uncoupling of mitochondrial respiration, might be favoured if the cell is under stress and unable to cope with more ROS from OXPHOS, even if the TCA cycle and OXPHOS are capable of normal function. ROS is also known to inactivate glyceraldehyde-3-phosphate

dehydrogenase (GAPDH), the 6th step of glycolysis. A reduction in the activity of this enzyme results in a build-up of glyceraldehyde-3-phosphate, acting as a metabolic switch to utilise the pentose phosphate pathway (PPP). This forms part of the cell's antioxidant response, as the first three reactions in the PPP generate NADPH; a reducing agent. Inactivation GAPDH also inhibits the downstream reactions of glycolysis (reviewed in Metallo and VanderHeiden, 2013).

To try and get a better view of the whole picture of what is happening to the metabolic pathways in senescence, some groups are using metabolic screening techniques. Toren Finkel and co-workers used a multi-platform approach to perform an unbiased metabolic screen of OIS and PEsen fibroblasts. They were able to identify 292 compounds in the cell pellets of IMR90 fibroblasts induced to senescence either by over expression of Ras, or through proliferative exhaustion, including metabolites found in a wide array of biochemical pathways, mainly amino acids, carbohydrates, lipids and nucleotides. There were significant differences between the profile of the PEsen cells and the profile of the OIS cells, which cannot be attributed to bias in measurement or tissue specific differences (which might have explained some of the variability on the other more targeted studies) as the same procedures were applied to all groups and the cells were all IMR90. It was observed for example that in OIS the concentration of free fatty acids was 5-10 fold higher than in the PEsen cells, and that there were higher rates of fatty acid oxidation (Quijano et al., 2012). These findings further demonstrate the difficulty in teasing out the effects specific to the senescent growth arrest from the other effects of the cellular stress causing the senescent growth arrest. Compounding this problem, Quijano and colleagues had no way of determining which metabolic changes were associated with growth arrest that could be transient compared to the irreversible growth arrest associated with senescence as they had no transiently growth arrested cell control group.

The senescence phenotype: summary

The phenotype of senescent cells is variable depending on tissue type, senescence induction mechanism and external environment, so in order to identify senescent cells it is necessary to look for more than one characteristic. The most common features used for identification of senescent cells are a failure to replicate when stimulated, SAβ-gal activity, a lack of proliferation markers and the presence of a known senescence inducer (such as oncogene expression, telomere attrition, or irreparable DNA double strand breaks (IrrDSB)) as well as cell cycle inhibitors such as $p16^{INK4A}$. Despite the lack of proliferation senescent cells remain highly metabolically active (Quijano et al., 2012) and studying this metabolic activity gives insight into the molecular process underlying the senescence phenotype, although it is difficult to separate the features related to the senescent growth arrest from features resulting from the senescence inducing stress itself.

Another major feature of senescent cells, although not well understood, is the SASP. Furthermore, several factors included in the SASP are known to be regulated by metabolic enzymes, possibly providing another link between metabolism and senescence associated pathologies, as the collection of secreted collection of inflammatory mediators and other proteins that make up the SASP undoubtedly provide the link between senescent cells and their role in *vivo*.

1.3 Senescence *in vivo*

Initially suspected of being an event that only occurred in cell culture due to sub-optimal conditions, there is now mounting evidence that cellular senescence has important functions *in vivo*. However, there may also be negative effects of senescence.

1.3.1 Senescence during development

In 2013 it was reported that senescent cells had been found at certain stages in the development of human embryos. Muñoz-Espin and colleagues showed that distinct populations of cells within the mesonephric tubules (which act like a kidney for the embryo while the kidneys develop, once the kidney structure is complete the mesonephric tubes disappear) and endolymphatic sac (which functions to help with hearing and maintain balance by filtering and collecting the endolymph of the cochlear and vestibular canals in the ear), are growth arrested before being cleared by the immune system (Muñoz-Espín et al., 2013). The cells were identified as senescent because they were positive for SAβ-gal and negative for the proliferation marker Ki67, although the cells were negative for γH2AX, a DDR protein, so the authors concluded that DNA damage was not a mechanism in the senescence induction, the heterochromatin markers tri-methylated lysine 9 histone H3 (H3K9me3) and the heterochromatin protein 1 gamma (HP1γ) were detected and these are both associated with SAHFs (Aird and Zhang, 2013). Further investigation using murine embryos found increased expression of $p21^{WAF1}$, the cell cycle inhibitor, that was regulated by TGF-β, Similar to Mothers Against Decapentaplegic 2 (SMAD 2) and the PI3K/Forkhead Box O (FOXO) pathway, but not $p16^{INK4A}$ or p53. This mechanism has not been observed *in vitro* however another group also observed cells in what appeared to be a senescent state regulated by $p21^{WAF1}$ during embryonic development in chicks and mice, and suggested that senescence evolved as a regulatory and instructive mechanism in development that can also be activated under pathological conditions later in life (Storer et al., 2013).

1.3.2 Senescence in wound healing

The removal of senescent cells by macrophages observed in developing embryos (Muñoz-Espín et al., 2013) is also known to occur in other *in vivo* settings such as wound healing; a function carried out by fibroblasts. As the main component of connective tissue, fibroblasts play a critical role in extracellular matrix (ECM) production and homeostasis,

which is vital for support and repair in most tissues and organs throughout the human body (reviewed in McAnulty, 2007). The spindle shaped cells, characterised by their expression of vimentin (the most abundant intermediate filament protein found in fibroblasts), are of mesenchymal origin and form a variety of 'subtypes', from contractile myofibroblasts in cardiac muscle to non-contractile dermal fibroblasts in skin. Fibroblasts continuously synthesise ECM proteins such as procollagens, at a rate of 3.5 million procollagen molecules/cell/day (McAnulty et al., 1991) however between 10 and 90% of these are degraded before leaving the cell by cathepsins D, B and L. Regulation of this process is important in adaptive collagen production during wound healing – and is achieved via production of MMPs as well as MMP inhibitors (TIMPs), which regulate degradation of the ECM in response to cell-cell and cell-matrix interactions (Seltzer et al., 1994). In the event of chronic wound healing, if excessive ECM is produced by fibroblasts then fibrosis can occur, resulting in deleterious tissue scarring which can lead to organ failure such as seen in liver fibrosis or pulmonary disease. There is evidence to suggest that in order to prevent fibrosis in the later stages of normal wound healing, fibroblasts are driven to a non-proliferative state by the matricellular protein CCN1 via integrin signalling, resulting in growth arrest by $p16^{INK4A}$ (Jun and Lau, 2010). Senescent cells ameliorate fibrosis by secreting MMPs (Pitiyage et al., 2011) which break down the excess ECM before being cleared by the immune system (Krizhanovsky et al., 2008) in what is termed 'immuno-surveilance'. Immuno-surveilance is carried out by different immune cells depending on the context of the senescence (reviewed in Hoenicke and Zender, 2012), probably because of different chemokine and cytokine messages being produced as part of the senescence induction and tissue specific SASP. Furthermore, the observation that senescent fibroblasts and endothelial cells secrete platelet derived growth factor -AA at wound sites, which promotes differentiation of myofibroblasts and therefore accelerates wound closure provides another example of the *in vivo* biological functions of senescent cells.

1.3.3 Senescence and cancer

1.3.3.1 Senescence as a tumour suppressor mechanism

In vitro experiments where expression of oncogenes *RAS* and *RAF* (sometimes to supra-physiological levels) were observed to induce senescence, as already described in section 1.1.5.1, leading to the hypothesis that senescence could be a tumour suppression mechanism *in vivo.* The first evidence in support of this hypothesis came in 2005 when it was reported that Eμ-N-Ras transgenic mice (expressing constituently active Ras in the haematopoietic compartment) that were also $p53^{+/-}$or Suv39h (Suppressor of variegation 3-9 homolog 1; a chromatin remodelling enzyme) negative succumbed to invasive T-cell lymphoma while Eμ-N-Ras mice with functioning p53 or Suv39h eventually succumbed to non-lymphoid neoplasia much later. It was observed that the primary lymphocyte proliferation, and therefore lymphoma formation, was directly stalled by a Suv39h1-dependent senescent growth arrest (Braig et al., 2005). Further convincing evidence came from the discovery that congenital human melanocytic nevi, which are benign tumours that rarely progress to melanoma, contain activating murine sarcoma viral (V-Raf) oncogene homolog B1 (BRAF) or neuroblastoma V-Ras oncogene homolog (NRAS) mutations and concomitantly displayed elevated levels of the senescence effector protein $p16^{INK4A}$ (Michaloglou et al., 2005). Many subsequent examples of senescence playing a role in preventing tumour formation in the presence of oncogene expression or loss of a tumour suppressor protein have been documented (see reviews Salama et al., 2014; Bennett, 2016), however it has been suggested that OIS is dependent not only the oncogene expression but also the level of other molecules such as $p16^{INK4A}$, as freshly isolated neonatal fibroblasts do not senesce in response to *RAS* (Benanti and Galloway, 2004).

As with wound healing, clearance of senescent cells appears to be an important part of the response to the damage/pathological condition that induced the cells to become senescent in the first place. Failure of the immuno-surveilance process can lead to deleterious effects of senescence, and reasons for this failure are not fully understood;

although a declining immune system with age would seem to be a reasonable explanation in older individuals (Wang et al., 2011a).

1.3.3.2 Senescent cells as a driver of neoplastic transformation

A permanent growth arrest in response to oncogene expression or loss of a tumour suppressor protein can prevent uncontrolled neoplastic growth in the offending cell but there is evidence that subsequent changes in the senescent cell secretome may promote neoplastic transformation and cancer growth in neighbouring cells. Krtolica and colleagues reported that senescent fibroblasts promoted growth of neoplastic epithelial cells in culture, and moreover showed that when immortal human keratinocyte cell line HaCaT cells were injected into severe combined immunodeficiency (SCID) mice with senescent fibroblasts formed tumours more frequently and that were larger than when HaCaT cells were injected with pre-senescent fibroblasts (and HaCaT cells injected without any fibroblasts formed no tumours) (Krtolica et al., 2001). Subsequent studies have had similar results (Liu and Hornsby, 2007; Coppé et al., 2010b) and it has also been suggested that energy metabolites that have been observed to be secreted by senescent cells, such as lactate and 3-hydroxybutyrate (3OHB), can participate in the SASP by providing energy to developing cancer cells (Bonuccelli et al., 2010; Capparelli et al., 2012) and there is evidence that direct addition of these molecules can increase mitochondrial activity in some cancer cell lines (Martinez-Outschoorn et al., 2010).

It seems paradoxical that having undergone what appears to clearly be a tumour suppressor mechanism the cells would then promote tumourigenesis in other cells. Some have proposed it to be an example of antagonistic pleiotropy; a biological process that can be both beneficial and harmful to the organism depending on that organism's age (Williams, 1957), because once an organism has reproduced any process that affects them negatively later in life does not get de-selected for by natural selection. In the case of senescence and cancer, it is possible that in young organisms that harbour few senescent and pre-malignant cells, the factors secreted by the senescent cells are not

present in high enough concentration to have an effect the neighbouring cells, or cells in young organisms respond differently to the signals, possibly because they harbour less damage than cells in older organisms. Indeed, age is the biggest risk factor for cancer (Fransen et al., 2013).

1.3.4 Senescence and ageing

Biological or organismal ageing is often defined by the functional capacity of organs (Chang and Harley, 1995; Melk et al., 2000), which declines with both chronological age and life-shortening conditions such as progeria (Burtner and Kennedy, 2010). This decline in organ function is also sometimes referred to as 'functional senescence' (Grotewiel et al., 2005) and occurs at different rates in each individual, such that a person's chronological age might not exactly correspond with their biological age (Baker and Sprott, 1988; Belsky et al., 2015). Functional senescence may well be driven by cellular senescence, as it is accepted that the number of senescent cells increases with age in a variety of mammalian tissues (Dimri et al., 1995; Paradis et al., 2001; Jeyapalan et al., 2007). It is not known whether this rise is caused by increased generation, decreased elimination, or both. Whatever the reason for their accumulation, the age-related increase in senescent cells occurs in mitotically competent tissues, which are those that give rise to cancer and ageing related disorders (Herbig et al., 2006; Jeyapalan et al., 2007) and proof that the presence of senescent cells is not just correlated to these pathologies but is causal is mounting. For example Baker and colleagues used a pro-geroid mouse model to show that elimination of the accumulated senescent cells prevents the onset of signs of organismal ageing: cataracts, sarcopenia and loss of subcutaneous fat, which are three major ageing phenotypes (Baker et al., 2011), and more recently using the same model Baker and colleagues showed that naturally occurring $p16^{INK4A}$ cells are involved in age related degeneration of multiple organs including heart and kidney (Baker et al., 2016). Furthermore clearance of senescent cells using a senolytic drug can also rejuvenate haematopoietic stem cells (Chang et al., 2015).

The molecular mechanisms behind the effect of cellular senescence on functional senescence and biological ageing are not yet well understood, although there are some examples of experimental evidence which shed a little light on the subject, such as work linking the aged appearance of wrinkled older skin to the matrix degrading factors secreted by senescent dermal fibroblasts (Hornebeck, 2003). Also, it has recently been confirmed using conplastic mice that mitochondrial DNA (mtDNA) affects health span and longevity by influencing mitochondrial proteostasis, ROS generation, insulin signalling, obesity, telomere shortening and mitochondrial dysfunction (Latorre-Pellicer et al., 2016). As already discussed in section 1.2.4 on page 56, mitochondria play an important role in senescence and the SASP and so may prove to be a link between cellular senescence and organismal ageing.

There is also an interest in astrocyte senescence in the context of age related neurodegenerative diseases like Parkinson's and Alzheimer's. It has been recorded that astrocytes cultured from the brains of aged rats stain positively for SAβ-gal and are less able to maintain the survival of co-cultured neurons, suggesting an age related decline in neuroprotective activity may be linked to senescence (Pertusa et al., 2007). This is supported by subsequent studies of autopsied human brain tissue; both $p16^{INK4A}$ and the SASP factor MMP3 increase significantly with age and are even higher in affected cortical brain tissues from patients who had suffered with Alzheimer's disease, relative to age-matched controls (Bhat et al., 2012). In autopsied brains of sufferers of Parkinson's disease an increase in the number of astrocytes with elevated $p16^{INK4A}$ expression and γH2AX in the substantia nigra pars compacta (the region of the brain that specifically degenerates in Parkinson's disease), compared to age-matched controls has also been observed (Chinta et al., 2015). Astrocytes play an extremely important role in synaptic transmission and information processing by neural circuits as well as regulating blood flow and metabolism in neurons and synapses (reviewed in Benarroch, 2005), so changes to their metabolism and secretome, such as is associated with senescent cells would be expected to cause disruption to surrounding cells.

Although experimental evidence for the involvement of senescent cells in organismal ageing *in vivo* is accumulating, there are many challenges to getting conclusive answers to questions on why senescent cells are accumulating and how they are interacting with surrounding cells.

1.3.5 The challenges of studying senescence *in vivo*

Although there are many *in vivo* models of *functional* senescence, including the nematode worm Caenorhabditis elegans, budding yeast (Saccharomyces cerevisiae), the fruit fly Drosophila melanogaster (reviewed in Gems and Partridge, 2013), and mouse models such as the Senescence Accelerated Mouse (SAM), of which there are 12 strains exhibiting accelerated onset of different aspects of ageing such as loss of bone density, decline in cognitive function and hair loss (Takeda et al., 1997); the challenges faced when studying *cellular* senescence *in vivo* are considerable. Firstly the lack of a single defined phenotype and incomplete understanding of the regulation of the multiple senescence phenotypes make it difficult to identify senescent cells with certainty. Because multiple markers are required, including staining for SAβ-gal activity it is not possible to monitor an individual organism's levels of senescent cells repeatedly over multiple time points. The pro-geroid model used by Baker *et al,* mentioned previously, which uses a transgene called INK-ATTAC for inducible elimination of cells expressing $p16^{INK4A}$cells (Baker et al., 2011) goes some way to address this problem, in the case of $p16^{INK4A}$ dependent senescence at least, because measurements can be taken in the same animal before and after removal of $p16^{INK4A}$ positive senescent cells.

While these model systems are incredibly useful for deducing genetic and molecular pathways involved in ageing and senescence, there are obvious differences between the model organisms and humans which could limit our understanding of human ageing and senescence. For example mice have a much shorter lifespan, much longer telomeres, and metabolic profiling has shown them to have a very different metabolic phenotype to humans (Tomás-Loba et al., 2013). With this in mind, it would be helpful to have a

biomarker of cellular senescence that could be measured non-invasively, so that multiple measurements could be made in humans over a time period to assess links between cellular senescence and phenomena such as functional senescence.

1.4 Biomarkers

Technically, a biomarker is defined as 'a characteristic that is objectively measured and evaluated as an indicator of normal biological processes, pathogenic processes, or pharmacological responses to a therapeutic intervention' (Group, 2001). In order to measure dynamic effects of treatments or time, it is important to measure a feature that is able to respond to these changes as quickly as possible, and increasingly more studies are making use of the metabolome in order to do this (James and Parkinson, 2015). The metabolome is the collection of small molecules that are interacting as reactants, intermediates and waste products of the countless biochemical reactions that are constantly occurring to keep cellular processes going, such as the break down and synthesis of carbohydrates, lipids and nucleotides. As we have already seen, all of these processes are known to be altered in senescence. The study of the metabolome is known as metabolomics.

1.4.1 Capturing the metabolome

Metabolomics as we know it today relies on the use of nuclear magnetic resonance (NMR) spectrometry and mass spectrometry (MS).

NMR spectrometry takes advantage of the fact that the nucleus of all atoms is charged and has a "spin" (I), a specific form of angular momentum. The value of I depends on the atom and some atoms, such as ^{1}H and ^{13}C, have an I value of 1/2. When a nucleus with I=1/2 is put into a magnetic field, it will align itself with the magnetic field in a low energy state but can be forced to align itself against the magnetc field if it absorbs enough energy. By pulsing radio waves through the sample in a magnetic

field, the low energy nuclei flip to align against the field, and their relaxation back to the low energy state can be measured as emitted radio waves. Because in a molecule the atoms are also subject to the small magnetic effects of neighbouring electrons and atoms as well as the magnetic field in the spectrometer, the nuclei will absorb energy at slightly different frequencies than they would if it were just a single atom; this is known as the chemical shift and is reflected in the radio waves detected during the relaxation and can be plotted as intensity versus frequency. The resulting spectra vary depending on what the nuclei with I=1/2 are surrounded by; if a nucleus is shielded by many electrons then it will require a higher energy frequency to elevate it to a high energy state, and if it is attached to a highly electronegative element it will be less shielded and require less energy. By studying the chemical shifts it is possible to determine the structure of a molecule and therefore identify it. For example when using 1H NMR, each hydrogen nucleus will produce a peak in the spectrum at a slightly different and frequency depending on what the hydrogen is bound to in the molecule, and the pattern of peaks produced will be unique for each molecule. The intensity of the signal is proportional to the number of hydrogen present, allowing quantification when a standard of known concentration is included in the sample.

There are several benefits to using NMR; unlike MS it is a non destructive technique so precious samples can be recovered for other analysis, and very little sample preparation is required. However it is not as sensitive as MS, and a larger sample volume is required.

The first use of MS (which at the time was called a parabola spectrograph) was by J.J. Thomson and his research assistant F.W. Aston at the University of Cambridge in 1912. Thomson and Aston measured the deflection of neon ions travelling through a magnetic and electrical field by capturing the deflected ions on photographic plates, and observed two areas of the photographic plate had been hit by the neon ions. They deduced that this was due to a difference in the mass-charge ratio of the ions and reasoned that there must be two stable isotopes of neon (Thomson, 1913). Aston

modified the parabola spectrograph to enable electromagnetic focusing (and discovered many more isotopes), and A.J. Dempster further improved the design to what is more recognisable as a mass spectrometer in 1918 (Dempster, 1918). The basic principles of mass spectrometry are that once introduced the sample is ionised (electrons must be removed from atoms in the sample to make positive ions. There are several ways of ionising the sample, the most widely used of which are summarised in table 1.2 on the next page) and passes into the vacuum of the mass analyser. The sample ions are accelerated, so that they all have the same kinetic energy, and as they pass through the magnetic field the positive ions get deflected. The lighter the ion, the greater the deflection and also the more charged (positive) the ion, the greater the deflection. The scattered ion beam hits an electronic detector and is transformed into a digital signal for recording and analysis.

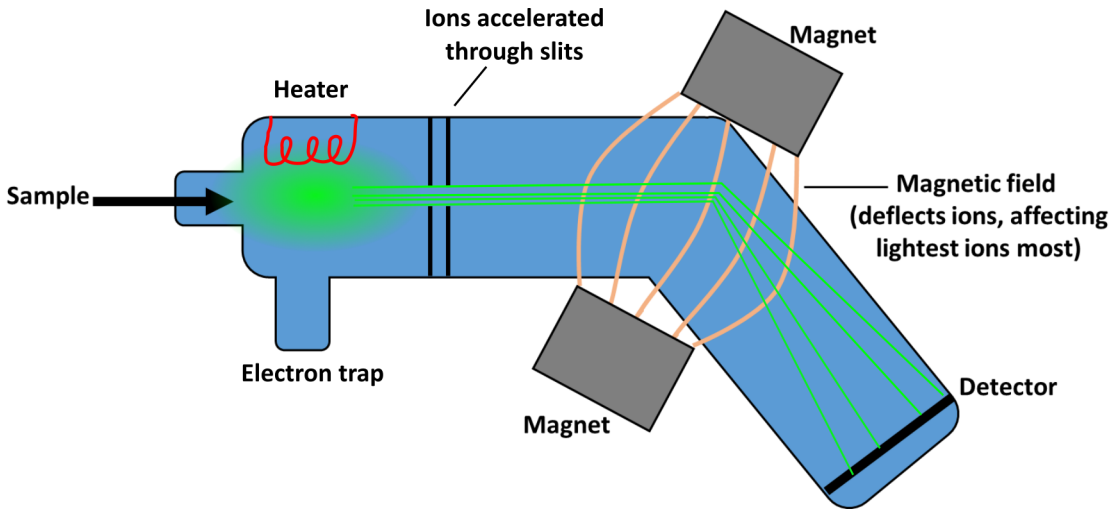

Figure 1.7: **The components of a basic mass spectrometer**.

In figure 1.7 the sample is ionised by Electron Ionistion or Electron Impact Ionisation (EI); whereby electrons, which are released from the metal coil in the electric heater, and are attracted to a positively charged electron trap, travelling through the gaseous sample on their way and knocking electrons from the atoms in the sample. This creates a reproducible collection of molecular ions and ionised molecular fragments for each molecule which can be used to help deduce structure and also can be compared to

libraries for identification, for analytes with a mass range under 1kDa. This method, and all the variants on it, requires that either the sample is already a gas, or that it is volatile and forms a gas when injected into the hot ionisation chamber.

In terms of metabolomics, MS became useful once it was coupled to chromatographic techniques, such as gas chromatography (GC) which were already being used to compare patterns of molecules in biological fluids of individuals (Pauling et al., 1971). Chromatography techniques such as GC and liquid chromatography (LC) alone could not produce the resolution or specificity necessary for accurate identification of the metabolites, and MS alone was not useful for biological mixtures of lots of unknown molecules. Today, different separation and ionisation techniques are used depending on the nature of the analyte in order to capture as much information as possible. Some of the most widely used configurations are described in table 1.2.

Table 1.2: **Common separation, ionisation and detection methods used in mass spectrometry**

Gas chromatography (GC)	Separation of analytes	The sample is vaporised and forced along a column in a carrier gas such as helium or nitrogen (the mobile phase). The column is lined with a polymer (the stationary phase) and as the analyte compounds interact with the stationary phase they will 'stick' in the column for differing lengths of time, known as the retention time. This method is suitable for analysing both organic and inorganic molecules, although they must either be volatile or able to be volatilised by derivitisation.

Name	Function	Description
Liquid chromatography (LC)	Separation of analytes	The sample is dissolved in a liquid mobile phase and drawn through a column containing particles of solid phase using gravity. As with GC, components of the analyte mixture will interact with the stationary phase for differing lengths of time depending on factors such as polarity, resulting in different retention times. This method is suitable for analysing organic molecules and polymers.
High performance liquid chromtography (HPLC) or ultra-high performance liquid chromatography (UHPLC)	Separation of analytes	Similar to LC but with a high operating pressure acting on the mobile phase, giving better resolution during separation.

Name	Function	Description
Electron spray ionisation (ESI)	Ionisation	The sample is dissoved in a volatile, polar solvent and pumped through a stainless steel capillary into the ionisation chamber of a mass spectrometer. At the end of the capillary a high voltage is applied, releasing the sample as charged droplets which are carried forward in a neubulising gas and the solvent evaporates as a heated drying gas (usually nitrogen) is passed over it leaving just analyte ions to enter the accelerator. Because the evaporation of the polar solvent occurs in a vacuum, each ion can gain multiple charges which decreases the mass/charge (z) ratio and makes it possible to get spectra for large molecules. This form of ionisation is useful for polar samples in the range <100Da - 100,000,000Da, so is often used when working with un-denatured proteins. Both positive and negative ions can be generated, with positive mode being used preferentially for proteins and peptides and negative mode used for saccharides and oligonucleotides.
Nanospray ionisation (NI)	Ionisation	Similar to ESI but uses a lower flow rate and less sample is needed.

Name	Function	Description
Electron impact ionisation (EI)	Ionisation	A gas phase sample is bombarded with electrons which knock electrons from analyte atoms creating ions. This is the most common method of ionisation in MS but is only useful for analytes under 1kDa.
Chemical ionisation (CI)	Ionisation	This method first requires the EI of a reagent gas such as methane or isobutane under high pressure so that reagent ions are forced to react with neutral reagent molecules and once the sample is introduced the reagent ions react with the sample, producing sample ions. CI causes less fragmentation than EI so more information can be gathered about the mass of the molecule, again only for analytes with a mass range under 1kDa.
Desorption chemical ionisation (DCI)	Ionisation	A variation on standard CI in which the sample is loaded onto a filament which is then heated very rapidly in the CI plasma, the rapid ion formation reduces fragmentation still further, although requires very fast scan speeds on the recorder.
Matrix assisted laser desorption ionisation (MALDI)	Ionisation	The sample is mixed with a matrix before being exposed to a laser at 337nm. The matrix absorbs the ultraviolet wavelengths and some of it rapidly vapourises along with the sample.

Name	Function	Description
Time of flight mass spectrometry (TOF MS)	Mass spectrometry	Rather than measuring the electromagnetic deflection of analyte ions, in TOF MS exploits the fact that the velocity of the particles is dependent on the mass/charge ratio (once they all have been given the same kinetic energy in the acceleration stage) and the accelerated ions are timed as they travel to the detector. This has the advantage that many more ions will be detected than in other MS set ups where ions can be lost to the walls of the instrument following deflection (although this "filtering" can be useful too).
Tandem mass spectrometry (MS/MS)	Mass spectrometry	Once ions of interest have been identified in a first round of MS and have been fragmented by dissociation (i.e. they have collided with an inert gas) they are filtered through to a second mass spectrometer for those fragments to be further separated by their mass/charge ratio.

1.4.2 The use of metabolomics in biomarker discovery

Humans have been using the detection of small molecules to diagnose disease since ancient times; as early as 1500-2000BC Chinese doctors used ants as a means of assaying urine, with sweet urine (a result of the presence of glucose in the urine) attracting ants used as a marker of diabetes. The more recent advances in NMR, GCMS and LCMS have enabled the discovery of new biomarkers, for example elevated plasma levels of

trimethylamine-N-oxide has been identified as a predictor of cardiovascular disease, using LCMS (Wang et al., 2011b) and elevated levels of sarcosine in urine has been described as a marker of prostate cancer (Sreekumar et al., 2009), although this finding has not yet translated to the clinic. Advances in tandem mass spectroscopy have also been essential in newborn screening, which requires just a dried drop of blood to identify amino and fatty acids indicative of inherited metabolic disorders before symptoms begin to show in the child, enabling faster treatment and a better patient outcome (Chace et al., 2002).

More recently these technologies have also been applied to finding metabolites associated with ageing, which may give insights into the processes involved in age related diseases. For example Cristina Menni and colleagues used metabolomic screening in 6055 humans, including twins, to identify a panel of 22 metabolites that correlate with age and of which some specifically correlate with age related decline in health such as bone density changes and lung function, and were associated also with birth weight. The authors were also able to combine the metabolomics data with epigenetic studies to link the metabolic profiles to methylation profiles, which is useful for studying molecular mechanisms that might be determined at a young age and what effect they have on long term health and ageing (Menni et al., 2013).

1.4.2.1 Data handling

The large amount of data generated from metabolomics screens can also be used as a source of information by other researchers looking for something different in the metabolome, so researchers are encouraged to deposit data sets into databases such as Metabolights (Haug et al., 2013) where they can be freely accessed. Moreover, improved organisation and annotation is continuing to increase the usefulness of the data, an example of this this the Husermet project which has documented the serum metabolome profile of 1200 healthy UK individuals and annotated it according to meta data such as sex, age, weight and whether the individual smokes. This resource gives a

valuable example of baseline variation as a result of these common factors which may impact other studies (Dunn et al., 2014).

1.5 Aims of this thesis

The primary aim of this work is to identify a novel biomarker for senescent fibroblasts which is robust in regard to cell type and senescence induction mode, and which can be measured non invasively.

In order to achieve this aim it is necessary to not only establish models of fibroblast senescence but also models of transient growth arrest so that molecules associated with growth arrest that will most likely be present in senescent cells but are not related to the permanent cell cycle arrest characteristic of senescent cells, can be ruled out. Furthermore, it will be necessary to model as far as possible the cellular stress that can lead to senescence induction, but without inducing senescence, so that molecules associated with the stress, which also will probably be present in senescent cells but not involved specifically in permanent cell cycle arrest, can also be discounted (the identification of induction type specific molecules will also help with this aim).

To capture candidates that are likely to be detectable in body fluids and therefore amenable to a non invasive test, the search for a marker will be focused on the molecules secreted into the tissue culture media, and to ensure as many candidates are identified as possible a non targeted metabolomics approach will be used.

The secondary aim of the thesis is to use smaller scale targeted experiments to validate candidates identified in the metabolomics screen, and identify transcriptional and protein level changes that could explain the elevation of the marker.

If successful in these aims the data generated will provide a detailed and thorough snapshot of the secreted metabolic phenotype of senescent fibroblasts that once uploaded to the database Metabolights will be available to other researchers to compare with their data and mine for their own interests. We will have identified a robust,

senescence specific secreted biomarker that is present in multiple senescence induction models and in multiple tissue types but is not present in transient growth arrest, which if validated *in vivo* could be extremely useful for the study of the role of senescence in human ageing and disease and also provide a non invasive marker to assess the success of treatments that aim to eliminate senescent cells.

Insights into why this marker is specifically elevated can potentially inform us of what metabolic pathways are essential for senescence and this will improve our understanding of the complex senescence phenotype as well as providing potential targets for the elimination of senescent cells or the activation of senescence in proliferating cells.

Chapter 2

Validating the senescence models

2.1 Introduction

In order to identify biomarkers specific to senescence, therefore distinct from both proliferating and transiently growth arrested cells but generic across replicative and stress induced senescence, it was necessary to have *in vitro* models of all of these states to make a comparison of their secreted metabolome. In this chapter I will describe the senescence models used and the techniques used to validate their growth arrest status.

2.1.1 Models used in this study

Two models of senescence were used in this study; replicative senescence (PEsen) induced by long term culturing under standard conditions, and irreparable DNA double strand break stress induced senescence (IrrDSBsen), induced using 20Gy gamma irradiation (Pitiyage et al., 2012). Both models were induced in fibroblasts from two different tissues (IMR90 from lung and NHOF1 from the bottom lip of an adult) wherever possible, and in the original, untargeted screens more cells types were used, to increase the likelihood of finding a genuinely generic senescence marker.

2.1.2 Growth arrest controls

Although the senescence induction mechanisms used to generate the senescence models are already established and we were confident the cells generated would be senescent, it could not be assumed that everything detected in the metabolome of those cells would be unique to senescent fibroblasts. It was predicted that there would be some shared features between transiently growth arrested and senescent metabolomes, as well as shared features between the metabolomes of cells with repairable and irreparable DNA double strand breaks, because many of the same cellular processes would be occurring in those situations. Therefore to be able to tease out events unique to senescence, controls were produced to account for repairable DNA double strand breaks and transient growth arrest.

2.1.2.1 Repairable DNA strand breaks

Previous work by Francis Rodier and colleagues had already established that a relatively low dose of 0.5Gy gamma radiation does cause DNA damage, but to an extent which can be resolved by the DDR (Rodier et al., 2009). As the IrrDSBsen model used in this study is also induced by gamma radiation, 0.5Gy was a good control for both the reversible DNA damage but also the experimental procedure of treating cells in suspension with ionising radiation.

2.1.2.2 Transient growth arrest

Finding a suitable growth arrest control for replicative senescence was slightly more difficult because there was no particular treatment that could be controlled for; the cells were simply cultured under standard conditions for a long time. One method of inducing a transient growth arrest, which has already been used in studies to elicit transient growth arrest (Rosner et al., 2013), is to serum starve cells. By only adding very small volumes of foetal calf serum to the culture media (0.1% vol/vol) the cells are denied growth factors and mitogens so are not stimulated to divide, resulting in

a growth arrest. The limitation of this technique is that the cellular metabolism is affected by changes in concentrations of serum. Despite this limitation the model was still considered useful as there were already studies published using that method. The ideal control however, would share the same nutritional and stimulatory environment, so that it would be reasonable to suppose that any differences in the metabolic phenotype were likely due to a specific feature of senescence which is not present in transiently growth arrested cells under the same conditions.

2.1.2.3 Confluence

When normal fibroblasts come into contact with other cells they undergo contact inhibition of proliferation (Wieser et al., 1990), initiating a growth arrest that is reversible if the interaction between cell surfaces is broken. This method of growth arrest allows the use of the same growth media across the growing, growth arrested and PEsen groups which is an advantage.

2.1.3 Identifying senescent cells

As explained in the previous chapter, the senescence phenotype is variable, so to ensure the most robust results several markers were chosen to monitor the proliferation status of the cells used in the experiments. Table 2.1 on the next page summarises some key markers that can be used to assess the proliferation/growth arrest status of cells, and more detail about the markers selected for use in this study is given in the following subsections.

Marker Name	Target	Use	Method of Detection	Additional Notes
SAβ-Gal[1]	Lysosomal beta galactosidase activity	Detects cells with large lysosomal compartments, a feature of senescence	Histochemistry (has been used both *in vitro* and *in vivo*), flow cytometry	
BrdU	DNA replication	Detects cells in S phase; cells that remain negative are not preparing to divide	Immuno-cytochemistry, flow cytometry	
$p21^{WAF}$ (also known as $p21^{Cip1}$)	Cell cycle inhibition	Detects the presence of the CDK1, CDK2, CDK4/6 inhibitor, capable of arresting the cell cycle a the G1 S checkpoint	Western blot, RT PCR, immuno-cytochemistry, flow cytometry	Protein levels elevated in early stages of growth arrest
$p16^{INK4A}$	Cell cycle inhibition	Detects the presence of the CDK4/6 inhibitor, capable of arresting the cell cycle at the G1 S checkpoint	Western blot, RT PCR, immuno-cytochemistry, flow cytometry	Protein levels elevated in later stages of senescence induction
pRb/Rb	Cell cycle inhibition	Detects the phosphorylation state of Rb (cell cycle can only progress from G1 to S if Rb is phosphorylated)	Western blot, immuno-cytochemistry, flow cytometry	
MCM7 (also known as MCM2)[2]	Replication potential	Detects component of MCM complex, necessary for DNA replication	Western blot, immuno-cytochemistry	
Ki67	Replication potential	Detects presence of Ki67 a protein present at all stages of the cell cycle except G0, Ki67 expression is required for cell division	Immuno-cytochemistry	Function of Ki67 is unknown
DNA SCARS (CHK2, 53BP1, H2AX & activated p53 associated with PML bodies)[3]	Persistent DNA damage foci	Detects persistent irreparable DNA damage foci which can regulate aspects of the senescence phenotype	Multi-label co-localisation (immuno-cytochemistry)	Individual components of SCARS can also be used to detect DNA strand breaks
SAHF (macroH2A, HP1 & H3K9Me2/3)[4]	Cell cycle inhibition	Detects heterochromatin domains that silence genes necessary for cell cycle progression	Multi-label co-localisation (immuno-cytochemistry)	

Table 2.1: **Markers of senescence**. Although none of these markers alone is definitive of senescence, using combinations of markers can be informative about the extent and mechanism of growth arrest. 1 (Debacq-Chainiaux et al., 2009)2(Nakatsuru et al., 1995)3(Rodier et al., 2011)4(Narita et al., 2003b)

2.1.4 Markers used in this thesis

Because it is not practical to measure all of the possible markers of senescence, a selection were chosen that cover the key phenotypic areas: growth arrest, morphological changes, loss of replicative potential, signs of senescence inducing mechanism and cell cycle inhibitors.

2.1.4.1 Growth arrest

Growth arrest was monitored by recording the doubling of cell populations, with the prior knowledge that generally populations that have gone through over 45 doublings are replicatively old and likely to contain an increasing population of senescent cells. If the population was growing at a rate that would not enable one population doubling within a month then the cells were considered growth arrested.

2.1.4.2 Morphological changes

An increase in cell size was observed but not measured in this study, although the presence of enlarged lysosomes was ascertained using the SAβ-gal assay.

2.1.4.3 Loss of replicative potential

The presence of Ki67, which is associated with proliferation, and MCM7, which is required for DNA replication, were monitored to establish whether growth arrested cells had lost the potential to replicate.

2.1.4.4 Markers of the senescence induction mechanism

Both the PEsen and IrrDSBsen models used in this thesis were expected to senesce via a DDR so markers of the SAHF and DNA-SCARS would be useful. In the present study, an established model of DNA double strand break induction was used which had already been validated using 53BP1 and ɣH2AX (Rodier et al., 2009), so 53BP1 foci alone was deemed sufficient to monitor DNA double strand break induction.

2.1.4.5 Cell cycle inhibitors

The cell cycle inhibitor $p16^{INK4A}$ was chosen because it often gradually accumulates in senescence and should not be present in transiently growth arrested cells, unlike $p21^{WAF1}$ which can become elevated even in transient growth arrest by p53 as part of the DDR (Robles and Adami, 1998).

2.1.5 Summary

Before the search for a senescence specific biomarker could begin, it was important to characterise the senescent and control model's phenotypes, so that the information could be used to better understand the relevance of the metabolic phenotypes to senescent growth arrest. This was done using several markers of senescence namely monitoring of the population doubling rate, SAβ-gal staining, Ki67, MCM7, 53BP1 foci and $p16^{INK4A}$ which, although individually not perfect, when considered together should give an accurate picture of the level of senescence within a population and the extent of DNA damage clearance.

To be able to tease out biomarkers specific to senescence later in the study, it was important to find relevant controls that would account for the test conditions and also transient growth arrest. The former was easily addressed by inclusion of relatively young (in terms of population doublings) proliferating cells under the same culture conditions. To control for the conditions of ionising radiation and DNA damage a low dose (0.5Gy) of gamma radiation was applied to cells to induce recoverable DNA damage, and to control for transient growth arrest both serum starved and confluent populations were generated. Although both of these growth arrest control have confounds, taken together they should provide a reasonable picture of transient growth arrest for the purposes of excluding findings which are a feature of growth arrest but not specifically senescence, later in the thesis.

2.2 Materials and methods

2.2.1 Cell culture

In order to find a generic biomarker applicable to many tissue types, a range of human cells were utilised. Normal human oral fibroblasts from an adult's cheek (age and sex unknown) (NHOF1) and lower lip (21 year old female) (NHOF5) were isolated and cultured from healthy volunteers by Dr. Gayani Pityiage (Pitiyage et al., 2011), normal new born human foreskin fibroblasts (HFF) were isolated and cultured by Dr. June Munro (Munro et al., 2001). Normal human lung fibroblasts (16 weeks gestation female) (IMR90) were purchased from the American Type Culture Collection (ATCC) (ATCC-CCL-186), as were normal new born human skin fibroblasts (BJ) (ATCC CRL-2522). Colon fibroblasts (Colon) were a generous gift from Professor Chris Paraskeva, University of Bristol.

All of these cells were cultured under the same conditions: using DMEM (4.5g/L glucose) supplied by Lonza (BE12-604F/12) supplemented with penicillin and streptomycin antibiotics (Life Technologies 15070-063) to a final concentration of 50U/mL, and L-glutamine (Life Technologies 25030-081) to a final concentration of 2mM, containing 10% vol/vol HyClone Foetal Clone II foetal bovine serum (Thermo Scientific SH30066.02), at 37°C in humid Eppendorf Galaxy S incubator with 10% CO_2/90% air. Flasks were kept at roughly 80% confluence, and medium was replenished every 3-4 days. Once cells became more than 80% confluent, or were needed for an experiment, they were washed once with warm (37°C) PBS containing 0.02% weight/vol EDTA before being incubated for 5 minutes with PBS containing 0.1% weight/vol trypsin and 0.01% weight/vol EDTA (1mL/10cm^2 dish). Following cell detachment the trypsin was neutralised by the addition of serum containing media (3mL media for every 1mL trypsin solution), and cells were counted manually using a haemocytometer to enable calculation of the cumulative mean population doublings (cmpds). Cmpds were used throughout the study as a measure of chronological age, and were calculated using the

formula:

$mpd = 3.32((\log_{10}\text{cell number yield})-(\log_{10}\text{cell number input}))$ (Munro et al., 2001)

2.2.2 DNA double strand break induction

To create irreparable DNA double strand breaks, in order to generate stress-induced senescent cells, the cells were exposed to gamma radiation by Anthony Price and his colleagues at the Wingate Institute, Whitechapel, London. Exposure to 0.5 and 20 Gray (Gy) was performed at a dose rate of 1.4Gy per minute, with the cells in suspension in 4°C DMEM. Cells were re-plated and returned to the incubator as quickly as possible following the treatment, and cultured for a total of 20 days under standard conditions.

2.2.3 "Collection"

Because the sample type collected in the final experiments was cell culture media, conditioned over 24 hours (referred to in this thesis as the "collection period"), all cell pellets were also collected and cells for immunohistochemistry fixed following the same protocol as would be applied to collect the conditioned media.

2.2.3.1 Growth arrest control: Confluence

The protocol for collection of the media from the confluent cells, which were used as a control for growth arrest, required slightly more time between plating of the cells and the start of the collection period, to enable the cells to become properly confluent and growth arrested. This protocol was optimised to get as many cells growth arrested (Ki67 negative) as possible whilst also not allowing irreparable DNA double strand breaks to develop (the cells must also be negative for large 53BP1 foci), and the optimum conditions were found to be plating the cells 4 days before collection was due, and replenishing the media every day within that time. Media volume added to the flasks during the collection period was increased to produce a cell number:volume ratio as similar as possible to that found in the other flasks with cells growing at the usual

density.

2.2.3.2 Growth arrest control: Serum starvation

Transient growth arrest induced by serum starvation in low serum media also required optimisation to get as many growth arrested cells as possible without inducing irreparable DNA double strand breaks. Cells were plated four days before collection was due, 24 hours after plating the cells were washed with 1xPBS and media was replaced with DMEM containing additional glutamine and antibiotics as in the standard media but containing only 0.1% vol/vol foetal calf serum.

2.2.4 Collection of cell pellets for western blot analysis

For PEsen experiments the PEsen and growing cells and in IrrDSBsen experiments all cells were seeded at a density of $5x10^5$cells per T75 flask approximately 24 hours before the collection period was due to start. For PEsen experiment growth arrest controls low serum or confluence experiments, cells were seeded 4 days before the collection period was due to begin. At the start of the collection period media was replaced with 3mL freshly made media. Flasks were allowed to equilibrate to 10% CO_2 before being sealed with Parafilm to prevent evaporation. 24 hours later, after the removal of the medium, the cells were washed with warm 1x PBS and incubated at room temperature with 1mL trypsin/EDTA solution (as previously described) while the media was being processed. Incubating the cells in the trypsin at room temperature rather than at 37°C slowed the action of the trypsin slightly and allowed more time to process the media before the cells detached fully. Following detachment the trypsin was neutralised by addition of 3mL serum containing media and the cells were counted. The cell suspension was then centrifuged at 800 rpm for 5 minutes to produce a cell pellet, which was resuspended in 1mL 1xPBS and transferred to an Eppendorf tube. A pellet was obtained

by centrifuging the cell suspension at 13,000 rpm in a microfuge for 5 minutes and the PBS was aspirated, then the pellet was snap frozen on ethanol/dry ice (EtOH/dry ice) and stored at -80°C.

2.2.5 Immunocytochemistry

2.2.5.1 Preparation of cells for staining

Young growing cells were plated into 8 well chamber slides (LabTek II, Nunc, catalogue number 154534) at a density of $2.8x10^3$ cells/well (except for when confluence was desired, then cells were plated at $1.66x10^4$ cells/well), at the same time as the flasks were seeded ready for the collection of media and pellets, and all media changes were carried out in parallel. At the same time as media and pellets were collected from the flasks, the media was removed from the chamber slides and the cells were washed once with warm PBS, then fixed with 4% weight/vol formaldehyde at room temperature for 45 minutes. Following fixation the cells were washed twice with PBS and stored at 4°C in PBS until staining.

2.2.5.2 Immunostaining

For both Ki67 (proliferation marker) and 53BP1 (DNA damage foci marker), the same protocol applies. First the cells were permiablised for 20 minutes in PBS containing 1% vol/vol Triton X-100, then the plastic chambers were removed so the slides could be washed briefly in a Coplin Jar with PBS containing 0.1% vol/vol Tween 20 (PBS-T). After washing, a solution of 0.1% weight/vol bovine serum albumin (BSA) in PBS-T (blocking buffer) was applied to the slide for 30 minutes at room temperature to block non specific reactive sites. Primary antibodies were diluted in blocking buffer (the DAKO mouse monoclonal anti-Ki67 clone MIB-1, lot number 20003301, the Millepore mouse kappa monoclonal anti 53BP1 MAb 3802 lot number 2279539, and the Abcam

mouse kappa monoclonal MOPC-21 non specific IgG ab18443 lot number GR107754-3 were all used at a 1:1000 dilution), and 40µl was incubated on each well for 2 hours at room temperature (care was always taken to dry the space between wells with a small piece of tissue to avoid antibody solutions running onto the wrong wells), in a humidity chamber consisting of damp tissue paper in the base of a slide box, with the slides resting horizontally on the top directly under the close fitting lid. Next, the slides were washed again in PBS-T and incubated with secondary antibody (Abcam Alexa Fluor 488 goat anti-mouse IgG (H+L) A11001 lot number 1219843) for 1 hour protected from light in the humidity chamber. Following a last wash in PBS-T, coverslips were applied using Vectashield Mounting Medium with DAPI (H-1200 Vector Laboratories) which is a non-hardening mountant, so the coverslips were sealed with a border of nail varnish before being stored at 4°C, protected from light.

2.2.5.3 Image acquisition

Images were obtained using the MetaMorph software package (MetaMorph Microscopy Automation & Image Analysis Software, Molecular Devices LLC) on a Leica DM4000B epi-fluorescence upright microscope with QIClick camera containing a Sony IC285 CCD chip for image acquisition. Gain and exposure time were set using young proliferating cells as positive control for Ki67, and senescent cells as a negative control for Ki67 and vice versa as controls for 53BP1. A minimum of 3 12 bit images were taken in different locations within each well, so that a minimum of 100 cells were imaged from different areas of the well.

2.2.5.4 Ki67 image analysis

All scoring was carried out using the open source image analysis software ImageJ and FIJI (Rasband, 1997; Schneider et al., 2012). The process described below has been

scripted as a macro, with the help of Dr. Steven West at the University of Oxford, which can be performed using either ImageJ or Fiji, in a semi-supervised manner (the computer runs through the analysis itself, but the images are displayed on the screen for the user to check in case the thresholding encountered any problems, as is sometimes the case with completely negative images. If there were any problems noticed with a particular image, the user has to go back and manually score that image). The DAPI image was auto-thresholded using Otsu's thresholding algorithm (OTSU) and dark background settings. The 'fill holes' and 'watershed' tools were used to automatically add a 1 pixel thick line to separate any touching nuclei. Nuclei were then defined as regions of interest (ROI) using 'analyse particles' options, excluding any objects touching the edges of the image, and including anything over 400 pixels in size to be shown as an outline and added to the ROI manager. The corresponding Alexa 488 image was then opened, auto thresholded in the same way (although importantly no "fill holes" or "watershed" was applied to these images) and the 'analyse particles' options were applied to show count masks of objects over 400 pixels in size, that have circularity between 0-1 and exclude any objects on the edge. These measurements were not added to the ROI manager. The ROI manager was then used to show the outlines of the nuclei overlaid on the count masks from the Alexa 488 image, by selecting 'show all', an example screen shot can be seen in figure 2.1. Using the 'measure' tool in the ROI manager tool bar produces a table containing information on the size, shape, and integrated density. Objects with 0 recorded for integrated density were recorded as negative for Ki67, objects with a positive value for integrated density were recorded as positive. The results were exported to an Excel spreadsheet, and the overall score was recorded as number of positive nuclei as a percentage of total nuclei.

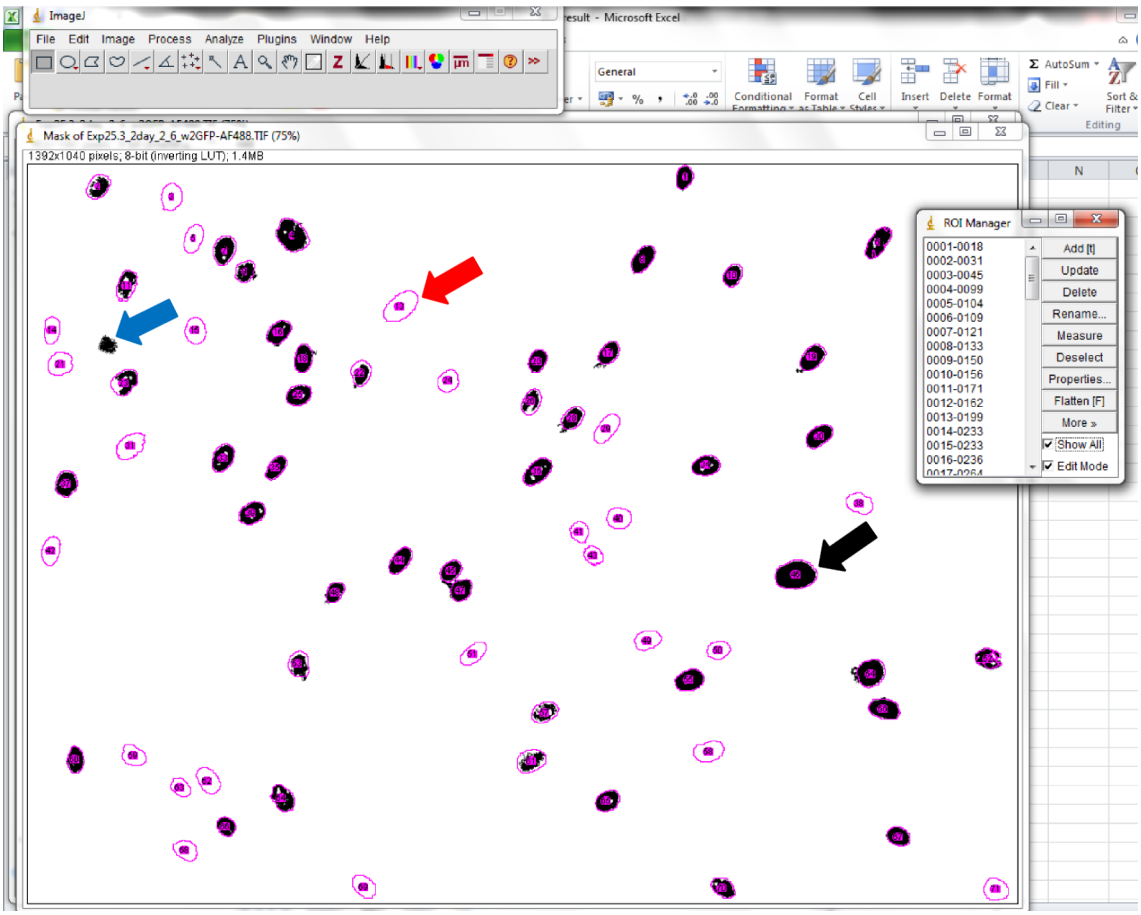

Figure 2.1: **Region of interest overlay on Ki67 staining**. Screen shot showing the region of interest (ROI), which has been defined by the thresholded DAPI image depicting the nuclei, overlaid onto the thresholded Ki67 image in ImageJ. The black arrow indicates a ROI containing positive Ki67 staining, the red arrow indicates a nuclear outline ROI that is negative for Ki67, and the blue arrow indicates fluorescent artefact in the 488 channel that does not fall inside a ROI and therefore will not be counted.

2.2.5.5 53BP1 image analysis

As 53BP1 foci are also in the nucleus, first the ROI was defined as described for the analysis of Ki67 staining in section 2.2.5.4 on page 92 , then using positive and negative control cells (young proliferating as negative and previously verified senescent cells as positive) a value of noise tolerance was defined in 'find maxima' tool such that any foci that would manually be scored as large in the positive control are detected as maxima, but any small foci in the negative control are not picked up. The value for noise

tolerance was kept constant for all images, and 'find maxima' was used to report a foci as a single point. The ROI were then overlaid and 'measure' from the ROI toolbar was used to generate a table of measurements, including integrated density, of each nuclei. The integrated density of one pixel (single point) is 255, so the integrated density of each nucleus was divided by 255 to obtain the number of foci in each nucleus, and the overall scoring reports the percentage of cells that scored positive (i.e. had at least one large foci).

2.2.5.6 Senescence associated beta-galactosidase (SAβ-gal) staining

SAβ-gal staining was performed using a kit (Histochemical Senescence Detection Kit (K320-250) from BioVision, Inc.). Cells were plated at a density of 8000 cells/well in a 12 well tissue culture plate and the media was refreshed in the afternoon of the following day at 5pm or later. 24 hours later, the media was removed and the cells were washed with warm PBS before being fixed and incubated with staining solution for 16 hours at 37°C in atmospheric ppCO_2, protected from light, in accordance with the kit instructions. The staining was achieved by hydrolysis of the colourless X-Gal in the staining solution, by the SAβ-gal enzyme (now known to be lysosomal beta galactosidase; senescent cells have larger lysosomes and much more of this enzyme than non- senescent cells) which yields galactose and 5-bromo-4-chloro-3-hydroxyindole. The latter then spontaneously forms a dimer which is oxidized to the insoluble blue precipitate 5,5'-dibromo-4,4'-dichloro-indigo, which can be detected visually (Debacq-Chainiaux et al., 2009).

After the staining solution had been removed, the cells were washed twice with PBS and counter-stained using nuclear fast red (to make the nuclear fast red solution 5g of aluminium sulfate (Sigma, Cat# 368458-500G) was dissolved in 100mL water in a glass beaker, and the water level marked. 0.1g nuclear fast red (N8002 Sigma Aldrich) was then added before slowly heating to the boil in a fume hood. After cooling the water

level was topped back up to 100mL, the solution was centrifuged to 12000 rpm and the supernatant filtered through a 0.45µm syringe filter to get rid of any precipitate). 500µl per well of staining solution was added and incubated for 15-20 minutes at room temperature, the cells were then washed twice with PBS. Images of the stained cells were taken at 100x magnification on a Nikon Eclipse TE2000-S inverted light microscope with Nikon camera model LHM100C-1. A minimum of 6 images were taken (depending how many cells are in view; ideally 100 cells in total at least) from different areas of the well. Cells were scored manually and reported as positive cells as a percentage of total cells.

2.2.6 Western blotting of $p16^{INK4A}$ and MCM7

Cell pellets collected as previously described in section 2.2.4 on page 90 were thawed on wet ice and lysed in 50µl RIPA buffer (150 mM sodium chloride, 1.0% (vol/vol) Triton X-100, 0.5% (weight/vol) sodium deoxycholate, 0.1% (weight/vol) sodium dodecyl sulphate (SDS), 50mM Tris, pH 8.0, stored at -20°C in 10mL aliquots) containing protease inhibitor cocktail (cOmplete EDTA free, Roche) according to manufacturer's instructions. The pellet was disrupted by pipetting, then centrifuged for 20 minutes at 12000rpm at 4°C to remove cell debris. The supernatant was transferred to a new tube on ice and a protein standard curve was prepared using bovine serum albumin (BSA) ranging in concentration from 0-2mg/mL. DC Protein Assay (Bio-Rad) reaction mixture was added to samples and the standard curve in a clear, flat bottomed 96 well plate (Primaria 353872, BD Falcon) and after 15 minutes incubation at room temperature the light absorbance was measured at 750nm by plate reader (Fluostar Optima, BMG Labtech). The concentration of protein in samples was calculated from the standard curve and the original samples diluted to 2µg/µL in RIPA buffer and loading buffer (4X Laemlli Sample Buffer #161-0747, Bio-Rad) and then boiled at 95°C for 5 minutes to denature the protein. The prepared samples were then stored at -20°C until needed.

The proteins in the cell lysate were separated by molecular weight using sodium dodecyl sulphate poly acrylamide gel electrophoresis (SDS-PAGE) with the NuPage Mini Cell system and pre-cast gels (Novex Protein NuPAGE Mini Gels, 4-12% Bis-Tris) and using 1X NuPage running buffer (NuPAGE MOPS SDS Running Buffer (20X) NP0001). A molecular weight marker was run on at least one end of the gel (BioRad Precision Plus dual colour ladder #161-0374) as a reference for the size of the protein bands. Gels were run for 120 minutes at 90V before the proteins were transferred from the gel to a membrane for detection. Immediately prior to exposure to the gel, the nitrocellulose membrane (with a pore size 0.45µm) was incubated in transfer buffer (Tris-glycine buffer: 25mM Tris, 192mM glycine, 10% vol/vol methanol), then carefully arranged on top of the gel in the middle of a sandwich of filter paper and sponges, all soaked in cold transfer buffer. The transfer was performed at 4°C (in a cold room) in transfer buffer for 90 minutes, at 30V.

Once the proteins had been transferred from the gel to the membrane, the membrane was incubated in blocking buffer consisting of Tris buffered saline containing 0.1% vol/vol Tween 20 (TBS-T) with 5% weight/vol milk (Marvel Original dried Skimmed Milk) for 1 hour at room temperature under gentle agitation, to block reactive sites.

Using the molecular weight marker as a guide, the membranes were cut horizontally at a molecular weight between that of the protein of interest (either $p16^{INK4A}$ at 16KDa or MCM7 at 81KDa) and the loading control (β-actin at 46KDa), to allow primary antibodies for different targets to be incubated with the membranes in parallel. The primary antibody targeting $p16^{INK4A}$(Anti-CDKN2A/p16INK4a EP4353Y(3) ab81278 from Abcam, UK) was diluted 1:2000 in blocking buffer, the primary antibody targeting MCM7 (Anti-MCM7 EP1974Y ab52489 from Abcam, UK) was diluted to 1:2000, the primary antibody targeting β-actin was diluted 1:20,000 in blocking buffer and incubated with the membrane overnight at 4°C, under gentle agitation. The next day the membranes were washed three times in TBS-T, 5 minutes per wash on a medium speed rocker, prior to incubation with secondary antibody (horse radish peroxidase (HRP)

conjugated goat anti rabbit, from Thermo Fisher Scientific, USA) 1 hour at room temperature with gentle agitation. A final set of washes in TBS-T were performed and the protein bands were visualised using an enhanced chemiluminescent substrate of HRP (Pierce ECL Western Blotting Substrate). Membranes were incubated with substrate solution containing luminol and peroxide for 2 minutes, then excess liquid was dabbed off and the membrane was exposed to light sensitive film (Amersham Hyperfilm ECL 28906837, GE Healthcare) in a dark room. The film was developed using the Xograph Film Autoprocessor 5.7 and scanned using a Cannon LiDE 210 scanner so that the protein bands could be analysed using the densitometry feature of ImageJ.

2.3 Results

In order to identify a metabolic marker specific to senescence it was necessary to control for features of transient growth arrest and the radiation treatment as well as proliferation. As explained in the chapter introduction, serum starvation and confluence were chosen as growth arrest control conditions for PEsen, and 0.5Gy gamma radiation was chosen as a control for the radiation treatment used to generate IrrDSBsen cells. These groups were characterised using markers of growth arrest and DNA damage induction, and these results are discussed below.

2.3.1 Generation of PEsen fibroblasts

2.3.1.1 Growth arrest

A slow rate of population doubling was observed in PEsen cells relative to growing controls; a representative example showing the rate of doubling over 4 days in young and old fibroblasts can be seen in figure 2.2.

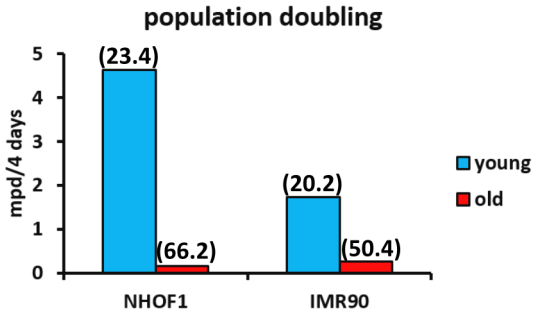

Figure 2.2: **Mean population doublings (mpd) achieved by "young" and "old" IMR90 and NHOF1 fibroblasts over a period of 4 days**. The number in brackets above the bars represents the cumulative mean population doublings (cmpd) for that particular population.

2.3.1.2 Morphological changes

Phase contrast images of fixed cells that had been exposed to X-gal (see figure 2.3) show both morphological changes (larger, flatter cell shape, in some cases multi-nucleated) and increased β-galactosidase activity (as evidenced by accumulation of blue pigment) in populations of fibroblasts which had gone through over 50 population doublings and had failed to complete one population doubling in a month.

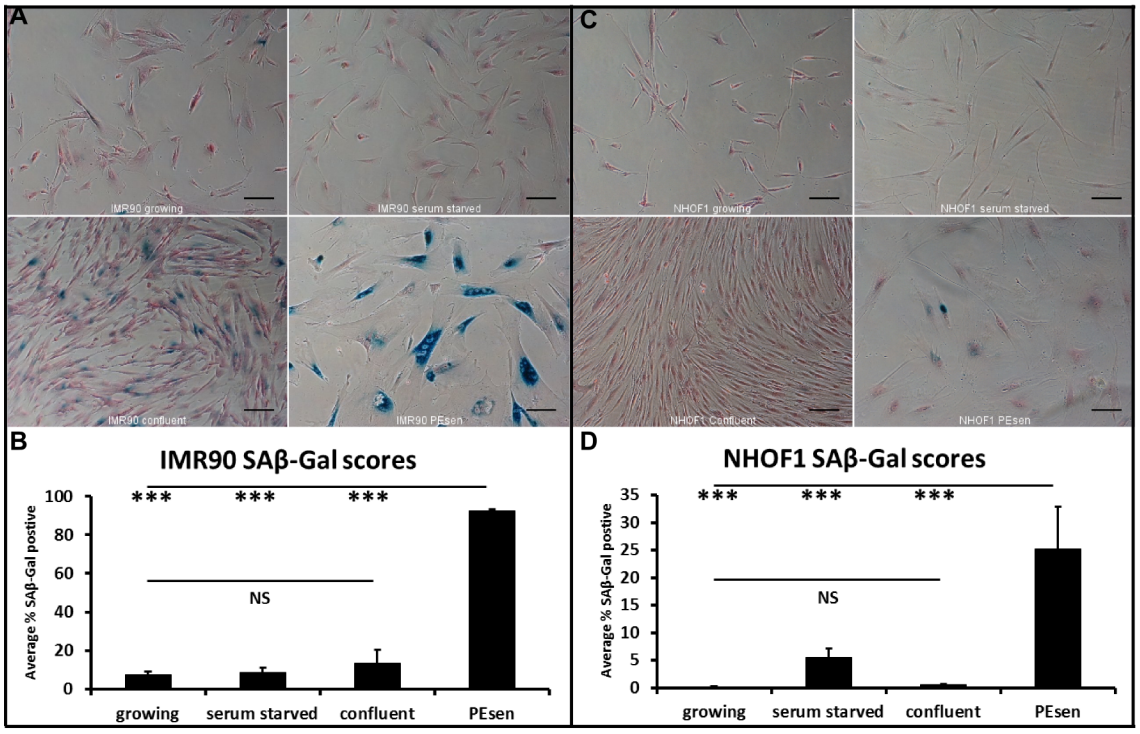

Figure 2.3: **SAβ-gal staining of PEsen and growth arrest controls**. Top panels show representative images of growing, serum starved, confluent and PEsen IMR90 (A) and NHOF1 (C) cells treated with X-gal; blue pigment has accumulated in cells with high beta galactosidase activity. Scale bars represent 50μm. Bottom panels show average % cells staining positive for SAβ-gal in IMR90 (B) and NHOF1 (D). n=3 NS: not significant ***$p<0.01$ with 1 way ANOVA, Tukey's post hoc analysis

2.3.1.3 Replicative potential

Replicative potential was assessed by both Ki67 (figure 2.4) and MCM7 protein level (figure 2.5).

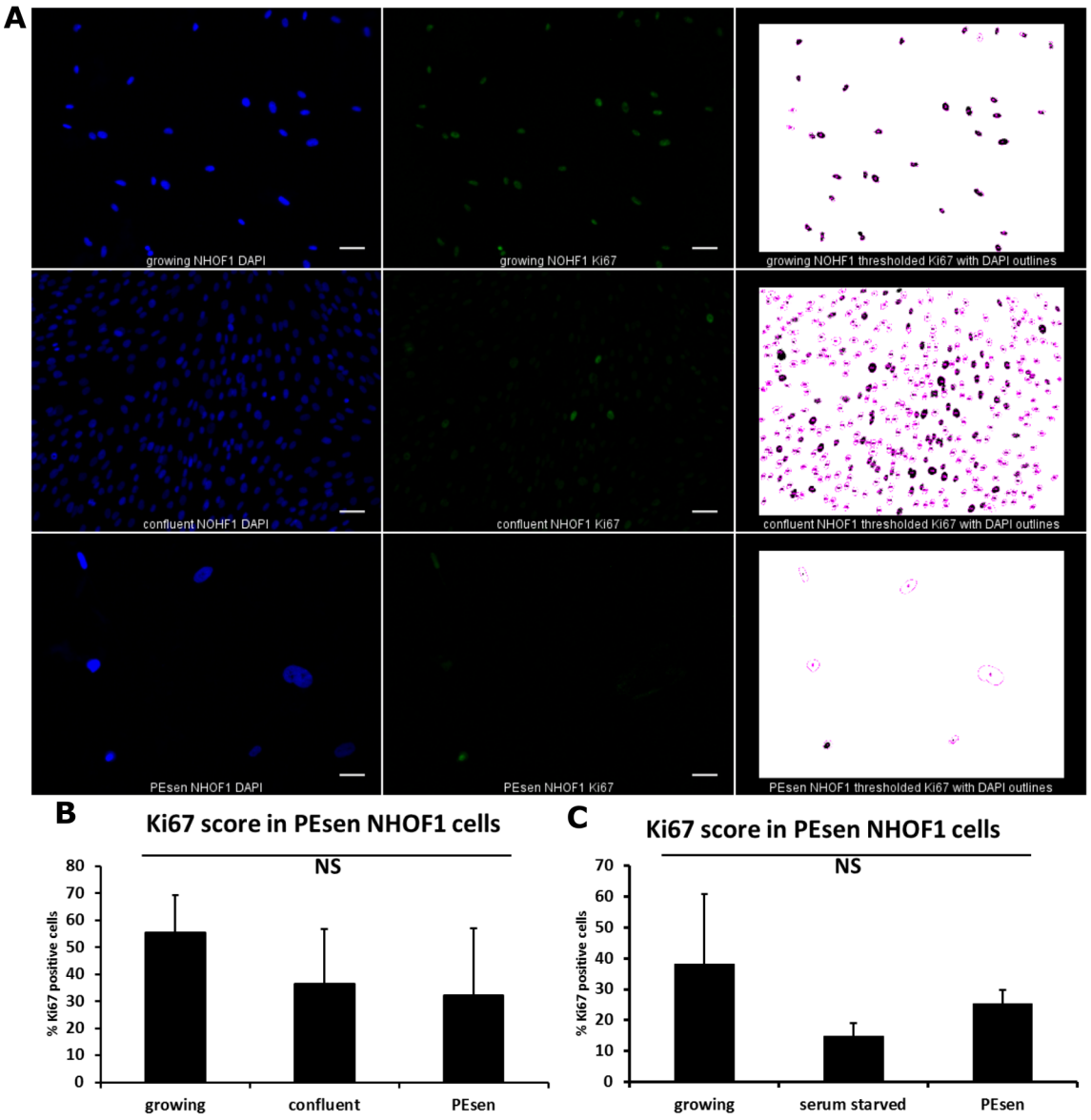

Figure 2.4: **Ki67 staining in PEsen NHOF1 and growth arrest controls A** Representative DAPI (blue) and Ki67 (green) staining in young, confluent, serum starved and PEsen cells (left and middle columns of images). The right hand column shows ImageJ thresholded image overlays, depicting which nuclei in the image were positive for Ki67. Scale bars represent 50µm. Bar charts **B** and **C** show the mean score for each group across three repeats. Error bars represent standard deviation from the mean. n=3 NS = not significant with 1 way ANOVA.

As figure 2.4 shows, the thresholding method identified fewer Ki67 positive nuclei in serum starved, confluent and PEsen populations compared to the young growing population however the trend was not significant when a 1 way ANOVA was applied.

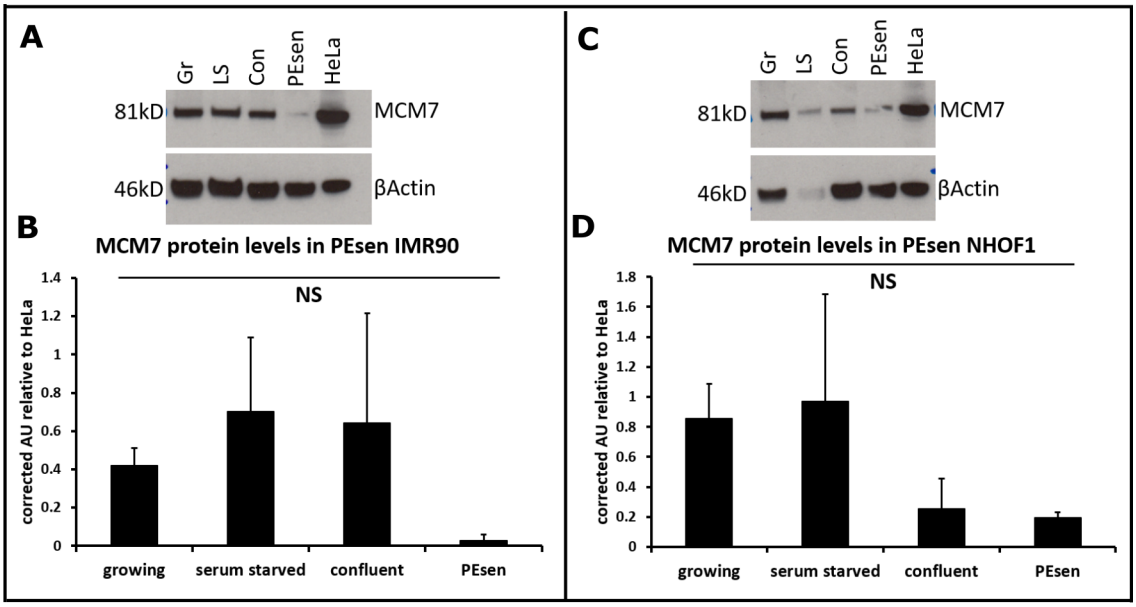

Figure 2.5: **MCM7 protein level in PEsen fibroblasts. A** and **C** are representative western blots of MCM7 protein levels in PEsen, growing (Gr), serum starved (LS) and confluent (Con) controls with β-actin loading control, in IMR90 and NHOF1 respectively. **B** and **D** show average MCM7 protein levels in PEsen and growth arrest controls already described in A and C. n=3 error bars represent standard deviation from the mean NS= not significant with a 1 way ANOVA.

Figure2.5 shows MCM7 levels decreased in both IMR90 and NHOF1 PEsen compared to growing cells but the trend was not statistically significant. The large error bars on the growth arrest control cells show there is a high level of variability in the confluent and serum starved cells, although in general they appear to retain higher levels of MCM7 than PEsen cells.

2.3.1.4 Senescence inducing mechanism (DDR)

53BP1 foci are indicative of a DDR, and large foci accumulate when there is irreparable DNA damage.

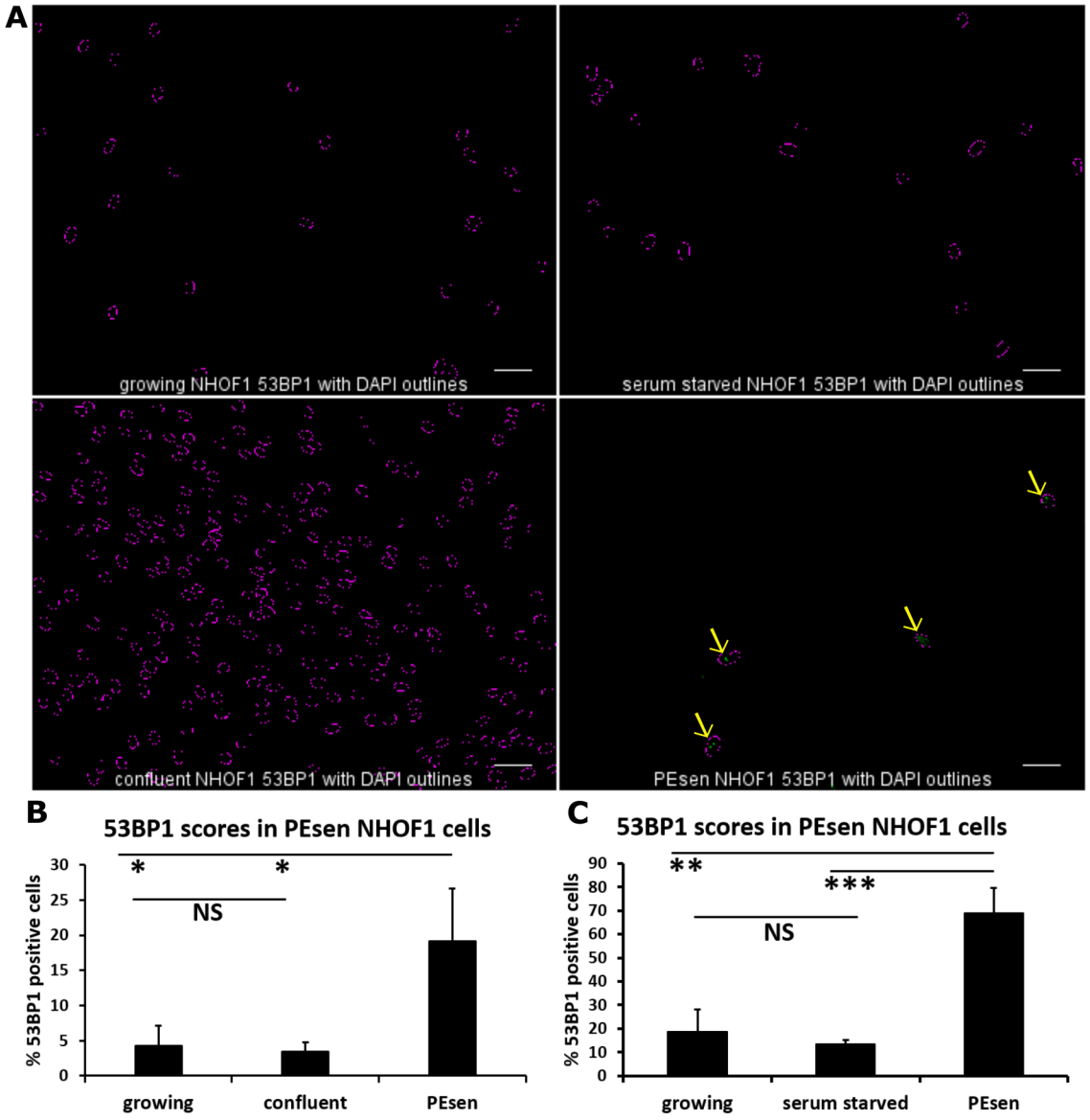

Figure 2.6: **53BP1 staining in PEsen and growth arrest controls**. **A** ImageJ nuclear outline overlays (magenta dotted lines) on 53BP1 foci staining (green) in growing, serum starved, confluent and PEsen NHOF1 cells. Yellow arrows point to 53BP1 foci, which can only be seen in the nuclei of PEsen cells. Scale bar represents 50µm. **B** the mean percentage of cells positive for 53BP1 foci for each group across three repeats. n=3 Error bars represent standard deviation from the mean. NS = not significant *p<0.05 **p<0.01 ***p<0.001 with 1 way ANOVA using Tukey's post hoc analysis.

Figure 2.6 shows that PEsen cells have many more 53BP1 foci than the other groups and this trend was found to be statistically significant with a 1 way ANOVA and Tukey's post hock analysis, while the growing and growth arrest control cells did not show a statistical difference in the number of 53BP1 foci.

2.3.1.5 Cell cycle inhibition

To confirm that senescence had not been induced in the growth arrest control cells western blots were performed to assess the levels of $p16^{INK4A}$, a CDK inhibitor. As can be seen in figure 2.7 there was a statistically significant increase in $p16^{INK4A}$expression in PEsen IMR90 cells compared to growth arrested and growing controls, however NHOF1 PEsen cells did not show any detectable $p16^{INK4A}$ protein (figure 2.8).

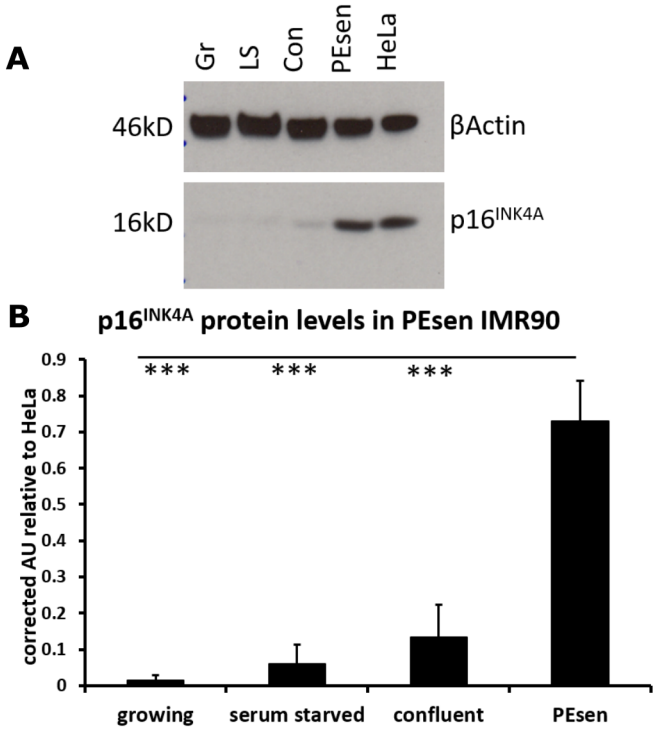

Figure 2.7: **$p16^{INK4A}$ protein level in PEsen IMR90 and growth arrest controls.** **A**. Representative western blot of $p16^{INK4A}$ protein levels in PEsen IMR90 cells as well as growing (Gr), serum starved (LS) and confluent (Con) controls, with β-actin loading control. **B**. Average $p16^{INK4A}$ protein levels in PEsen IMR90 and controls as in A, quantified relative to HeLa. Error bars represent standard deviation from the mean, n=3 ***$p<0.001$ with 1 way ANOVA and Tukey's post hoc analysis.

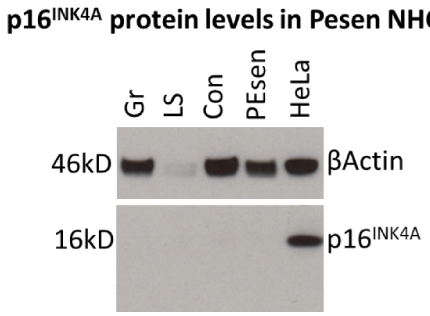

Figure 2.8: **p16^{INK4A} protein level in PEsen NHOF1 and growth arrest controls.** Representative western blot of p16^{INK4A} protein levels in PEsen NHOF1 cells as well as growing (Gr), serum starved (LS) and confluent (Con) controls, with β-actin loading control. No signal for p16^{INK4A} was detected in any of the NHOF1 lysates, so no quantification was performed.

2.3.2 Generation of DNA double strand break stress induced senescent fibroblasts

The same approach was used to characterise the IrrDSBsen fibroblasts

2.3.2.1 Growth arrest

In the 18 days after irradiation with 20Gy gamma, both NHOF1 and IMR90 IrrDSBsen populations did not proliferate, where as the 0Gy control cells continued to complete multiple population doublings in that time. An example is shown in figure 2.9.

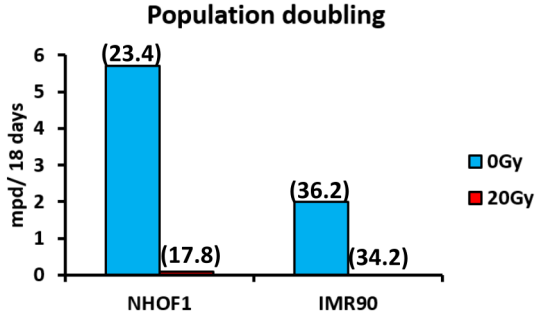

Figure 2.9: **Mean population doublings (mpd) achieved by IMR90 and NHOF1 fibroblasts that had been subject to 20Gy gamma or 0Gy gamma radiation, over a period of 18 days**. The number in brackets above the bars represents the cumulative mean population doublings (cmpd) for that particular population.

2.3.2.2 Morphological changes

SAβ-gal levels were increased after 20 days in cells that were exposed to 20Gy gamma compared to growing cells and cells that had been exposed to 0.5Gy gamma in both IMR90 (figure 2.10) and NHOF1 (figure 2.11).

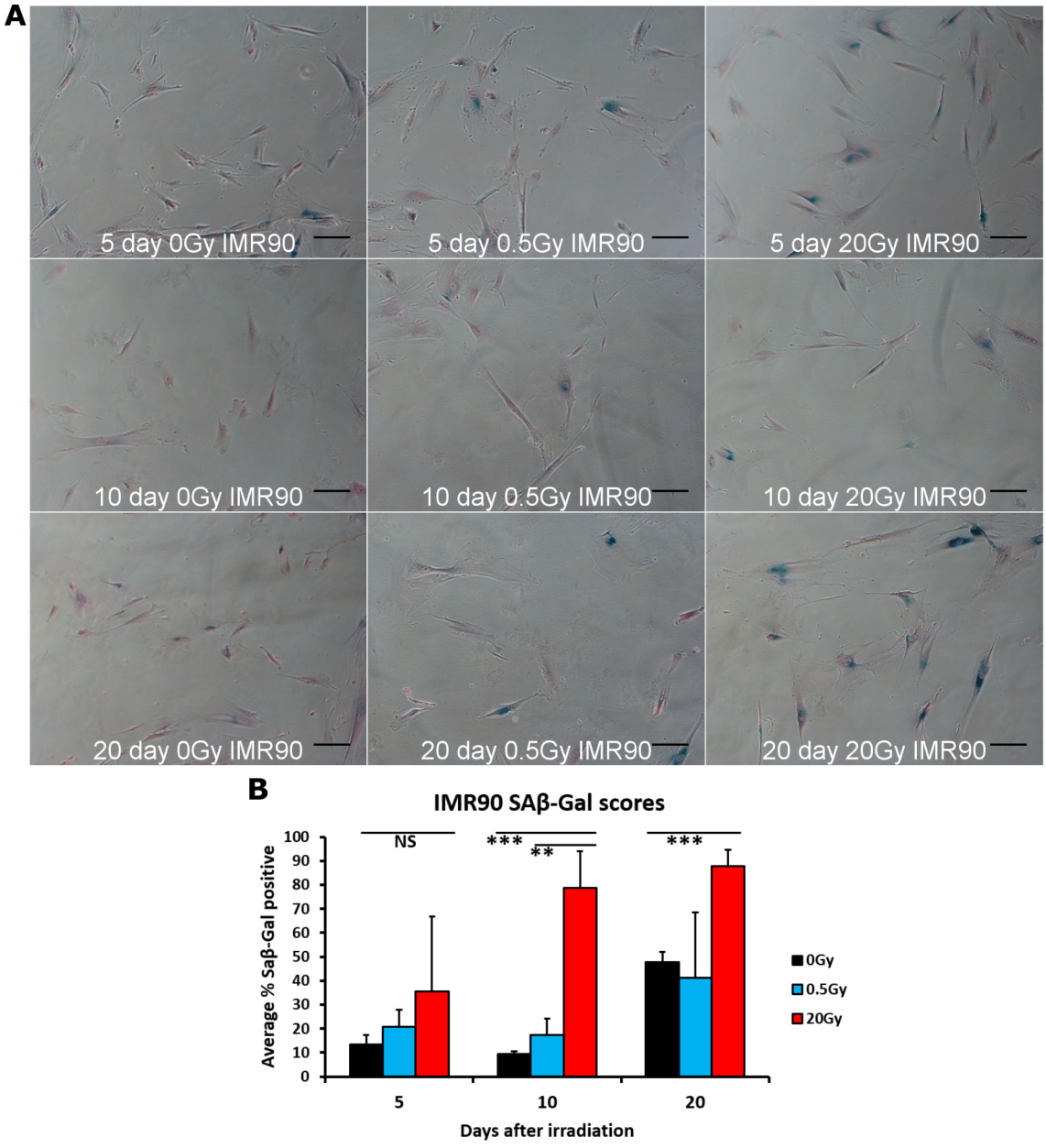

Figure 2.10: **A** Representative SAβ-gal staining of 0Gy 0.5Gy and 20Gy treated IMR90 at 5, 10 and 20 days after treatment. Scale bar represents 50μm. **B** Average % SAβ-Gal scores 0Gy 0.5Gy and 20Gy treated IMR90 at 5, 10 and 20 days after treatment. Scale bars represent standard deviation from the mean. N=3 NS = non significant, **p<0.01 ***p<0.001 with 1 way ANOVA and Tukey's post hoc analysis.

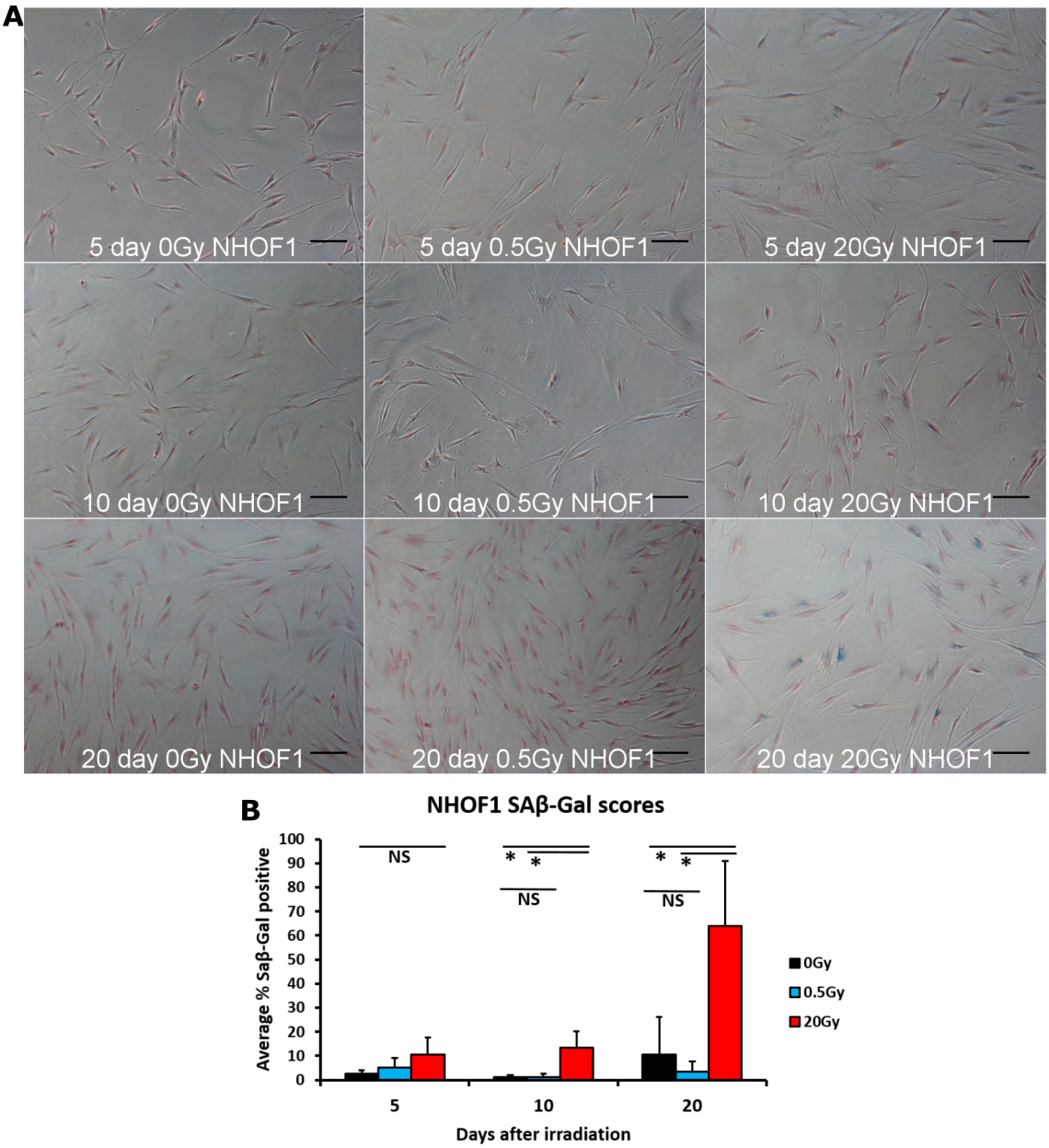

Figure 2.11: **A** Representative SAβ-gal staining of 0Gy 0.5Gy and 20Gy treated NHOF1 at 5, 10 and 20 days after treatment. Scale bar represents 50μm. **B** Average % SAβ-Gal scores 0Gy 0.5Gy and 20Gy treated NHOF1 at 5, 10 and 20 days after treatment. Scale bars represent standard deviation from the mean. N=3 NS = non significant, *p<0.05 1 with 1 way ANOVA and Tukey's post hoc analysis.

2.3.2.3 Replicative potential

The levels of the proliferation marker Ki67 declined over time in both IMR90 and NHOF1, and in NHOF1 the effect of 20Gy irradiation caused a statistically significant decrease compared to controls as early as 5 days after treatment (see figure 2.13) al-

though interestingly in IMR90 the decline in Ki67 following 20Gy was not significantly different to the decline in controls until the 20Gy time point (figure 2.12).

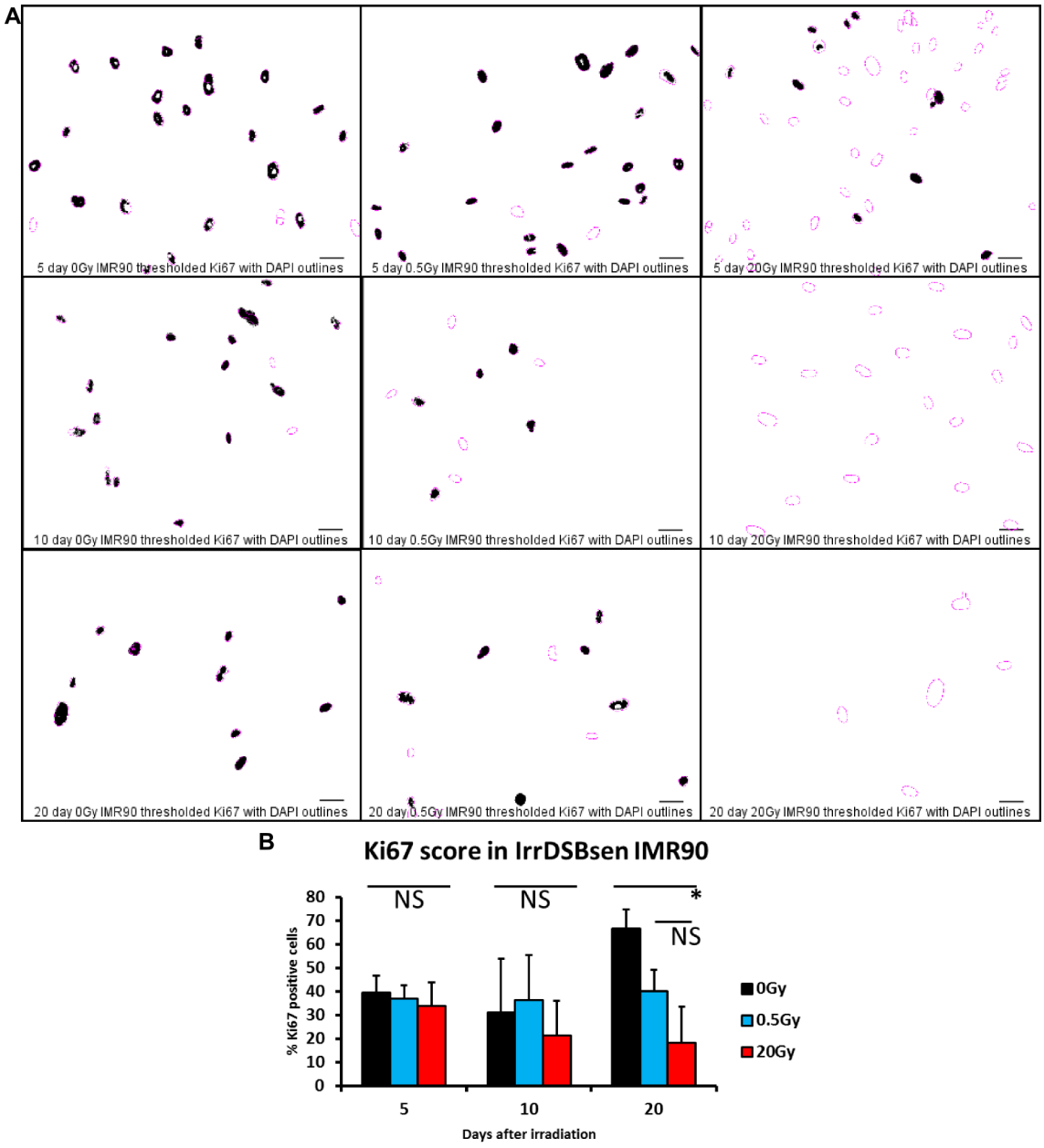

Figure 2.12: **A** Thresholded Ki67 staining with nuclear regions of interest (identified using DAPI) shown as magenta outlines, in IMR90 cells 5, 10 and 20 days after a 0, 0.5 and 20Gy dose ionising radiation. Scale bar represents 50µm. **B** Mean Ki67 scores for each group across three repeats. Error bars represent standard deviation from the mean. NS = not significant *$p<0.05$, 2 way ANOVA with Tukey's post hoc analysis.

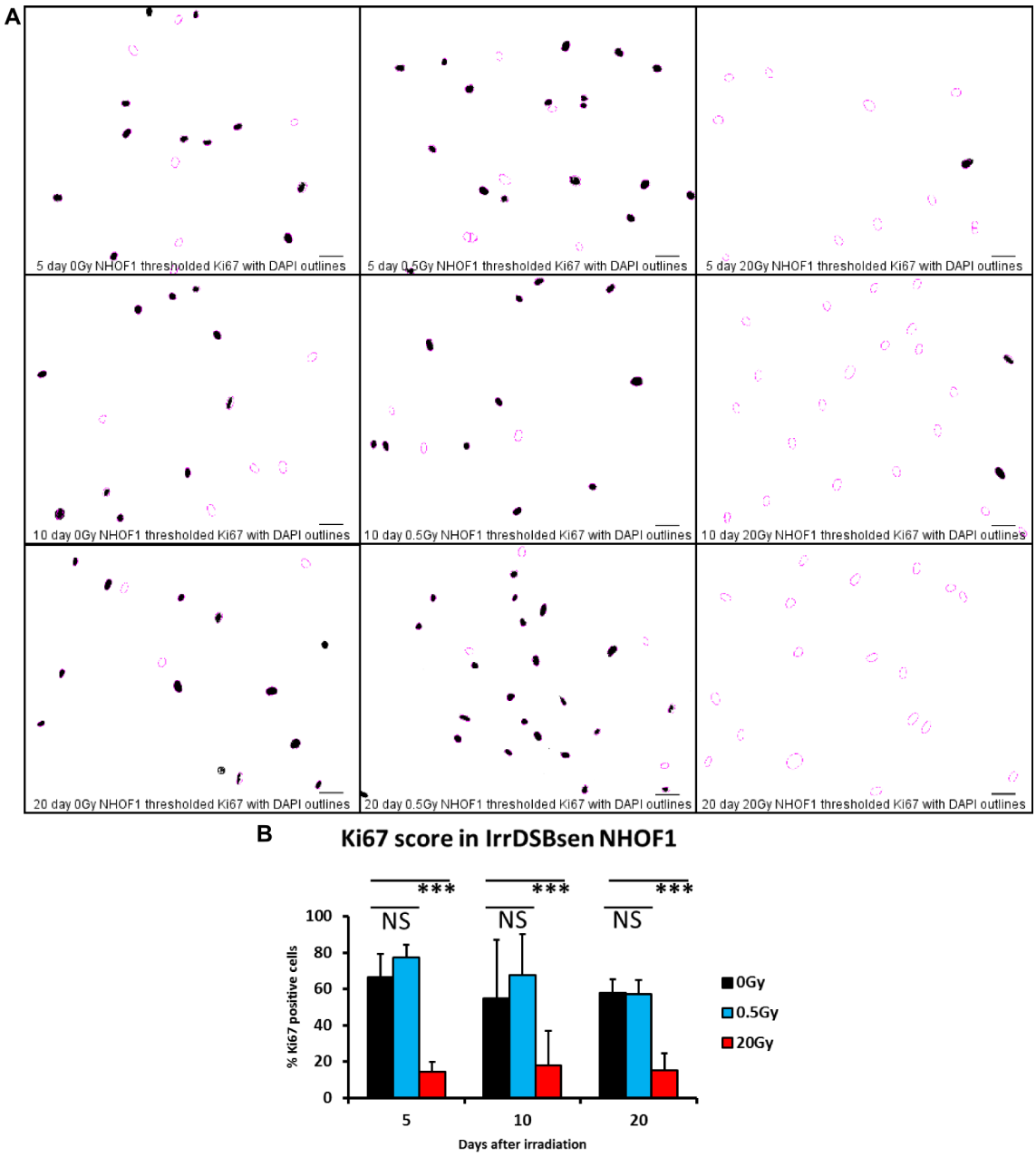

Figure 2.13: **A** Thresholded Ki67 staining of NHOF1 cells 5, 10 and 20 days after exposure to 0Gy, 0.5Gy and 20Gy, showing nuclear regions of interest (identified using DAPI) shown as magenta outlines. **B** Average percentage Ki67 positive NHOF1 cells 5, 10 and 20 days after exposure to 0Gy, 0.5Gy and 20Gy. Error bars represent standard deviation from the mean, n=3 NS= not significant ***$p<0.001$ with 2 way ANOVA using Tukey's post hoc analysis.

Further assessment of replicative potential was made using the marker MCM7, showing that in IMR90 the decline in MCM7 following 20Gy gamma radiation is statistically significant at just 5 days (figure 2.14) and a similar pattern is seen in NHOF1 although

it was not statistically significant (figure 2.15).

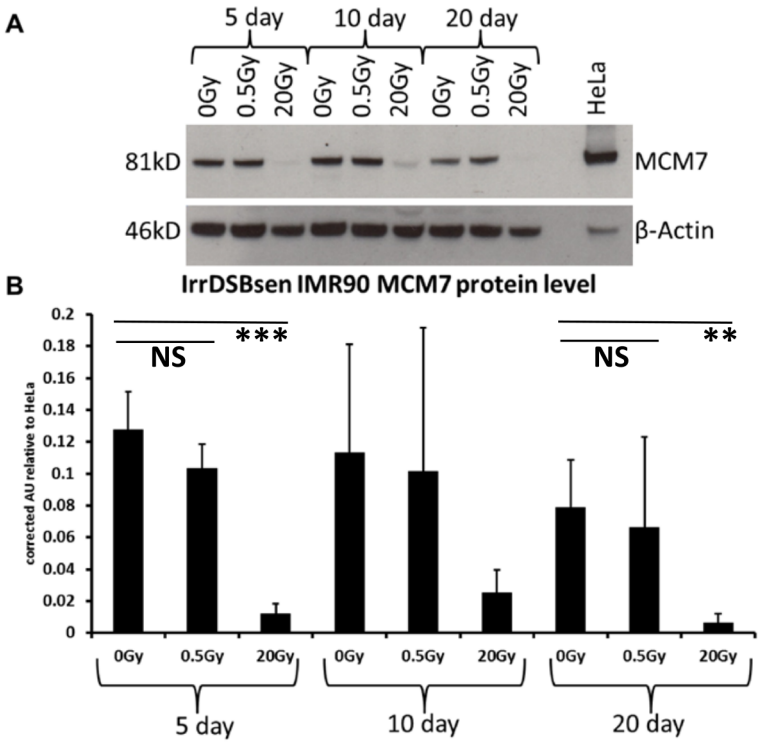

Figure 2.14: **MCM7 protein levels in IrrDSBsen IMR90 A** western blot showing MCM7 protein levels in IMR90 cells treated with 0Gy, 0.5Gy and 20Gy on days 5, 10 and 20 after treatment. **B** Average MCM7 protein levels in IMR90 cells treated with 0Gy, 0.5Gy and 20Gy on days 5, 10 and 20 after treatment. Error bars represent standard deviation from the mean. For day 10 0Gy and 0.5Gy n= 2, for all other points n=3. NS = not significant ***p<0.001 **p<0.01 with a 1 way ANOVA and Tukey's post hoc analysis (on 5 day and 20 day data points only)

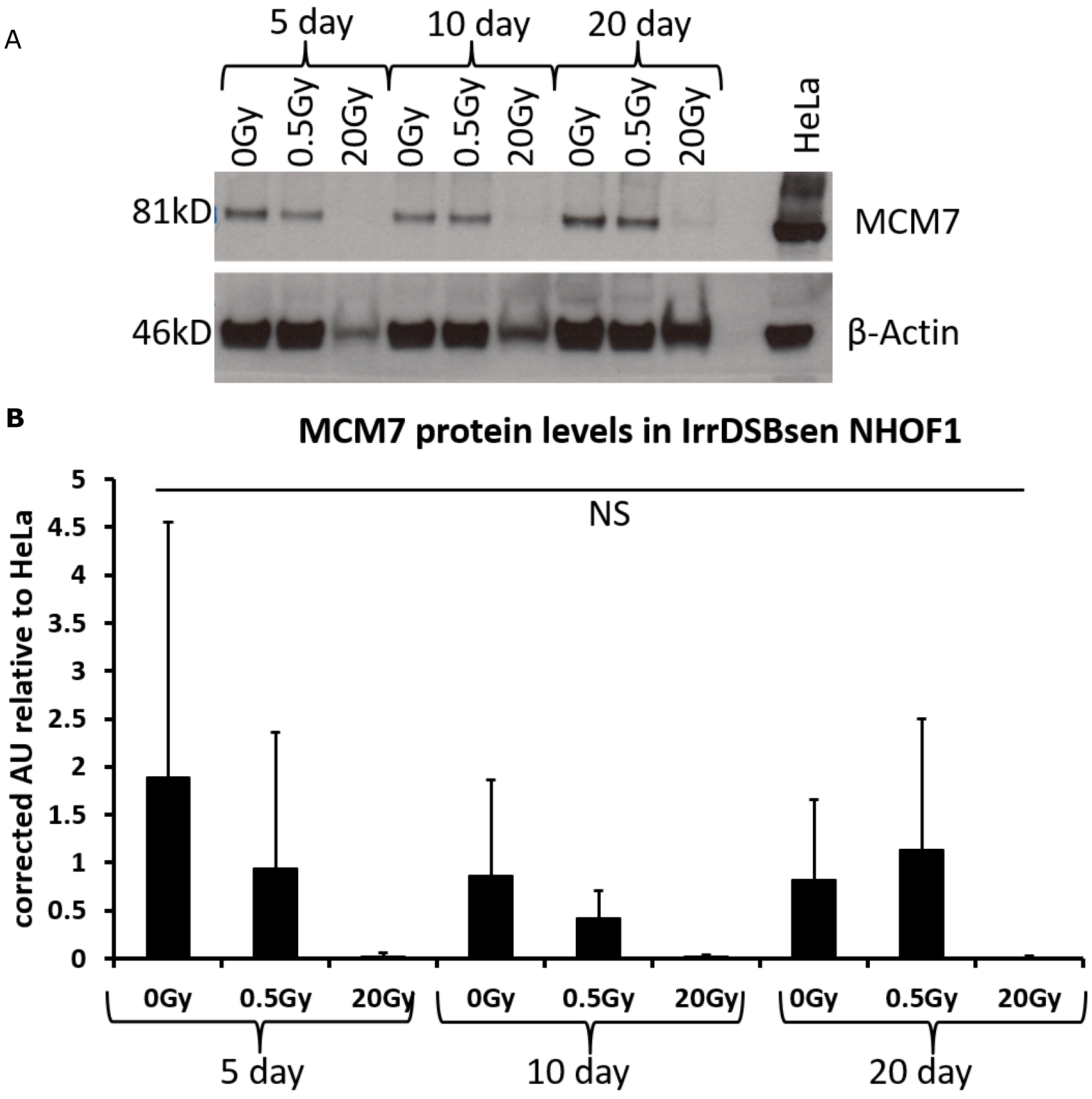

Figure 2.15: **MCM7 protein levels in IrrDSBsen NHOF1 A** Representative western blot showing MCM7 protein levels in NHOF1 cells treated with 0Gy, 0.5Gy and 20Gy on days 5, 10 and 20 after treatment. B Average MCM7 protein levels in NHOF1 cells treated with 0Gy, 0.5Gy and 20Gy on days 5, 10 and 20 after treatment. Error bars represent standard deviation from the mean, n=3. NS= not significant with a 2 way ANOVA with Tukey's post hoc analysis

2.3.2.4 Senescence inducing mechanism (DDR)

53BP1 staining shows an induction of DNA double strand breaks by day 5 that are sustained for the 20 day time period in the 20Gy treatment group but not in the 0Gy or 0.5Gy populations in both IMR90 and NHOF1, a trend which was not statistically

significant in IMR90 (figure 2.16) but was highly statistically significant in NHOF1 (figure 2.17).

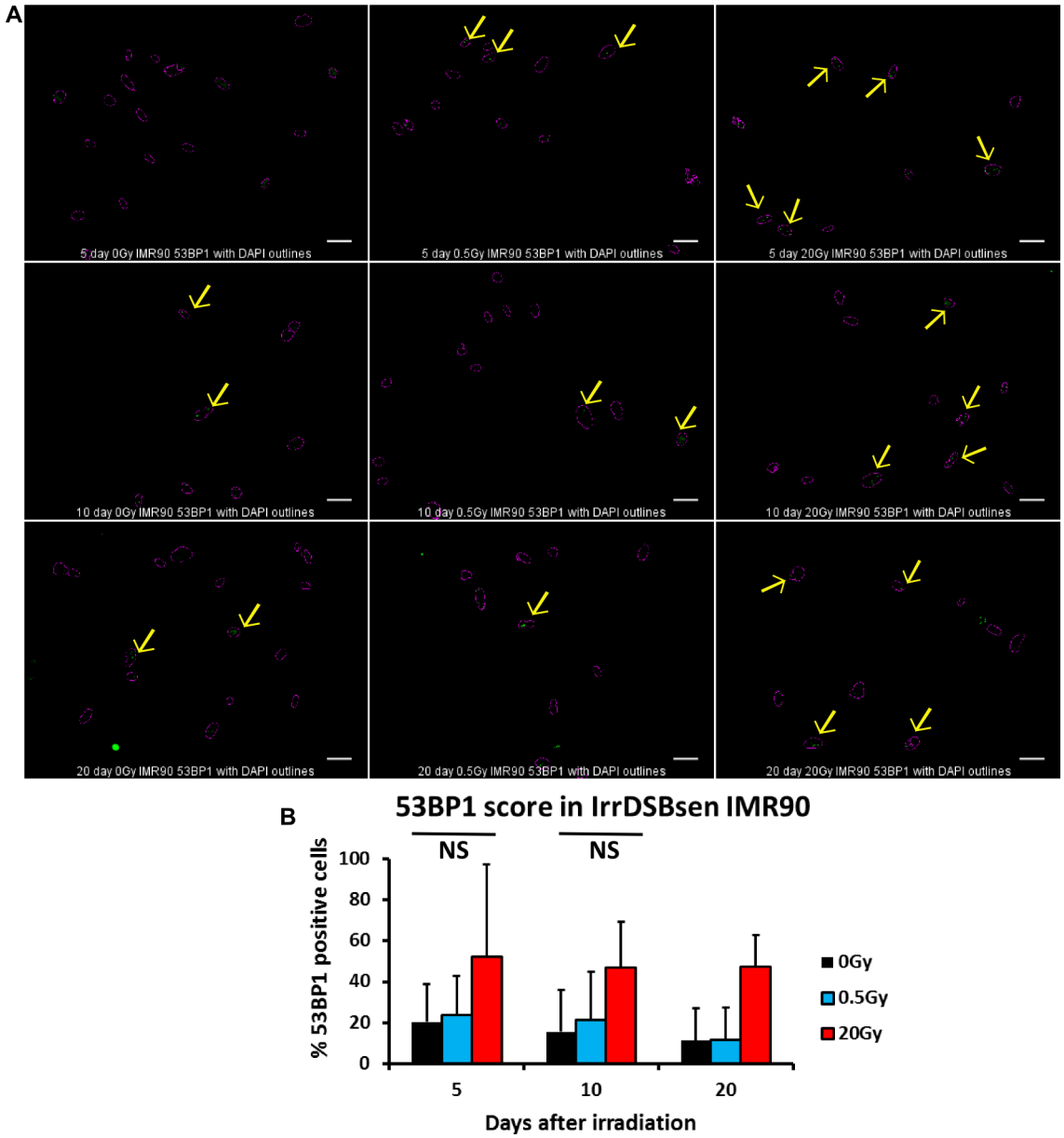

Figure 2.16: **53BP1 staining in IrrDSBsen IMR90 A** ImageJ nuclear overlays (magenta dotted lines) on 53BP1 foci (green, highlighted by yellow arrows) in IMR90 after 0, 0.5 or 20Gy ionising radiation on 5, 10 and 20 day time points. Scale bar represents 50µm. **B** shows the mean score for each group across three repeats. Error bars represent standard deviation from the mean, n=3 in 5 and 10 day groups, n=2 in day 20 group due to damage on the slide. NS = not significant with 1 way ANOVA.

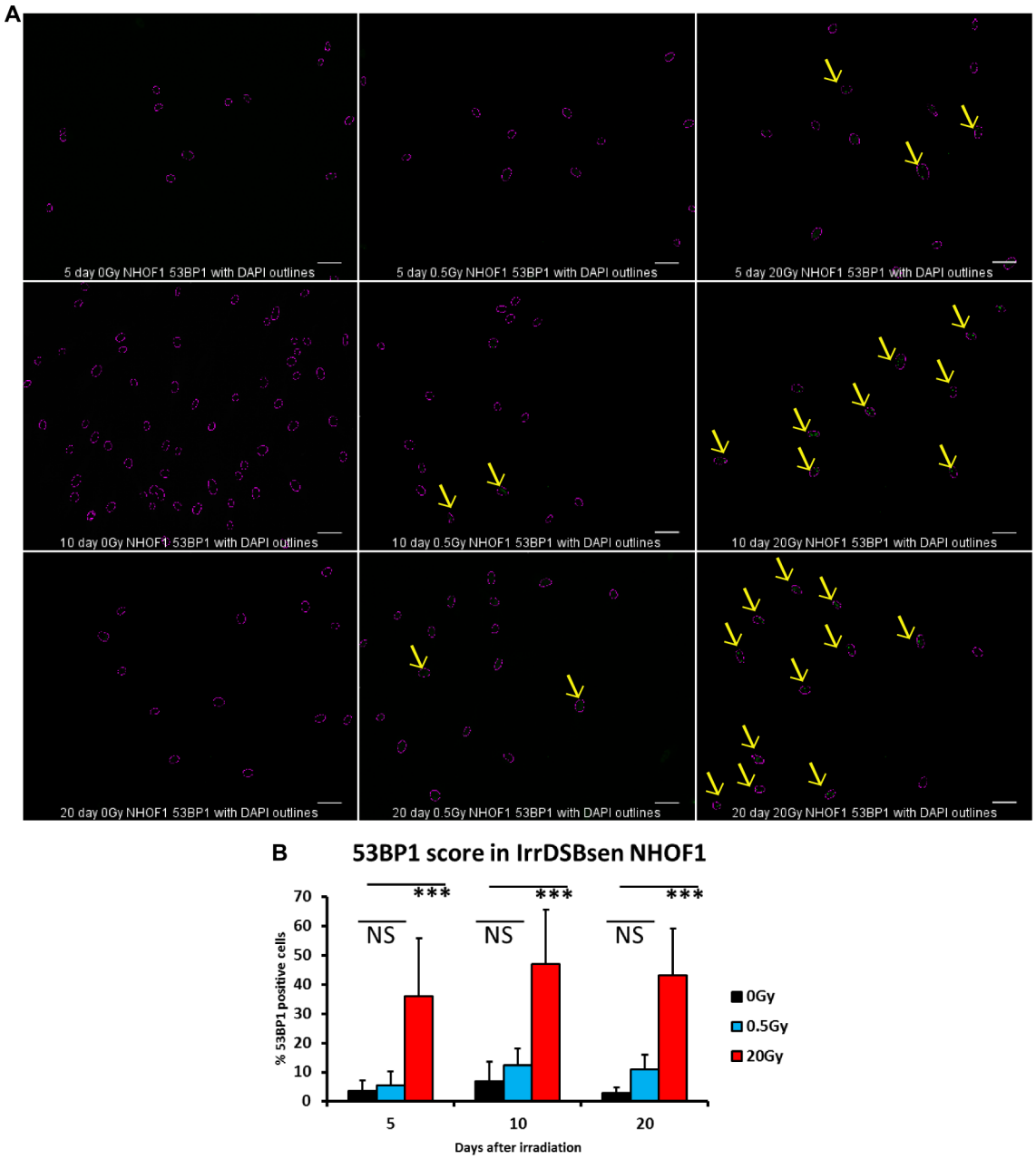

Figure 2.17: **53BP1 staining in IrrDSBsen NHOF1 A** ImageJ nuclear overlays (magenta dotted lines) on 53BP1 foci (green, highlighted by yellow arrows) in NHOF1 after 0, 0.5 or 20Gy ionising radiation on 5, 10 and 20 day time points. Scale bar represents 50µm. **B** shows the mean score for each group across three repeats. Error bars represent standard deviation from the mean. NS = not significant ***$p<0.001$, 2 way ANOVA with Tukey's post hoc analysis.

2.3.2.5 Cell cycle inhibition

Protein levels of the cell cycle inhibitor $p16^{INK4A}$ were measured using western blot. $p16^{INK4A}$ levels did appear to increase in IMR90 cells following irradiation with 20Gy however the trend was weak and not statistically significant (figure 2.18) and $p16^{INK4A}$ was undetectable in NHOF1 (figure 2.19).

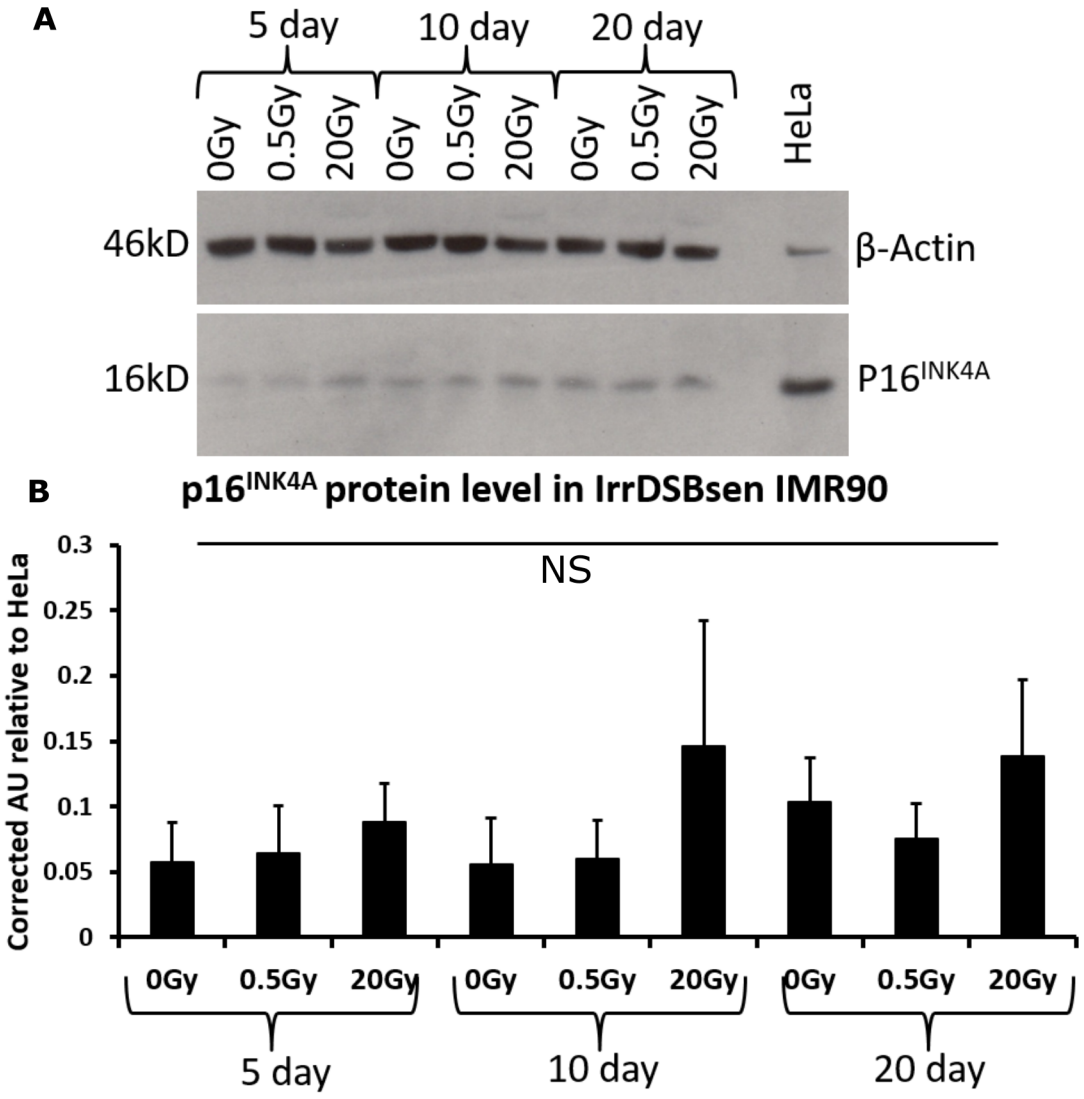

Figure 2.18: **p16^{INK4A} protein levels in IrrDSBsen IMR90 A**. Representative western blot of IMR90 lysate showing a slight increase in p16^{INK4A} levels over time and with 20Gy gamma irradiation, and the loading control β-actin. **B** shows densitometry analysis of 3 biological repeats of the same treatment, relative to the same HeLa lysate on each blot and corrected for loading against beta actin. Error bars represent standard deviation from the mean. n=3 NS = not significant with 2 way ANOVA.

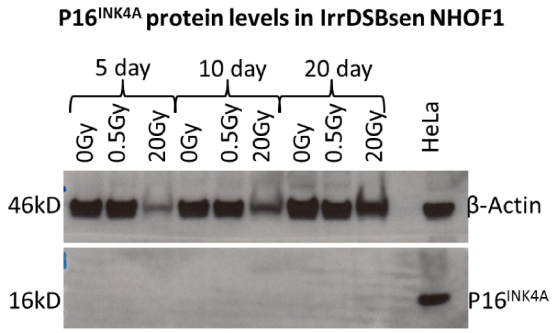

Figure 2.19: **p16INK4A protein levels in IrrDSBsen NHOF1**. Representative western blot of $p16^{INK4A}$protein levels in IrrDSBsen NHOF1 cells. No signal was detected from any of the NHOF1 lysates so no quantification has been carried out. n=3.

2.4 Discussion

This chapter set out to characterise the models of senescence used in this thesis, to ensure that information gained in later experiments regarding the metabolome can be interpreted as accurately as possible. By employing the growth arrest controls confluence and serum starvation, as well as the irradiation exposure control 0.5Gy, all of which have been shown in this chapter to show markers of growth arrest but not DNA double strand breaks or senescence, greater confidence can be placed in the outcomes of the experiments in the remainder of the thesis.

2.4.1 Differences in the population doubling rate and SAβ-gal activity between both senescence induction modes and cell lines

Firstly, it was observed that both the PEsen and IrrDSBsen cells had an extremely slow doubling rate compared to young and unirradiated controls. The growth of the IrrDSBsen cells was slower than the PEsen cells, as can be seen when comparing figure 2.2 on page 99 with figure 2.9 on page 105. This could be because the PEsen population is likely to be a heterogeneous mix of cells ranging from some which are still dividing,

some which are just entering senescence and some which are fully senescent, whereas the IrrDSBsen population of cells all received the same strong, senescence inducing stimulus at the same time so the growth arrest is much more synchronous. This may be an important observation to consider later when comparing the metabolomes of the two models.

Next we considered the morphology of the PEsen and IrrDSBsen populations, by looking at phase contrast images of cells stained for SAβ-gal activity. In both IMR90 and NHOF1 cells the PEsen population comprised cells with a larger cell size and a statistically significantly higher percentage positive for SAβ-gal activity whereas the growth arrest controls retained their normal size and did not have significantly elevated levels of SAβ-gal activity compared to growing controls (see figure 2.3 on page 100). There is a difference between the cell lines in terms of intensity of staining and total percentage of cells that stained positive; the young growing IMR90 population had an average of just under 10% of cells positive for SAβ-gal activity, whereas the young growing NHOF1 population had 0%, which was increased with PEsen to over 90% positive in IMR90 compared to 25% positive in NHOF1. This observation could reflect a difference in the lysosome compartment of the cells generally or it could suggest the IMR90 cells are more senescent generally. Further insight into this observation can be gained by looking at figures 2.10 on page 106 and 2.11 on page 107, which show the SAβ-gal staining of IrrDSBsen IMR90 and NHOF1 and the 0.5Gy reversible strand break control compared to growing cells. Both cell lines have a significant increase in SAβ-gal activity following 20Gy gamma which is evident after 10 days but is at its highest after 20 days. As with the PEsen model, IMR90 cells have a higher baseline SAβ-gal activity than NHOF1, and interestingly the IrrDSBsen NHOF1 cells averaged over 60% positive for SAβ-gal activity compared to just 25% in the PEsen population suggesting that the IrrDSBsen NHOF1 population is generally more senescent than the PEsen population. This supports the theory that the rate of growth was even slower in IrrDSBsen cells than in PEsen cells because a larger proportion of the cells

are fully senescent. Comparing the two cell lines it is also evident that there are some underlying differences between IMR90 and NHOF1 in terms of rate of doubling and SAβ-gal activity. These observations taken together suggest that the IMR90 population may be physiologically older than the NHOF1 population, or may be more sensitive to senescence inducing stimuli. Importantly, the growth arrest controls for both PEsen and IrrDSBsen in both IMR90 and NHOF1 were found to be not significantly different to the growing controls, regardless of the baseline SAβ-gal activity.

2.4.2 Proliferative potential

Ki67 staining was used to assess the percentage of cells in cycle. Unfortunately Ki67 data on PEsen was only obtained for NHOF1, so we cannot compare PEsen Ki67 levels between the two cell lines, or between the two induction mechanisms for IMR90. In NHOF1 Ki67 decreased more drastically at 20 days after 20Gy (IrrDSBsen) than in the equivalent senescent model PEsen, as we would expect based on the relative growth rates and SAβ-gal activity of the populations. Despite the decrease in Ki67 in PEsen NHOF1 not being statistically significant relative to growing controls, there is a clear trend and importantly there was also a decline in Ki67 levels in both the confluence and serum starved growth arrest controls, indicating that the conditions used are creating populations of cells more phenotypically similar to senescent cells than growing cells. The IrrDSBsen model in NHOF1 appears to give a more robust decrease in Ki67 staining across all time points which was statistically significant and also importantly there was no statistical difference in the Ki67 levels in the 0Gy growing control and the 0.5Gy irradiation/repairable DNA double strand break control indicating that the damage is indeed reversible and does not induce senescence.

The Ki67 score in the IrrDSBsen IMR90 cells was not significantly different to 0Gy or 0.5Gy controls until the 20 day time point, unlike in NHOF1 cells. This maintenance of Ki67 in IrrDSBsen IMR90 relative to controls is quite puzzling, as the cells were exhibiting several other signs of being senescent from a much earlier point. As the

presence of Ki67 only tells us the cells are not in G_0 it is possible that more of the cells had arrested at some other point in the cycle. Another factor that certainly influenced this result, is the fact that the percentage of cells positive for Ki67 in the 0Gy and 0.5Gy control groups is lower on days 5 and 10 than on day 20, so the perceived decrease in Ki67 in 20Gy treated cells after 20 days is more attributable to an increase in Ki67 in the 0Gy control rather than a large decrease in the 20Gy group, although the experiment was repeated 3 times and at days 5 and 20 there is little variation between the data from the repeats suggesting that this pattern is not a result of experiment variation. As we have already seen from the population growth rate and SAβ-gal, IMR90 cell populations likely have a higher proportion of senescent cells, so the observation that the 0Gy and 0.5gy have generally lower levels of Ki67 than the equivalent NHOF1 cell populations is not surprising.

MCM7 protein levels are also an indicator of proliferative potential as it is a protein required for replication fork formation, and should be independent of which phase cells have arrested in. MCM7 protein levels should therefore help to ascertain whether there are indeed more growth arrested cells in the control populations of IMR90 cells, in which case the MCM7 levels in those controls would be low relative to a positive control (HeLa) and relative to NHOF1. Indeed for PEsen, figure 2.5 on page 102 demonstrates that IMR90 growing cells have roughly half the level of MCM7 protein expression seen in NHOF1, when both are compared to HeLa. Both lines show the same trend for decrease of MCM7 in PEsen relative to growing cells, although the relationship was not statistically significant in either cell line. In IMR90 both growth arrest controls retained higher levels of MCM7 on average than the PEsen group, indicating that they have not lost the potential to proliferate despite being growth arrested. In NHOF1 the serum starved cells retained high levels of MCM7 however on average the confluent cells did exhibit a reduction in MCM7 protein levels similar to those seen in the PEsen group. It is probable that the variability is due to the dynamic nature of transient growth arrest; although much effort was given to optimising the conditions so that cells were

just growth arrested, but not engaging senescence entry mechanisms, it is very difficult to get populations of cells consistently within the narrow phenotype requirements when externally they look practically identical to growing cells. The variability would almost certainly reduce with a larger sample size, however under the time constraints it wasn't possible to achieve.

The decline in MCM7 levels in 20Gy but not 0.5Gy relative to 0Gy in the IrrDSBsen model was more obvious, and in the case of IMR90 was statistically significant (see figure 2.14 on page 110). There was considerable variation in the NHOF1 MCM7 protein levels and as a result the 20Gy specific decline in MCM7 was not statistically significant but the trend is still clear.

So far the data suggests that the senescence induction methods have been successful in causing an increase in the number of growth arrested cells in the population which have lost the potential to replicate, and that the growth arrest control conditions serum starvation and confluence have also caused a growth arrest, but one that is not permanent as the cells retained markers of proliferative potential. Next we looked at whether there was evidence of a DDR occurring in our PEsen an IrrDSBsen populations as well as their associated controls.

2.4.3 Evidence of a DDR

The DNA damage repair protein 53BP1 is recruited to sites of DNA damage so immunostaining of this protein was used to assess DNA damage response foci. Again unfortunately data on 53BP1 in PEsen was only collected for NHOF1, so we can only make the comparison between PEsen and IrrDSBsen in that cell line. In PEsen NHOF1 it was clearly demonstrated that the DDR was being engaged, as there was a statistically significant increase in the percentage of the population that contained 53BP1 foci in PEsen compared to growing controls and crucially both growth arrest controls contained very similar levels of 53BP1 positive cells to the growing control, confirming that the mild stress used to growth arrest them was not causing damage that could

lead to senescence engagement via DDR (figure 2.6 on page 103).

In NHOF1 IrrDSBsen there was a slight elevation in the number of cells treated with 0.5Gy engaging the DDR, although the number was highly statistically significantly different from cells treated with 20Gy, which had much higher levels of DDR positive cells even from day 5. This is consistent with the findings of researchers that much of the DNA damage induced by even 1Gy ionising radiation is resolved within 24 hours(Schultz et al., 2000) and confirms that the 0.5Gy dose is a good control for repairable strand breaks and the irradiation treatment. The sustained elevation in 53BP1 over 20 days strongly suggests that senescence is being induced via a DDR in this model, as we would expect. IMR90 cells subjected to 20Gy and 0.5Gy show the same trend as NHOF1, with an increase in 53BP1 in 20Gy cells from 5 days that is maintained to 20 days compared to 0Gy and a slight increase in 53BP1 in 0.5Gy treated cells compared to 0Gy, however the results were not statistically significant. We can see that the baseline level of 53BP1 in IMR90 is a little higher than in NHOF1, suggesting that the overall slower rate of growth and increased level of SAβ-gal staining could be due to on-going low levels of DNA damage in this cell line.

2.4.4 $p16^{INK4A}$ protein levels

IMR90 PEsen cells showed a large increase in the level of $p16^{INK4A}$ protein expression compared to growing controls; further evidence that the PEsen IMR90 population is largely fully senescent. As expected the growth arrest controls did not cause a significant increase in $p16^{INK4A}$ protein level, demonstrating that the growth arrest induced in these cells is transient and not engaging senescence pathways. In PEsen NHOF1 however no $p16^{INK4A}$ protein could be detected. The presence of a protein band in HeLa demonstrates that there was not a technical issue with the blot or antibody, so the lack of $p16^{INK4A}$ could suggest that PEsen NHOF1 are not fully senescent, although if this were the case we would still expect to some signal in the PEsen population, it could also suggest that NHOF1 are senescing via a $p16^{INK4A}$ independent mechanism. Inter-

estingly a previous student had identified individual $p16^{INK4A}$ positive NHOF1 cells in a less senescent population and additionally it has been informally observed that NHOF1 cell growth rate slows at around 45mpds increasing again until the population undergoes senescence at around 65mpds. One explanation for this could be that a subset of the NHOF1 population is $p16^{INK4A}$ positive; these cells senesce around 45mpds due to elevation of $p16^{INK4A}$ and are outgrown by a $p16^{INK4A}$ negative population which then goes on to senesce through a different mechanism after further population doubling. Unfortunately there was not time to investigate this result further.

No $p16^{INK4A}$ was detected in IrrDSBsen NHOF1 either, and even in IMR90 which are known to have constituently high levels of $p16^{INK4A}$ the build up of $p16^{INK4A}$ was not very substantial, as can be seen from figure 2.18. Again this result cannot be put down to any problems with the blot or antibody, because the HeLa lysate repeatedly gave good signal as shown in the representative blots in figures 2.18 and 2.19, therefore it appears likely that the IrrDSBsen induction mechanism does not require elevation of $p16^{INK4A}$.

2.4.5 Summary

The aims of this chapter were to characterise the phenotype of the models used in this thesis and verify that the controls showed signs of reversible growth arrest. These aims were largely met; both PEsen and IrrDSBsen models showed signs of permanent growth arrest induced via DNA double strand breaks, while the growth arrest controls serum starvation and confluence showed signs of a transient growth arrest that was not engaging the DDR. The control for irradiation treatment and repairable DNA damage, 0.5Gy gamma radiation, also seems appropriate as there was no long lasting DNA damage response and the populations did not become growth arrested. Some observations were made that will be useful later when comparing the metabolomes of the two senescence models and cell lines, such as the observation that the IMR90 cell populations appear to be harbouring low levels of DNA damage, are slower growing

and senesce via $p16^{INK4A}$ in PEsen but possibly not IrrDSBsen conditions. NHOF1 on the other hand appear to have less senescent cells in the young population, which have lower levels of DNA damage than IMR90, and possibly do not up-regulate $p16^{INK4A}$ in PEsen or IrrDSBsen conditions. Overall in both lines a more robust phenotype was seen in the IrrDSBsen populations compared to the PEsen and this has been attributed to the heterogeneous nature of the PEsen population compared to the IrrDSBsen population. Going forward it will be interesting to see if these differences are reflected in the secreted metabolome.

Chapter 3

The metabolome of senescent fibroblasts

3.1 Introduction

3.1.1 The study of small molecules

The metabolome

Within each cell, every single process is underpinned by chemical reactions in which molecules are precursors, reactants, intermediates, waste products, catalysts and inhibitors; leaving behind a metabolic footprint known as the metabolome. The study of this biochemical signature of cellular processes is called metabolomics.

What the metabolome can uniquely tell us

While genomics has uncovered a wealth of markers that predispose to disease, and transcriptomics and proteomics give us insight into the structure and function of cellular components, it is the addition of information on the metabolome which can ultimately tell us what processes have actually been occurring within the cell. In addition, the use of mass spectrometry coupled to liquid and gas chromatography allows high throughput, accurate identification and quantification of metabolites in small volumes of biological

fluids that can be taken repeatedly from the same subject (for example blood, urine, saliva, and cell culture media), making metabolomics the ideal method to study dynamic biological systems.

Metabolon

Some of the techniques commonly used in the field of metabolomics were outlined in Chapter 1; each technique has its strengths and weaknesses that make it better for detecting certain types of molecule, so when performing untargeted exploratory screens to identify novel biomarkers it is preferable to use multiple platforms to capture as many components of the metabolome as possible. To gather comprehensive and reliable metabolomic profiles of senescent versus growing fibroblasts we sent conditioned media samples to Metabolon, the industry leading commercial metabolomic screening service that uses a proprietary platform called DiscoveryHD4. Using a library of over 4500 known metabolites built from pure reference standards to identify metabolites detected with a combination of GCMS and UHPLC MS/MS in positive and negative detection modes allows rapid, accurate and reproducible metabolite identification, with verification performed by specialist chemical spectral analysts. The aim of using a commercial screening service was to identify the strongest candidates for biomarkers of senescence which could then be followed up on smaller scale using the technology available locally.

3.1.2 Summary

In this chapter the methods used to assess the secreted metabolome of the senescence and growth arrest models described in the previous chapter will be explained, from the untargeted screen performed by Metabolon which was used to identify candidate markers and highlight altered metabolic pathways, to the search for a more local and affordable targeted method of following up these findings.

3.2 Materials and methods

3.2.1 Collection of conditioned media

3.2.1.1 General protocol

On the 18th day following irradiation for IrrDSBsen, or once cells were deemed replicatively senescent for PEsen, cells were counted and re-plated at a density of 5x10^5 cells per T75 flask (Thermo Fisher), in 12mL culture media. The following day (except in the case of the confluent and low serum experiments, the conditions for these collections are detailed below) the media in the flasks was replaced with freshly made DMEM (made as described earlier), with the reduced volume of 3mL per T75 flask. A 3mL aliquot of this freshly prepared media, that had not been exposed to cells, was centrifuged and frozen in exactly the same manner as outlined below for the samples, to act as a control for the baseline media constituents. The flasks were allowed to equilibrate to 10% CO_2 /90% air in the 37°C incubator before being sealed with Parafilm to prevent evaporation. The flasks were then incubated for 24 hours to allow the media to become conditioned, before the media were collected into 30mL tubes and centrifuged at 800xg for 2 minutes to remove any dead cells or other debris. The media were then split between 3 or more Eppendorf tubes as 1mL aliquots and centrifuged again at 13,000 rpm in a microfuge. The media was then transferred to fresh Eppendorf tubes and snap frozen in a bath of EtOH/dry ice for at least 15 minutes before being transferred to a -80°C freezer for storage.

3.2.1.2 Growth arrest control: Confluence

The protocol for collection of the media from the confluent cells, which were used as a control for growth arrest, required slightly more time between plating of the cells and the start of the collection period, to enable the cells to become properly confluent and growth arrested. This protocol was optimised to get as many cells growth arrested (Ki67

negative) as possible whilst also not allowing irreparable DNA double strand breaks to develop (the cells must also be negative for large 53BP1 foci), and the optimum conditions were found to be plating the cells 4 days before collection was due, and replenishing the media every day within that time. Media volume added to the flasks during the collection period was increased to produce a cell number:volume ratio as similar as possible to that found in the other flasks with cells growing at the usual density.

3.2.1.3 Growth arrest control: Serum starvation

Transient growth arrest induced by serum starvation in low serum media also required optimisation to get as many growth arrested cells as possible without inducing irreparable DNA double strand breaks. Cells were plated four days before collection was due, 24 hours after plating the cells were washed with 1xPBS and media was replaced with DMEM containing additional glutamine and antibiotics as in the standard media but containing only 0.1% vol/vol foetal calf serum.

3.2.2 Collection of cell pellets

Cell pellets were always collected at the same time as the conditioned media, or under identical conditions. Cells were seeded at a density of $5x10^5$ cells per T75 flask and the following day the media was replaced with 3mL freshly made media. Flasks were allowed to equilibrate to 10% CO_2/90% air before being sealed with Parafilm to prevent evaporation. 24 hours later, after the removal of the medium, the cells were washed with warm 1x PBS and incubated at room temperature with 1mL trypsin/EDTA solution (as previously described) while the media was being processed. Incubating the cells in the trypsin at room temperature rather than at 37°C slowed the action of the trypsin slightly and allowed more time to process the media before the cells detached fully.

Following detachment the trypsin was neutralised by addition of 3mL serum containing media and the cells were counted. The cell suspension was then centrifuged at 800 rpm for 5 minutes to produce a cell pellet, which was re-suspended in 1mL 1xPBS and transferred to an Eppendorf tube. A pellet was obtained by centrifuging the cell suspension at 13,000 rpm in a microfuge for 5 minutes and the PBS was aspirated, then the pellet was snap frozen on EtOH/dry ice and stored at -80°C.

3.2.3 Metabolon's analysis platforms

Metabolon is a leading commercial metabolomics phenotyping company based in the USA with proprietary analysis platforms and informatics systems that offer the most comprehensive metabolomics platform for screening biological samples available. The protocols used to prepare and analyse the samples we sent are as follows (adapted from descriptions provided by Metabolon):

3.2.3.1 Sample Preparation

Samples were thawed and a recovery standard was added prior to protein removal by precipitation with methanol of a 100µl (this process was performed using the automated MicroLab STAR® system from Hamilton Company). The resulting extract was divided into four fractions: one for analysis by UPLC/MS/MS (positive mode), one for UPLC/MS/MS (negative mode), one for GCMS, and one for backup. Samples were placed briefly on a TurboVap (Zymark) to remove the organic solvent. Each sample was then frozen and dried under vacuum. Samples were then prepared for the appropriate instrument, either UPLC/MS/MS or GC/MS.

3.2.3.2 UPLC/MS/MS

The LC/MS portion of the platform was based on a Waters ACQUITY ultra-performance liquid chromatography (UPLC) and a Thermo-Finnigan linear trap quadrupole mass spectrometer, which consisted of an ESI source and linear ion-trap mass analyser. The sample extract was reconstituted in acidic or basic LC-compatible solvents, each of which contained 8 or more injection standards at fixed concentrations to ensure injection and chromatographic consistency. One aliquot was analysed using acidic positive ion optimized conditions and the other using basic negative ion optimized conditions in two independent injections using separate dedicated columns. Extracts reconstituted in acidic conditions were gradient eluted using water and methanol containing 0.1% vol/vol formic acid, while the basic extracts, which also used water/methanol, contained 6.5mM ammonium bicarbonate. The MS analysis alternated between MS and data-dependent MS/MS scans using dynamic exclusion.

3.2.3.3 GCMS

The samples for GCMS analysis were re-dried under vacuum desiccation for a minimum of 24 hours prior to being derivatised under dried nitrogen using bistrimethyl-silyl-triflouroacetamide. The GC column was 5% phenyl and the temperature ramp was from 40° to 300° C in a 16 minute period. Samples were analysed on a Thermo-Finnigan Trace DSQ fast-scanning single-quadrupole mass spectrometer using electron impact ionization. The instrument was tuned and calibrated for mass resolution and mass accuracy on a daily basis.

3.2.3.4 Quality assurance

Additional samples were included with each day's analysis. These samples included extracts of a pool created from a small aliquot of the experimental samples and process

blanks. Quality control (QC) samples were spaced evenly among the injections and all experimental samples were randomly distributed throughout the run. A selection of QC compounds was added to every sample for chromatographic alignment, including those under test. These compounds were carefully chosen so as not to interfere with the measurement of the endogenous compounds.

3.2.3.5 Data extraction and compound identification

Raw data was extracted, peak-identified and QC processed using Metabolon's hardware and software. These systems are built on a web-service platform utilizing Microsoft's .NET technologies, which run on high-performance application servers and fibre-channel storage arrays in clusters to provide active failover and load-balancing. Compounds were identified by comparison to library entries of purified standards.

3.2.3.6 Data analysis

The profile of a sample of unconditioned media (collected at the beginning of the media conditioning period) was subtracted from the profile of conditioned media samples, to give an indication of whether metabolites were being secreted or depleted in the conditioned media. The scaled intensity values for each metabolite were then normalised to the average cell count over the collection time period.

Principal components analysis

The un-targeted metabolomic screens performed by Metabolon provided a huge amount of data; turning this overwhelmingly large collection of numbers into a wealth of information was made possible using multivariate analysis. The primary method used was Principal Components Analysis (PCA), which is a dimension reduction technique that transforms correlations in the data into new variables (latent variables, or components)

and lists them in descending order based on how much of the total variance in the data is represented by that component. PCA aims to reduce the number of variables by creating components that explain as much of the variance as possible. Often, 80-90% of the variance in a data set can be explained by the first 4 or 5 components, which are referred to as the "principal components". By looking at what original variables caused the separation of these components (which variables loaded onto which components, described by the loading scores) it is possible to identify which metabolites were different between the control groups and the senescent groups. This analysis was performed by Metabolon.

Random forests analysis

Random forests is a supervised machine learning technique that uses a subset of the available data, which has identifying true class information associated with it, to construct a "training tree" that the remaining data, known as the "out-of-bag" (OOB) variables, are passed down to obtain a class prediction for each variable (in this thesis the variables are levels of metabolites, and the classes are the cell groups i.e. senescent versus growing). This process is repeated thousands of times, using all of the data but never passing data used to create a tree down that particular tree, to produce the forest. The final classification of each sample is determined by computing the class prediction frequency ("votes") for the OOB variables over the whole forest. For example, if the random forest consists of 50,000 trees; 25,000 of which had been used to make a prediction for sample 1, and of the 25,000, 15,000 trees classified the sample as belonging to Group A and the remaining 10,000 classified it as belonging to Group B, then the votes are 0.6 for Group A and 0.4 for Group B, so the final classification will be Group A. This method is unbiased, because the prediction for each sample is based on trees built from a subset of samples that do not include that sample. When the full forest is grown, the class predictions are compared to the true classes, generating the "OOB error rate" as a measure of prediction accuracy. The prediction accuracy can therefore

be used as an unbiased estimate of how well sample class can be predicted in a new data set.

To determine which metabolites make the largest contribution to the classification, a "variable importance" measure is calculated. Metabolon used the "Mean Decrease Accuracy" (MDA) as this metric. The MDA is determined by randomly altering a variable, running the observed values through the trees, and then reassessing the prediction accuracy. If a variable is not important, then this procedure will have little change in the accuracy of the class prediction (permuting random noise will give random noise). By contrast, if a variable is important to the classification, the prediction accuracy will drop if that variable is changed, and this is recorded as the MDA. The result is an "importance" rank ordering of biochemicals; typically the top 30 biochemicals are given as the output of the analysis, forming a list of metabolites that are potentially worthy of further investigation.

3.2.4 Enzymatic quantification of lactate

Extracellular lactate was quantified using an enzymatic assay from BioAssay Systems (Enzychrom L-Lactate Assay Kit ECLC-100). Frozen aliquots of conditioned media as well as the blank media controls were thawed on ice, and kept on ice at all times. A standard curve of L-Lactate at concentrations ranging from 0 to 1mM was prepared in serum free DMEM. Media samples were diluted in distilled water 4 or 8 times. Corresponding diluted media and serum free media controls were also used. Initial testing showed that endogenous enzyme activity in the media was negligible/ non-existent. Diluted media samples were added to clear, flat bottomed 96 well plates (Primaria 353872, BD Falcon) in triplicate. A reaction mix containing Assay Buffer, 3-(4,5-dimethylthiazol-2-yl)-2,5-diphenyltetrazolium bromide (MTT), NAD, and an enzyme mix was then added, and a time zero (T0) measurement at 565nm was taken using a plate reader (Fluostar Optima, BMG Labtech). After 20 minutes incubation at room temperature a second measurement was taken at 565nm. The T0 measurement was sub-

tracted from final measurement, and relevant media controls subtracted from sample measurements before the results were multiplied by relevant dilution factors and original concentrations derived from the equation of the line of the standard curve. Values were corrected for cell number.

3.2.5 Quantification of citrate

3.2.5.1 Enzymatic assays

The Citrate Colorimetric/Fluorometric Assay Kit was obtained from BioVision (K655-100). For the colorimetric assay, conditioned and unconditioned media were diluted 1:10, 1:50 and 1:100 in Assay Buffer and a standard curve of 0 to 10nmol/ well prepared. All were added to a clear flat bottomed 96 well plate (Primaria 353872, BD Falcon) in triplicate and a reaction mix containing buffer, enzyme mix, developer and probe was then added. The plate was protected from light for the incubation period of 30 minutes at room temperature. Absorbance was measured at 570nm (Fluostar Optima, BMG Labtech), and the concentration of citrate in the samples was determined from the standard curve. The blank media values were subtracted from all conditioned media values before being corrected for cell number. For the fluorescent assay, samples were not diluted and a slightly different range of standard curve of citrate, ranging in concentration from 0 to 1nmol/well, was used. The samples were added to a black 96 well plate (Nunclon Delta Black microwell S1), and the reaction mix was then made and added in the same way as for the colorimetric assay. The plate was protected from light and incubated at room temperature for 30 minutes before being read in a fluorescence plate reader (Fluostar Optima, BMG Labtech) at excitation wavelength 535nm, emission 587nm. The concentration of citrate in the conditioned media samples was determined from the standard curve, and again unconditioned blank media values were subtracted from conditioned media values and finally the values were corrected for cell number.

3.2.5.2 Precipitation of citrate

Citrate has been successfully quantified in urine using a precipitation method, so we decided to see if it would be sensitive enough to work with culture media using a method described by Lewis (Lewis, 1990). A standard curve was made using sodium citrate dehydrate (Sigma) ranging from 0 to 4.5mM in unconditioned cell culture medium. To each 4mL sample of conditioned cell culture medium 100µl 25% vol/vol NH_4OH (Sigma) was added, the samples were mixed by vortexing before addition of 900µl 0.2M $MgCl_2$ and then centrifuged at 4000xg for 10 minutes to remove phosphates. The supernatant was transferred to a fresh tube and the pH was adjusted to 2.0 with HCl. Then, 250µl 18mM $FeCl_3$ was added and the tubes were mixed by vortexing, before 200µl was transferred to a clear, flat bottomed, 96 well plate and the absorbance was immediately read at 390nm (Fluostar Optima, BMG Labtech). The citrate concentration was determined from the standard curve.

3.2.5.3 Proton Nuclear Magnetic Resonance (1H NMR)

1H NMR uses the nuclear magnetic resonance of hydrogen -1 nuclei (the absorption and re-emission of a pulse of electromagnetic radiation by the hydrogen nuclei) to generate a spectrum of peaks that vary depending on the electron environment of each hydrogen in a molecule. From these spectral signatures molecules can be identified, and, because the intensity of the peaks are proportional to the number of hydrogens present, the number of molecules can be quantified when a standard of known concentration is run. Here 4,4-dimethyl-4-silapentane-1-sulfonic acid (DSS) was chosen because it is highly water soluble and its extremely low electronegativity means its peak occurs at much lower chemical shift than any naturally occurring molecules, so is not overlapped by anything in the samples. Because the resonance frequency of the 1H nucleus (or indeed any nucleus) is proportional to the magnetic field strength, it is vital that the field strength remains stable and to facilitate this deuterium oxide (D2O) was added to the samples. D2O resonance can be continuously detected in a different channel to the 1H resonance because the resonance frequencies are very different, and this signal is

used by the spectrometer to inform a feedback loop that adjusts the current accordingly to maintain a stable field strength during the acquisition of the 1H resonance.

600µl of sample medium was added to a NMR tube with 10% vol/vol D2O (151882 lot#STB04343V, Sigma Aldrich) and 10% weight/vol DSS (DLM-32-1 lot# I-15653 Cambridge Isotope Laboratories, Inc.). Tubes were taken on wet ice directly to the NMR facility in the Joseph Priestley Building, School of Biological and Chemical Sciences, Queen Mary University of London. Data were acquired by Dr. Harold Toms with Bruker AV600; 600 MHz using 5mm inverse/BB auto-tuning probe with Z gradient, using the software package TopSpin. The signal from the water in the media, which was the main constituent of the samples, was suppressed, the signals Fourier transformed, and the base line and phase were corrected, using TopSpin. Peaks were identified in MNova Lite by comparing blank media to media containing sodium citrate, and confirmed by comparing to reference peaks in the human metabolome database (HMDB) (Wishart et al., 2013).

3.2.5.4 Targeted GCMS

A collaboration was set up with the laboratory of Dr Jake Bundy at Imperial College London. There I was shown how to derivitise the samples by Dr Sarah Davies, and a detection method was developed with Mr. Mark Bennett.

GCMS requires the molecule(s) of interest to be volatile, thermally stable, and to not have functional groups that can be adsorbed onto the injector. For this reason the sample needed to be derivatised (chemically altered) to ensure reproducible peak heights and shapes for citrate. Two derivitising agents were chosen; methoxyamine hydrochloride, which reacts with carbonyl groups to form an oxime derivative, and n-methyl-n-(trimethylsilyl) trifluoroacetamide (MSTFA), which replaces active hydrogens on OH, NH or SH groups with a silyl group. In order for the MSTFA to be effective at derivitising the molecules of interest all the water needed to be removed from the sample, otherwise the abundance of active hydrogens in the water would make the derivatisation of anything else very inefficient. In addition, to prevent unnecessary

clogging of the injector, proteins also needed to be removed from the samples which was done by precipitation with methanol. Just as with NMR, an internal standard of known concentration (deuterated citrate at 0.1mM final concentration) was added to each sample at the beginning of the sample preparation process so that any loss of the sample due to problems during the sample preparation or GCMS itself could be accounted for. To make the assay quantitative, a calibration curve of 0mM, 0.01mM, 0.05mM, 0.1mM, 0.2mM, 0.4mM, 0.6mM 0.8mM and 1mM citrate was prepared in unconditioned culture media using sodium citrate and extracted, dried, derivatised and run alongside the samples.

Firstly, samples were defrosted on wet ice, randomised, and then mixed by vortexing. 25µl of sample was added to an Eppendorf containing 2.5µl internal standard (1mM $d_4$citrate), before protein was extracted from the solution by addition of 50µl -20°C methanol. The tubes were vortexed again and then centrifuged at 4°C for 10 minutes at 14,000rpm and the precipitated protein pellet was discarded. The supernatants were then transferred to deactivated glass vials (from Agilent, catalogue number 5183-4432) and the samples were either freeze dried over night (this method was used in early experiments until the freeze drier broke) or dried in a SpeedVac (much easier and faster, this method was quickly adopted after the breakdown of the freeze drier) for 30 minutes at 40°C. 20µl 20mg/mL methoxyamine hydrochloride in anhydrous pyridine was added (under a fume hood as pyridine is harmful if inhaled, swallowed, or absorbed through the skin) and the vials were vortexed to mix, briefly centrifuged, then incubated at 30°C for 90 minutes under 1400 rpm agitation in an Eppendorf Thermo Mixer. After another brief centrifugation, 80µl MSTFA + 1% (vol/vol) TMCS in anhydrous pyridine was added to each vial (again in the fume hood), the vials were vortexed and centrifuged again and then incubated at 37°C for 30 minutes under 1400 rpm agitation in the Eppendorf Thermo Mixer. The sample was collected in the bottom of the vial with another brief centrifugation, then using a glass Pasteur pipette each sample was transferred to a deactivated glass insert (Agilent catalog number 5183-2088) which was

then replaced in the vial, so that the injector needle could reach the small sample volume. The samples were then centrifuged once more, and carefully checked for the presence of any precipitate, which could clog the GCMS sample injector. If there was precipitate in the insert, the supernatant was transferred to a new insert without disturbing the precipitate pellet at the bottom.

The GCMS was carried out in pulsed splitless mode on a Hewlett Packard HP6890 series GC system with Agilent 6890 series injector and a 30m long 250μm dimeter capillary column (Agilent, model number 19091s-433HP5MS) using a flow rate of 1mL/minute, and a Hewlett Packard 5973 Mass selective detector. The acquisition was done in either full scan (for example in the optimisation of the method for detecting citrate, and to trouble shoot when the spectra derived looked abnormal) or selective ion monitoring mode (SIM). When in SIM mode the ion masses detected were: 273.0, 350.0, 465.0, 276.0, 375.0, 469.0, 347.0, and 378.0 and the dwell time for all of these ions was 50ms.

Once the spectra had been obtained, the ratio of the 4 peak heights from the most abundant ions of citrate (at 273, 347, 375 and 465) to the corresponding ions from deuterated citrate (at 276, 350, 378 and 469) was taken, to normalise across samples. The concentration of citrate in the samples was calculated from the equation of the line obtained from plotting the calibration curve.

3.2.6 Treatment of cells with lactate, 3OHB and citrate

Young growing IMR90 and NHOF1 cells were plated at a density of 5000 cells/well in a 12 well tissue culture plate in standard DMEM containing 10% vol/vol foetal calf serum as previously described. 24 hours later the medium was replaced with 2mL of a mixture of DMEM and Ham's F12 (1:1 mix), with antibiotics, glutamine and serum added as normal, containing either 1mM citrate, 10mM lactate, 10mM 3OHB or no treatment. The treatments were applied to triplicate wells and cells were cultured for one month, constantly exposed to the treatments. Once one well became confluent, all the wells were trypsinised, counted, and replated at 5000 cells/well in standard DMEM before having the treatment re-applied 24 hours later. The cumulative mean population

doublings were averaged across the three wells for each repeat of the experiment due to the variable nature of manual cell counts, and plotted over time for each treatment to compare rate of growth.

3.3 Results

3.3.1 Untargeted metabolomics screens identified candidate biomarkers of senescence

In total, as part of this project four metabolomic screens have been performed by Metabolon, and with each screen the quality of the data improved as the protocols were refined. For example it became apparent that it was important to keep the cell density to media volume ratio consistent between flasks, and that scaling down the experiments (using flasks with an area smaller than 75cm^2) led to more variable results. It was also noticeable that in the earlier screens some of the senescent groups were not as old as others, making it more difficult to pull out differences in the metabolome. Despite this, even in the early experiments with lower quality data, it was evident that several areas of cellular metabolism were altered in senescence, as shown in the random forest analysis in figure 3.1, which was generated by Metabolon using data from PEsen and growing NHOF1, NHOF5, Colon, BJ and IMR90 fibroblast lines.

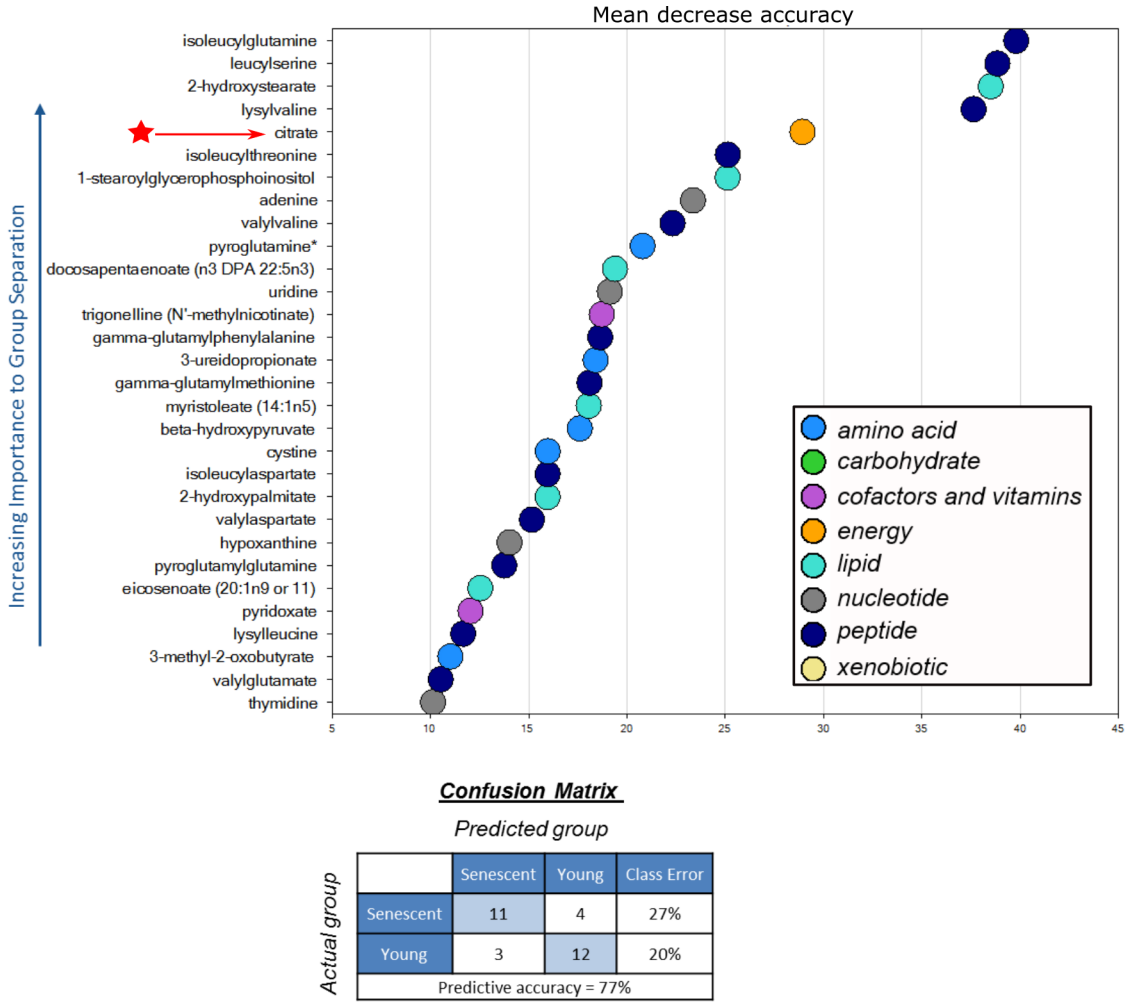

Figure 3.1: **Random forests analysis of PEsen versus growing fibroblasts** (produced by Metabolon). The y axis lists metabolites in order of importance for the predictive model built in the 'forest' to differentiate between conditioned media from senescent and growing cells. The confusion matrix shows how good the predictions made by the forest were; a 77% predictive accuracy is more than would be expected by chance (50%)The red star and arrow highlight citrate, a metabolite in the "energy" pathway group which ranked 5th in importance to separation of senescent and growing extracellular profiles.

The random forest lists the metabolites in order of importance for the predictive model built in the 'forest' to differentiate between conditioned media from senescent and growing cells. The confusion matrix shows how good the predictions made by the forest were; a 77% predictive accuracy is more than would be expected by chance (50%) so we can be reasonably confident that the metabolites selected by the random forest are truly important in the metabolic pathways that are different in PEsen and growing

cells.

The majority of highly important molecules suggested in this model are peptides, lipids and amino acids, although the TCA cycle intermediate ("energy" metabolite) citrate is also listed as highly important. However this experiment did not include the growth arrest controls, so it's difficult to tell if the changes detected are specific for senescence compared to transient growth arrest.

In another screen, which focused on one cell line (NHOF1) but included the growth arrest controls validated in the previous chapter, Metabolon used another multivariate analysis technique to identify differences between experimental groups; principal components analysis (PCA). The PCA plot Metabolon produced is shown in figure 3.2.

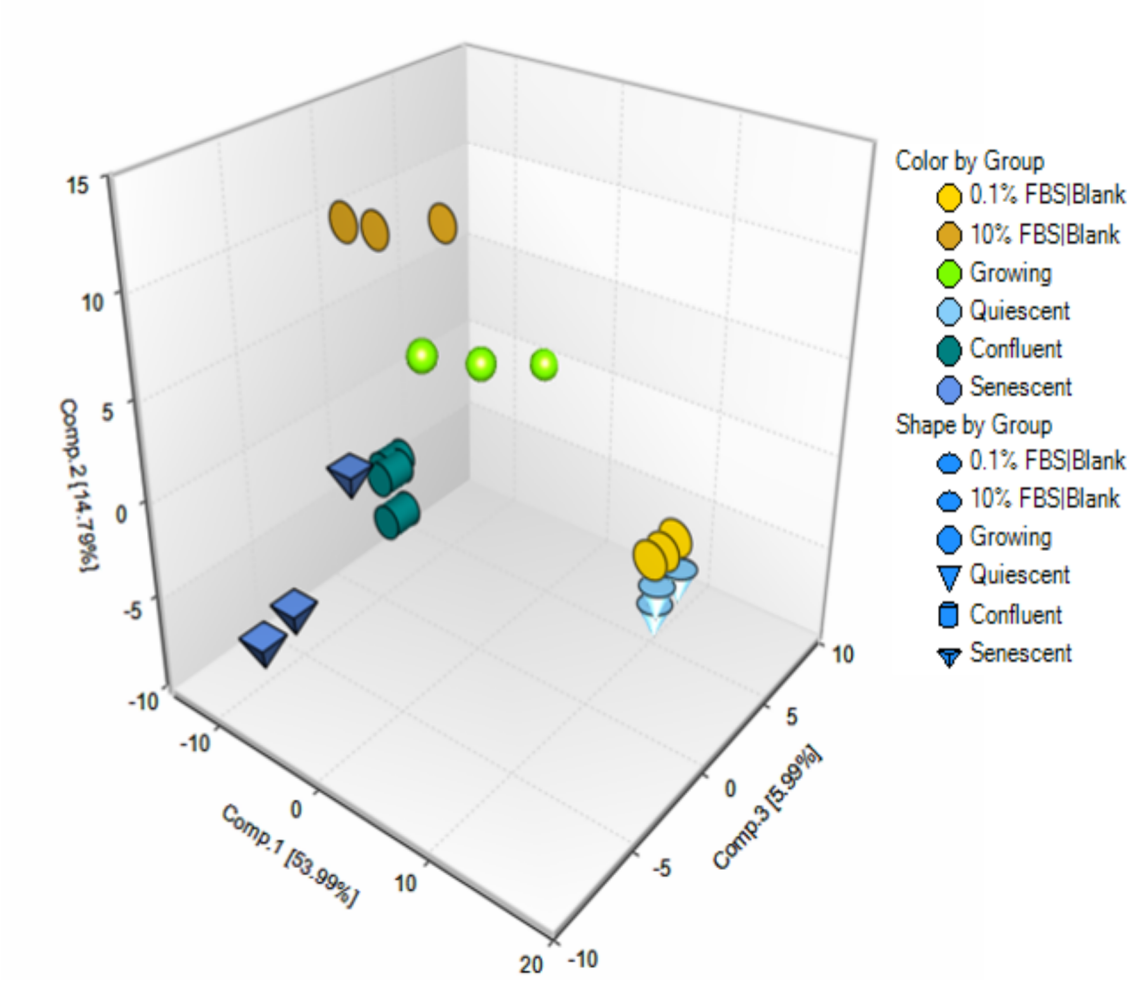

Figure 3.2: Principal component analysis of metabolomic data from PEsen (labelled senescent) growing, confluent and serum starved (labelled quiescent) NHOF1 conditioned culture media. The x, y and z axis show the 1st 2nd and 3rd components The number in square brackets represents the percentage of the total variance explained by that component.

The PCA plot shows there is clear separation of the groups, except for the 0.1% vol/vol serum blank and serum starved growth arrest control, which appear to be closely related. It also appears that the confluent growth arrest control profile is the closest to the senescent cell profile. To see if this separation was related to the molecules identified as important across multiple fibroblast lines in the random forest analysis, direct comparisons were made between the levels of metabolites in the groups previously identified: peptides, lipids, amino acids and energy metabolism.

3.3.1.1 Peptide metabolism in PEsen

The particular peptide molecules identified in the random forest were not found to be specifically altered in the study using the growth arrest controls but other metabolites in the same pathway were either significantly depleted or elevated (figure 3.3 and figure 3.4).

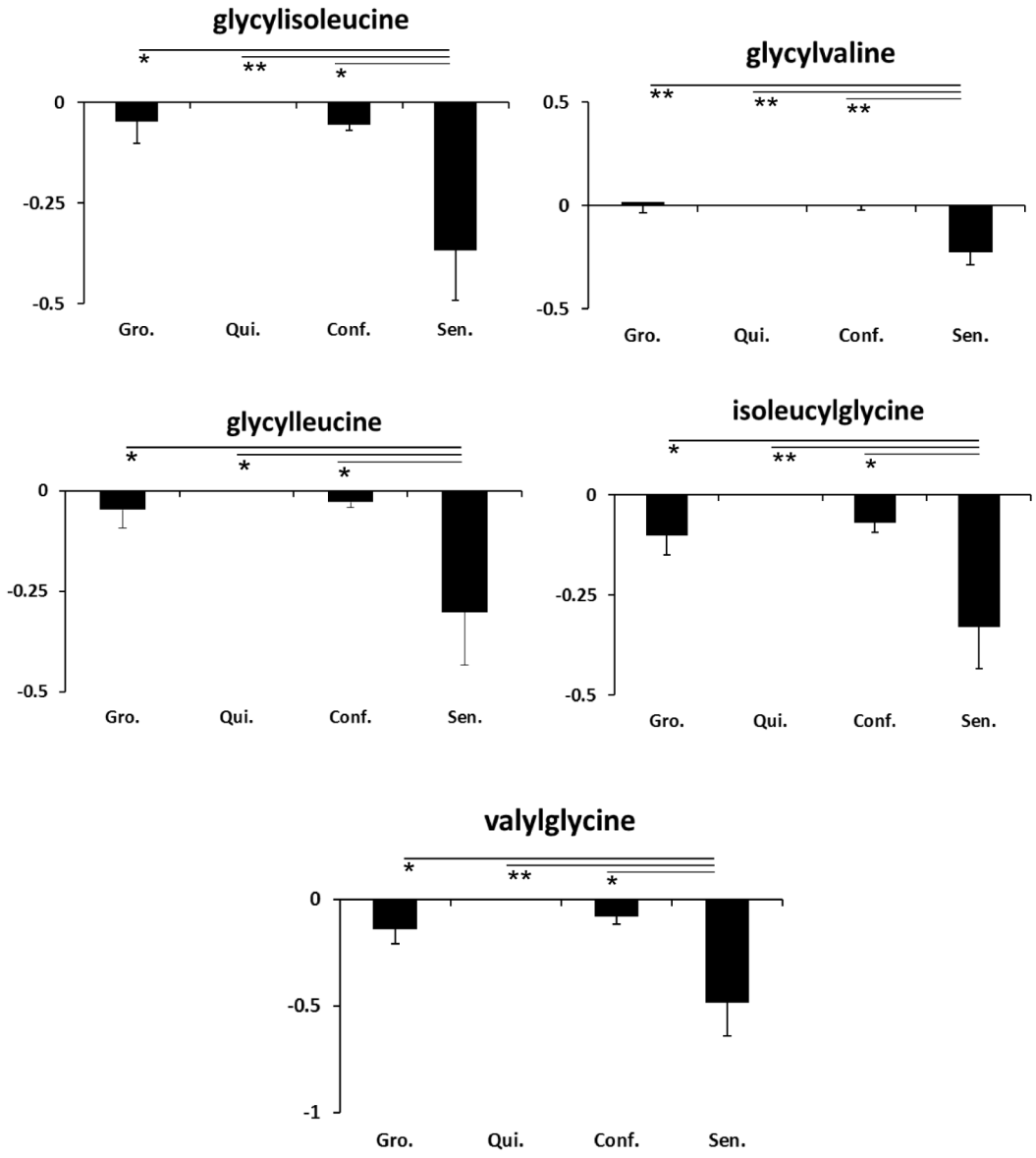

Figure 3.3: **Extracellular dipeptide levels in PEsen NHOF1 and growth arrest controls**. Several dipeptides were specifically depleted in PEsen (Sen) NHOF1 relative to growing (Gro), serum starved (Qui) and confluent (Conf) cells. The y axis on all the graphs represents the net scaled intensity of each metabolite normalized to 1×10^5 cells/mL, error bars represent standard deviation from the mean. n = 3 *p<0.05, **p<0.01 with 1 way ANOVA and Tukey's post hoc analysis.

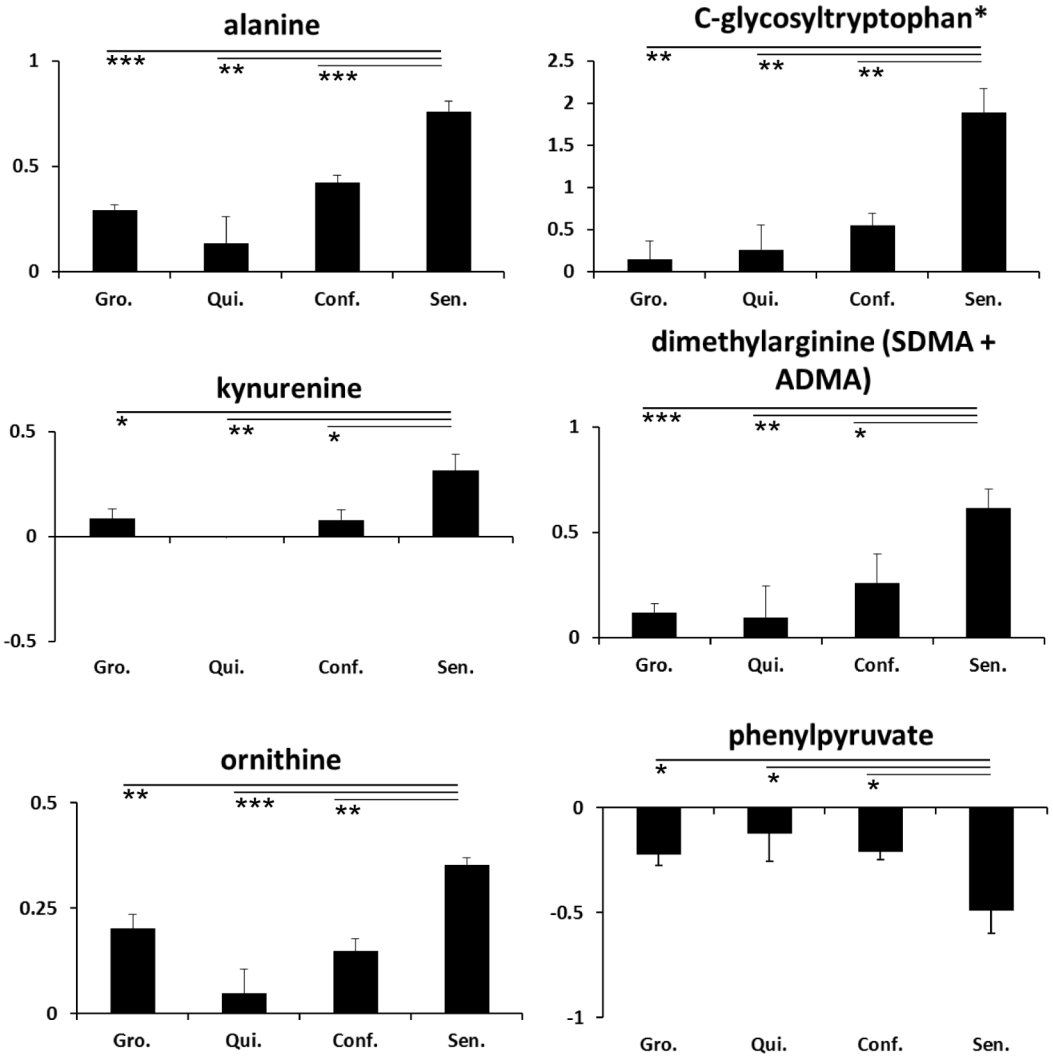

Figure 3.4: **Extracellular amino acid levels in PEsen NHOF1 and growth arrest controls.** Several amino acids were specifically elevated or depleted in PEsen (Sen) NHOF1 relative to growing (Gro), serum starved (Qui) and confluent (Conf) cells. The y axis on all the graphs represents the net scaled intensity of each metabolite normalized to 1×10^5 cells/mL, error bars represent standard deviation from the mean. n = 3 *p<0.05, **p<0.01 with 1 way ANOVA and Tukey's post hoc analysis.

3.3.1.2 Lipid metabolism in PEsen

As with the peptides, the particular lipids highlighted by the random forest were not found to be specifically modulated in the screen using the growth arrest controls, but metabolites in the same pathways were specifically elevated or depleted in PEsen relative to growth arrest controls. Figure 3.5 shows some essential fatty acids and figure 3.6

shows some phospholipids that were specifically modulated.

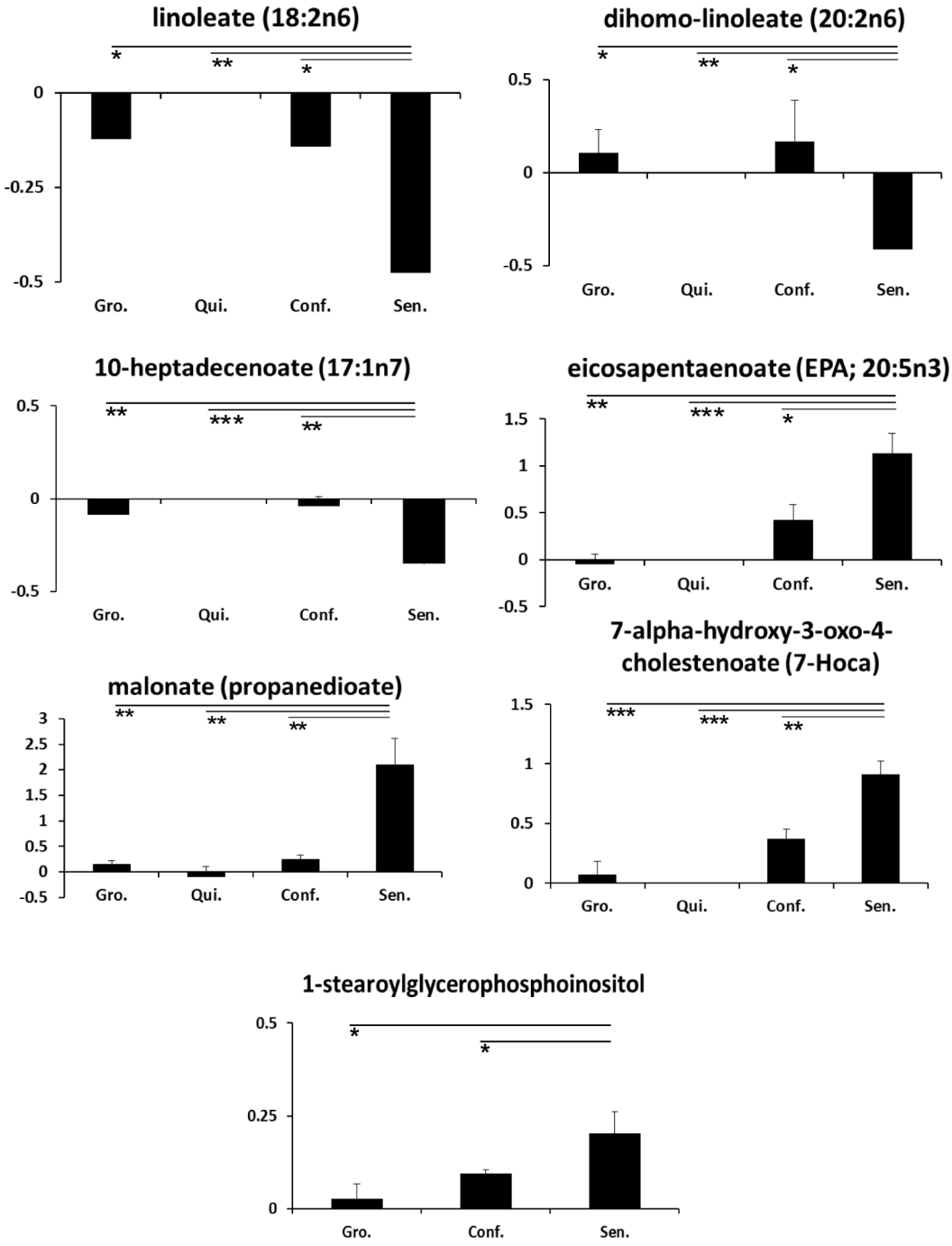

Figure 3.5: **Extracellular essential fatty acid levels in PEsen NHOF1 and growth arrest controls**. Several essential fatty acids were either specifically depleted or specifically elevated in PEsen (Sen) NHOF1 relative to growing (Gro), serum starved (Qui) and confluent (Conf) cells. The y axis on all the graphs represents the net scaled intensity of each metabolite normalized to 1×10^5 cells/mL, error bars represent standard deviation from the mean. n = 3 *p<0.05, **p<0.01 ***p<0.001 with 1 way ANOVA and Tukey's post hoc analysis.

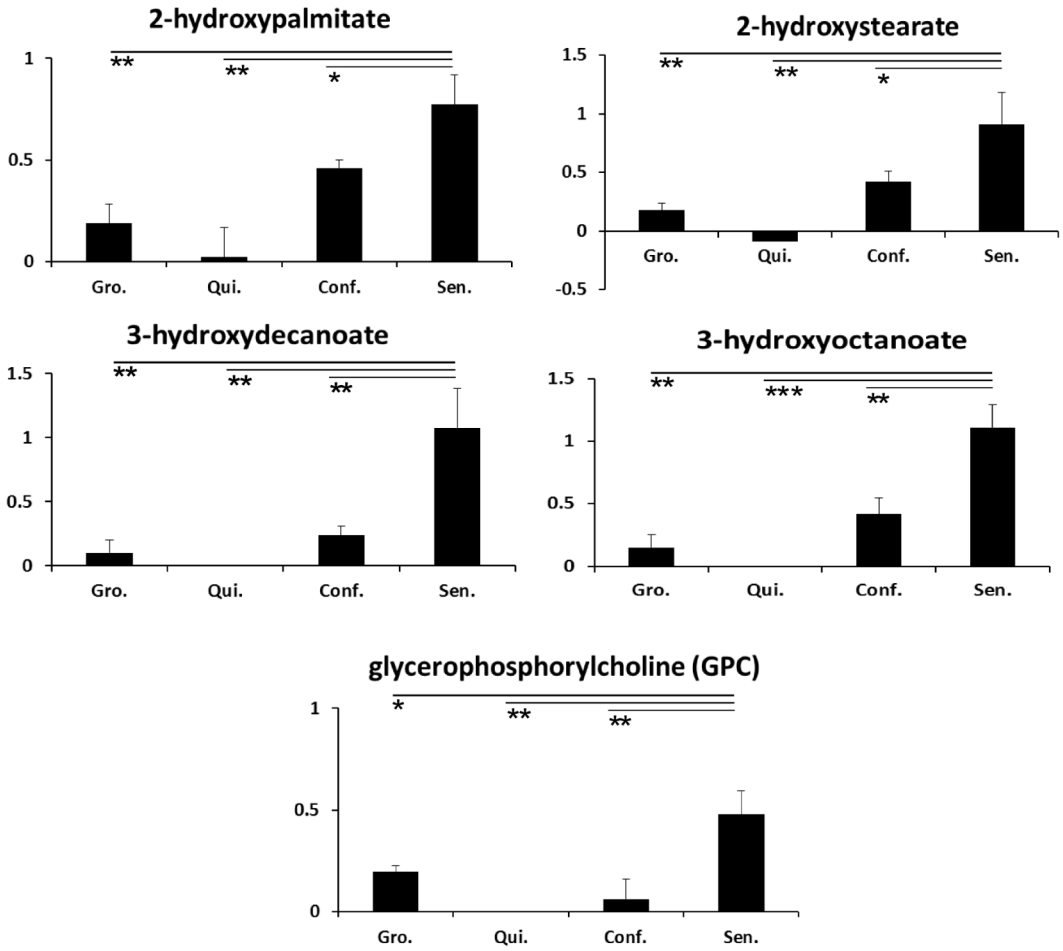

Figure 3.6: **Extracellular phospholipid levels in PEsen NHOF1 and growth arrest controls.** Several phospholipids were specifically elevated in PEsen (Sen) NHOF1 relative to growing (Gro), serum starved (Qui) and confluent (Conf) cells. The y axis on all the graphs represents the net scaled intensity of each metabolite normalized to 1 $\times$ 10^5 cells/mL, error bars represent standard deviation from the mean. n = 3 *p<0.05, **p<0.01 ***p<0.001 with 1 way ANOVA and Tukey's post hoc analysis.

3.3.1.3 Energy metabolism in PEsen

Several biochemicals involved in the central energy metabolism pathways were elevated or depleted in the conditioned media of PEsen NHOF1 relative to growth arrest controls, and once again a significant change in the level of citrate was detected (figure 3.7).

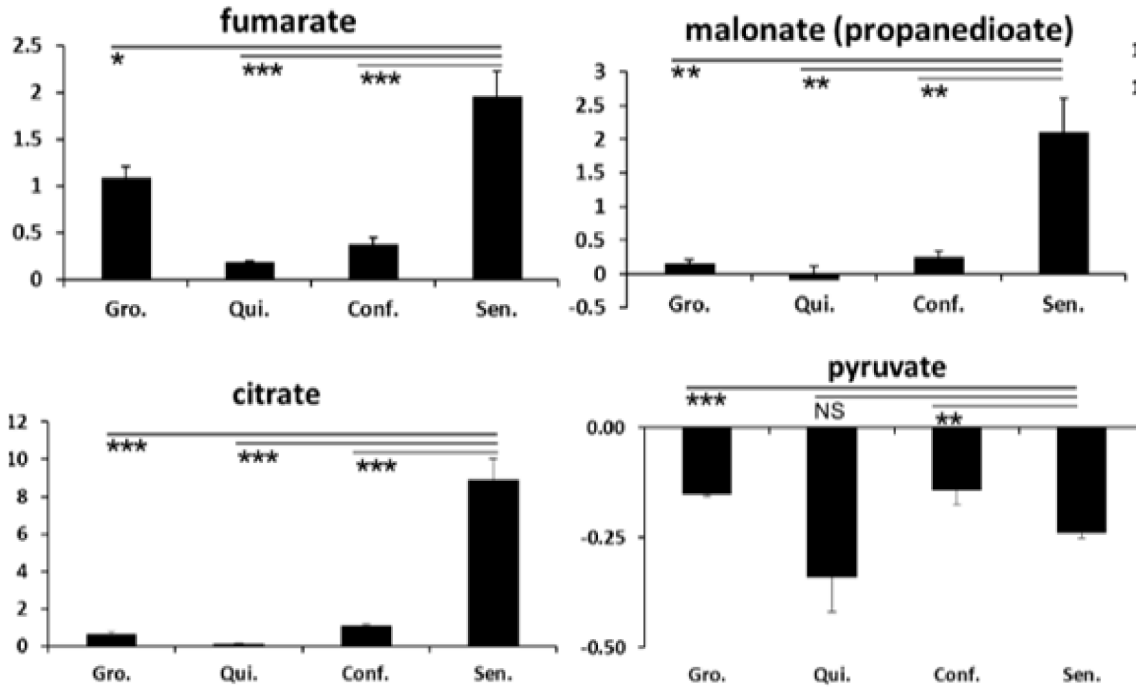

Figure 3.7: **Extracellular energy metabolite levels in PEsen NHOF1 and growth arrest controls**. Several energy metabolites were either specifically depleted or specifically elevated (including citrate) in PEsen (Sen) NHOF1 relative to growing (Gro), serum starved (Qui) and confluent (Conf) cells. The y axis on all the graphs represents the net scaled intensity of each metabolite normalized to 1×10^5 cells/mL, error bars represent standard deviation from the mean. n = 3 *p<0.05, **p<0.01 ***p<0.001 with 1 way ANOVA and Tukey's post hoc analysis.

For further insight into the metabolic state of the cells, intracellular levels of metabolites involved in three key energy metabolism pathways were examined. As shown in figures 3.8 and 3.9, intracellular levels of several metabolites of glycolysis and the PPP were elevated compared to growing and growth arrested controls, while TCA metabolites were generally depleted.

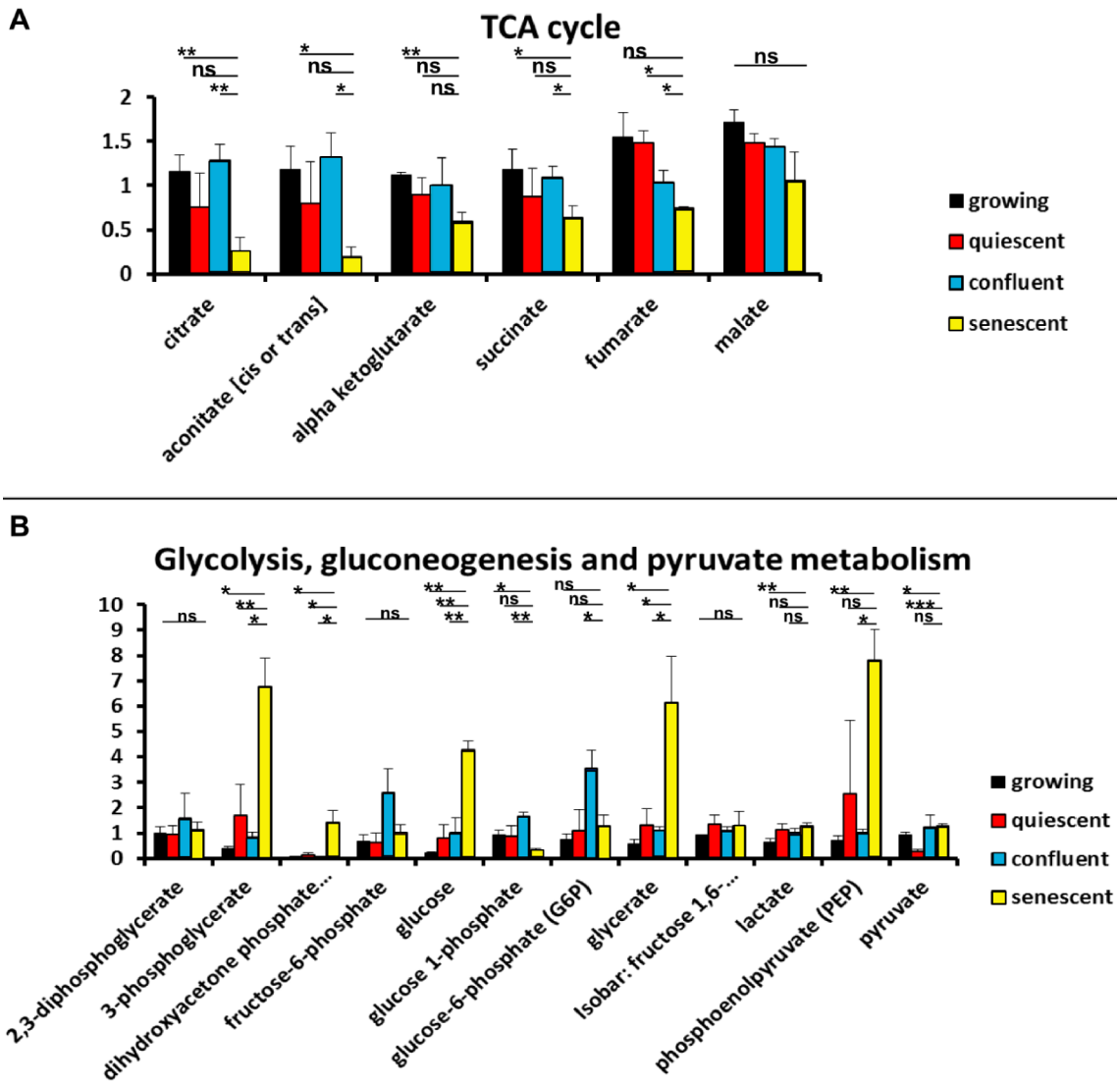

Figure 3.8: **Intracellular energy metabolite levels from the TCA cycle, glycolysis and gluconeogenesis in PEsen NHOF1 and growth arrest controls. A** Intracellular levels of TCA metabolites **B** Glycolytic metabolites in PEsen NHOF1 and growth arrest controls. The y axis on both graphs represents the net scaled intensity of each metabolite normalised to $1x10^5$ cells/mL, error bars represent standard deviation from the mean. n = 3 ns = not significant *p<0.05, **p<0.01 ***p<0.001 with 1 way ANOVA and Tukey's post hoc analysis.

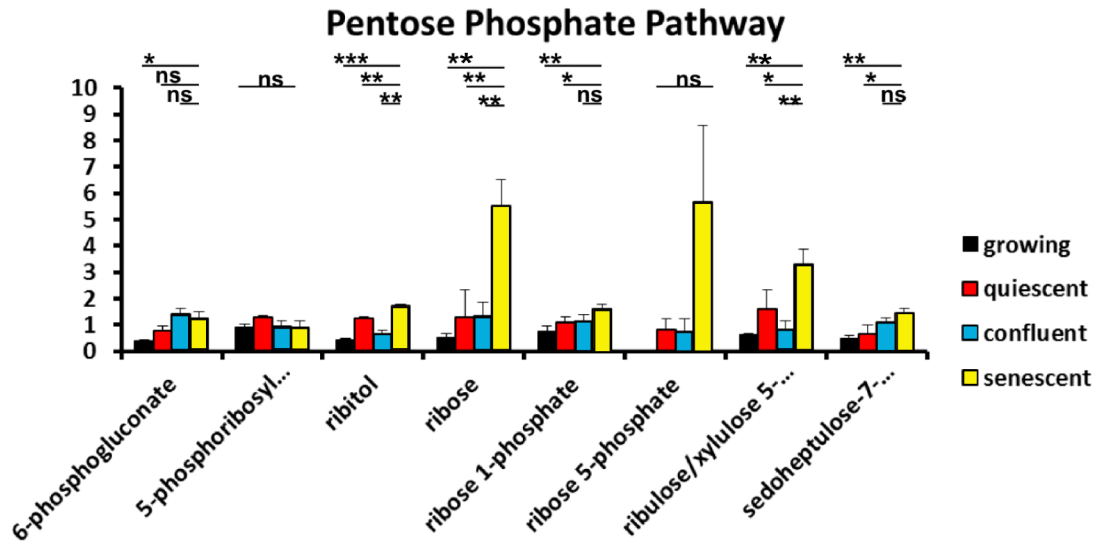

Figure 3.9: **Intracellular energy metabolite levels from the PPP in PEsen NHOF1 and growth arrest controls**. The y axis represents the net scaled intensity of each metabolite normalised to $1x10^5$ cells/mL, error bars represent standard deviation from the mean. n = 3 ns = not significant *p<0.05, **p<0.01 ***p<0.001 with 1 way ANOVA and Tukey's post hoc analysis.

Adding further insight into the metabolic state of the cells, levels of intracellular ADP were also detected (figure 3.10). Although not statistically significant, there was a clear trend for depletion of this molecule in senescent NHOF1 compared to growth arrest controls.

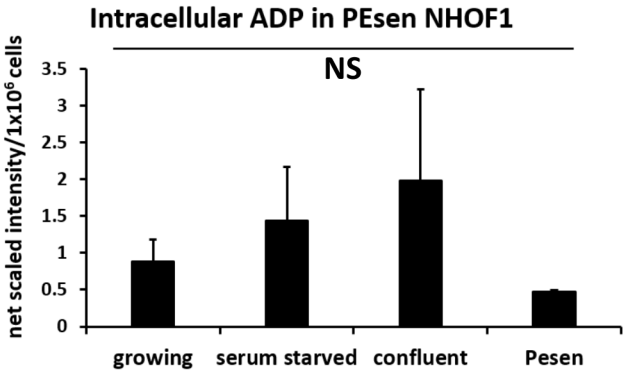

Figure 3.10: **Intracellular levels of adenosine di-phosphate (ADP) in PEsen NHOF1 and growth arrest control**s. n=3 error bars represent standard deviation from the mean NS = not significant with 1 way ANOVA.

Intracellular levels of AMP were also measured and were significantly depleted in

PEsen cells compared to growing controls (figure 3.11).

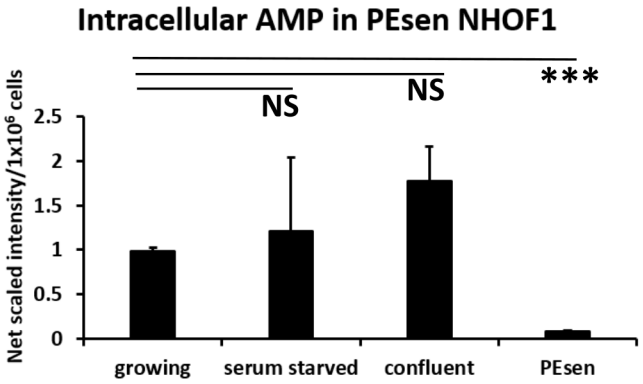

Figure 3.11: **Intracellular levels of adenosine mono-phosphate (AMP) in PEsen NHOF1 and growth arrest controls normalised to cell number**. n=3 error bars represent standard deviation from the mean NS= not significant ***p<0.001 with a 1 way ANOVA and Tukey's post hoc analysis.

Intracellular levels of acetyl Co-A were elevated in PEsen NHOF1 and growth arrest controls compared to growing controls, a relationship which was statistically significant in PEsen and serum starved cells (figure 3.12).

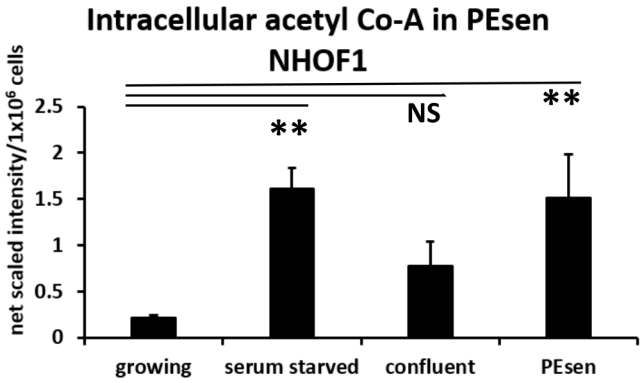

Figure 3.12: **Intracellular levels of acetyl Co-A in PEsen NHOF1 and growth arrest controls normalised to cell number**. n=3 error bars represent standard deviation from the mean NS= not significant **p<0.01 with a 1 way ANOVA and Tukey's post hoc analysis

Co factors are essential for metabolic pathways to function, as they facilitate the transfer of electrons from one molecule to the next. The intracellular levels of three key co factors are shown in figure 3.13.

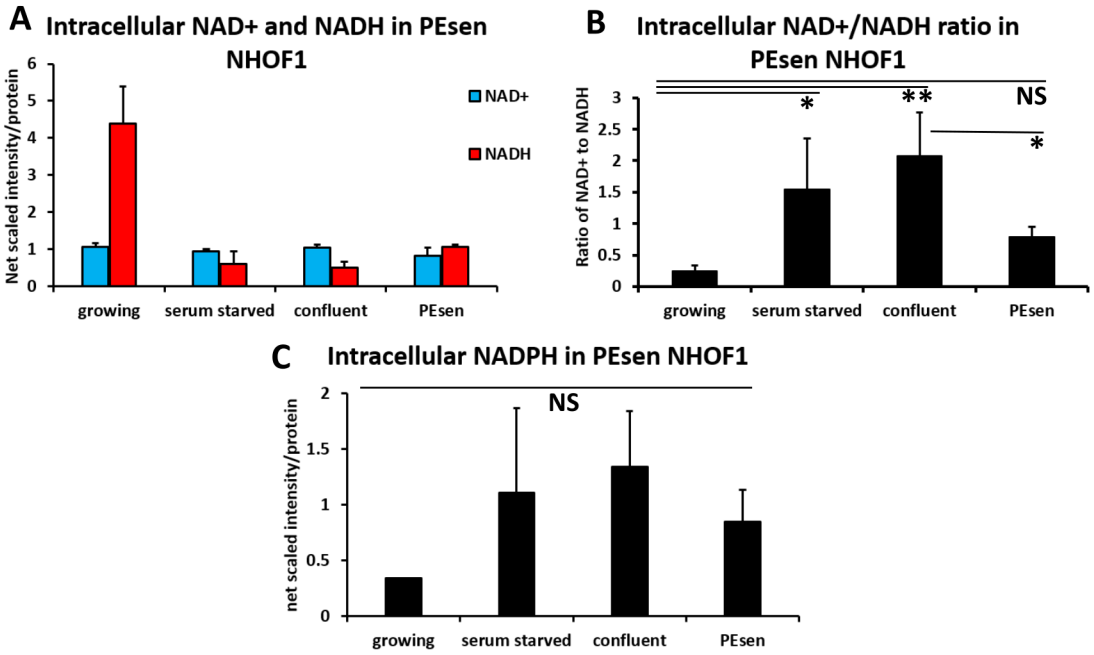

Figure 3.13: **Intracellular levels of NAD+, NADH and NADPH in PEsen NHOF1 and growth arrest controls**. **A** Average intracellular levels of NAD+ and NADH in PEsen as well as serum starved and confluent growth arrest controls and growing control NHOF1, normalised to protein. n=3 error bars represent standard deviation from the mean. **B** Ratio of intracellular NAD+ to NADH measured in PEsen as well as serum starved and confluent growth arrest controls and growing control NHOF1, normalised to protein. n=3 error bars represent standard deviation from the mean. NS = not significant, *p<0.05, **p<0.01 with a 1 way ANOVA and Tukey's post hoc analysis. **C** Average intracellular levels of NADPH in PEsen as well as serum starved and confluent growth arrest controls and growing control NHOF1, normalised to protein. n=3 error bars represent standard deviation from the mean NS= not significant with a 1 way ANOVA.

3.3.1.4 Citrate

Because citrate was specifically picked up in repeated screens, and is involved in energy metabolism which is known to be altered but is not yet well understood in senescence (see section 1.2.4 on page 56) it was decided that citrate would be a good candidate marker to focus on.

Looking at the data for citrate across multiple PEsen fibroblast cell lines there was indeed a clear trend for citrate elevation in the PEsen cells, although it was not statistically significant for all lines (see figure 3.14). Overall if all the lines are considered together the increase in citrate in PEsen cells was statistically significant (figure 3.15),

and as already shown in figure 3.7 on page 146, citrate was not elevated in transient growth arrest.

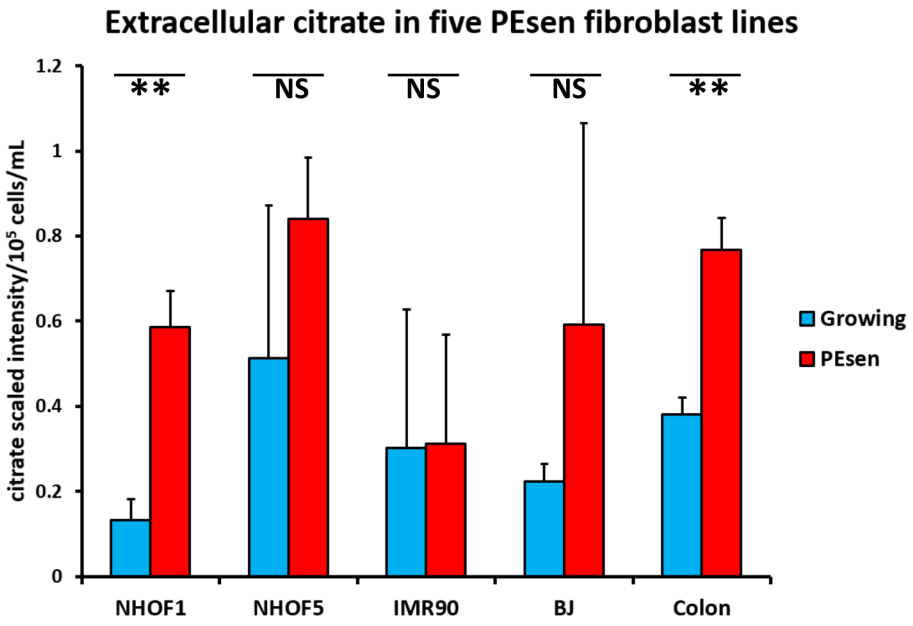

Figure 3.14: **Extracellular citrate in PEsen cells from five fibroblast lines compared to growing controls.** GCMS performed by Metabolon. Error bars represent standard deviation from the mean, n=3 NS= not significant,**p<0.01 with a Student's T test

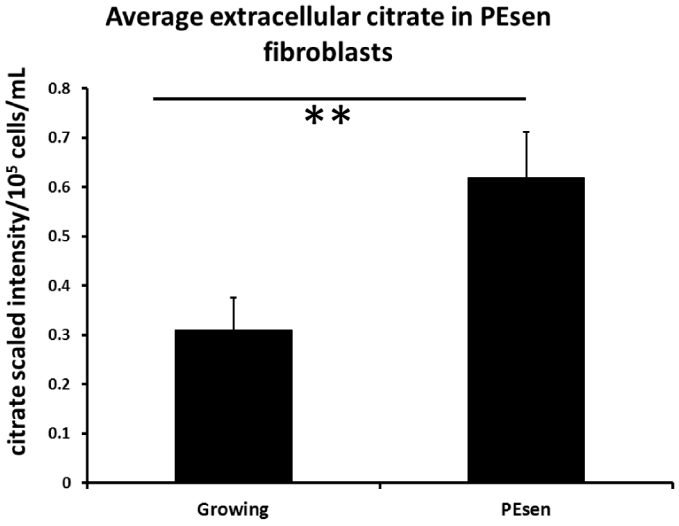

Figure 3.15: **Average extracellular citrate in PEsen cells from five fibroblast lines compared to growing controls**. GCMS performed by Metabolon. n= 5 error bars represent standard error of the mean, **p<0.01 Student's T test.

An elevation of citrate was found in another untargeted metabolomics screen of

multiple cell lines, this time in IrrDSBsen fibroblasts (figure 3.16).

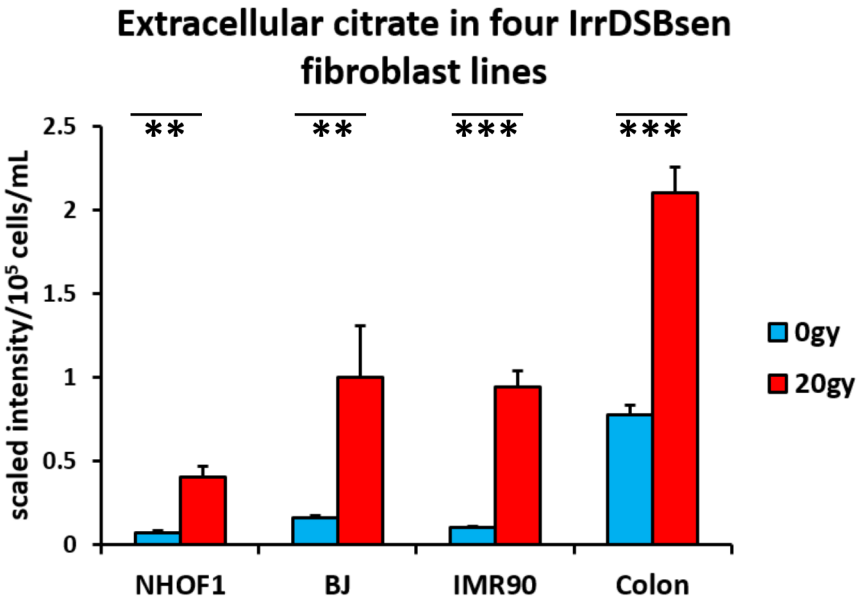

Figure 3.16: **Extracellular citrate in IrrDSBsen (20Gy) cells** from four fibroblast lines compared to growing controls (0Gy). GCMS performed by Metabolon. Error bars represent standard deviation from the mean, n=3 per group. **p<0.01, ***p<0.001 with Student's T-test.

Furthermore, citrate was not found to be elevated in cells that received 0.5Gy gamma radiation, the control used for repairable DNA damage, as shown in figure 3.17.

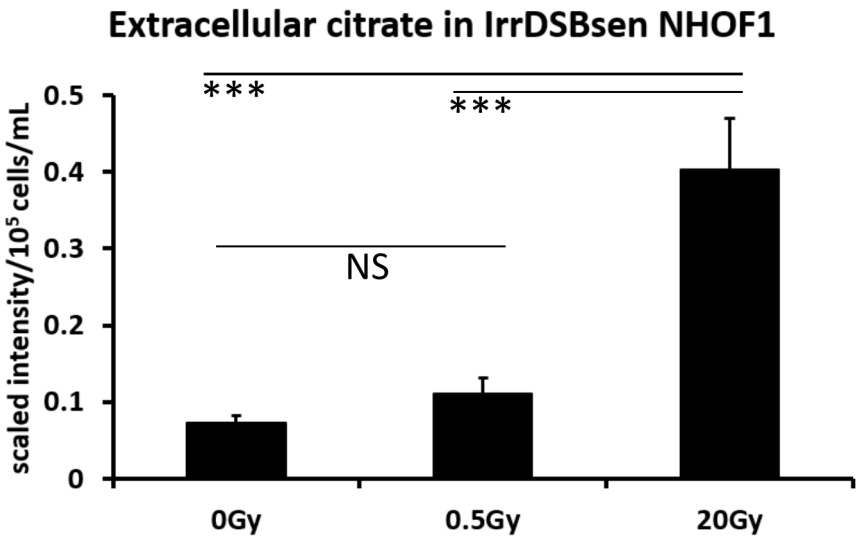

Figure 3.17: E**xtracellular citrate measured in IrrDSBsen NHOF1 cells with 0Gy and 0.5Gy controls.** GCMS performed by Metabolon. n=3, error bars represent standard deviation from the mean, NS= not significant, ***p<0.001 with 1 way ANOVA and Tukey's post hoc analysis.

3.3.1.5 Lactate

In addition to citrate, lactate was of interest as it had been reported in the literature that it is released from senescent cells present in the tumour stroma and acts as a metabolic fuel for cancer cells (Bonuccelli et al., 2010; Whitaker-Menezes et al., 2011). Figure 3.18 shows the relative levels of extracellular lactate in five PEsen fibroblast lines, and only one line (Colon fibroblasts) showed an elevation in lactate following PEsen. When all the cell lines are combined there is no significant elevation of lactate (figure 3.19).

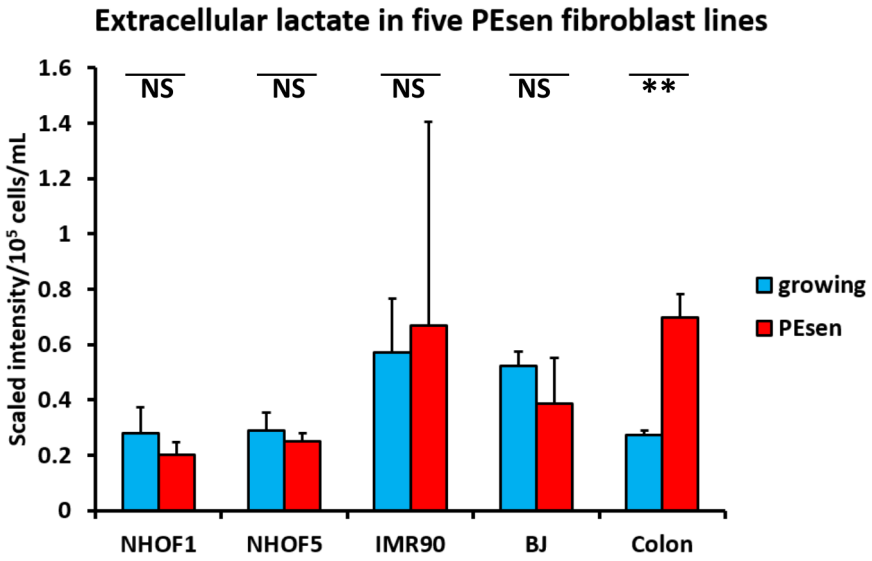

Figure 3.18: **Extracellular lactate in five PEsen fibroblast lines.** GCMS performed by Metabolon. Error bars represent standard deviation from the mean, n=3 NS= not significant, **p<0.01 with Student's T test.

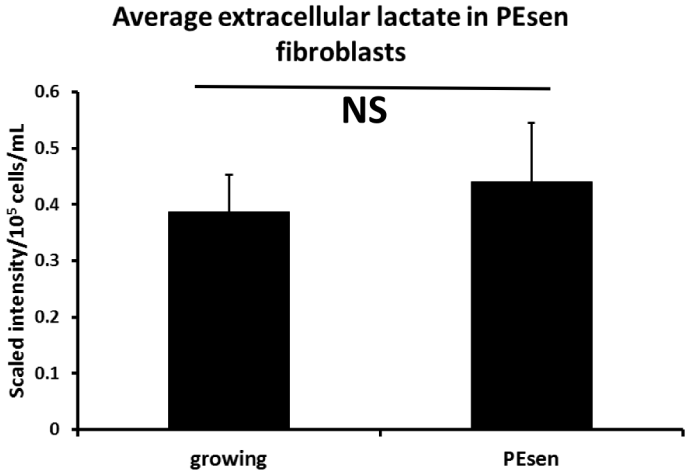

Figure 3.19: Average extracellular lactate in 5 PEsen fibroblast lines. GCMS performed by Metabolon. Error bars represent standard error of the mean, n=5 NS= not significant with Student's T test.

This result was confirmed in another screen of PEsen using the growth arrest controls (shown in figure 3.20).

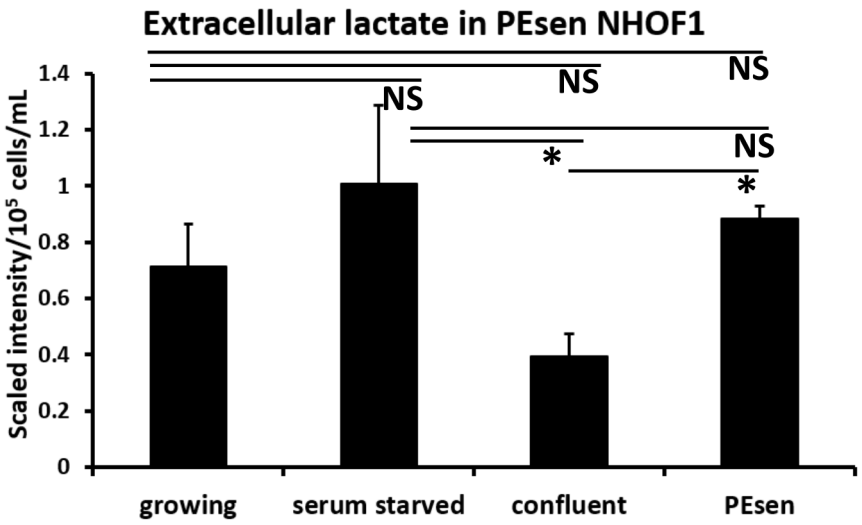

Figure 3.20: **Extracellular lactate in PEsen NHOF1 cells and growing, serum starved and confluent controls**. GCMS performed by Metabolon. Error bars represent standard deviation from the mean, n=3 NS= not significant, *p<0.05 with a 1 way ANOVA and Tukey's post hock analysis.

In IrrDSBsen fibroblasts however there was an increase in extracellular lactate following senescence, except in NHOF1, as shown in figure 3.21, and overall across all of the cell lines the increase was statistically significant (figure 3.22).

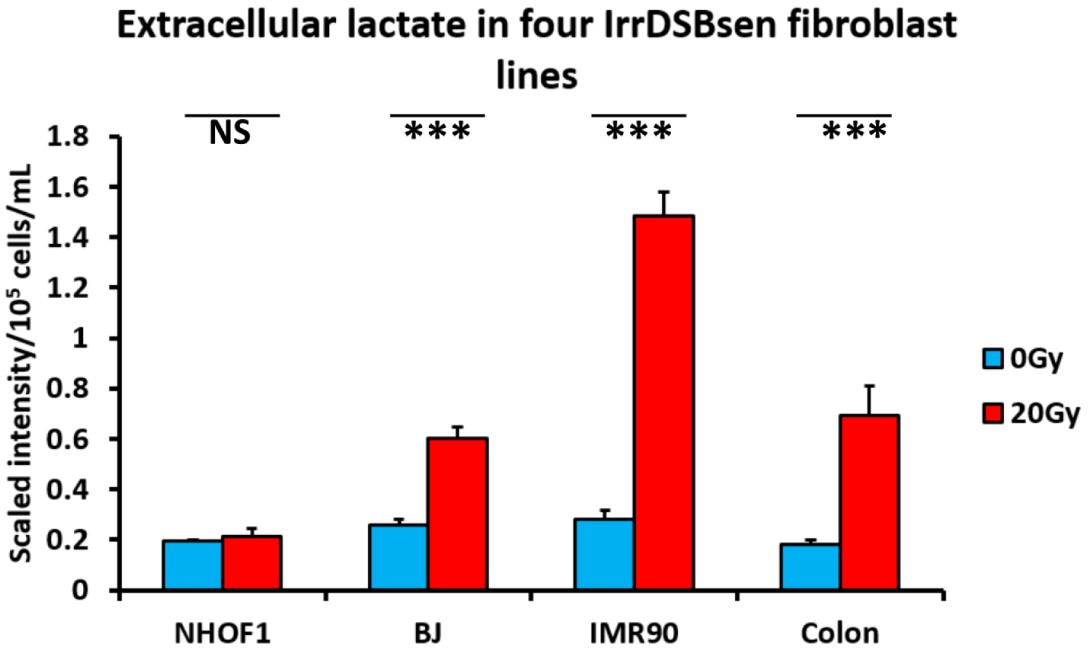

Figure 3.21: **Extracellular lactate measured in four IrrDSBsen (20Gy) and growing control (0Gy) fibroblast lines.** GCMS performed by Metabolon. n=3 NS= not significant, **p<0.01 ***p<0.001 with Student's T test.

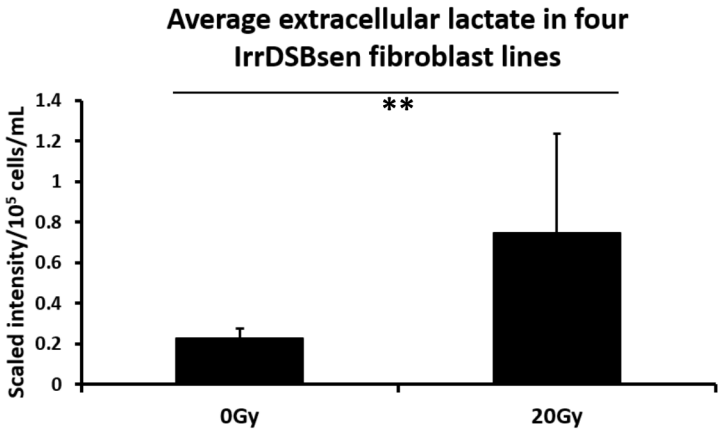

Figure 3.22: A**verage extracellular lactate in four IrrDSBsen fibroblast lines**. GCMS performed by Metabolon. n=12 **p<0.01 with Student's T test

The screen that covered the 0.5Gy control for IrrDSBsen was carried out in NHOF1 only, and in accordance with the previous result there was no elevation of lactate seen in this experiment (figure 3.23).

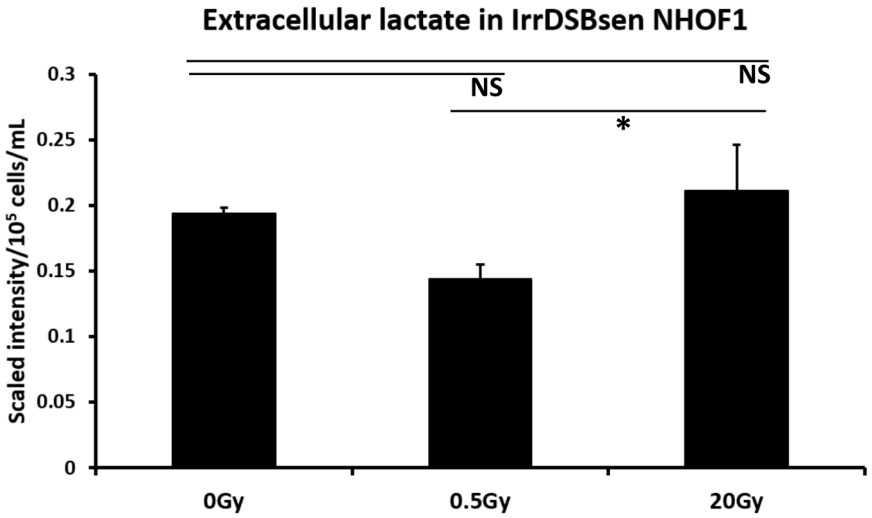

Figure 3.23: **Extracellular lactate measured in IrrDSBsen NHOF1 cells with 0Gy and 0.5Gy controls.** GCMS performed by Metabolon. n=3, error bars represent standard deviation from the mean NS = not significant *p<0.05 with 1 way ANOVA and Tukey's post hoc analysis.

3.3.1.6 Reduction-oxidation (redox) homeostasis

The untargeted screens also detected that several metabolites related to redox homeostasis were specifically elevated in PEsen compared to the other groups (figure 3.24) and while none are suitable as biomarkers of senescence, because redox homeostasis is often affected in many pathologies, this finding could give insight into the regulation and maintenance of the senescence phenotype.

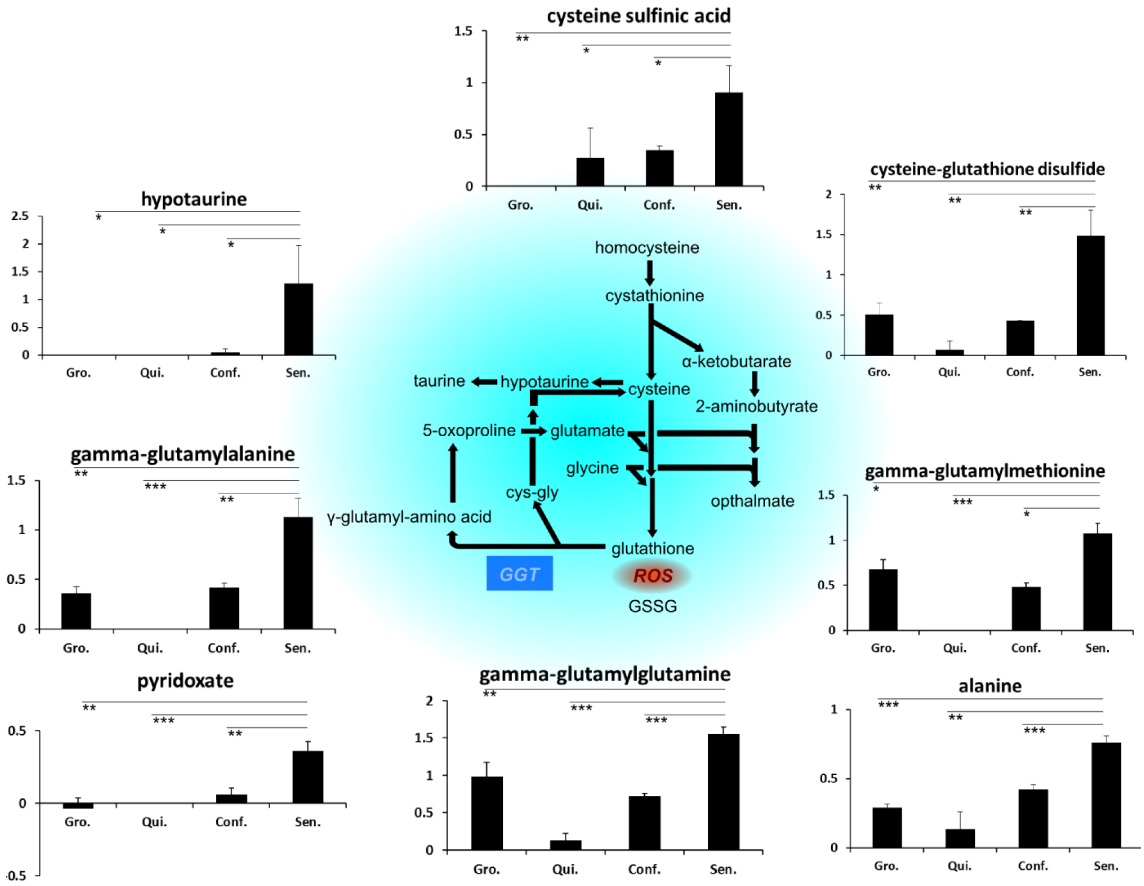

Figure 3.24: **Gamma glutamyl redox homeostasis pathway and related metabolites detected in the conditioned media of PEsen (Sen.) NHOF1** and serum starved (Qui.) and confluent (Conf.) growth arrest controls compared to growing (Gro.) controls. The graphs show net scaled intensity normalised to $1x10^5$cells/mL, n=3, error bars represent standard deviation from the mean. *p<0.05, **p<0.01, ***p<0.001 with unpaired two ample T Test. GGT: gamma glutamyl transferase; ROS: reactive oxygen species. Figure taken from James et al., 2015.

3.3.2 The secretome is not a product of increased biomass

The decision to normalise extracellular metabolite levels to cell number rather than total protein content was made because the primary aim of the work was to identify a secreted biomarker that could potentially be used to detect the presence of increased numbers of senescent cells in an individual simply from the metabolite levels detected in their blood serum. In that scenario, the desired result is the accurate detection of an increased population of senescent cells, and as an increased cell size is part of the senescence phenotype the effect the increased size has on the levels of metabolites

secreted is irrelevant. Nevertheless, ascertaining whether the increase in extracellular citrate is a product simply of increased overall protein content and therefore an up-scaled citrate production, in which case the fold increase in citrate would be expected to be similar to the fold increase in total protein, or whether it is a specific increase in citrate independent of the increase in total protein, is usefull information for deducing the source of increased extracellular citrate. Graph A in figure 3.25 on the following page shows that the ratio of citrate normalised by cell number to citrate normalised by protein in growing, serum starved and confluent cells is around 1 for both intracellular and extracellular citrate, meaning there is hardly a difference between the levels of citrate recorded using normalisation with either method. In PEsen cells however both intracellular and extracellular citrate had a ratio of around 3, meaning that normalising to cell number was giving a reading of citrate 3 times higher than if it were normalised to protein. This effect must be due to the increased biomass of the senescent cells, however it does not completely explain the scale of the elevation in extracellular citrate. As shown in graph B in figure 3.25 on the next page, while the PEsen citrate scaled intensity value when normalised to cell number is roughly 3 times greater than when normalised to protein, it is more than 8 times greater than the scaled intensity values of citrate in growing and growth arrested cells. The increase in extracellular citrate is not proportional to the increase in protein content of the senescent cells. Furthermore, when normalised to protein the levels of extracellular citrate detected were still higher in PEsen than in growing, serum starved or confluent cells.

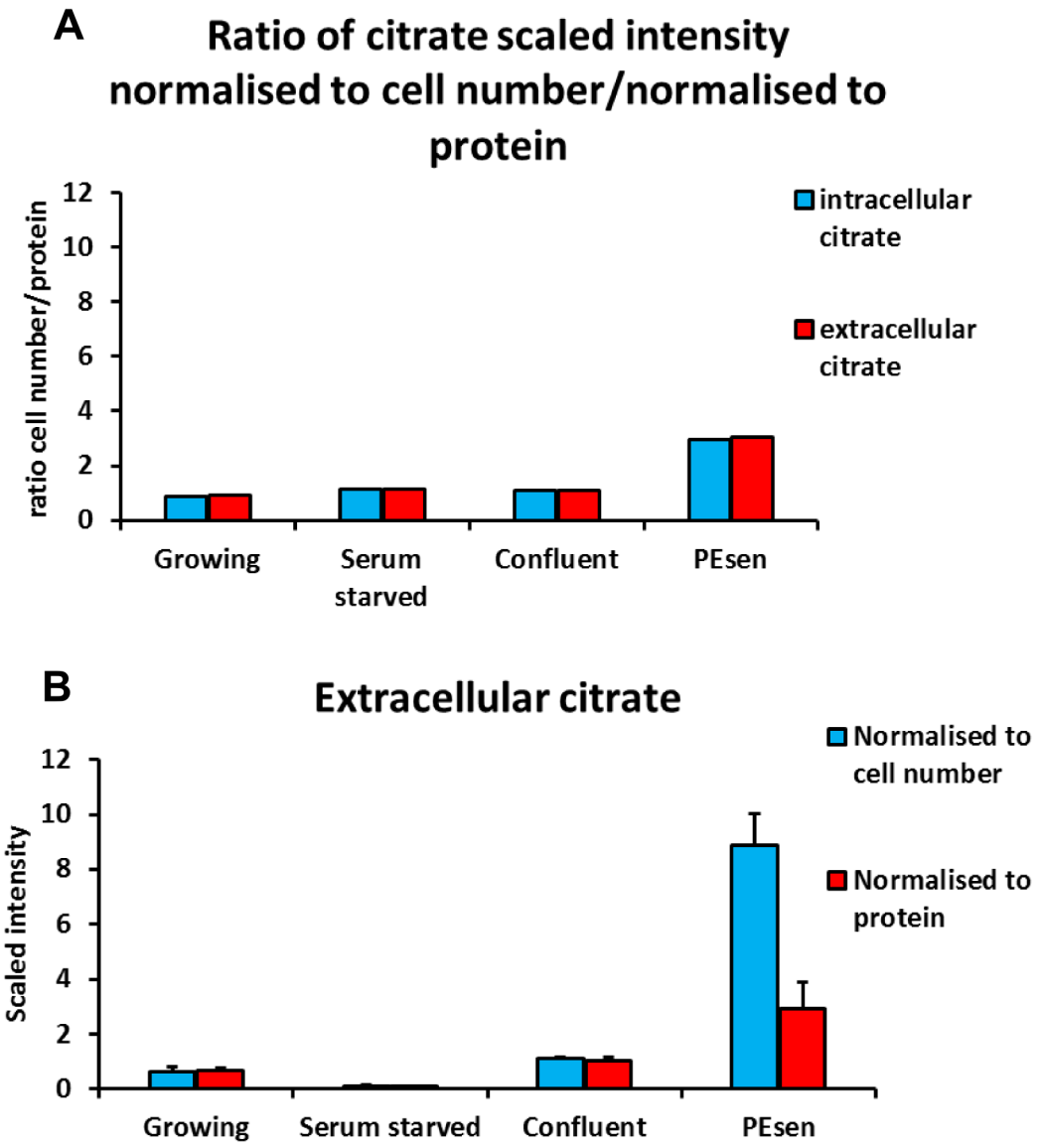

Figure 3.25: **Normalisation of citrate to cell number compared with normalisation to protein**. **A** The ratio of both intracellular citrate (blue bars) and extracellular citrate (red) citrate normalised by cell number to citrate normalised by protein. **B** The scaled intensity values of extracellular citrate normalised to cell number (blue bars) and normalised to protein (red bars) n=3 error bars represent standard deviation from the mean.

Interestingly intracellular levels of citrate decrease in PEsen relative to controls if citrate is normalised to protein, and appears unchanged if normalised to cell number, as figure 3.26 on the following page shows. Whichever method is used, citrate is not elevated inside the cell despite its accumulation outside the cell.

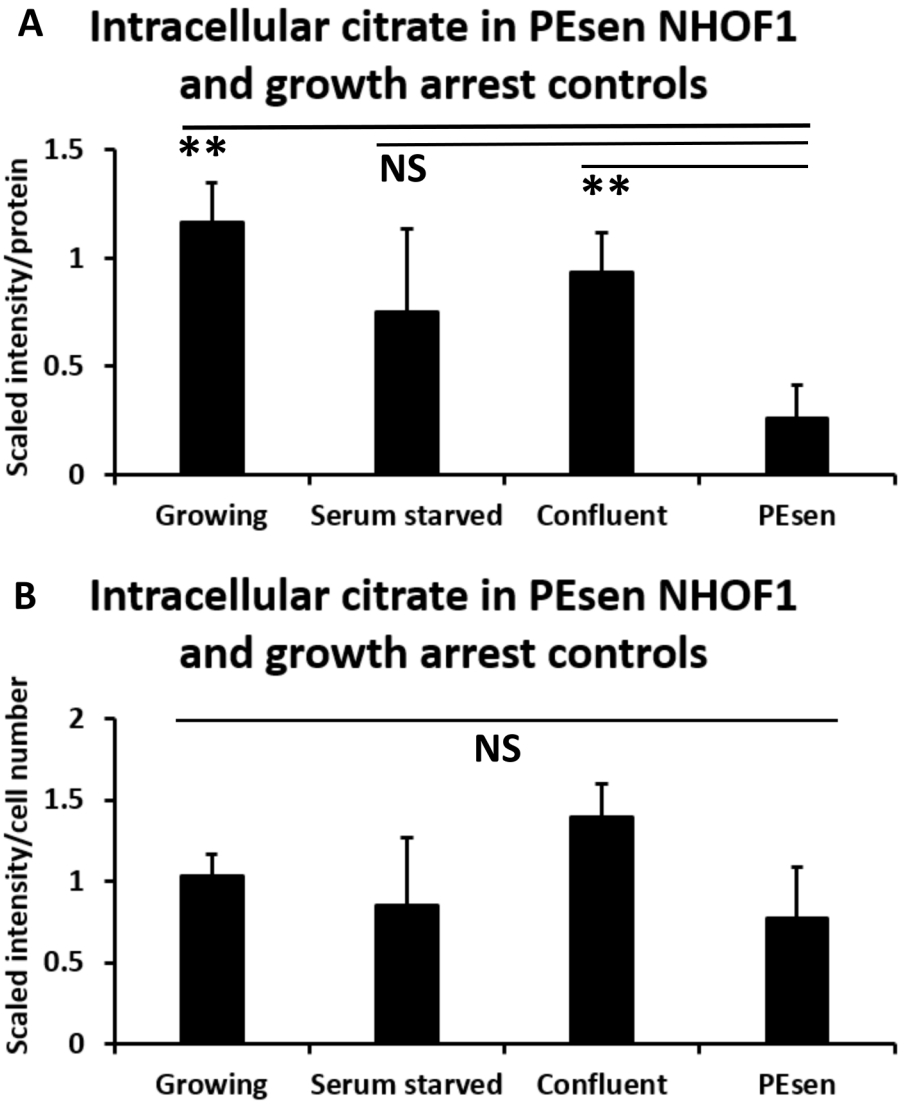

Figure 3.26: **Intracellular citrate levels in PEsen NHOF1 and growth arrest controls. A** Intracellular citrate normalised to protein **B** Intracellular citrate normalised to cell number. N=3 error bar represent standard deviation from the mean NS = not significant **p<0.01 with a 1 way ANOVA and Tukey's post hoc analysis.

3.3.3 Targeted methods used to support findings from untargeted screens

Attempts to confirm the result from the Metabolon screen using an enzymatic assay to quantify the extracellular lactate produced the opposite finding than had been seen in the untargeted screens: lactate was elevated in PEsen but not in IrrDSBsen. There was a trend for increased extracellular lactate in PEsen compared to young growing

cells although the relationship was not statistically significant as shown in figure 3.27, however when all lines were considered together lactate was significantly elevated in PEsen (figure 3.28).

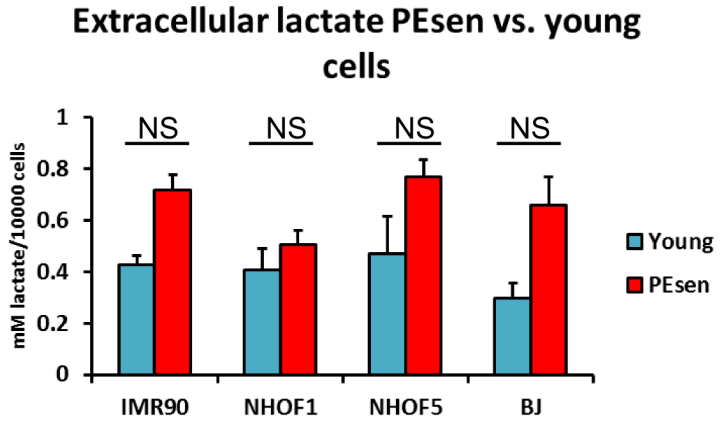

Figure 3.27: **Extracellular lactate measured in four PEsen fibroblast lines using an enzymatic assay**. Error bars represent standard deviation from the mean n= 3 NS = not significant with a Student's T test.

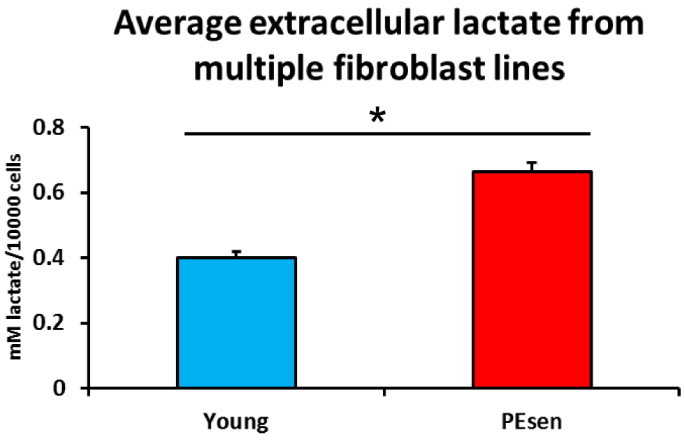

Figure 3.28: **Average extracellular lactate measured in four PEsen fibroblast lines using an enzymatic assay**. Error bars represent standard error of the mean n= 4 *p<0.05 with a Student's T test.

However the increase in extracellular lactate measured in IrrDSBsen IMR90 cells was not statistically significant (figure 3.29 on the next page).

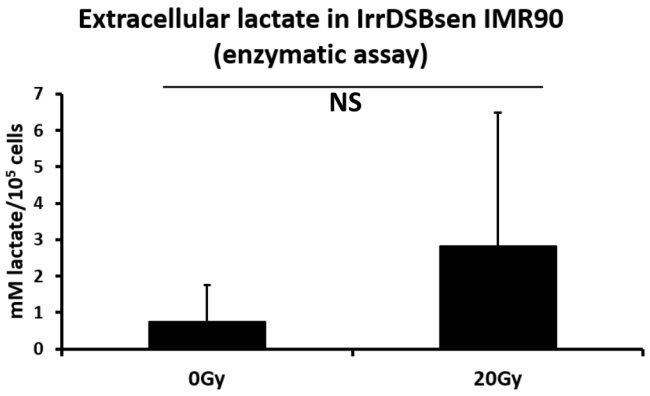

Figure 3.29: **Extracellular lactate in IrrDSBsen IMR90 measured by enzymatic assay**. Error bars represent standard deviation from the mean, n=3 NS= not significant with Student's T test.

Attempts to use an enzymatic assay to quantify citrate were not successful. The assay worked as demonstrated by the production of a standard curve in figure 3.30 **A,** however no citrate was detectable in any tests of conditioned media, and once the background (determined from blank media) had been subtracted values were usually negative, the opposite result to the Metabolon screen. An example of results from one of the pilot experiments is shown in figure 3.30 **B.**

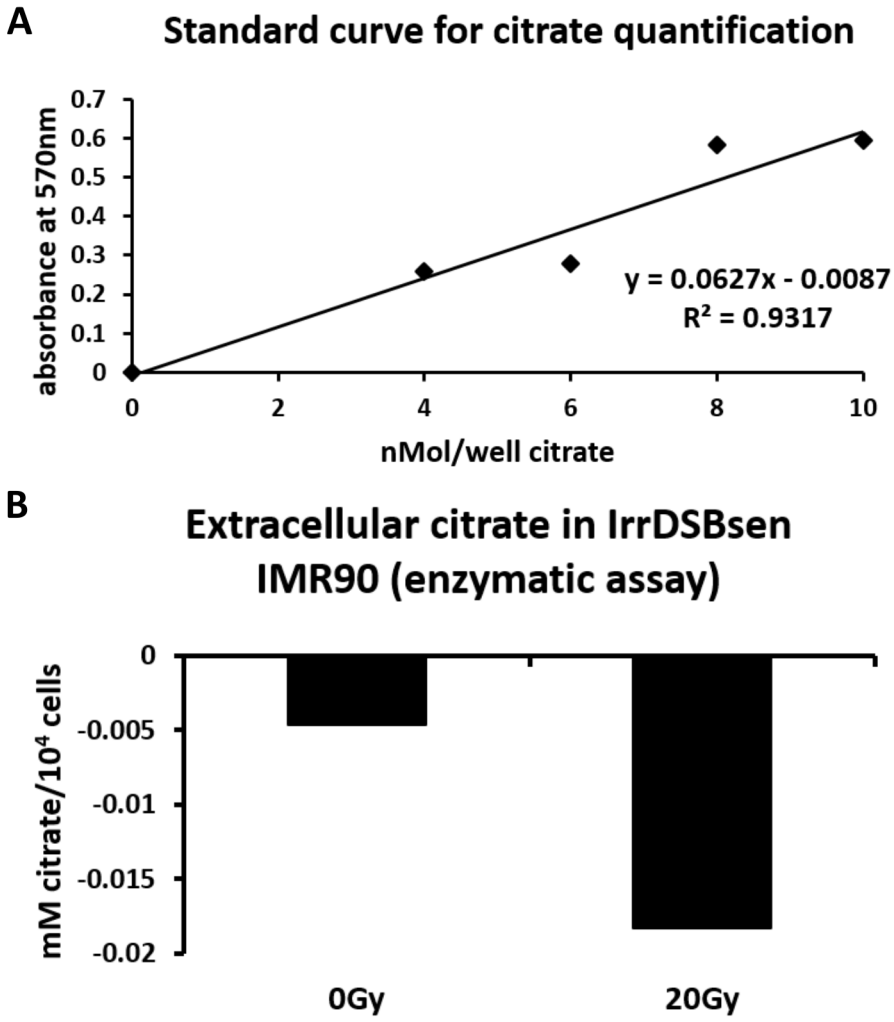

Figure 3.30: **Extracellular citrate in IrrDSBsen IMR90 measured using enzymatic assay A** Standard curve from the pilot test of enzymatic citrate quantification, showing linear relationship between increasing concentration of citrate in cell culture media and absorbance at 570nm **B** Pilot experiment showing extracellular citrate measured in IrrDSBsen IMR90. n=1.

Attempts to detect citrate by precipitating it out of solution were also unsuccessful, as shown in figure 3.31. In standard cell culture media that many samples had already been collected in, the phenol red interfered with the assay and the standard curve was not very linear (**A**). Removal of phenol red from the media improved the linearity slightly (**B**) however the presence of lactate in the media reduced the linearity (**C-D**).

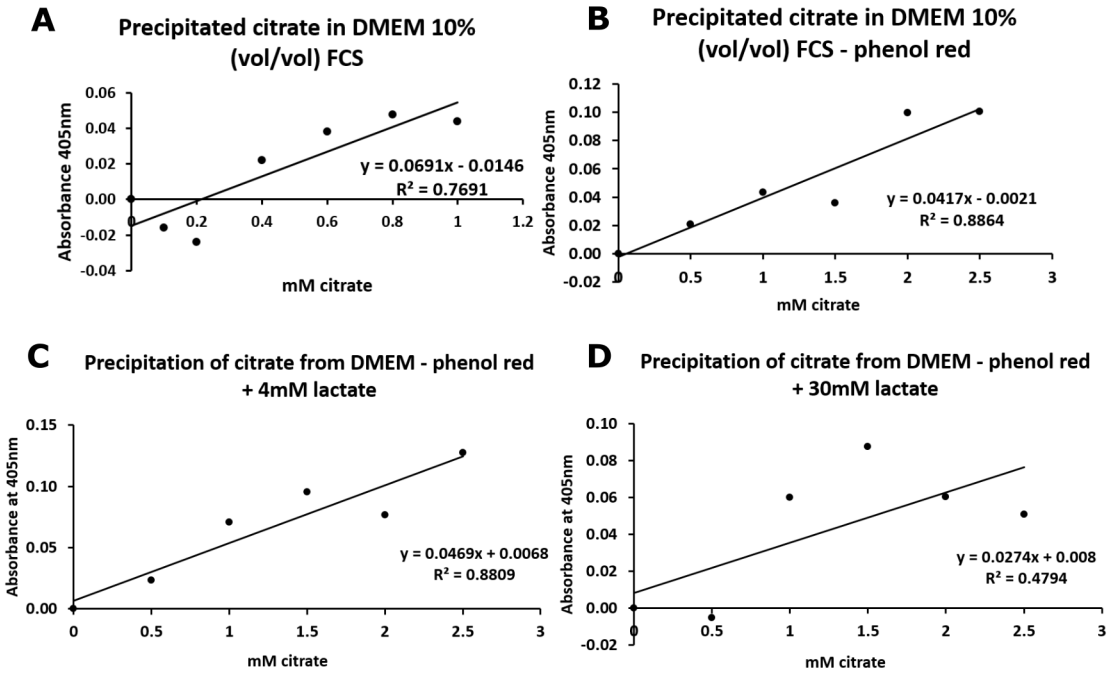

Figure 3.31: **Quantification of precipitated citrate A** standard curve of precipitated citrate in DMEM 10% (vol/vol) foetal calf serum (FCS). **B** a standard curve of precipitated citrate in DMEM 10% (vol/vol) FCS without phenol red (kit recommendation). **C** standard curve of precipitated citrate in DMEM 10% (vol/vol) FCS without phenol red but with 4mM lactate added. **D** standard curve of precipitated citrate in DMEM 10% (vol/vol) FCS without phenol red but with 30mM lactate added.

NMR initially appeared promising for detection of citrate in the conditioned media, with a spiked in citrate standard giving peaks in an area of the spectrum not occupied by other peaks present in unconditioned media (see figure 3.32 on the following page)

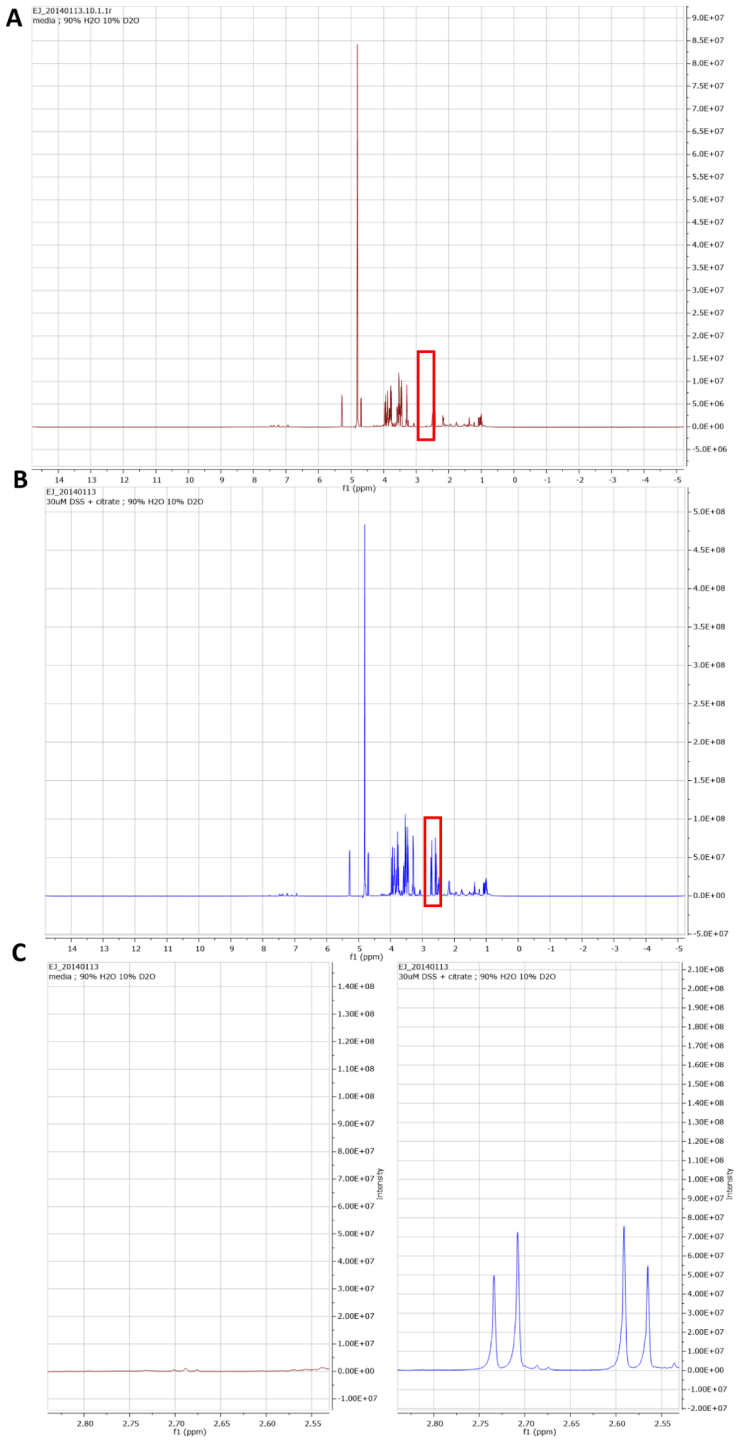

Figure 3.32: **Detection of citrate in DMEM using NMR**. NMR spectra as shown in MNova Lite from **A** unconditioned DMEM, red box shows where peaks from citrate would be expected **B** unconditioned DMEM containing 0.1mM citrate**,** red box shows the area where peaks from citrate would be expected **C** magnified area of spectrum (unconditioned DMEM on the left, DMEM containing 0.1mM citrate on the right) where peaks from citrate would be expected.

However citrate was undetectable in media from IrrDSBsen NHOF1 and IrrDSBsen

IMR90 (example data shown in figure 3.33).

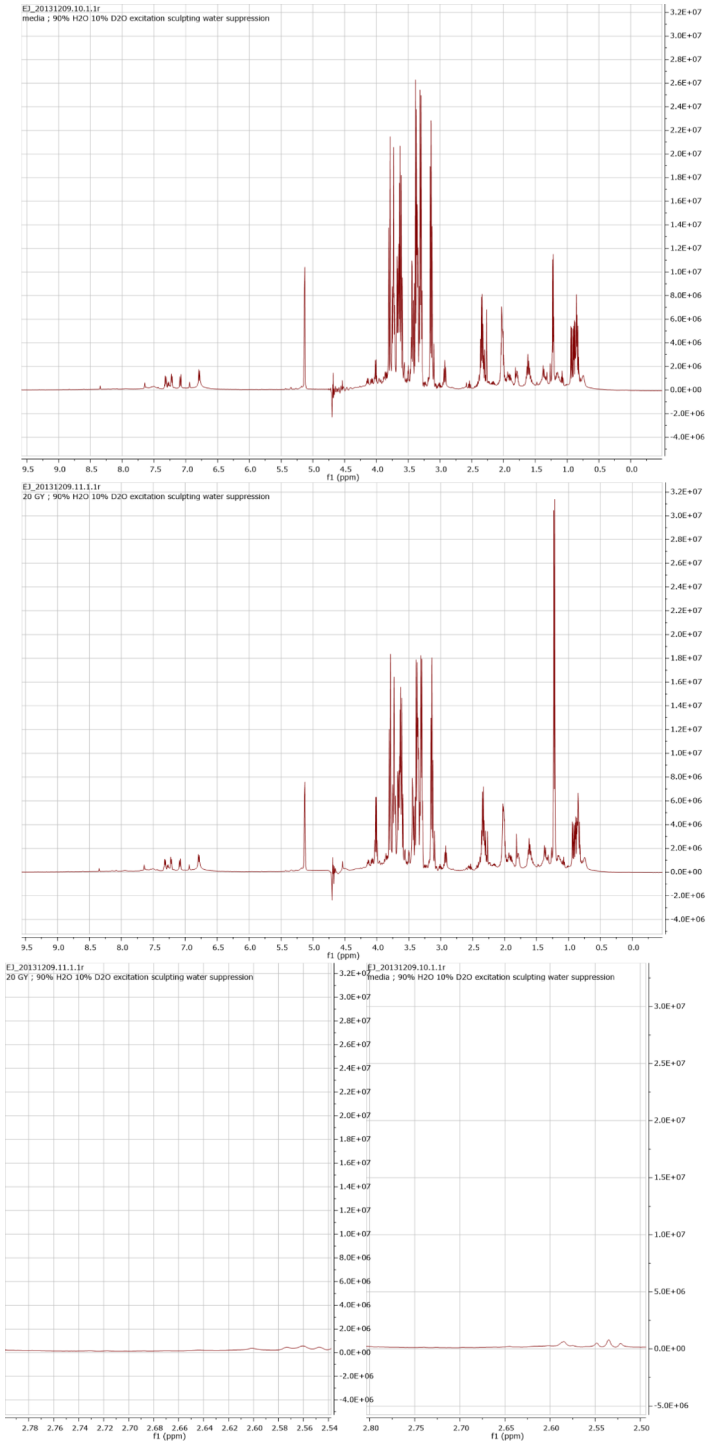

Figure 3.33: **NMR of IrrDSBsen NHOF1 conditioned media**. NMR spectra as shown in MNova Lite from **A** unconditioned DMEM **B** conditioned DMEM from IrrDSBsen NHOF1 **C** magnified area of spectrum where citrate would be seen.

Citrate was successfully measured using GCMS with the help of Mark Bennett and Sarah Davies at Imperial College London. The spectra of the ions used to measure

citrate have been plotted in figure 3.34.

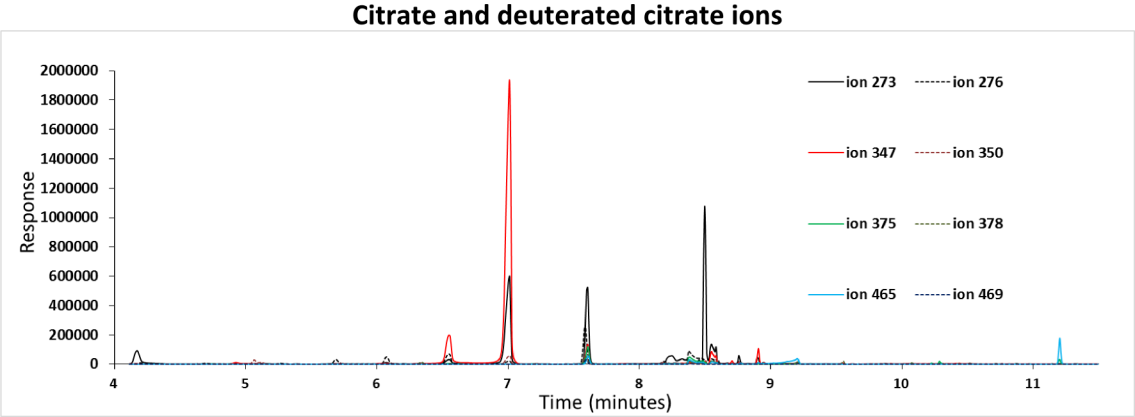

Figure 3.34: **Detection of citrate using GCMS.** Example spectra of the ions used to identify citrate in DMEM using GCMS.

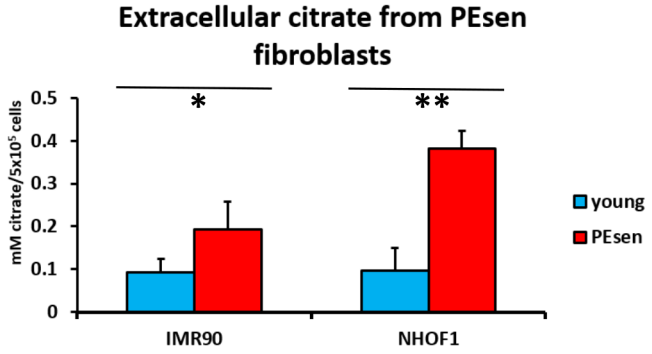

Figure 3.35: **Extracellular citrate measured in PEsen fibroblasts using GCMS**. Concentration of extracellular citrate from NHOF1 and IMR90 fibroblasts that are senescent due to proliferative exhaustion (PEsen) compared to growing controls, and normalised to cell number n=3 per group *p<0.05 **p<0.01 with a Student's T Test.

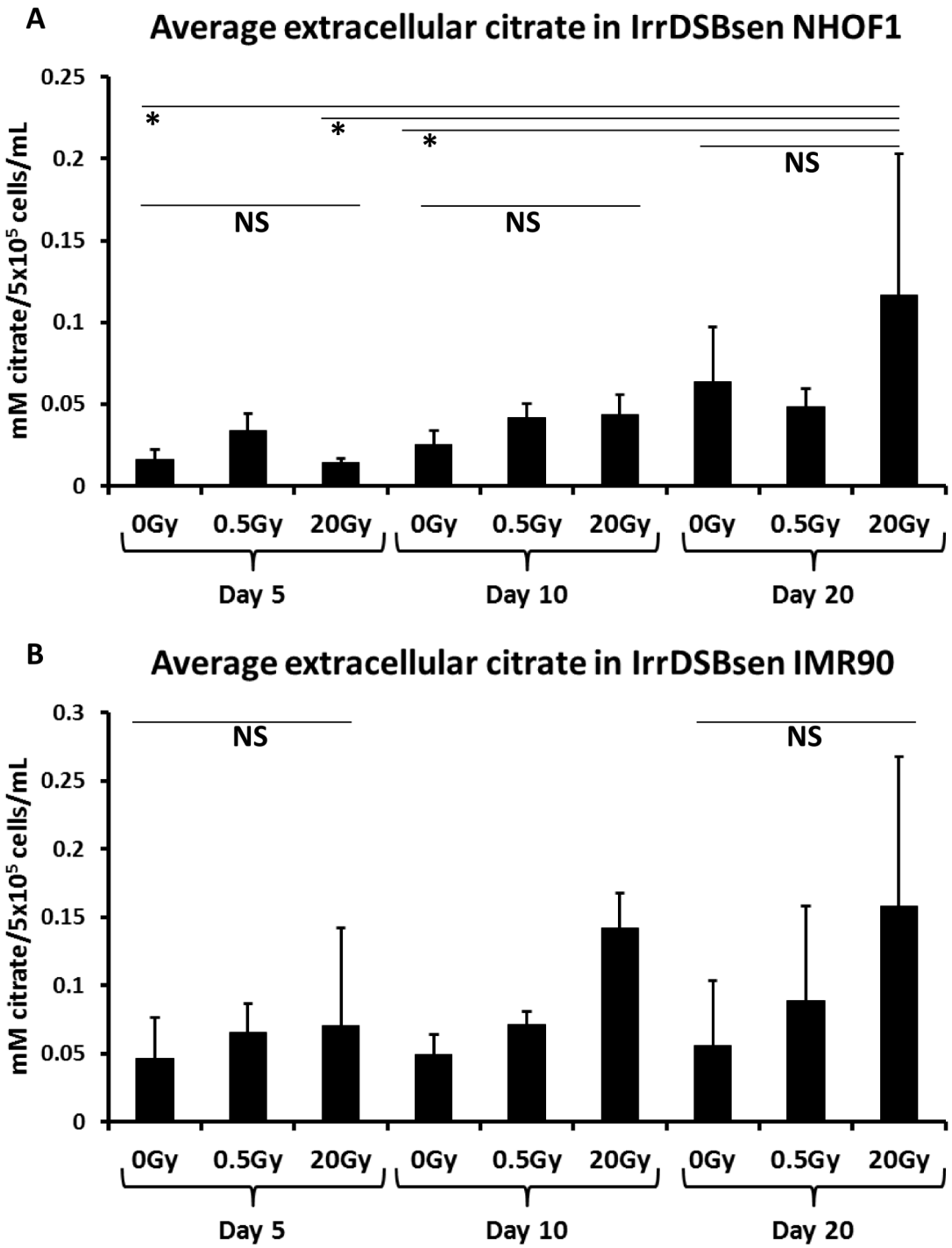

Figure 3.36: **Extracellular citrate measured in IrrDSBsen fibroblasts using GCMS**. **A** Extracellular citrate in NHOF1 5, 10 and 20 days after irradiation with 0, 0.5Gy and 20Gy gamma. n=3 error bars represent standard deviation from the mean NS = not significant *p<0.5 with a 1 way ANOVA and Tukey's post hoc analysis. **B** Extracellular citrate in IMR90 5, 10 and 20 days after irradiation with 0, 0.5Gy and 20Gy gamma. n=3 except for day 10 0Gy and 0.5Gy where n=2. error bars represent standard deviation from the mean NS = not significant *p<0.5 with a 1 way ANOVA and Tukey's post hoc analysis

Lactate and the ketone 3OHB had previously been reported to act as a metabolic fuel for cancer cells (Capparelli et al., 2012); to see if these molecules or citrate had any effect on normal fibroblast growth rates young NHOF1 cells were cultured in media containing either lactate, citrate or 3OHB for approximately 1 month and their growth rate was monitored. There was very little effect on growth as figure 3.37 shows.

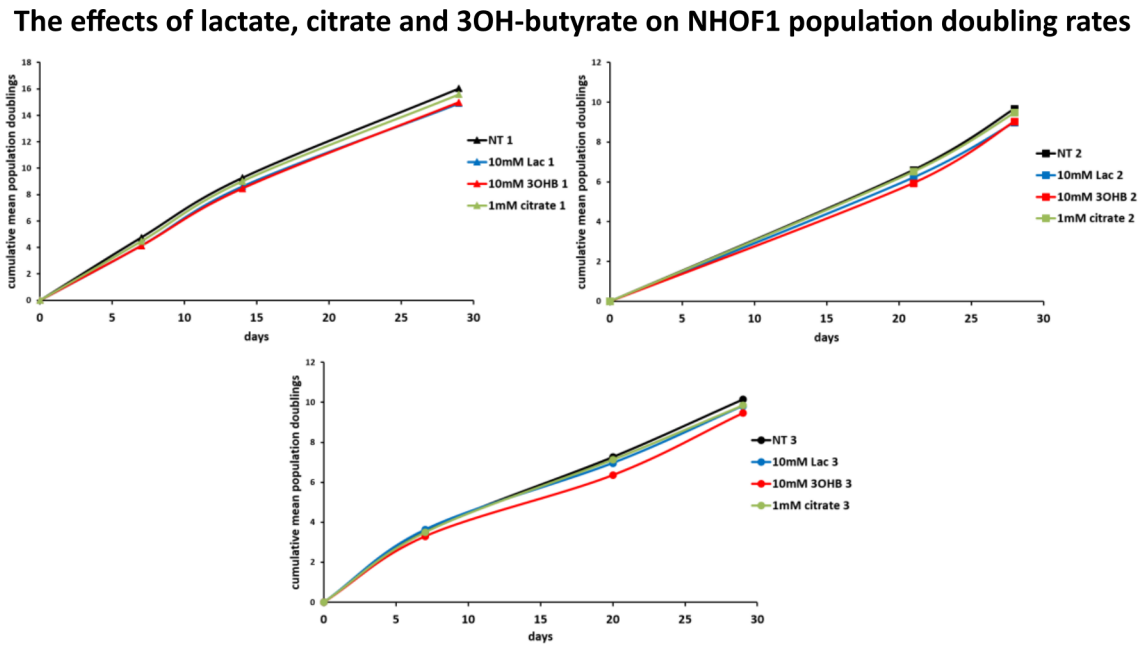

Figure 3.37: **The effect of lactate, citrate and 3OHB on cell population doubling rates in NHOF1** measured by manual cell counts over approximately 30 days. n=3.

3.4 Discussion

In this chapter we examined the secreted metabolome of senescent fibroblasts with the aim of finding a secreted biomarker of senescence. The untargeted screens gave an overview of the general metabolic phenotype of the different cell groups, allowing comparisons to be made between the profile of the senescent cells with the profiles of growing and growth arrest controls. The untargeted screens highlighted key pathways that were altered in the senescent models including peptide metabolism, lipid metabolism, redox homeostasis and energy metabolism. Importantly, one molecule was consistently elevated specifically in senescence (it was not elevated in the growth arrest or irradiation

controls) over multiple screens; citrate. In order to use citrate as a marker of senescence in experiments that aimed to manipulate the senescent phenotype and deduce the mechanism behind its elevation, it was necessary to find a targeted method that was sensitive, accurate and affordable. In this section the findings of the untargeted screens will be examined and the methods of targeted citrate analysis tested will be discussed.

3.4.1 Comparison of growth arrest controls

While both serum starved and confluent cells were very useful for teasing out which changes were specific for senescence rather than common to both senescence and transient growth arrest, the PCA plot in figure 3.2 on page 141 shows that the detected profile of confluent cells was more similar to that of PEsen cells than any other group. This suggests that confluence may be a more suitable control for PEsen than serum starvation. The profile of serum starved cells was very similar to the unconditioned 0.1% vol/vol serum media, which could suggest the serum starved cells had very low metabolic activity over the 24 hour collection period as it would appear that there were not many changes in the the metabolite levels. Senescent cells however are known to remain metabolically active, and this is supported by figure 3.2 which shows the profile of PEsen NHOF1 cells is separate from the unconditioned 10% vol/vol DMEM.

3.4.2 Metabolomic screens confirm that several metabolic pathways are altered in senescence

The untargeted metabolomic screens highlighted several altered metabolic pathways in senescent cells, as over multiple screens different molecules belonging to the same pathway were either significantly elevated or depleted.

3.4.2.1 Peptide metabolism

The finding that multiple dipeptides, all of which are products of incomplete catabolism of proteins, are depleted (figure 3.3 on page 142) in the conditioned media of senescent

cells suggests that dipeptides are being taken up from the media which is interesting because it has been demonstrated that senescent cells have impaired proteosome activity, so are unable to effectively break down proteins that have sustained severe oxidative damage (Sitte et al., 2000). Instead of recycling or releasing energy from proteins from within the cells, perhaps senescent cells rely on uptake of dipeptides to serve their energy needs. Although according to the Human Metabolome Database (HMDB) the dipeptides that were elevated in this study have no known biological function other than to be further broken down, it is possible that these dipeptides are beneficial to the cells in other ways that have not yet been discovered, as was found for the dipeptide carnosine. Carnosine has been shown to delay senescence through its ability to promote protein turnover (McFarland and Holliday, 1994).

Some amino acids were elevated in the media of senescent cells, including kynurenine (figure 3.4 on page 143). Kynurenine is a product of tryptophan metabolism and has been associated with age related neurodegenerative diseases such as Alzheimer's disease (Schwarcz et al., 2012). A relationship between senescence in the brain, for example astrocyte senescence, and neurodegeneration has been previously observed (Bhat et al., 2012) but is not well understood. The observation that extracellular kynurenine is specifically elevated in senescence, if replicated in astrocytes could offer further mechanistic insight into the link between senescence, ageing and neurodegenerative disease.

Overall it would appear that senescent cells have impaired proteosome activity, as already reported (Sitte et al., 2000) but are taking up and breaking down exogenous dipeptides, causing the observed increase in extracellular amino acids. Alternatively, these findings could be explained by the specific secretion of protease enzymes from senescent cells, as part of the SASP, which has been reported in the literature (Coppé et al., 2010a). External breakdown of the dipeptides would account for both their depletion and the increase in amino acids, although further investigation would be required before any conclusions could be made regarding this observation.

3.4.2.2 Lipid metabolism

The observed elevation of glycerophoshorylcholine (GPC) in senescent cells (figure 3.6 on page 145) is in agreement with data from a study of senescent cells using NMR (Gey and Seeger, 2013). GPC is formed from the breakdown of phosphatidylcholine and is a major form of choline storage, so its elevation in senescence suggests choline metabolism and phospholipid degradation is important in senescence. Overall the depletion of essential fatty acids such as the membrane lipid linoleate combined with the apparent degradation of phospholipids suggests there is extensive membrane catabolism occurring in senescent cells.

Interestingly, one of the phospholipids that was specifically elevated in senescent fibroblasts was malonate, which is a known inhibitor of succinate dehydrogenase. Succinate dehydrogenase is an enzyme involved in both the TCA cycle and complex II of the electron transport chain, and inhibition of this enzyme could impact dramatically on the cells ability to utilise those methods of energy generation, giving weight to the theory that senescent cells have compromised mitochondrial function and favour glycolysis over the TCA cycle.

3.4.2.3 Redox homeostasis

The increase in gamma-glutamyl amino acids and other gamma-glutamyl pathway intermediates in senescent cells (figure 3.24 on page 158) suggests that the gamma-glutamyl pathway is active in senescence. The gamma-glutamyl pathway plays a crucial role in redox homeostasis within cells as it is a mechanism of regenerating reduced glutathione (GSH), a tripeptide formed of cysteine, glutamate and glycine that reduces peroxides and mops up radicals which would otherwise cause damage to proteins, lipids and DNA.

Oxidative stress is reported to be high in senescent cells (Hubackova et al., 2012) and is thought to be linked to mitochondrial dysfunction, which can induce senescence (Wiley et al., 2016). It is therefore not surprising to find that oxidative defence pathways appear to be active. Furthermore, the senescence effector protein p53 plays an

important role in redox homeostasis independently of senescence. At high levels p53 is able to increase ROS by suppressing antioxidant genes such as manganese superoxide dismutase at the promoter level (Drane et al., 2001), or by trans-activating ROS generating enzymes for example quinone oxidoreductase (Polyak et al., 1997). Conversely, p53 can also trans-activate and up-regulate antioxidant enzymes such as glutathione peroxidase 1 (Sablina et al., 2005). It has been proposed that by manipulating the balance of ROS p53 is able to regulate cell fate, causing apoptosis, autophagy and senescence (Liu et al., 2008).

The observation that the gamma-glutamyl pathway is active is in agreement with there being high levels of ROS in the senescence models used, because it suggests there is a demand for the reducing agent GSH. High levels of ROS could be indicative of either low levels of p53, consistent with loss of the p53 induction and activation of antioxidant enzymes, or high levels of p53 consistent with suppression of antioxidant genes. Of these two options, the most likely is that there are low levels of p53 in the senescent cells, because the levels of ROS induced in the presence of high levels of p53 often induces apoptosis, not senescence (Liu et al., 2008), and it has been established that during the course of senescence induction and stabilisation an initial increase in p53 activation is followed by an increase in $p21^{WAF1}$ and subsequent decline in p53, with the senescent state usually being maintained by $p16^{INK4A}$ (Stein et al., 1999).

3.4.2.4 Energy metabolism

One measure of the energy status of the cells is the relative level of ATP to ADP or AMP. Although intracellular ATP was not detected in the metabolomic screen, intracellular ADP levels were measured (see figure 3.10 on page 148) and did not increase in PEsen, although they did show a slight elevation in the growth arrest controls (which was not statistically significant). This is important because if ATP is considered the "cellular energy currency", ADP is effectively evidence of spent ATP (the breaking of a phosphate bond in ATP releases energy, leaving ADP which can be recycled back to

ATP). Having more ADP than ATP is a sign of metabolic imbalance; the cell is using up ATP faster than it can generate it. While the ratio of ATP:ADP could not be calculated here, it is reasonable to assume that as the intracellular levels of ADP in PEsen NHOF1 were not higher than in growing controls, it is unlikely that there is a metabolic imbalance in those cells. Furthermore, AMP was significantly depleted in PEsen NHOF1 but not growth arrest controls (figure 3.11 on page 149) which contradicts findings by Zwerschke and colleagues, who reported that senescent cells have elevated AMP (Zwerschke et al., 2003). Both ADP and AMP activate AMP-activated protein kinase (AMPK) when elevated, which has multiple effects on cell metabolism. AMPK has been shown to increase glucose transport into the cell, promoting glycolysis, as well as increasing fatty acid oxidation, mitochondrial biogenesis and autophagy, all of which should increase ATP production to restore the balance of energy (reviewed in (Choudhary et al., 2014). The fact that AMP and ADP are low in PEsen cells suggests that either adequate ATP is being generated in senescent cells or that senescent cells are not utilising ATP. Given that the PCA analysis showed a clear separation between PEsen and unconditioned media (figure 3.2 on page 141) it must be assumed that PEsen cells are metabolically active, so the latter explanation can be rejected. Therefore PEsen cells must be generating ATP, either through glycolysis coupled to the TCA cycle and oxidative phosphorylation, or alternatively by glycolysis.

The observation that senescent cells have increased glycolytic activity but an impaired TCA cycle has also been recorded in a study of dermal fibroblasts. The authors described an increase in glycolytic activity that was not matched by TCA activity combined with decreased activity in the malate - aspartate shuttle, resulting in a metabolic imbalance and a depletion of ATP (and therefore accumulation of ADP). ATP depletion is known to activate nutrient sensors and promote the transcription of glycolytic enzymes, which exacerbates the phenotype (Zwerschke et al., 2003). However, as figure 3.10 on page 148 shows, we did not find an accumulation of intracellular ADP in senescence, in fact the opposite was observed. The growth arrest controls however did

display an increase in intracellular ADP (figure 3.10 on page 148), indicating that while cellular stress does induce a metabolic imbalance and a build up of ADP results, the scenario is not not the same in established senescence.

The accumulation of the TCA cycle intermediates citrate and fumarate in the conditioned media of senescent fibroblasts could support the theory that the TCA cycle remains active in senescence. In addition the depletion of pyruvate from the media, which is converted to acetyl Co-A before entering the TCA cycle, could be due to a reduced level of glycolysis, because pyruvate is a product of glycolysis and its depletion from the media indicates that more is being consumed than produced. Acetyl Co-A is not only used in the TCA cycle however, it is also required for acetylation of proteins, so acetyl-Co-A produced from breakdown of pyruvate is not necessarily all going into the TCA cycle. In addition the accumulation of acetyl Co-A seen in PEsen and growth arrested NHOF1 (figure 3.12 on page 149) could be an indication that the TCA cycle is not functioning optimally. Another way of assessing the activity of the TCA cycle is to look at the NAD+/NADH ratio. As figure 1.6 on page 58 illustrates, the TCA cycle generates NADH from NAD+. and in growing cells there is a relative abundance of NADH compared to NAD+ however in growth arrested and senescent cells NADH levels fall, while NAD+ levels are maintained (figure 3.13 on page 150). This could also support the case that the activity of the TCA cycle is reduced in senescence.

In contrast to the suggestion that the senescent cells could be exhibiting reduced glycolytic activity, when data from IrrDSBsen conditioned media is taken into account an increase in extracellular lactate is observed. Lactate is also a product of glycolysis, and its elevation is generally associated with a glycolytic phenotype. As demonstrated in Chapter 2, it seems likely that the phenotype exhibited by IrrDSBsen is stronger because a higher percentage of the cells are fully senescent at the time of measurement whereas in the PEsen experiments the percentage was much lower. It is possible therefore that there is a gradual shift in metabolism over time as the senescent phenotype develops. A shift away from the TCA cycle towards a more glycolytic metabolism may be due to

declining mitochondrial function in senescence. Several studies have already shown that mitochondrial dysfunction can induce senescence (Passos et al., 2007; Moiseeva et al., 2009; Velarde et al., 2012; Wiley et al., 2016) and recent work by Clara Correia-Melo and colleagues has demonstrated that mitochondrial biogenesis is necessary for much of the senescence phenotype (Correia-Melo et al., 2016).

The data on intracellular metabolites in PEsen NHOF1 also show an increase in several metabolites associated with PPP activity (see figure 3.8 on page 147). The PPP (a schematic of which is shown in figure 3.38 on the following page) is a pathway that breaks down glucose and produces ribose-5-phospahte (in the oxidative arm of the pathway) which can be used in nucleotide metabolism, or recycled back to glucose-6-phosphate (in the non-oxidative arm of the pathway) and re-enter the oxidative arm of the pathway. The oxidative arm of the PPP also generates NADPH, a reducing equivalent used in lipid synthesis as well as forming a vital part of the cells oxidative defence by facilitating the reduction of oxidised glutathione (Winkler et al., 1986). Interestingly, intracellular NADPH was elevated in PEsen and growth arrest controls (see figure 3.13 on page 150) although the increase wasn't found to be statistically significant. When considered together with the elevation of several PPP metabolites it does suggest that PPP activity is increased in growth arrest and particularly in senescence. The observation that PPP activity is increased in senescent cells supports previous suggestions that senescent cells have an active oxidative stress response.

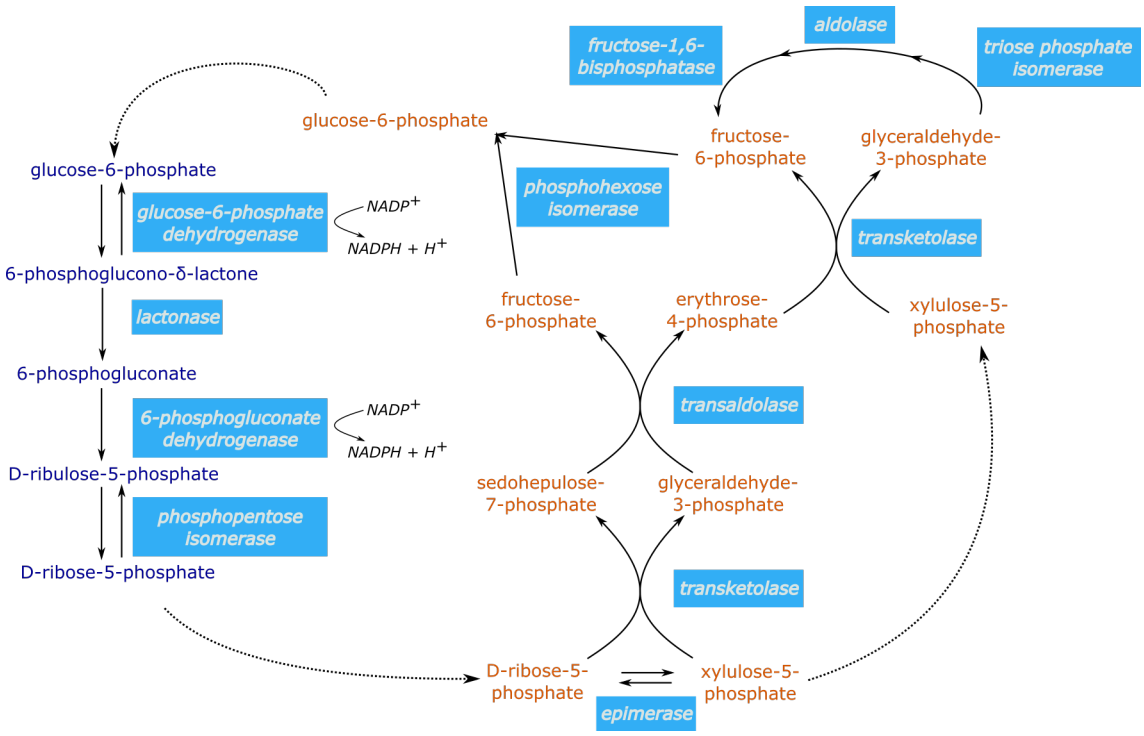

Figure 3.38: **The pentose phosphate pathway (PPP)** Blue boxes represent enzymes, blue text represents the intermediates in the oxidative arm of the PPP and orange text represents intermediates in the non-oxidative arm of the PPP. Solid arrows represent the direction of reaction and dotted arrows show where the product of one reaction is involved at a different section of the pathway. NADP+ = nicotinamide adenine dinucleotide phosphate NADPH = reduced nicotinamide adenine dinucleotide phosphate

3.4.3 Extracellular citrate is specifically elevated in senescence

As well as forming part of the general energy metabolism signature of senescent cells, citrate was the only molecule to be elevated across all of the screens with statistical significance. It was significantly elevated relative to growth arrest controls in PEsen NHOF1 fibroblasts (figure 3.7 on page 146), as well as being significantly elevated in PEsen cells from other tissues relative to growing controls (figure 3.14 on page 151), and was also significantly elevated in IrrDSBsen cells from multiple lines relative to 0Gy controls (figure 3.16 on page 152), and in IrrDSBsen NHOF1 relative to 0.5Gy radiation controls (figure 3.17 on page 153). Interestingly, intracellular citrate was not elevated (figure 3.26 on page 161). This is important because citrate is known to directly inhibit glycolysis via inhibition of phosphofructokinase (Newsholme et al., 1977), however in

PEsen NHOF1 cells at least, intracellular citrate is not elevated compared to growing cells (see figure 3.26 on page 161) so would not be expected to have any increased inhibitory effect on glycolysis.

Attempts to replicate this result using enzymatic kits and precipitation were not successful, due to interference from other molecules present in the media. NMR was also unsuccessful, most likely due to the low total amount of citrate present in the media as we were able to identify peaks corresponding to citrate when it was spiked into the media, so there was not a problem with the method used. Targeted GCMS was successfully used to detect elevated citrate in IrrDSBsen compared to 0.5Gy and 0Gy controls (figure 3.36 on page 169) and PEsen (figure 3.35 on page 168) although the data was more variable than that acquired by Metabolon. This is probably due to the extra variation introduced during preparation and derivitisation of the samples as Metabolon used an automated system to extract and derivitise the samples, which is a technically demanding process involving small volumes of liquid. Any inaccuracy in the volumes pipetted both before drying and during the derivitisation impacts on the calculation of the original concentration in the sample. In the targeted analysis I manually pipetted each sample individually at all of the steps, so small errors were more likely than in the original screens. Despite the increased variation, the method was successful in quantifying extracellular citrate.

Citrate therefore appears to be a strong candidate for a secreted marker of senescence. Indeed, a search of the literature revealed that citrate plays a role in several cell processes reported be altered in senescence (Lee et al., 2015), and has even been linked to ageing in humans (Menni et al., 2013).

3.4.3.1 Role of citrate in cell biology

Citrate is a tricarboxylate produced from acetyl Co-A by the enzyme citrate synthase (CS) in the mitochondria. It is then either broken down by aconitase 2 (ACO2) in the TCA cycle to form isocitrate, or exported from the mitochondria into the cytoplasm

by the selective transporter SLC25A, where it can be broken down to isocitrate by aconitase 1 (ACO1) or used by ATP citrate lyase (ACLY) to generate acetyl Co-A and NADPH which are important for fatty acid metabolism and acetylation of proteins, and NAD^+ which is necessary for glycolysis. More citrate can be transported into the cytoplasm from outside the cell if needed through SLC13 transporter family members NaDC1, NaDC3 and NaCT (Gopal et al., 2007; Mycielska et al., 2009)(see figure 3.39).

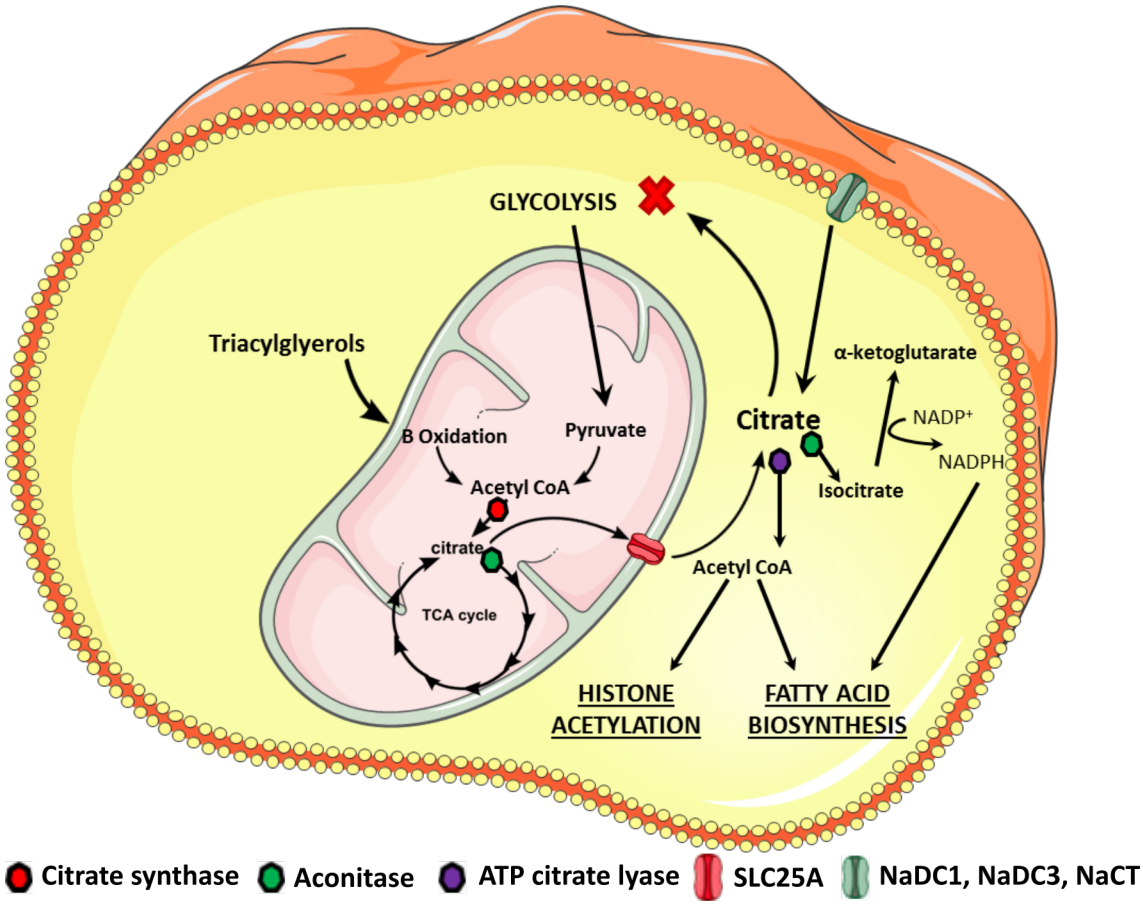

Figure 3.39: **Fate of citrate within the cell.** Citrate is produced in mitochondria by citrate synthase, it then either remains in the mitochondria and enters the TCA cycle where it is broken down by aconitase 2 to isocitrate, or is transported across the mitochondrial membrane into the cytoplasm by the SLC25A citrate carrier. Once in the cytoplasm citrate can inhibit glycolysis via phosphofructokinase, can be converted to isocitrate by aconitase 1, or to acetyl Co-A by ATP citrate lyase. Additional citrate can be transported across the plasma membrane through the SLC13 family members NaDC1, NaDC3 and NaCT (reviewed in Mycielska et al., 2009).

Citrate is present in the blood usually at around 0.1mM (Costello and Franklin, 1991), although there is not much literature on where this citrate comes from, Gopal

suggests that it comes mainly from dietary intake, with the possibility that some citrate is released from cells by an unknown mechanism (Gopal et al., 2007). In prostate luminal epithelium however there is a known mechanism for citrate transport across the plasma membrane from the cytoplasm to the extracellular space; an isoform of the mitochondrial citrate transporter SLC25A which is translocated to the plasma membrane (Mazurek et al., 2010). Unlike other tissues, the prostate produces large amounts of citrate and releases it in the expressed prostatic secretion at concentrations up to 150mM, with final concentration in the seminal fluid of up to 50mM (Kavanagh, 1994). It has been observed that incubating spermatozoa in 10mM citrate (and 10mM lactate) increases ATP production (Medrano et al., 2006), so it is likely that these high concentrations of citrate act as metabolic fuel for the spermatozoa. Given that intracellular citrate levels in senescent cells are not elevated, it seems reasonable to assume that the extracellular elevation is due to an active process of transport across the plasma membrane, possibly in the same way citrate is transported across the plasma membrane of prostate epithelium. Although currently the only data on intracellular citrate in senescent cells are part of an untargeted screen that was not quantitative, the relative levels of intracellular citrate in senescent cells to growing cells compared with the relative level of extracellular citrate in senescent cells to growing cells suggest that senescent cells are not only exporting citrate while the growing cells are not but are either producing more citrate or not breaking down citrate as readily as growing cells.

While the concentrations detected in this thesis were not as high as recorded in the prostatic secretions, it is not known what the local concentrations surrounding senescent cells *in vivo* might be. To see if lower levels of citrate or lactate were capable of promoting proliferation in normal fibroblasts we incubated cells in media containing either 10mM lactate, 1mM citrate or 10mM 3OHB (a molecule also previously reported to be used as a metabolic fuel (Bonuccelli et al., 2010)) and measured the population doubling rate. The addition of these molecules did not have a positive effect on the growth rate of the cells, however the effect on the metabolism of the cells was not

investigated.

3.4.4 Summary

In this chapter citrate was identified as a strong candidate for a secreted biomarker of senescence in fibroblasts; fulfilling the primary aim of this project. The metabolomic screens also showed that energy, lipid and protein metabolism were altered in senescent cells as well as redox homeostasis pathways, which give insight into the overall metabolic status of senescent cells. Taken together the data suggest that senescent cells have increased glycolytic and PPP activity, whereas the TCA cycle appears to be less active. This shift in metabolism may be in response to oxidative stress, as several metabolites involved in redox homeostasis were also elevated. These data are also consistent with reports in the literature that senescent cells have dysfunctional mitochondria (Hutter et al., 2004; Passos et al., 2007; Ghneim and Al-Sheikh, 2010; Wiley et al., 2016), as functioning mitochondria are necessary for the TCA cycle and OXPHOS to occur and moreover dysfunctional mitochondria are are ineffective at neutralising ROS (Balaban et al., 2005). In the next chapter we will discuss the experiments which were undertaken to try and understand more about what is regulating these changes and how citrate is involved.

Chapter 4

Regulation of the metabolome in senescence

4.1 Introduction

In the previous chapter the TCA cycle intermediate citrate was identified as a specific secreted marker of senescence. Several metabolic pathways were also identified as altered in both PEsen and IrrDSBsen. In this chapter we will look more closely at proteins that may be involved in the regulation of those pathways and therefore could directly or indirectly influence the levels of extracellular citrate.

4.1.1 Proteins involved in glucose metabolism

Firstly, as citrate is an intermediate in the TCA cycle, and the untargeted screens identified energy metabolism as a pathway generally altered in senescence, qPCR was used to investigate any changes at the transcriptional level of proteins involved in the TCA cycle and the closely related pathways glycolysis and the PPP. Enzymes directly involved in the generation (citrate synthase (CS)) and breakdown (ACLY, ACO1 and ACO2) of citrate were also assessed at the transcriptional level and the results confirmed at the protein level using western blots.

4.1.2 Proteins involved in oxidative stress response

Redox homeostasis was another pathway identified as important in differentiating between senescent cells and growing or growth arrested controls. The metabolic pathways active in a cell can be affected by the levels of ROS present, and furthermore ROS is known to induce senescence. For this reason transcriptional regulation of proteins involved in cellular oxidative stress response was examined, and levels of ROS were measured.

4.1.3 Senescence effector proteins

To determine the importance of the senescence effector proteins $p16^{INK4A}$, $p21^{WAF1}$ and p53, conditioned culture media was analysed from fibroblasts lacking these proteins. Preliminary data has also been gathered on the relationship between telomere length and extracellular citrate levels.

4.1.4 Summary

This chapter will address the second aim of the thesis; to elucidate the mechanism behind the elevation of citrate in senescent cells, using a combination of molecular techniques (qPCR and western blot) and cell biology (knockout of senescence effector proteins).

4.2 Materials and methods

4.2.1 Cell culture

Routine culture was performed using the same reagents and techniques as described in previous chapters, although some different cell lines were used for this work. Normal human lung fibroblasts (Loxo26) along with isogenic knockout of p53 (Loxo26 $p53^{-/-}$) and $p21^{WAF1}$ (Loxo26 $p21^{-/-}$) were a kind gift from John Sedivy at Brown University USA. Gordon Peters at the Cancer Research UK London Research Institute kindly

gave us human dermal fibroblasts homozygous for a 19 base pair deletion in exon 2 of the *CDKN2A* gene that encodes $p16^{INK4A}$, and so are $p16^{INK4A-/-}$(Leiden) (Stott et al., 1998).

NHOF1 cells were immortalised by Professor Ken Parkinson (Queen Mary University of London) by expression of TERT. To distinguish between the telomere lengthening and non canonical functions of TERT, TERT-HA was used (TERT-HA is TERT with a c- terminal haemaglutinin (HA) tag. TERT-HA is catalytically active but does not lengthen telomeres (Counter et al., 1998)), and the vector control NHOF1 pBabe Puro was also created. The vectors were provided by Professor Robert Weinberg (Massachusetts Institute of Technology).

4.2.2 Measurement of reactive oxygen species (ROS)

$1x10^5$ adherent cells were incubated for 1 hour with 1μM H_2DCFDA (2',7'-dichlorofluoroscin diacetate, catalog number 287810 from Calbiochem) in DMEM containing 10% vol/vol FBS. After trypsinisation as described previously, the cell suspension was centrifuged at 1000rpm for 5 minutes. The cell pellet then was re-suspended in 500μl 1xPBS at 37°C and the suspension was transferred to FACS tubes with 1μl of DAPI added to enable cell viability counts. With the help of Dr Gary Warnes at the Blizard Flow Cytometry Core Facility, a Beckton Dickinson BD LSRII flow cytometer was used to detect cells that had sufficient ROS to oxidise the non-fluorescent product of H_2DCFDA to the fluorescent 2', 7' –dichlorofluorescein (DCF). DCF has excitation and emission spectra of 495 nm and 529 nm respectively. As a positive control, cells treated with 1mM Tert-butyl-hydroperoxide (Luperox TBHP solution, 458139 lot#BCBG4467V Sigma Aldrich) for 2 hours were used, with or without recovery time prior to the assay and as a negative control, cells treated with the antioxidant PBN (N-tert-butyl-α-phenylnitrone B7263, Sigma Aldrich) at 1mM in DMEM containing 10% vol/vol FBS for 1 or 2 hours before assay were used. Non-viable cells as determined by DAPI staining were excluded from the counts, and cells within the gates of viable and positive for DCF were compared to

cells within the gates of viable but negative for DCF.

4.2.3 qPCR of transcripts involved in energy metabolism and oxidative stress response

4.2.3.1 RNA extraction

RNA was extracted using the RNeasy Mini Kit (Qiagen catalog number 74104). The cell pellet of approximately $5x10^5$ – $1x10^6$ cells was thawed on wet ice, lysed as per Qiagen recommendations in 350µl RLT buffer containing 1% vol/vol β-Mercaptoethanol, and homogenised using a QIAshredder spin column (Qiagen catalog number 79654). Total RNA was extracted using ethanol precipitation onto columns followed by elution in 30µl RNAse free water. Eluted material was re-incubated for 1 minute on the column before being spun off, to maximise the RNA yield.

4.2.3.2 RNA quantification and quality assessment

RNA was diluted 1:4 in Tris-EDTA (TE) pH 8.0 (5µl RNA + 15µl TE) and using a Nanodrop 1000 UV with a blank of 5µl RNAse free water + 15µl TE pH 8.0, the absorbance values at 260nm, 230nm and 280nm were recorded. The 260/280nm ratio and 260/230nm ratios were recorded to make sure that both values were close to 2.0 and that there was a single peak at 260nm., to ensure that the RNA was not contaminated with proteins, chaotropic salts or phenol. The Nanodrop 1000 calculated the concentration of RNA from the absorbance of UV light using the Beer- Lambert Law.

4.2.3.3 Complimentary DNA (cDNA) generation

cDNA was generated from mRNA using the RT2 First Strand Kit (from Qiagen, catalog number 330401) with on column DNAse digestion for 20 minutes at room temperature (RNAse free DNAse Set, Qiagen catalog number 79254). 400ng RNA was used per reverse transcription reaction, as per kit instructions. The reactions were carried out in duplicate or triplicate at 42°C for 15 minutes, and to stop the reaction the temperature was increased to 95°C for 5 minutes before the tubes were removed and put directly onto ice. All of the incubations were carried out in a PCR block (Venti 96 well

Thermal Cycler, Applied Biosystems).

4.2.3.4 qPCR arrays

384 (4 x 96) well array plates containing 4 replicate primer assays for each of 84 pathway-focused genes (Human Glucose Metabolism PAHS-006Z, SA Biosciences and Human Oxidative Stress PAHS-065Z, SA Biosciences) were used as well as 4 replicate primer assays for each of 5 housekeeping genes, 4 wells containing genomic DNA controls, 12 wells containing reverse-transcription controls, and 12 wells containing positive PCR controls. cDNA was mixed with Sybr Green Mastermix (Roche) and added to the plates using EZLoad covers; cDNA from senescent and matching young control cells from both IMR90 and NHOF1 were run together on each plate. Real Time PCR was carried out using the Roche LightCycler 480; 1 cycle of 10 minutes at 95°C to activate HotStart DNA polymerase, with 45 cycles of 15 seconds at 95°C and 1 minute at 60°C for data acquisition. Quantification of threshold crossing (CT) was done using the Light Cycler 480 Second Derivative Max. Analysis of the fold up or down regulation of genes was performed using the Excel-based PCR Array Data Analysis Templates for 384-well arrays (available for download from www.SABiosciences.com/pcrarraydataanalysis.php.), using the most stable housekeeping genes for normalisation (minimum of 2 used). 3 biological repeats were quantified in this way. A full list of genes for the Human Glucose Metabolism array and Human oxidative stress array along with a brief description of their functions can be seen in appendix A on page 270 and appendix B on page 285 respectively.

4.2.3.5 Western blot of PDK4, ACO1, ACO2 and ACLY.

Western blots were performed as described previously in Chapter 3 section 2.2.6 on page 96. The primary antibody targeting PDK4 (mouse monoclonal [ICBG5] ab110336 from Abcam UK), ACO1 (rabbit monoclonal [EPR7225] ab126595 from Abcam, UK), ACO2 (rabbit polyclonal ab71440 from Abcam, UK) or ACLY (rabbit polyclonal #4332 from Cell Signalling) was diluted 1:1000 in blocking buffer, and incubated with the membrane overnight at 4°C, under gentle agitation. The next day the membranes were

washed three times in TBS-T, 5 minutes per wash on a medium speed rocker, prior to incubation with secondary antibody (goat polyclonal anti-mouse IgG HRP conjugated ab6789 from Abcam UK, at a dilution of 1:5000, or goat polyclonal anti-rabbit IgG HRP conjugated, from Thermo Fisher Scientific, USA and 1:10,000) for 1 hour at room temperature with gentle agitation. A final set of washes in TBS-T were performed and the protein bands were visualised using an enhanced chemiluminescent substrate of HRP (Pierce ECL Western Blotting Substrate) as previously described. In the case of PDK4, which has a molecular weight of 47kDa very similar to that of β-actin, the membrane had to be stripped using mild stripping buffer (15g glycine, 1g SDS, 10mL Tween-20 adjusted to pH2.2 and brought to 1L with ultrapure water). Membranes were incubated in stripping buffer for 10 minutes with gentle agitation before being washed twice with PBS for 10 minutes each, then twice with TBS-T for 10 minutes each. The success of the stripping process was checked by applying HRP substrate and exposing the membrane to film for longer than the longest exposure time used to detect the first primary antibody, and developing it. If bands were visible the stripping process was repeated. If no bands were visible the membranes were then incubated in blocking buffer for 30 minutes before addition of primary rabbit anti-β-actin antibody as previously described in section 2.2.6 on page 96.

4.3 Results

4.3.1 Glucose metabolism

As some of the data from the metabolomic screen regarding the TCA metabolites was difficult to interpret (the elevation of citrate and fumarate in the media suggested the TCA cycle was active however intracellularly the levels of these metabolites was not elevated) a qPCR array was used to interrogate the mRNA levels of transcripts relevant to energy metabolism pathways. A list of all the genes assessed in the array and can be seen in appendix A.

Many genes coding proteins that had a role in glycolysis were significantly elevated in PEsen fibroblasts relative to growing controls, however in some cases there were quite dramatic cell type specific differences (see figure 4.1). For example the transcript for phosphoenolpyruvate carboxykinase 2 (PCK2) was down-regulated in PEsen NHOF1 but up-regulated in PEsen IMR90.

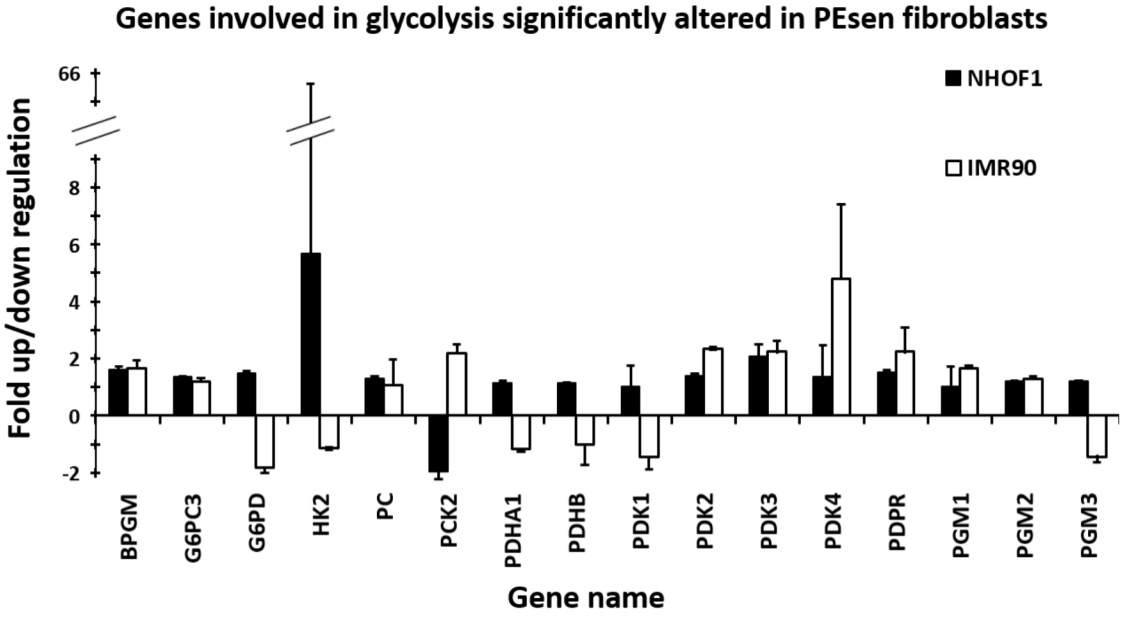

Figure 4.1: **Fold up/down regulation of genes involved in glycolysis regulation in PEsen fibroblasts**. Bars represent fold up/down regulation of genes in PEsen fibroblasts that were identified as being statistically significant from growing controls using a Student's T Test. n=3 error bars represent standard deviation from the mean.

Similarly, there were a number of genes relating to the TCA cycle that were significantly up-regulated in PEsen, although again in some cases the opposite result was seen in NHOF1 and IMR90 (figure 4.2).

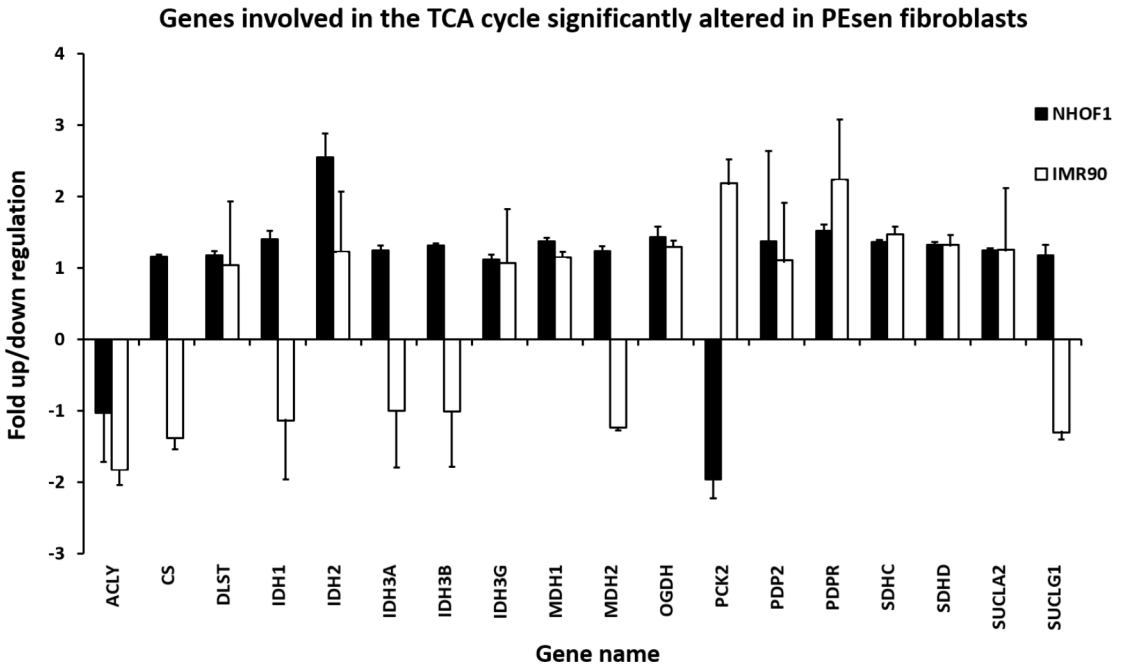

Figure 4.2: **Fold up/down regulation of genes involved in TCA cycle regulation in PEsen fibroblasts**. Bars represent fold up/down regulation of genes in PEsen fibroblasts that were identified as being statistically significant from growing controls using a Student's T Test. n=3 error bars represent standard deviation from the mean.

Some genes involved in the PPP were also significantly altered in PEsen fibroblasts, although only phosphoribosyl pyrophosphate synthetase 1 (PRPS1) in IMR90 showed a fold change larger than 2 (figure 4.3).

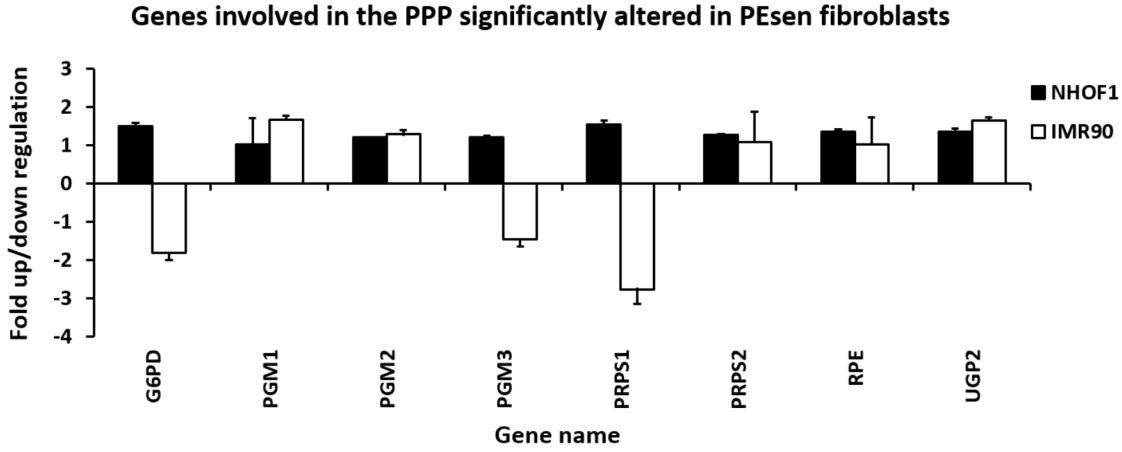

Figure 4.3: **Fold up/down regulation of genes involved in PPP regulation in PEsen fibroblasts**. Bars represent fold up/down regulation of genes in PEsen fibroblasts that were identified as being statistically significant from growing controls using a Student's T Test. n=3 error bars represent standard deviation from the mean.

As previous chapters have demonstrated, the IrrDSBsen model of senescence represents a more extreme phenotype than PEsen, so a more dramatic set of changes were expected at the transcriptional level in IrrDSBsen cells. In fact the difference was not very dramatic, except in the case of PDK4 which in IrrDSBsen was up-regulated by nearly 60 fold in IMR90 (figure 4.4) compared to an up-regulation of around 5 fold in PEsen. Generally the trend for up or down regulation of a certain gene was the same in both PEsen and IrrDSBsen, with a few exceptions in the genes associated with glycolysis; for example hexokinase 2 (HK2) was down-regulated in PEsen IMR90 but up-regulated in IrrDSBsen IMR90, although in PEsen the down-regulation was less than 2 fold, so not very substantial. In some cases fold up/down regulation of specific genes was not available for one or other of the senescence models because the quality of the data was not good enough, so some of the genes shown in the PEsen graphs are not found in the IrrDSBsen graphs for the same pathway and *vice versa.*

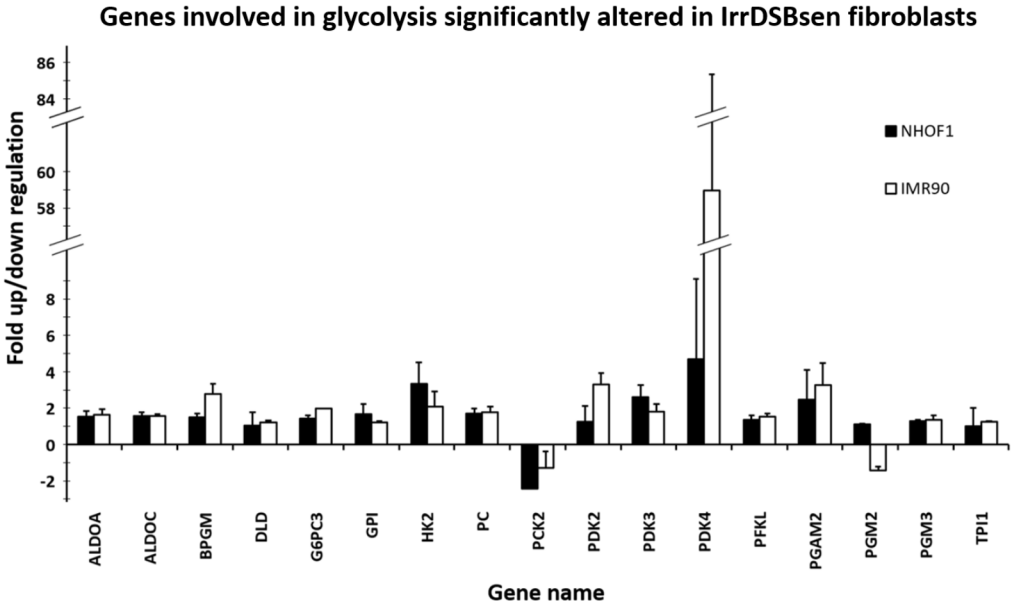

Figure 4.4: **Fold up/down regulation of genes involved in glycolysis regulation in IrrDSBsen fibroblasts.** Bars represent fold up/down regulation of genes in PEsen fibroblasts that were identified as being statistically significant from growing controls using a Student's T Test. n=3 error bars represent standard deviation from the mean.

The fold up/down regulation of genes involved in the TCA cycle was not remarkable even in IrrDSBsen (figure 4.5), and there were no contradictions regarding whether a

gene was up or down regulated between IrrDSBsen and PEsen.

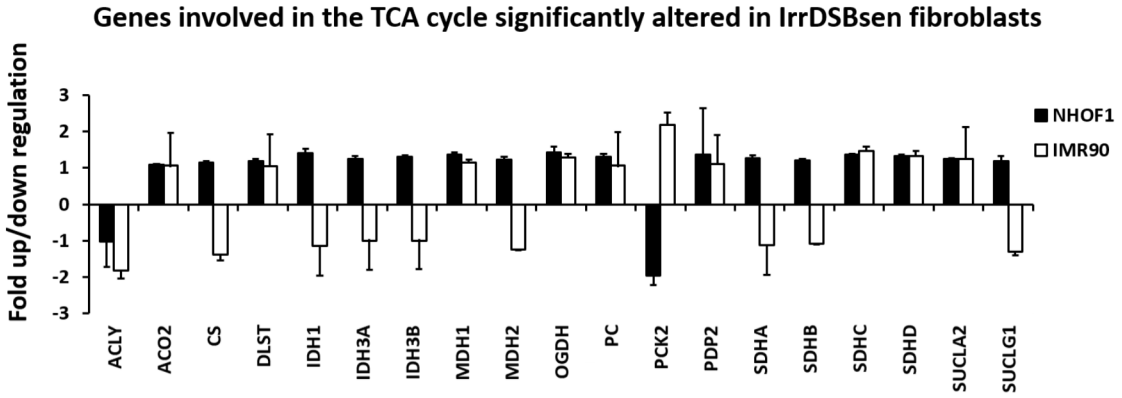

Figure 4.5: **Fold up/down regulation of genes involved in TCA cycle regulation in IrrDSBsen fibroblasts**. Bars represent fold up/down regulation of genes in PEsen fibroblasts that were identified as being statistically significant from growing controls using a Student's T Test. n=3 error bars represent standard deviation from the mean.

The PPP also did not show large fold changes in IrrDSBsen fibroblasts (figure 4.6) and many of the fold changes that were statistically significant were in the opposite direction to those shown in PEsen.

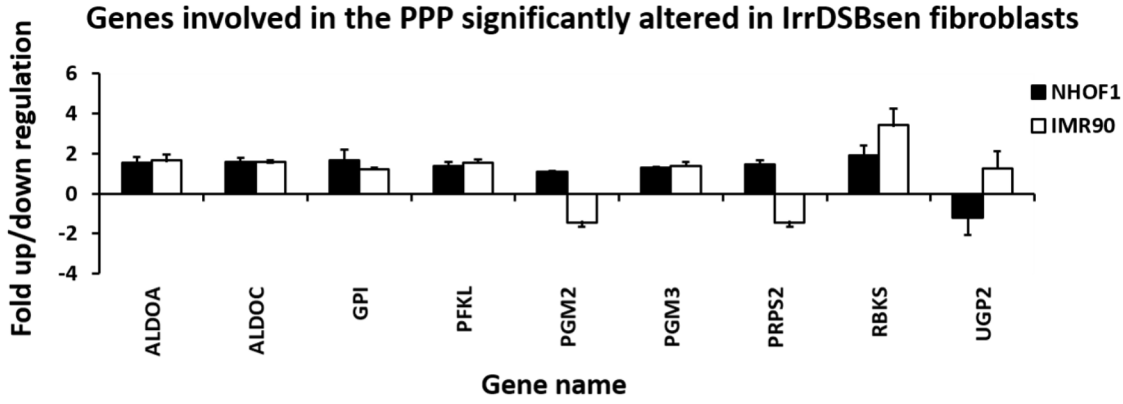

Figure 4.6: **Fold up/down regulation of genes involved in PPP regulation in IrrDSBsen fibroblasts**. Bars represent fold up/down regulation of genes in PEsen fibroblasts that were identified as being statistically significant from growing controls using a Student's T Test. n=3 error bars represent standard deviation from the mean.

When considering only genes with an up or down regulation of 2 fold or more in either IMR90 or NHOF1 fibroblasts, it becomes clear that at the transcriptional level senescence has no measurable effect on genes relating to the TCA cycle, but there are

several genes involved in glycolysis that are altered at the transcriptional level in both PEsen and IrrDSBsen senescence, as shown in figure 4.7.

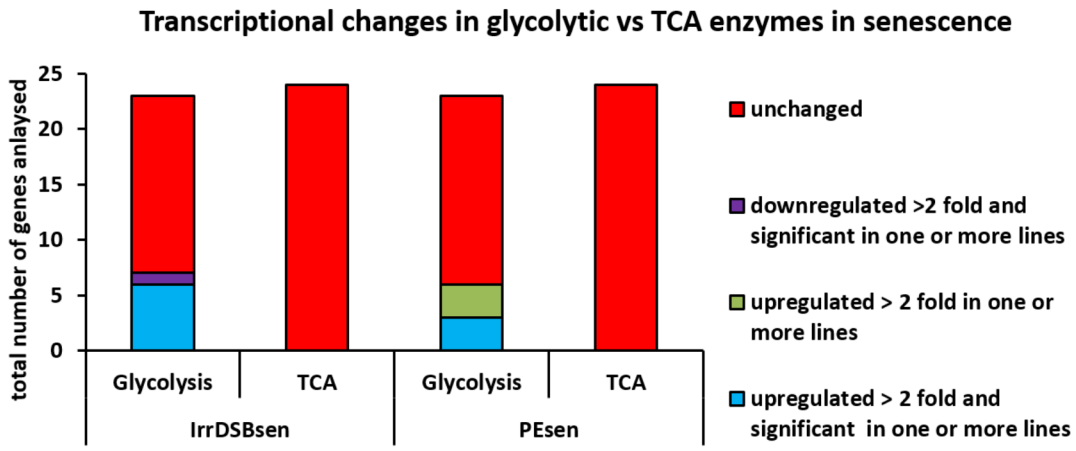

Figure 4.7: Total number of detected transcriptional changes in glycolysis compared to TCA cycle, in both IrrDSBsen and PEsen. Genes up or down regulated by 2 fold or more in either NHOF1, IMR90 or both lines were counted. n=3 per gene per cell line per senescence group. Statistical significance determined using a Student's T Test.

The gene with the largest fold change was PDK4. To see if this up regulation at the transcriptional level resulted in an increase at the protein level, and also to include growth arrest controls that it was not possible to run the qPCR, a western blot was performed on the lysates of growing, PEsen and growth arrested NHOF1 (figure 4.8) and IMR90 (figure 4.9). PDK4 protein was not elevated in PEsen in either line, although in IMR90 it was significantly elevated in confluent controls.

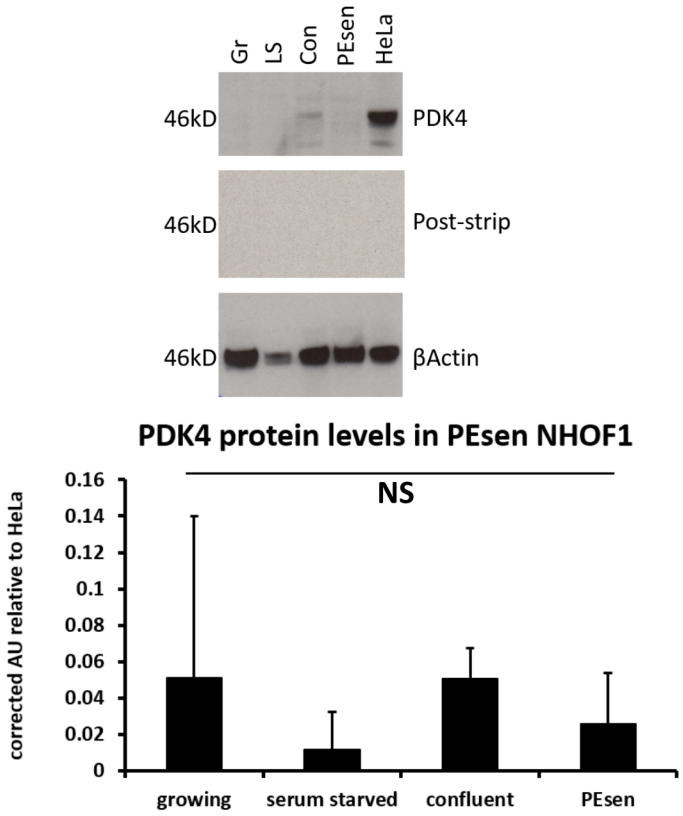

Figure 4.8: **PDK4 protein levels in PEsen NHOF1 and growth arrest controls**. **A** Representative western blot of PDK4 protein in PEsen NHOF1 cells as well as growing (Gr), serum starved (LS) and confluent (Con) controls, with β-actin loading control. **B** Average PDK4 protein level in PEsen NHOF1 and controls as in A, quantified relative to HeLa. Error bars represent standard deviation from the mean, n=3 NS= not significant with a 1 way ANOVA and Tukey's post hoc analysis.

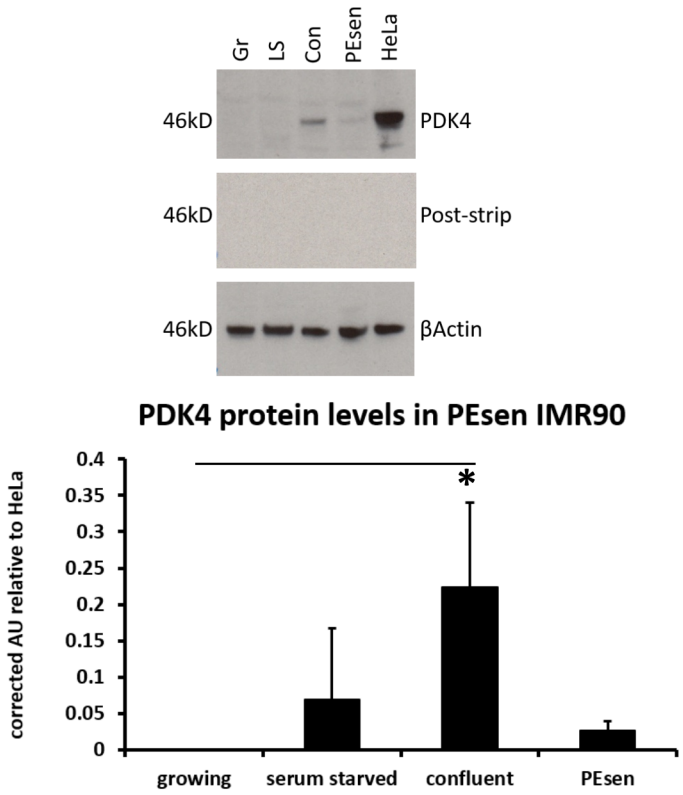

Figure 4.9: **PDK4 protein levels in PEsen IMR90 and growth arrest controls**. **A** Representative western blot of PDK4 protein in PEsen IMR90 cells as well as growing (Gr), serum starved (LS) and confluent (Con) controls, with β-actin loading control. **B** Average PDK4 protein level in PEsen IMR90 and controls as in A, quantified relative to HeLa. Error bars represent standard deviation from the mean, n=3 *$p<0.05$ with a 1 way ANOVA and Tukey's post hoc analysis.

In IrrDSBsen NHOF1 PDK4 was not detected, however in IrrDSBsen IMR90 there was a trend for PDK4 elevation that was not statistically significant (see figure 4.10). In NHOF1 it appears there could have been protein degradation in the 20Gy samples across all time points, or a miss calculation of protein content leading to under-loading of the gel for those groups.

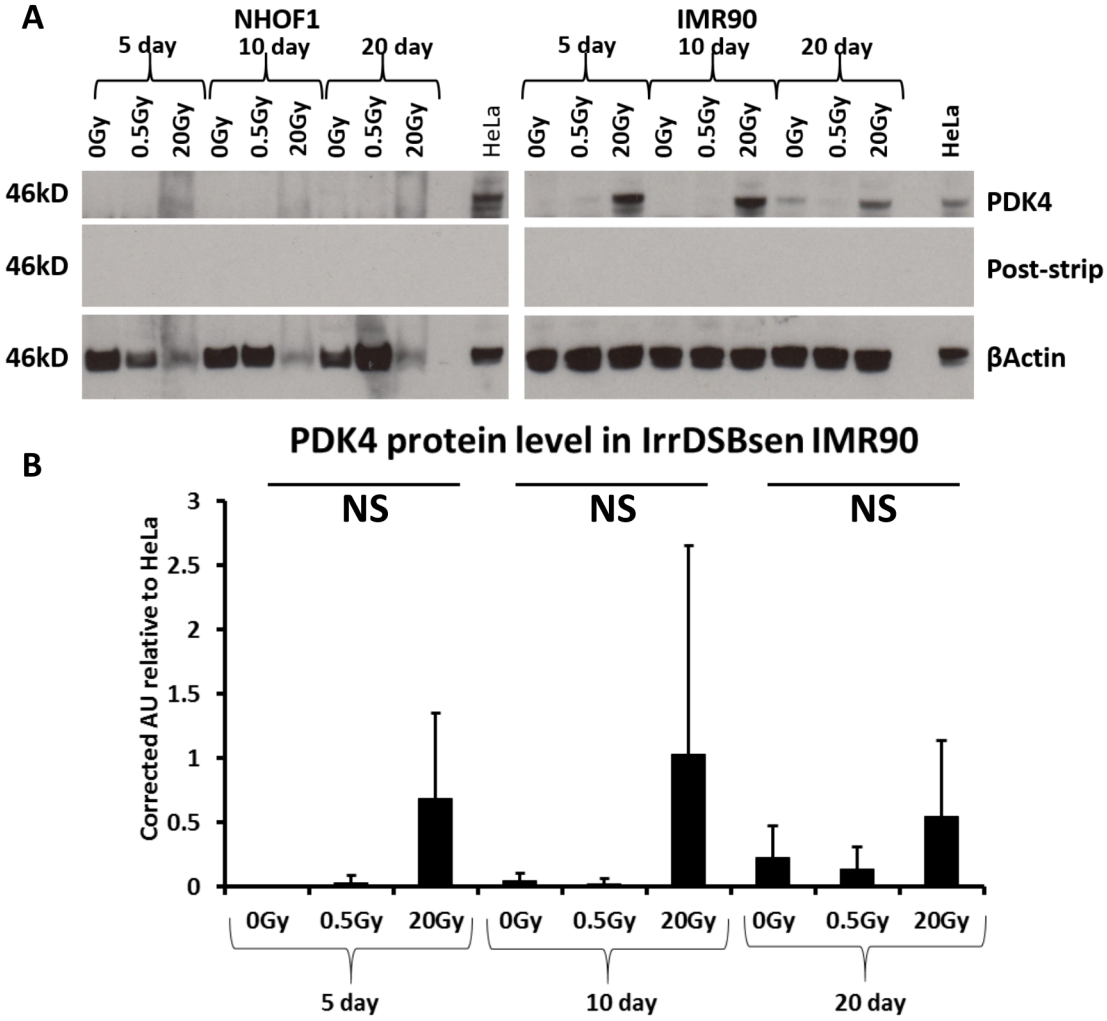

Figure 4.10: **PDK4 protein levels in IrrDSBsen NHOF1 and IMR90**. **A** representative western blot of PDK4 protein in NHOF1 and IMR90 fibroblasts 5, 10 and 20 days following 0Gy, 0.5Gy and 20Gy gamma radiation, with β-actin loading control. Because PDK4 and β-actin have the same molecular weight, the membrane was stripped to remove primary and secondary antibodies in between probing for each protein. The membrane was incubated with HRP substrate and exposed for to film for 15 minutes (post strip membrane) to ensure the strip was successful before the next primary (which was a different species to the first primary) to make sure that the signal detected with the second antbody was not contaminated by residual binding from the first primary antibody. **B** Average PDK4 protein levels in IrrDSBsen (20Gy) IMR90 and 0Gy and 0.5Gy controls 5, 10 and 20 days after gamma radiation relative to HeLa. n=3 error bars represent stadar deviation from the mean, NS = not significant with a 1 way ANOVA. No PDK4 was reliably detected in NHOF1 cell so densitometric analysis was not done.

4.3.2 Regulation of citrate

To assess the transcriptional regulation of enzymes that could potentially affect the accumulation of citrate observed in the previous chapter qPCR was used to measure the fold up or down regulation of genes coding for the enzymes ACLY, ACO1, ACO2 and CS. None of the genes had a fold change over 2 (figure 4.11).

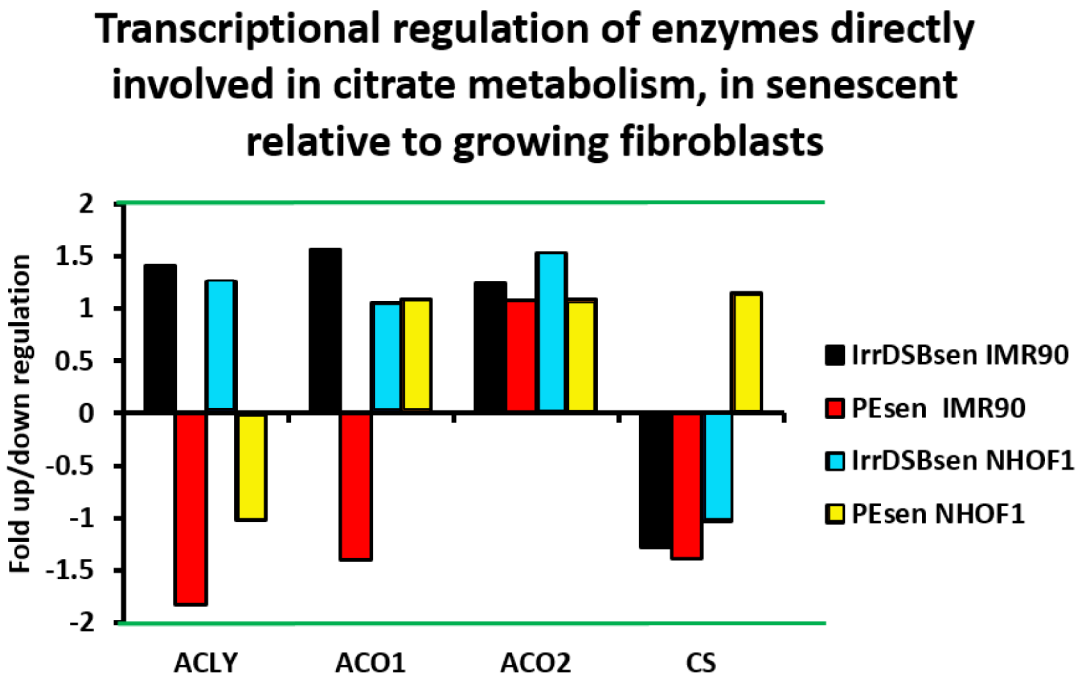

Figure 4.11: **Fold up/ down regulation of genes directly involved in citrate metabolism** (ACLY, ACO1, ACO2 and CS) in IrrDSBsen and PEsen NHOF1 and IMR90 fibroblasts relative to growing controls. n= 3. Green line marks 2 fold up/down regulation threshold, less than 2 fold change is considered not changed.

In case there was a post transcriptional modification that could cause there to be a difference in citrate related enzymes at the protein level in senescent fibroblasts, western blots were performed. In both NHOF1 and IMR90 there was no significant change in protein level of ACLY, ACO1 or ACO2 (figures 4.12 and 4.13).

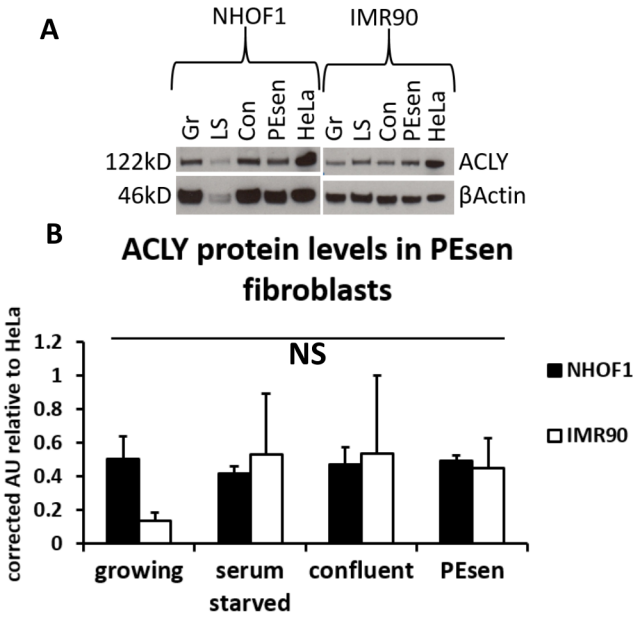

Figure 4.12: **ACLY protein levels in PEsen NHOF1 and IMR90 as well as growing and growth arrest controls**. **A** Representative western blot of ACLY protein in PEsen NHOF1 and IMR90 cells as well as growing (Gr), serum starved (LS) and confluent (Con) controls, with β-actin loading control. **B** Average ACLY protein level in PEsen NHOF1 and IMR90 and controls as in A, quantified relative to HeLa. Error bars represent standard deviation from the mean, n=3 NS= not significant with a 1 way ANOVA.

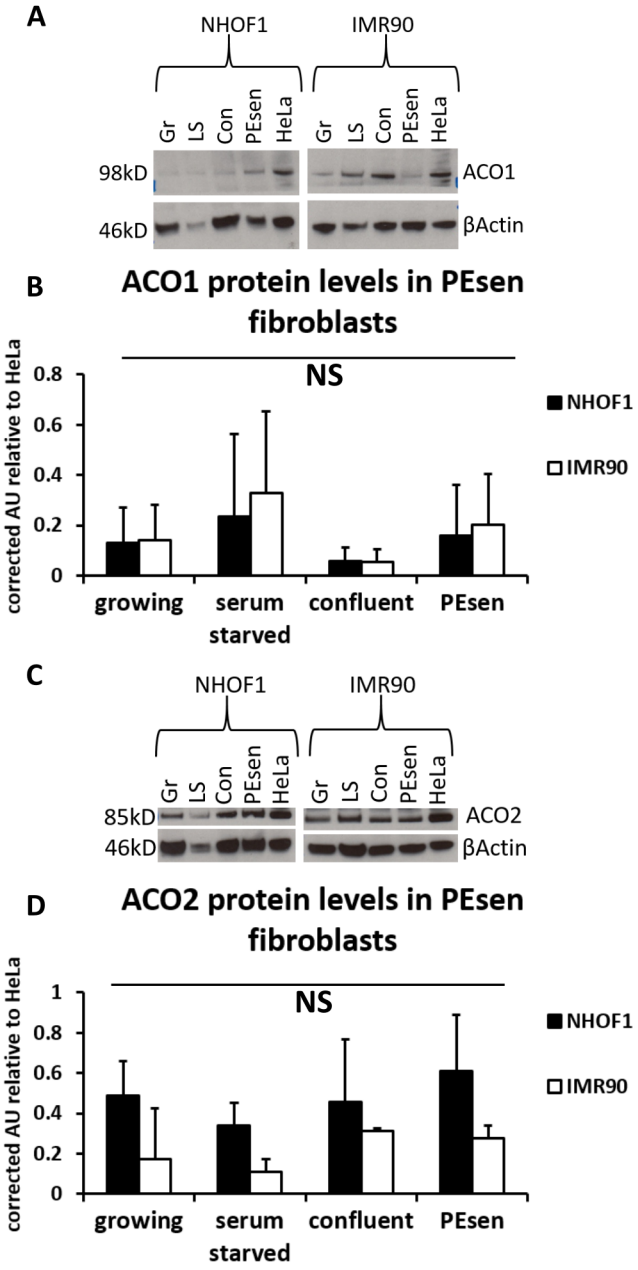

Figure 4.13: **Aconitase 1 (ACO1) and aconitase 2 (ACO2) protein levels in PEsen NHOF1 and IMR90 as well as growing and growth arrest controls**. **A** Representative western blot of ACO1 protein in PEsen NHOF1 and IMR90 cells as well as growing (Gr), serum starved (LS) and confluent (Con) controls, with β-actin loading control. **B** Average ACO1 protein level in PEsen NHOF1 and IMR90 and controls as in A, quantified relative to HeLa. Error bars represent standard deviation from the mean, n=3 NS= not significant with a 1 way ANOVA. **C** Representative western blot of ACO2 protein in PEsen NHOF1 and IMR90 cells as well as growing (Gr), serum starved (LS) and confluent (Con) controls, with β-actin loading control. **D** Average ACO1 protein level in PEsen NHOF1 and IMR90 and controls as in C, quantified relative to HeLa. Error bars represent standard deviation from the mean, n=3 NS= not significant with a 1 way ANOVA.

In IrrDSBsen there was also not a significant difference in the levels of ACLY for NHOF1 or IMR90, however IMR90 had more ACLY relative to HeLa than NHOF1 did after 20 days regardless of treatment (figure 4.14).

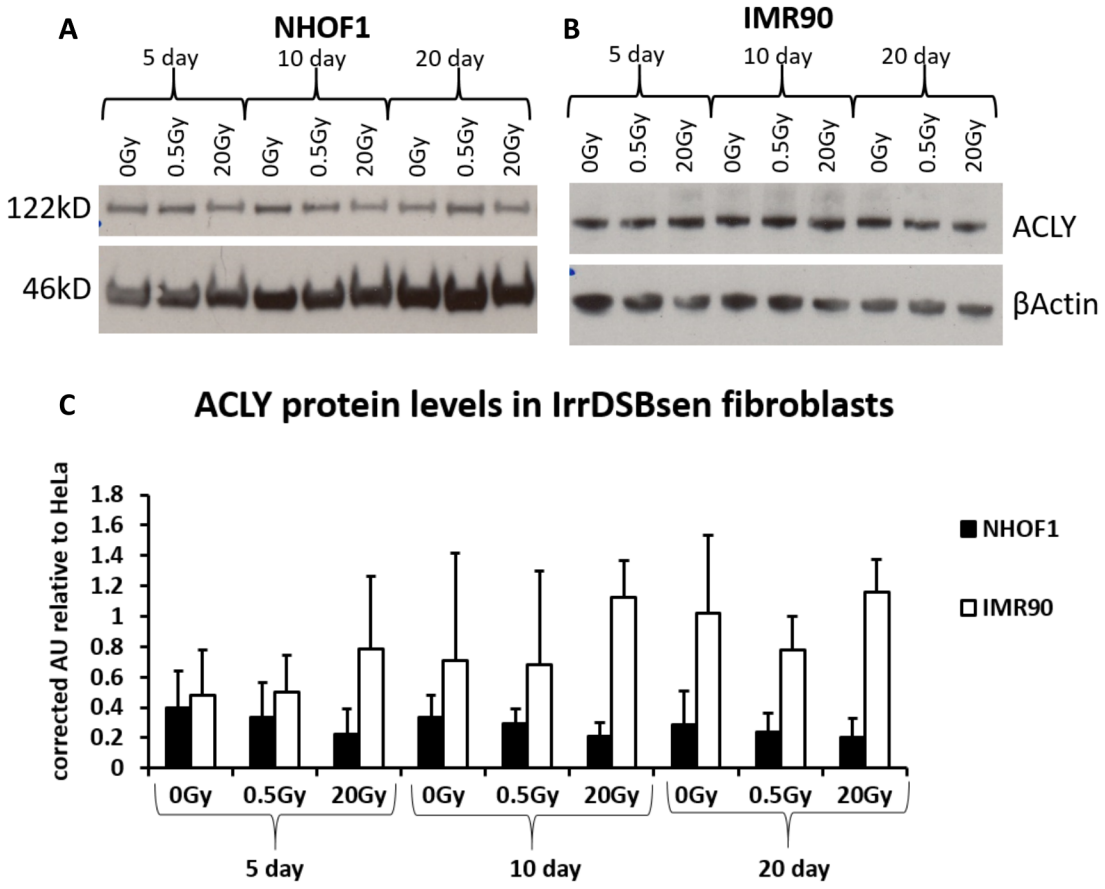

Figure 4.14: **ACLY protein levels in NHOF1 and IMR90 5, 10 and 20 days after exposure to 0Gy, 0.5Gy and 20Gy gamma radiation**. **A** Representative western blot of ACLY protein in IrrDSBsen (20Gy) NHOF1 and IMR90 cells as well growing (0Gy) and repairable DNA damage (0.5Gy) controls, 5, 10 and 20 days after radiation, with β-actin loading control. **B** Average ACLY protein level in IrrDSBsen NHOF1 and IMR90 and controls as in A, quantified relative to HeLa. Error bars represent standard deviation from the mean, n=3 except in the case of IMR90 day 10 0Gy and 0.5Gy which are n=2

Similarly IrrDSBsen NHOF1 and IMR90 did not elevate ACO1 or ACO2 protein levels relative to 0Gy controls, but the protein level of ACO1 in IMR90 was higher relative to NHOF1, regardless of treatment (figures 4.15 and 4.16).

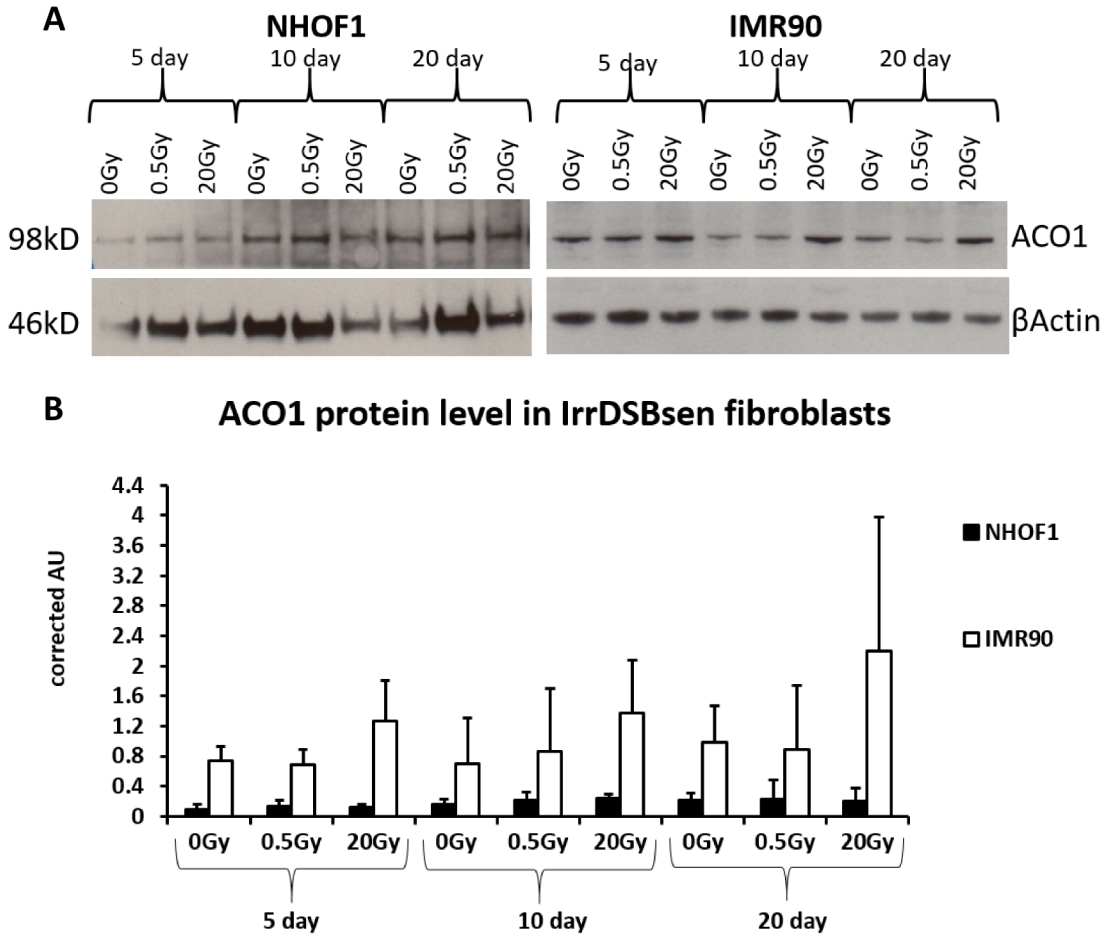

Figure 4.15: **Aconitase 1 (ACO1) protein levels in NHOF1 and IMR90 5, 10 and 20 days after exposure to 0Gy, 0.5Gy and 20Gy gamma radiation**. **A** Representative western blots of ACO1 protein in IrrDSBsen (20Gy) NHOF1 and IMR90 cells as well growing (0Gy) and repairable DNA damage (0.5Gy) controls, 5, 10 and 20 days after radiation, with β-actin loading control. **B** Average ACO1 protein level in PEsen NHOF1 and IMR90 and controls as in A, quantified relative to HeLa. Error bars represent standard deviation from the mean, n=3 except in the case of IMR90 day 10 0Gy and 0.5Gy which are n=2.

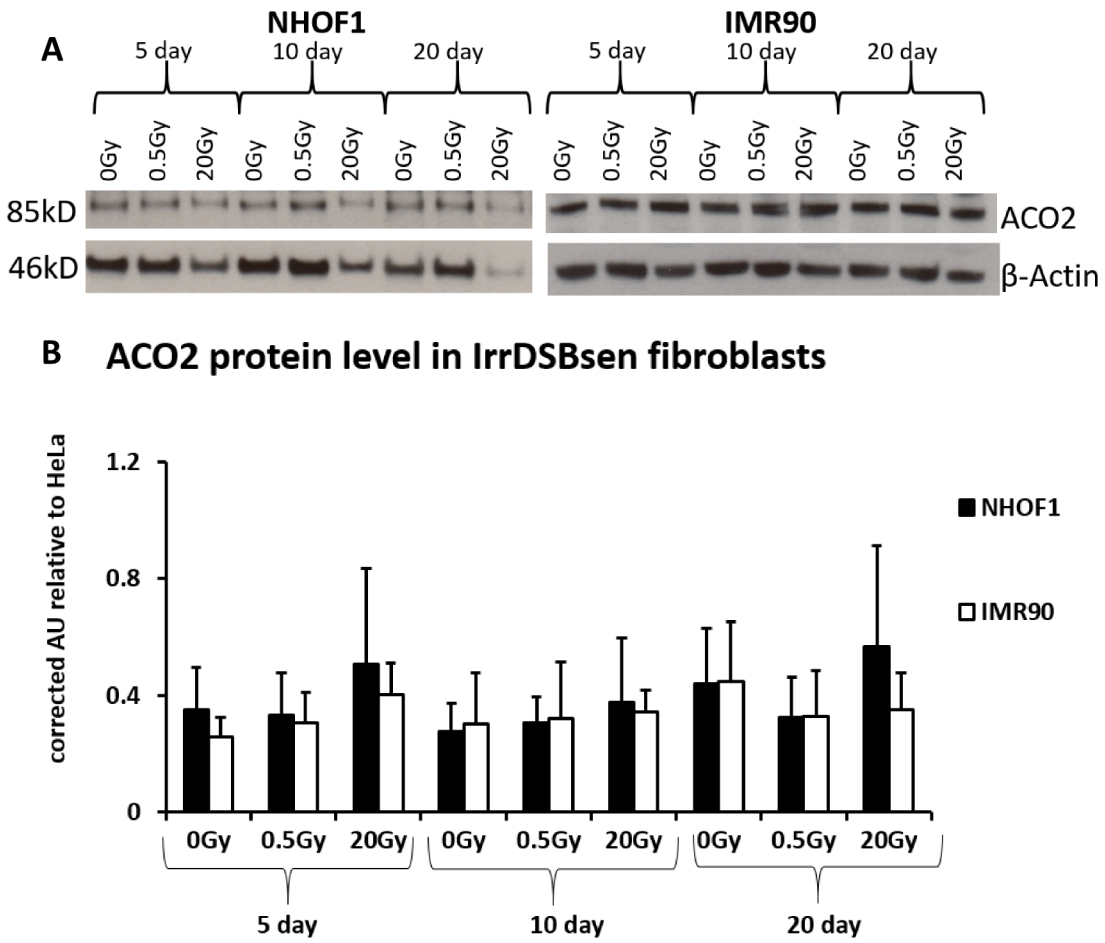

Figure 4.16: **Aconitase 2 (ACO2) protein levels in NHOF1 and IMR90 5, 10 and 20 days after exposure to 0Gy, 0.5Gy and 20Gy gamma radiation**. **A** Representative western blots of ACO2 protein in IrrDSBsen (20Gy) NHOF1 and IMR90 cells as well growing (0Gy) and repairable DNA damage (0.5Gy) controls, 5, 10 and 20 days after radiation, with β-actin loading control. **B** Average ACO2 protein level in PEsen NHOF1 and IMR90 and controls as in A, quantified relative to HeLa. Error bars represent standard deviation from the mean, n=3 except in the case of IMR90 day 10 0Gy and 0.5Gy which are n=2.

4.3.2.1 p53 restrains extracellular citrate

To see if p53 or the down stream senescence effector $p21^{WAF1}$ are involved in the regulation of citrate production or release from senescent cells, extracellular citrate levels were measured using targeted GCMS of the conditioned media from isogenic lung fibroblasts with knock out of p53 and $p21^{WAF1}$. The cells lacking p53 show elevated extracellular citrate, although none of the cells expressed an increased senescence phenotype as

demonstrated by SAβ-gal staining (figure 4.17). There was no significant difference between extracellular citrate in $p16^{INK4A-/-}$ cells and controls (figure 4.18).

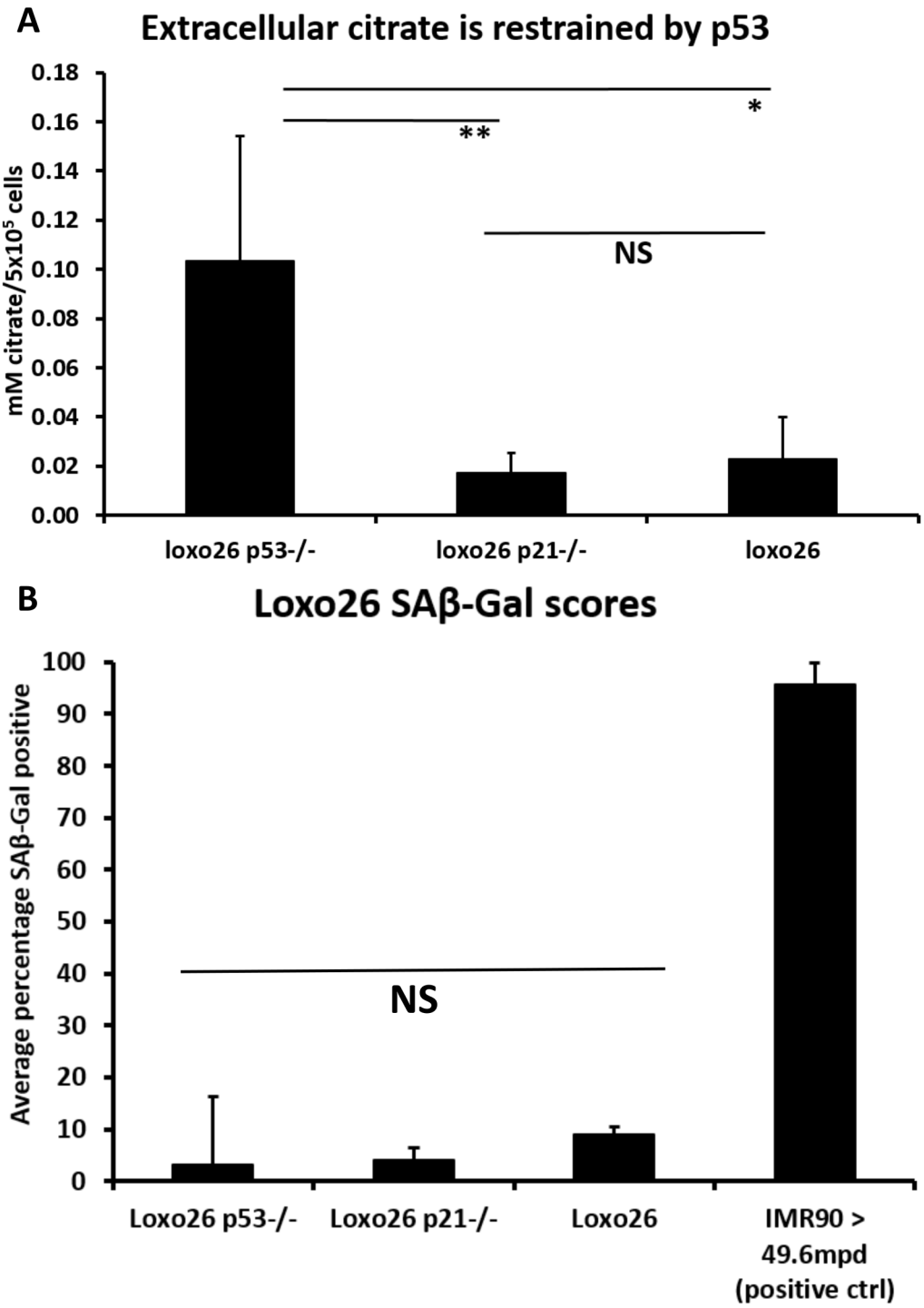

Figure 4.17: **Extracellular citrate in Loxo26 fibroblasts and isogenic p53$^{-/-}$ and p21$^{\mathbf{WAF1-/-}}$ controls. A** Extracellular citrate in Loxo26 fibroblasts and isogenic p53$^{-/-}$ and p21$^{\mathrm{WAF1-/-}}$ controls measured using targeted GCMS and normalised to cell count. N=3, error bars represent standard deviation from the mean, NS = not significant, *p<0.05, **p<0.01 with a 1 way ANOVA and Tukey's post hoc analysis. **B** SAβ-gal scores for Loxo26 and the isogenic p53$^{-/-}$, p21$^{\mathrm{WAF1-/-}}$ populations used for citrate quantification. IMR90 49.6mpd is a PEsen positive control for the SAβ-gal assay. n=3, error bars represent standard deviation from the mean, NS = not significant with a 1 way ANOVA.

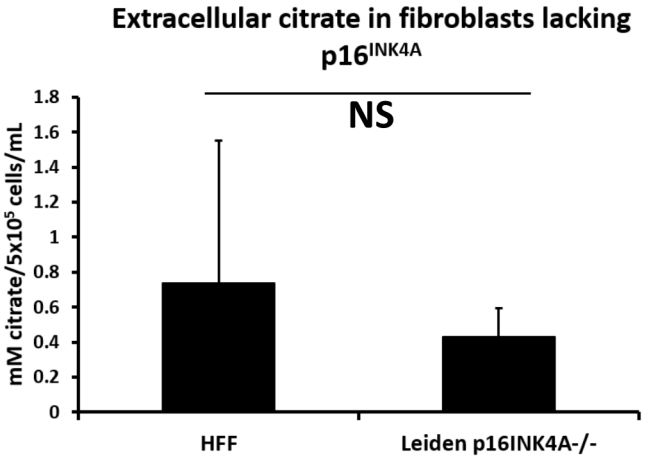

Figure 4.18: **Extracellular citrate in dermal fibroblasts lacking $\mathbf{p16^{INK4A}}$**(Leiden) and dermal normal fibroblasts (HFF) measured using GCMS. n=3 error bars represent standard deviation from the mean NS= not significant with a Student's t Test.

4.3.3 Oxidative stress response

Because redox homeostasis pathways are closely associated with senescence and the metabolomic screens suggested there was an oxidative stress response active in the senescent cells, and also because p53 (which restrains citrate (figure 4.17)) is known to regulate ROS (Liu et al., 2008), a qPCR array was used to assess the transcriptional regulation of some key oxidative stress response genes in PEsen and IrrDSBsen. All of the fold changes that were statistically significant were in the direction of up regulation, and NOX5, PNRP, PTGS1, PTGS2, SFTPD and SOD3 were all consistently up-regulated in both lines in both PEsen and IrrDSBsen (figure 4.19).

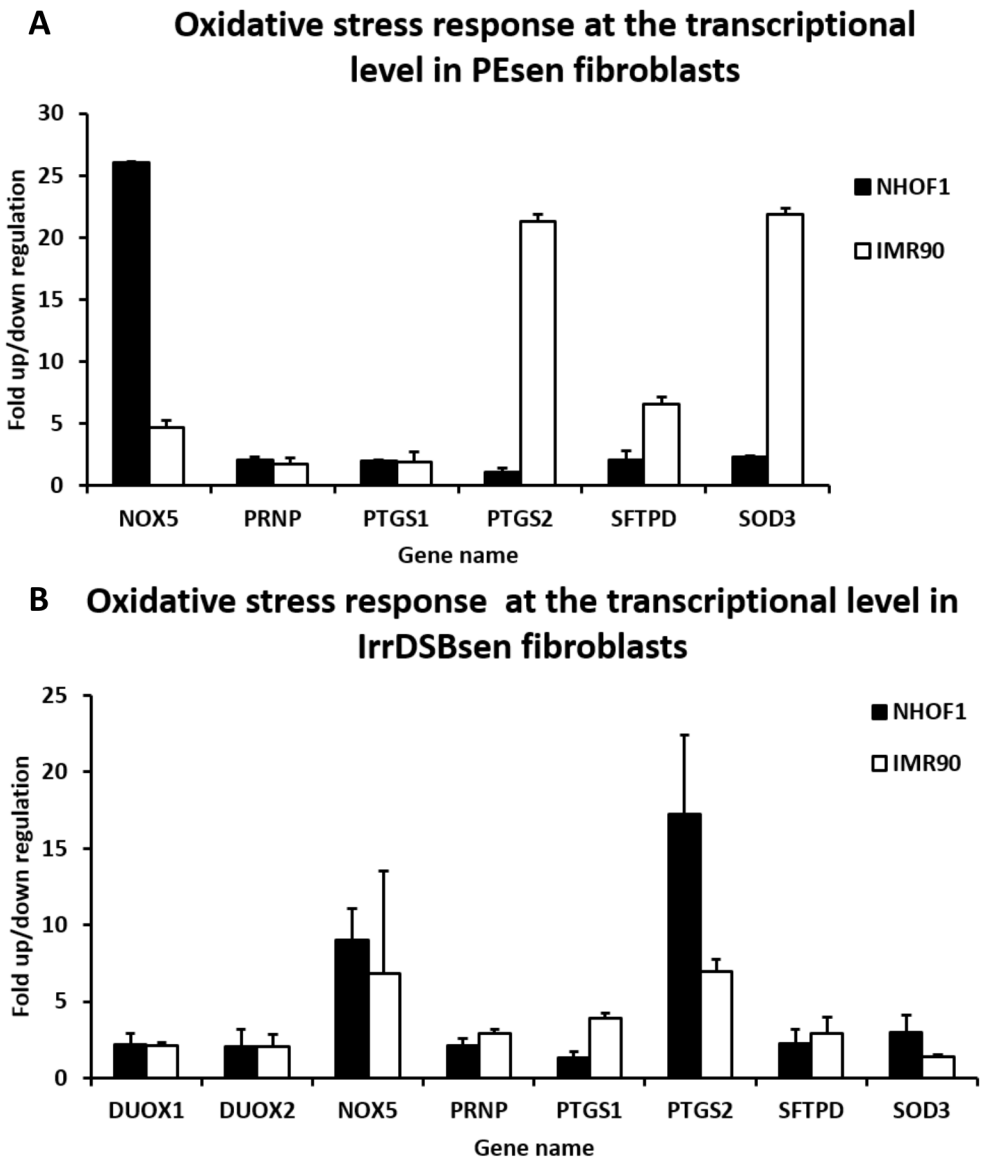

Figure 4.19: **Fold up/down regulation of genes involved in oxidative stress response in PEsen and IrrDSBsen fibroblasts**. **A** Fold up/down regulation of genes involved in oxidative stress response in PEsen NHOF1 and IMR90 fibroblasts that were identified as being statistically significant from growing controls using a Student's T Test. n=3 error bars represent standard deviation from the mean. **B** Fold up/down regulation of genes involved in oxidative stress response in IrrDSBsen NHOF1 and IMR90 fibroblasts that were identified as being statistically significant from growing controls using a Student's T Test. n=3 error bars represent standard deviation from the mean.

A breakdown of the types of proteins affected most by these transcriptional changes can be seen in figure 4.20 on the next page.

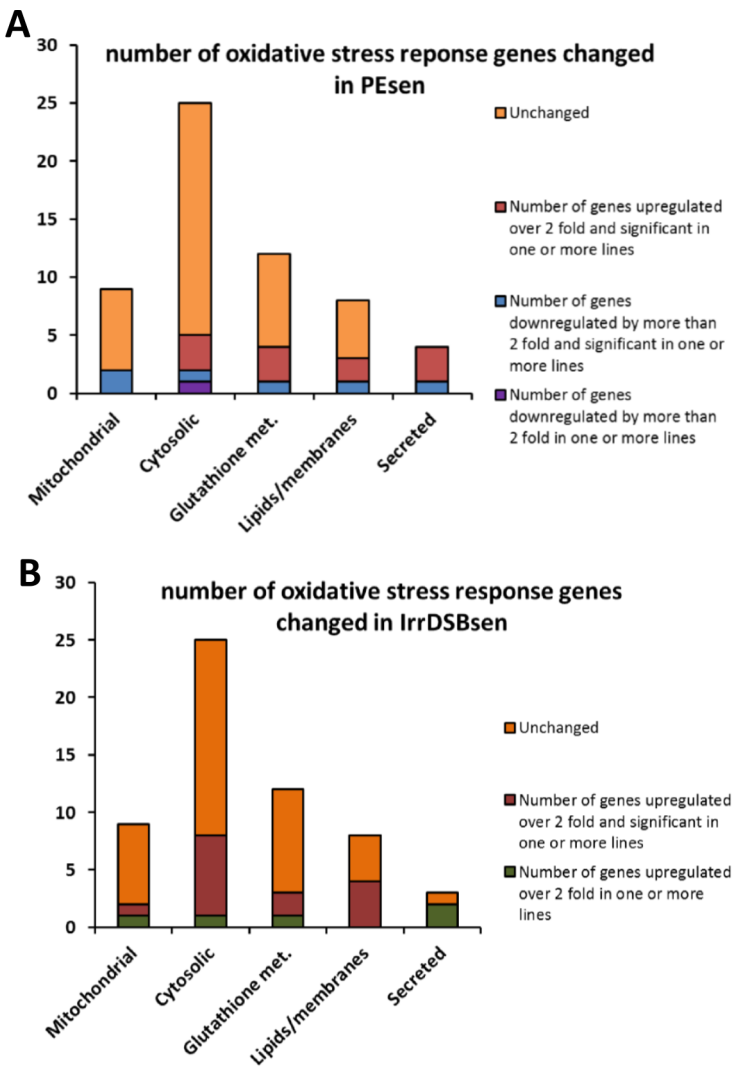

Figure 4.20: **Total number of detected transcriptional changes in genes for proteins involved in reducing reactive oxygen species in PEsen and IrrDSBsen fibroblasts**. Total number of detected transcriptional changes in genes for proteins involved in reducing reactive oxygen species damage in mitochondria, the cytosol, specifically in the glutathione pathway, in lipids and membranes and which are secreted from the cell in **A** PEsen and **B** IrrDSBsen. Genes up or down regulated by 2 fold or more in senescent compared to growing controls in either NHOF1, IMR90 or both lines were counted. n=3 per gene per cell line per senescence group. Statistical significance determined using a Student's T Test.

A DCF assay demonstrated that the levels of hydrogen peroxide in PEsen NHOF1 were elevated compared to growing controls however in IMR90 that was not the case, as shown in figure 4.21.

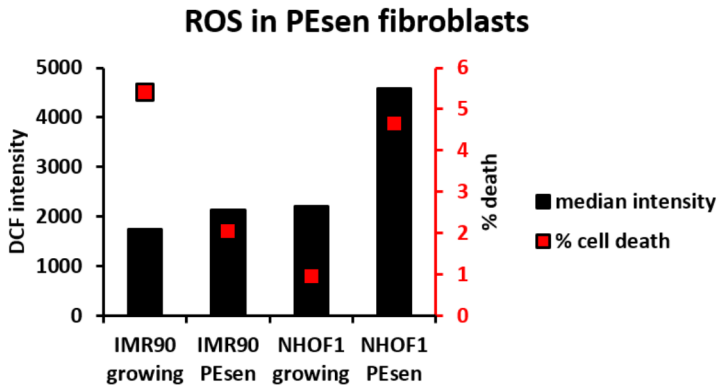

Figure 4.21: **Reactive oxygen species levels in PEsen and IrrDSBsen NHOF1 and IMR90 fibroblasts** determined by DCF intensity using a flow cytometer. n = 2.

To see if there was a link between senescence effector proteins and ROS the DCF assay was applied to fibroblasts lacking either $p16^{INK4A}$, p53 or $p21^{WAF1}$ along with matched controls. The assay revealed that cells lacking $p16^{INK4A}$ or p53 had elevated levels of ROS compared to controls, but that loss of $p21^{WAF1}$ did not have a significant effect on ROS levels (figure 4.22).

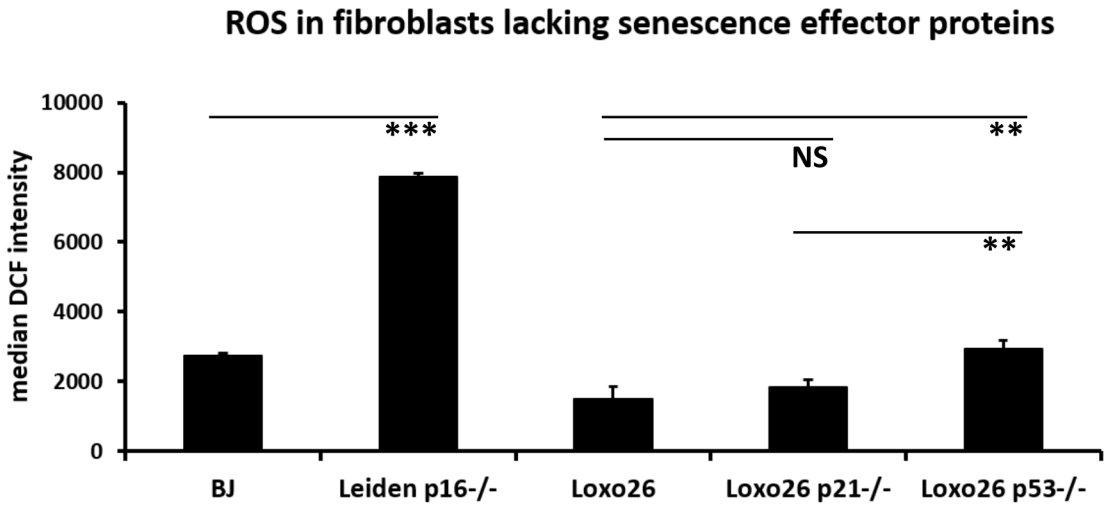

Figure 4.22: **Reactive oxygen species levels in fibroblasts lacking senescence effector proteins $p16^{INK4A}$(Leiden p16-/-), $p21^{WAF1}$ (Loxo26 p21-/-) and p53 (Loxo26 p53-/-),** compared with either tissue matched controls (BJ dermal fibroblasts as a control for Leiden dermal fibroblasts) or isogenic controls (Loxo26 lung fibroblasts as a control for $p21^{WAF1}$ and p53 knockout lung fibroblasts) determined by DCF intensity using a flow cytometer. n = 3, error bars represent standard deviation from the mean NS = not significant, **p<0.01 ***p<0.001 with a Student's T Test.

To examine the role of telomere length on the level of extracellular citrate, targeted GCMS was used to measure the extracellular citrate present in the conditioned media from NHOF1 cells expressing enzymatically active telomerase (NHOF1 TERT), or expressing telomerase lacking a key function necessary for lengthening telomeres (NHOF1 TERT HA), compared to the extracellular citrate in NHOF1 containing the vector control (NHOF1 puro). Collections of conditioned media were made after NHOF1 TERT HA and NHOF1 puro cell populations showed signs of PEsen. Preliminary results shown in figure 4.23 suggest that cells expressing TERT but not TERT HA do not have elevated extracellular citrate despite completing more population doublings than TERT HA and vector control cells were able to complete before ceasing to divide.

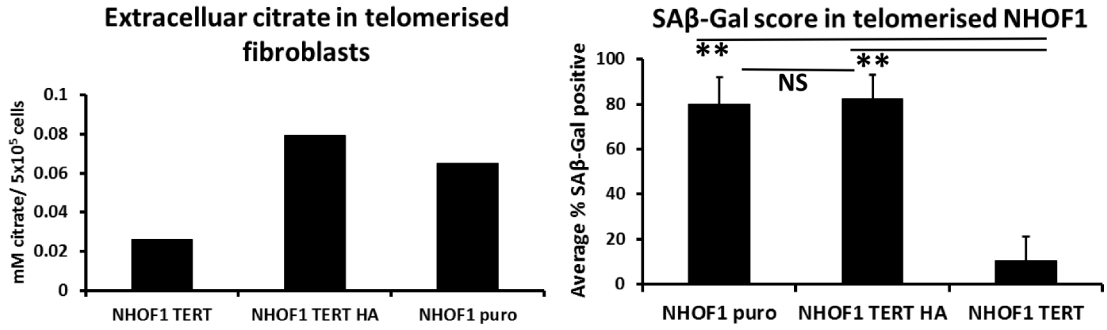

Figure 4.23: **Extracellular citrate in telomerised NHOF1 fibroblasts** with telomerase (NHOF1 TERT) at +55.3mpd, telomerase lacking telomere lengthening activity (TERT HA) at +17.8mpd compared to vector control (NHOF1 puro) at +9.9mpd measured using targeted GCMS n=1. The graph on the right shows the corresponding SAβ-gal scores for the cell populations used for citrate quantification. n=3 error bars represent standard deviation from the mean, NS= not significant, **$p<0.01$ with a 1 way ANOVA and Tukey's post hoc analysis.

4.4 Discussion

The aim of this chapter was to shed light on the mechanisms behind the elevation of citrate in the conditioned media of senescent cells and add further detail to the general metabolic state of senescent cells which was described in the previous chapter.

Firstly the transcriptional regulation of glucose metabolism (one of the pathways implicated in the metabolomic screen) was assessed using qPCR, this included enzymes

that directly regulate citrate, and key results were confirmed at the protein level using western blots. The impact of p53, $p21^{WAF1}$ and $p16^{INK4A}$ on levels of extracellular citrate were investigated using knock-out fibroblasts lines. The transcriptional regulation of redox homeostasis pathways (another of the pathways implicated in the metabolomic screen) was also assessed using qPCR and the levels of ROS in senescent cells were measured. Finally telomerised cells were used to assess the importance of telomere attrition to the accumulation of extracellular citrate in senescence.

The data described in this chapter helped to clarify the findings from the metabolomic screen and were also informative regarding the route of citrate elevation, although further work is required to determine the mechanism.

4.4.1 Regulation of energy metabolism in senescent fibroblasts

Firstly, transcriptional regulation of the pathways involved in energy metabolism was assessed because citrate is an intermediate in the TCA cycle, so its elevation might be explained by an increase or decrease in transcription of vital proteins in the TCA cycle or associated pathways. Furthermore the intracellular metabolic profile of NHOF1 suggested that senescent cells are glycolytic, an aspect of the phenotype that may be regulated at the transcriptional level.

qPCR analysis of a panel of transcripts of genes coding proteins involved in glycolysis, the TCA cycle and the PPP revealed that most of the transcriptional changes in energy metabolism during senescence were occurring in glycolytic enzymes. As figure 4.7 on page 193 shows, there were no fold up or down regulation changes in TCA cycle genes that were greater than two fold, whereas there were several statistically significant up and down regulations over 2 fold in glycolytic enzymes. The number of genes with a fold up regulation in glycolytic enzymes was still quite low (5 genes), but the one with the largest up regulation was pyruvate dehydrogenase kinase 4 (PDK4), a key gatekeeper enzyme. PDK4 is induced by metabolic stress such as starvation or glucose deprivation (Wu et al., 2000) and fatty acid flux (Abbot et al., 2005; Nahlé et al., 2008), and

regulates TCA cycle activity by inhibiting the pyruvate dehydrogenase complex (PDH) (Sugden and Holness, 2003), therefore preventing the conversion of pyruvate to acetyl co-A and lowering flux through the TCA cycle. An increase in this enzyme suggests that metabolism is being diverted away from the TCA cycle, supporting the intracellular metabolomic screen data which found increased glycolytic and PPP intermediates (figure 3.8 on page 147).

When PDK4 protein levels were investigated using western blot however, there was not a significant increase in PDK4 protein in PEsen or IrrDSBsen (figures 4.8, 4.9 and 4.10), although there was a non significant increase in IrrDSBsen IMR90 cells. Interestingly there was a significant increase in PDK4 protein in confluent IMR90, which could suggest that elevation in PDK4 and possibly diversion of metabolic flux away from the TCA cycle is more strongly associated with the cell dealing with the stress that induces the senescence rather than the actual senescence growth arrest itself.

Nevertheless, there did appear to be a glycolytic phenotype when considering the untargeted metabolomic screen data, that was distinct from the metabolic phenotype of the growth arrest controls, the fact that this difference in profiles is not fully explained by changes at the transcriptional level means there must be an involvement of post transcriptional changes.

A more detailed picture of the extent to which senescent cells use glycolysis, the TCA cycle and the PPP could be achieved with flux experiments. By replacing some of the glucose (or other substrates such as pyruvate or glutamine) in the culture media with glucose containing a stable heavy carbon isotope (^{13}C) and taking samples of cells for metabolite extraction at multiple time points starting immediately after addition of the media, the uptake and breakdown of the labelled glucose could be tracked along with the fate of the heavy carbon. The accumulation of heavy carbon in a particular pool of metabolites would enable the identification of the most active metabolic pathways.

4.4.2 Transcriptional regulation of enzymes directly involved in citrate metabolism

As an increase in extracellular citrate had been observed in senescent cells, it was expected that there would either be an increase in the production of citrate or a reduction in its breakdown. It had been previously reported in the literature that CS activity declines in senescence (Ghneim and Al-Sheikh, 2010), so a decrease in the enzymes that break down citrate (ACO1, ACO2 and ACLY) seemed most likely. It was surprising to find that there were no changes at the transcriptional level of the enzymes ACO1, ACO2 or ACLY (figure 4.11 on page 197), and no detectable changes in their protein levels either (figures 4.12 on page 198, 4.13 on page 199, 4.14 on page 200 and 4.15 on page 201).

These observations do not rule out the possibility that the enzyme activity is affected, and attempts were made to measure the activity of both ACO1 (in the cytoplasm) and ACO2 (in the mitochondria) in senescent fibroblasts. Unfortunately these attempts were not successful, due to incomplete separation of the mitochondrial and cytoplasmic cell fractions prior to running the assay. The protocol required a large number of cells and it was not possible to optimise the experiment in the time frame of this project. ACLYlyase, the other enzyme investigated that breaks down citrate, has previously been linked to senescence. Knock-down of ACLY has been shown to induce senescence, and in rat and human dermal fibroblast (HDF) cells ACLY protein levels were shown to be reduced (Lee et al., 2015), contrary to findings in this thesis. Unfortunately there was no time to measure ACLY activity, which can be measured indirectly by measuring the optical density change caused by oxaloacetate (a product of the reaction catalysed by ACLY in which citrate is broken down) reaction with NADH in the presence of excess malate dehydrogenase (Srere, 1959).

4.4.3 Post translational modification of enzyme activity

Attempts were also made to find evidence of post-translational modifications that could cause a reduction in enzymatic activity. 4-hydroxynonenal (4HNE) residues can form on proteins and affect their function following oxidative damage to lipids (Uchida and Stadtman, 1992), so an antibody targeting 4HNE was used on western blot membranes in an attempt to compare total 4HNE levels in senescent and growing fibroblasts, however this avenue of investigation was not pursued because the signal was extremely variable and a suitable positive control had not been characterised.

Although there was not time to properly optimise the measurement of ACO1 and ACO2 activity in this thesis, it has been reported that human prostate, the only tissue known to produce citrate in large volumes and export it out of the cell, has a reduced capacity to oxidise citrate due to rate limiting ACO2 (mitochondrial aconitase) activity, despite the protein levels remaining normal. This has been attributed to inhibition by zinc, which is present in high concentrations in prostate mitochondria (Costello and Franklin, 1981). Zinc accumulation in prostate is known to be due to hormonal regulation (Costello and Franklin, 1994), so it would be surprising if the *in vitro* results reported in this thesis were also due to specific inhibition of ACO2 by zinc. Nevertheless, inhibition of ACO2 by ROS (Yan et al., 1997) or fumarate (Ternette et al., 2013) as potential source of elevated citrate appears to be worth further investigation, in addition to ACLY.

4.4.4 The role of senescence effector proteins in extracellular citrate accumulation

The generous gifts of knockout p53, $p21^{WAF1}$ and $p16^{INK4A}$ made it possible to test the probable role of these proteins in the accumulation of extracellular citrate. While stable knockout ensured that there was a complete loss of the proteins of interest and enabled their stable culture, long term effects of the knockout and therefore the induction of compensatory mechanisms cannot be ruled out especially in the case of p53, which is

involved in numerous cellular processes. With this in mind ideally the results obtained using these cells will be confirmed using transient knock-down of the proteins, however there was not time to do this during the project.

4.4.4.1 $p16^{INK4A}$

Conditioned media collected from cells lacking p53, $p21^{WAF1}$ and $p16^{INK4A}$ were analysed using targeted GCMS. Cells lacking $p16^{INK4A}$ did not show any significant change in extracellular citrate relative to control cells (the control cells were not ideal as they were not isogenic, however they were from the same tissue type), so $p16^{INK4A}$ is not likely to be closely involved in citrate regulation. Given that the two cell lines most studied in this thesis had completely different expression levels of $p16^{INK4A}$ (NHOF1 did not have detectable levels of $p16^{INK4A}$ whereas IMR90 had low levels of $p16^{INK4A}$ in growing cells and elevated $p16^{INK4A}$ in senescence), yet both had elevated extracellular citrate in senescence, it was expected that $p16^{INK4A}$ probably did not play a key role in the extracellular accumulation of citrate. However, this still remains to be properly tested directly.

4.4.4.2 p53 and $p21^{WAF1}$

$p53^{-/-}$ fibroblasts showed a significant increase in extracellular citrate. This elevation was not related to senescence as an SAβ-gal assay showed the cells were negative for the characteristic blue stain (figure 4.17 on page 204), and suggests that p53 normally functions to restrain citrate. p53 could be either restraining citrate production, citrate export from the cells, or both but the fact that knockout of $p21^{WAF1}$ had no effect on citrate levels shows that the mechanism p53 is involved in to elevate citrate does not include the transcriptional activation of $p21^{WAF1}$.

The evidence that loss of p53 leads to an increase in extracellular citrate fits with the prior knowledge that established senescence is associated with low levels of p53. There are several ways in which the levels of p53 could be influencing the level of citrate and

metabolism in general in senescence.

4.4.4.3 Potential direct effects of p53

p53 is known to directly interact with several metabolic enzymes and transcriptionally regulate both metabolic enzymes and transporters of metabolic fuels.

Metabolic enzymes

Malic enzyme 1 (ME1) and malic enzyme 2 (ME2) convert malate to pyruvate and in doing so regenerate NADPH from NADP+. NADPH is required for reductive biosynthesis of lipids, and over expression of ME1 and ME2 results in increased total lipids. p53 has been shown to repress expression of ME1 and 2, as demonstrated by the elevation of both malic enzymes and subsequent increase in lipid levels in *TP53*$^{-/-}$ cells (Jiang et al., 2013). The phenotype observed in the previous chapter included the specific accumulation of multiple phospholipids in senescence (figure 3.6 on page 145) which might be explained by de-repression at the transcriptional level of ME1 and ME2 following a decline in p53 protein levels in established senescence. Furthermore PGM, a glycolytic enzyme, is inhibited by p53 (Kondoh et al., 2005) and TIGAR inhibits the glycolytic enzyme PFK1) by degrading fructose-2,6-bisphosphate which acts to stimulate PFK1 (Bensaad et al., 2006). Low p53 activity would therefore suggest that the inhibition of glycolysis via these routes would be alleviated.

As well as inhibiting glycolysis p53 acts to promote oxidative phosphorylation through transcriptional regulation of proteins necessary for mitochondrial respiration such as synthesis of cytochrome oxidase 2 (SCO2) which is critical to the formation of complex IV in the electron transport chain (Matoba et al., 2006).

NFkB

The transcription factors NFkB play several roles in senescence induction and maintenance, but it is also involved in some of the metabolic functions of p53.

p53 is necessary for the anti-glycolytic, pro-OXPHOS activities of NFkB, as demonstrated by Claudio Mauro and colleagues, who showed that inhibition of NFkB subunit RelA resulted in an increase in lactate production and a decrease in oxygen consumption, signs that the cells had become glycolytic. Expression of p53 in these cells reduced lactate production and increased oxygen consumption (Mauro et al., 2011). Furthermore, p53 inhibits the NFkB driven expression of GLUT3, a glucose transporter that increases glucose transport into the cell to fuel glycolysis (Kawauchi et al., 2008). Low levels of p53 activation would therefore be expected to result in repression of the anti-glycolytic activities of NFkB and an increase in the expression of GLUT3 and therefore glucose transport into the cell, supporting a glycolytic phenotype. These assumptions are yet to be tested.

Transport of metabolic fuel

As already mentioned p53 represses the expression of GLUT3 via NFkB, but p53 is also known to repress GLUT1 and GLUT4 which are also glucose transporters (Schwartzenberg-Bar-Yoseph et al., 2004). The product of glycolysis is lactate, and if cells are heavily reliant on glycolysis the build up of lactate can reduce the intracellular pH which inhibits glycolysis. in order to maintain a glycolytic metabolism the surplus lactate needs to be transported out of the cell via members of the monocarboxylate transporter family (Halestrap and Price, 1999). We have some evidence of increased extracellular lactate in senescence (see figure 3.22) suggesting that there may be increased transporter activity. MCT1 is repressed by p53 (Boidot et al., 2011), again suggesting that in late senescence with low levels of p53 activation glycolysis increases.

ROS

p53 also has a complex relationship with ROS regulation and depending on the context p53 can induce or repress ROS (Liu et al., 2008); in the case of substantially decreased p53 activity ROS has been shown to go up due to lack of transcription of several

antioxidant p53 target genes (Sablina et al., 2005). Redox homeostasis pathways were another aspect of the senescent phenotype studied in this chapter based on findings in the metabolomic screen, discussed in the next section.

4.4.5 Oxidative stress response

There is evidence that at the transcriptional level senescent cells launched an oxidative stress response including up-regulation of SOD3 (4.19 on page 206); an enzyme that catalyses the conversion of superoxide to to hydrogen peroxide (H_2O_2) and water and has been shown to reduce cellular oxidative stress (Serra et al., 2003). Interestingly several genes known to increase cellular oxidative stress were elevated in senescent cells as shown in figure 4.19 including the NADPH oxidases DUOX1 and 2 and NOX5. These proteins generate H_2O_2 and maintain the DDR (Fulton, 2009; Ameziane-El-Hassani et al., 2015) and their increased transcription would suggest that senescent cells have elevated levels of ROS. Indeed data from a DCF assay measuring intracellular H_2O_2 showed elevated ROS levels in PEsen fibroblasts (see figure 4.21). Elevated levels of ROS is generally associated with dysfunctional mitochondria (Wang et al., 2013), so it is likely that oxidative metabolism would be impaired in these cells, which is a possible reason for the observed glycolytic phenotype. If there had been more time this hypothesis could have been tested by measuring the membrane potential and respiration rate of the mitochondria in senescent cells (Brand and Nicholls, 2011) however unfortunately it was not possible to achieve in the time frame.

While the loss of of p53 in Loxo26 $p53^{-/-}$ did result in increased levels of ROS, as expected according to the literature (Sablina et al., 2005), interestingly the $p16^{INK4A}$ negative Leiden cells showed relatively higher levels of ROS (see figure 4.22) compared to both control cells and the Loxo26 $p53^{-/-}$, but did not show elevated levels of citrate (figure 4.18) suggesting that elevated citrate is not closely related to higher levels of ROS in senescent cells. However, this requires direct testing.

4.4.6 Telomerase

NHOF1 cells with added telomerase did not senesce despite undergoing more population doublings than were necessary to cause senescence in NHOF1 cells lacking telomerase, and preliminary citrate measurements show that citrate does not accumulate in the media of telomerised cells following long term culture (figure 4.23 on page 209), as would be expected when considering the knowledge that telomerase enables immortalisation by lengthening and maintaining telomeres (Vaziri and Benchimol, 1998). Unfortunately the citrate measurement data shown for telomerised cells only represents an n of one, due to technical issues with the GCMS which meant that the subsequent experimental samples could not be analysed in time for this thesis. If the pattern of the result remains the same when the final data points are added, the increase in extracellular citrate following PEsen in NHOF1 cells expressing telomerase with the HA tag which prevents it from lengthening or maintaining telomeres, immortalising cells, or avoiding replication crisis in cells (Counter et al., 1998), suggests that non-canonical functions of telomerase retained by TERT HA are not sufficient to prevent accumulation of citrate. If that is the case then citrate elevation is probably not due to DNA damage alone, because one of the non-canonical functions of telomerase is enhanced DNA damage response and resolution, not just at the telomere (Masutomi et al., 2005), although the extent of DDR/DNA damage in these cells was not examined here so this assumption remains to be tested. Another non-canonical function of telomerase is protection of mitochondrial DNA and improved mitochondrial function with less mitochondrial ROS generation (Ahmed et al., 2008). It was not possible to determine from the NHOF1 TERT data whether the lack of citrate accumulation was due to the telomere lengthening activity of telomerase or if all or part of the effect was due to the non-canonical functions such as the ability to protect mitochondria. The TERT HA expressing cells have the potential to answer this question; if the tagged telomerase is fully capable of localising to the mitochondria in the same way as TERT, then mitochondrial dysfunction is unlikely to be the cause of elevated citrate, as we would expect mitochondrial dysfunction to

be corrected in TERT HA expressing cells (which still senesce and show elevated citrate) however there is no evidence to demonstrate the HA tagged protein's ability to enter the mitochondria. Further investigations are necessary to establish the extent of mitochondrial damage in senescent cells expressing TERT HA.

4.4.7 Summary

Following the metabolomics study which identified citrate as a potential secreted biomarker of senescence, a number of approaches were used to try and elucidate the mechanism behind the elevation of citrate. These experiments also helped to further characterise the metabolic phenotype of the senescent fibroblasts, which, from the metabolomic screen, appeared to be glycolytic.

Regulation of glucose metabolism was assessed at the transcript level using a qPCR array which showed that there were not many large changes in fold up or down regulation of the metabolic enzymes involved in the TCA cycle, PPP or glycolysis but most of the changes were in the glycolysis pathway, supporting the theory that senescent cells predominantly use glycolysis to generate energy. However, this up-regulation could not be seen at the protein level in the key enzyme PDK4, so it would be useful to use labelled carbon glucose to measure how much of the glucose produces either lactate or PPP intermediates and how much enters the TCA cycle, to show definitively which pathways are preferentially used in senescence.

There was no change at the transcriptional level in enzymes that are directly involved in the breakdown and production of citrate, namely ACLY, ACO1, ACO2 and CS. This was confirmed at the protein level. Further work is needed to assess the activity of these enzymes, as post translational modifications or antagonists may be affecting their function.

Chapter 5

General Discussion

5.1 Introduction

The two key aims of this thesis were to firstly identify a candidate secreted biomarker of senescent fibroblasts, because such a marker that could be measured non invasively *in vivo* and non destructively *in vitro* would be extremely valuable in the study of senescence and potentially as a means of tracking the effectiveness of anti-ageing treatments. The second aim of the thesis was to elucidate the mechanism behind the elevation of any identified biomarkers, as this information would ensure appropriate use of the biomarker within the bounds of any limitations and also could potentially facilitate the manipulation of the senescence phenotype. In this chapter the extent to which these aims have been achieved will be discussed, along with additional insights gained as a consequence of the experiments undertaken in pursuit of the aims, and how the work will impact on the field of senescence. Lastly, some ideas on expansion of the work in the future will be discussed.

5.2 Citrate as a biomarker of senescent fibroblasts

The primary aim of the thesis was achieved in the identification of citrate as a secreted marker of senescence (described in chapter 3 section 3.3 on page 138), a result that was

specific to senescent fibroblasts and distinct from transiently growth arrested cells and cells with repairable DNA damage, but common to senescent fibroblasts from several tissue types. These factors make citrate an ideal candidate for a biomarker of senescence *in vivo.* In this section the need for a biomarker of senescence will be discussed along with an overview of the key achievements that faciltated the identification of citrate as a candidate marker and limitations of the work.

5.2.1 The need for a senescence biomarker

Senescent cells are known to accumulate *in vivo,* in pathologies such as neoplasia (Yang et al., 2006) and fibrosis (Pitiyage et al., 2011) as well as with age (Liu et al., 2009). However, without a non invasive biomarker of senescent cells it is impossible to carry out longitudinal studies to assess the role senescent cells are playing in these pathologies.

Current methodologies for identifying the presence of senescent cells *in vivo* usually require the tissue of interest to be removed and stained for SAβ-gal activity or other marker of senescence such as $p16^{INK4A}$, making it difficult if not impossible to take multiple measurements from the same individual over time and to monitor responses to interventions. While genetic manipulations of mice have enabled researchers to monitor accumulation of $p16^{LUC}$ cells in mice *in vivo* non destructively (Burd et al., 2013), this is only useful for senescence via $p16^{INK4A}$ and cannot be extended to humans. So far studying the general increase or decrease in senescent cells in humans has not been achieved, although studies on peripheral T- lymphocyte senescence have been successful (Liu et al., 2009).

Even the discovery of the SASP has not yet yielded any biomarkers; many of the reported proteins and factors are not commonly seen in all modes of senescence or tissue types tested, in fact recently a mode of senescence was described that did not show any of the inflammatory elements of the SASP (Wiley et al., 2016). The SASP therefore is not a direct result of the senescence growth arrest, rather it is related to other associated molecular changes that may also be present in other conditions such

as inflammation.

5.2.2 Biomarker discovery using metabolomics

The field of metabolomics has proven very useful for identifying biomarkers of disease in human body fluids such as blood and urine, thanks to technological advances which have brought down costs and increased throughput (reviewed in James and Parkinson, 2015). Increasing numbers of researchers are taking advantage of the ability to detect changes in metabolite levels, which reflect changes in cellular processes, in specific disease conditions or in response to intervention. The challenge still remains to be able to capture the entire metabolome; currently the separation techniques used each only enable certain classes of molecule to be identified, therefore to get a complete picture multiple platforms must be used. Thorough multi platform screens have been performed using human blood serum with the aim of describing the human serum metabolome, curated with metadata on age, gender, weight and lifestyle habits (Dunn et al., 2014) which is a useful resource for those trying to identify biomarkers in smaller more specific studies. Relevant to this work, several groups have used metabolomics to identify a signature of ageing, such as the study published by Christina Menni and colleagues in 2013 which identified a panel of 22 metabolites, including citrate, that strongly correlated with age (Menni et al., 2013). It was unknown at the time if any of the metabolites associated with ageing in humans were a direct consequence of increased senescent cells; the work in this thesis showing extracellular citrate is specifically elevated in senescent fibroblasts suggests there could be a link.

5.2.3 The contribution of this work to the field of senescence and human ageing

In this thesis the metabolomes of normal human senescent cells are described, and metabolite changes specific to permanent cell cycle arrest were identified, including the elevation of extracellular citrate. Importantly, it was possible to distinguish metabolite

changes that were common to aspects of the growth arrest that were reversible and those which were specific to permanent growth arrest. This distinction could only be made because of the robust controls used as part of the screening process; the characterisation of the senescent cells and growth arrest controls (serum starved and confluent) was necessary to determine the most appropriate experimental design but also highlighted some interesting differences between the cell types used. By using several markers to assess senescence, transient growth arrest and DNA damage, it was possible to optimise the culturing conditions so that metabolomes from fully senescent cells, transiently growth arrested cells and growing cells could be compared with confidence. Importantly for the understanding of the place of this work in the context of the wider literature, wherever possible at least two cell lines were used, including IMR90 which has been used in many other publications in the field. This thorough approach makes it unlikely that the findings of this work are a peculiarity of the cell type used.

The metabolomics screens revealed alterations to several metabolic pathways in senescent cells that were consistent with observations in other published studies, including redox homeostasis, protein metabolism, fatty acid metabolism and energy metabolism. The increase in gamma-glutamyl amino acids (see figure 3.24 on page 158) is indicative of increased gamma-glutamyl transferase activity; a key enzyme in the maintenance of antioxidant glutathione levels, a finding that agrees with older studies (Takahashi et al., 1978). Previous studies also show that the turnover of proteins decreases with age (Makrides, 1983), which is supported by the finding in this study that several dipeptides were depleted in the media of senescent cells (figure 3.3 on page 142). In the case of energy metabolism, depleted pyruvate and elevated TCA intermediates such as citrate and fumarate initially suggested the TCA cycle is very active in senescent cells. However when the internal metabolome, which showed there were lower levels of citrate, malate and succinate (but interestingly fumarate levels were sustained) inside senescent cells was taken into consideration, along with qPCR analysis of the enzymes involved in glucose metabolism that showed an increase in transcription of glycolytic enzymes; it

becomes increasingly likely that senescent cells are actually predominantly using glycolysis to generate ATP. As the TCA cycle enzymes are situated inside mitochondria, this result is perhaps not surprising because it is well documented that senescent cells have dysfunctional mitochondria (Passos et al., 2007). Previous work assessing the bioenergetics of senescent cells found that although cells had a decreased oxygen consumption rate, indicating decreased oxidative metabolism, the glucose taken up by the cells was not all being converted to lactate, the end product of glycolysis, and so the authors concluded that the cells must be using up the pyruvate in the TCA cycle (Zwerschke et al., 2003). This conclusion did not allow for the possibility that substrate might be shunted into the PPP, or that gluconeogenesis might be active. To address these issues flux experiments using the labelled substrates glucose, glutamine and pyruvate should be conducted over a combination of short (minutes) and long (hours) time-courses to establish which pathways are being preferentially used by senescent cells (intermediates in the favoured pathways will incorporate the labelled carbons from the substrates). Not only would this information add further detail to our knowledge of senescent cell biology, it may also be helpful in achieving the second aim of this project; understanding the mechanism behind the elevation of extracellular citrate, which will be discussed later.

The question of whether or not the *in vitro* work in this thesis will translate to a useful tool for studying senescence *in vivo* remains to be properly tested, although citrate has already been identified as highly correlated with human ageing *in vivo* in the study carried out by Menni and colleagues (Menni et al., 2013) as well as more recent studies (Dunn et al., 2014), proving that alterations in citrate levels in humans *in vivo* are both detectable and highly correlated with a condition known to be associated wit accumulation of senescent cells (ageing), making citrate an excellent candidate as a biomarker of senescence. In other species citrate has also been identified as a marker of ageing; for example in house flies (Yan et al., 1997), which is also important because previous work characterising the metabolome of ageing in non-human species

has shown many aspects of the metabolome to be species specific. For example, a metabolomic study of ageing in mice, which focused on lipids, reported many changes in lipid metabolism (Tomás-Loba et al., 2013) that were not found to be similar in our study of human senescent cells or the studies of human ageing already mentioned (Dunn et al., 2014; Menni et al., 2013). Finding aspects of senescence and ageing that are similar between species is vital if animal models are to be informative on human conditions.

To summarise this point; the work presented in this thesis represents a novel contribution to the field of senescence in two regards; firstly the wealth of data generated from the untargeted screening of the extra cellular metabolome of senescent and growing cells from multiple tissues, in two modes of senescence as well as growth arrest controls and intracellular metabolomes of one line will be deposited in the Metabolights database for other researchers to access and mine. Secondly, a candidate secreted biomarker of senescence has been identified, using rigorous controls to ensure it is specific for senescence and not related only to the induction stimulus or transient growth arrest.

5.3 The mechanism behind citrate elevation

The second aim of this thesis was to elucidate the mechanism driving the elevation of extracellular citrate in senescent cells. While progress has been made towards this goal, further work is needed to answer the two main questions: what pathway(s) is the citrate coming from and how is it being transported out of the cell? Figure 5.1 depicts the main candidates for investigation.

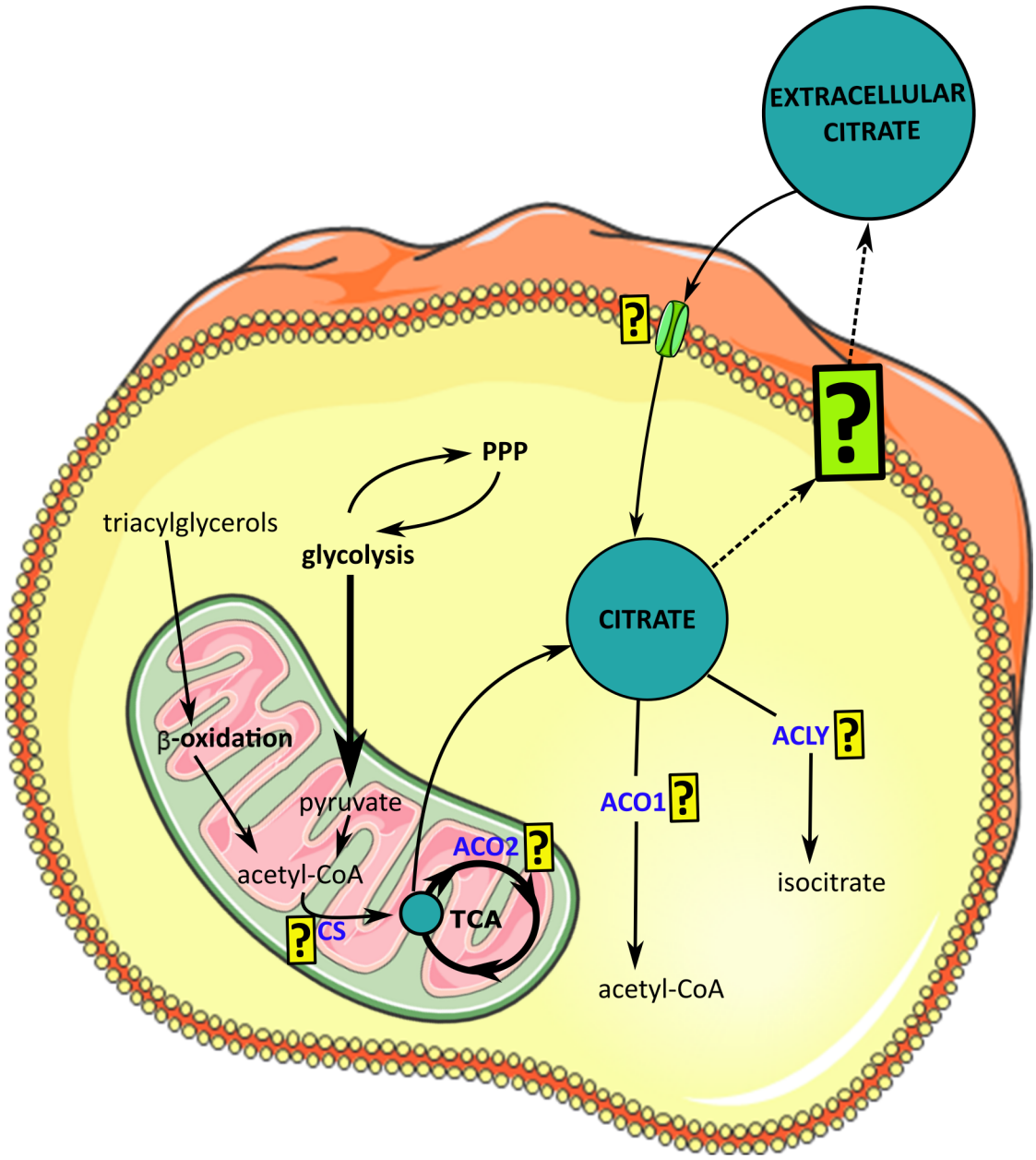

Figure 5.1: **Potential sources of citrate in the cell**. Citrate (teal circle) is produced from acetyl-CoA via the enzyme citrate synthase (CS). An increase in β-oxidation of triacylglycerols or glycolysis could result in an increase in mitochondrial acetyl-CoA, which could potentially result in n increase in citrate production via citrate synthase. A decrease in activity of either mitochondrial aconitase (ACO2) or cytosolic aconitase (ACO1) could result in a decrease in the rate of citrate breakdown, leading to its accumulation. Similarly reduction in ATP citrate lyase (ACLY) activity would also impair the breakdown of citrate and lead to its accumulation. The observation that citrate is depleted inside the cell but elevated outside suggests either a decrease in transport of citrate into the cell via NaCT/NaDC1/NaDC3 transporters (green channel), or transport out of the cell via an unknown mechanism (green box with ?). Yellow boxes containing ? signify unknown activity of neighbouring enzyme or transporter.

5.3.1 Where is the citrate coming from?

There are three main logical explanations for the observation that senescent cells have elevated extracellular citrate and lower levels of intracellular citrate than growing and growth arrested controls, which could be occurring together or in isolation. Firstly, it is possible that transport of citrate across the plasma membrane into the cell is somehow impaired. Secondly, there could be an increase in CS activity to produce citrate that is then transported out of the cell. Thirdly there could be a decrease in activity of the enzymes that break down citrate. The use of a blank media sample, corresponding to each collection of conditioned media, shows the relative increase in extracellular citrate compared to controls is genuinely an increase in citrate over the baseline levels seen in the media. This observation means we can probably discount the first of those options just described as the sole driver of increased extracellular citrate levels, because clearly some citrate at least must have exited the cell. The exit of citrate from the cell is assumed not to be from random leakage or diffusion because the movement would be against a concentration gradient, and furthermore overall the extracellular metabolome of senescent cells showed specific metabolites were depleted or enriched; there does not appear to have been a non specific leakage of intracellular metabolites. It is important to note that the metabolomic screen of intracellular metabolites was untargeted and not quantitative, so as yet it is not known if the amount of citrate outside the cell represents the same amount of citrate found usually inside the growing cells. If the amount of citrate in the extracellular compartment of the senescent cells is similar to the amount found inside growing cells, it would seem probable that transport of citrate across the plasma membrane from the cytosol to the extracellular space is the major factor of interest. However, if the extracellular citrate from senescent cells is more than the intracellular citrate in growing cells, then in addition to intracellular citrate being transported out across the plasma membrane, there must either be an increase in production of citrate or a decrease in the breakdown of citrate. Although the activity of CS has not been tested here, this thesis showed there was no transcriptional up-

regulation of the enzyme and based on current literature it is unlikely to have increased activity levels. CS is a mitochondrial enzyme, an organelle that is reported to become dysfunctional in senescence due to increased ROS (Passos et al., 2007) and additionally it has been reported that citrate synthase activity decreases in senescence (Ghneim and Al-Sheikh, 2010). The remaining options of decreased ACO or ACLY activity also have not been tested in this thesis, although none of these enzymes were down-regulated at the transcript or protein level. There is already substantial literature to suggest that ACO2 (mitochondrial aconitase) is likely inhibited, either by fumarate (which is sustained in senescent cells while other TCA intermediates declined, if the data are normalised to protein, or elevated if considered on an amount per cell basis) through succination of cysteine residues (Ternette et al., 2013) or carbonylation as a result of increased ROS (Yan et al., 1997), and silencing of ACLY has been demonstrated to induce senescence via p53 (Lee et al., 2015).

5.3.1.1 The role of senescence effector proteins

Given that extracellular citrate accumulation is specific to senescent cells, the impact of senescence effector proteins seemed a good place to look for possible regulation of the citrate accumulation. In chapter 2 it was observed that NHOF1 cells did not have detectable levels of $p16^{INK4A}$ in either PEsen or IrrDSBsen models, and while IMR90 did show elevation of $p16^{INK4A}$ in PEsen it was not apparent in IrrDSBsen. These varying levels of $p16^{INK4A}$ in groups that all showed elevated citrate suggests that the elevated citrate was probably not directly linked to $p16^{INK4A}$ levels. Further evidence in support of this came from the use of $p16^{INK4A}$ knock out cells (Leiden) and $p21^{WAF1}$ knockout and p53 knockout cells, which showed that relative to controls and the other knockouts, cells lacking p53 had elevated extracellular citrate; suggesting p53 restrains citrate but not via $p21^{WAF1}$.

5.3.2 How does citrate exit the cell?

While there are obvious routes for further investigation of whether there is more citrate being produced and whether or not its breakdown is being inhibited, the way forward for identifying how citrate is transported out of the cell is more challenging. As already mentioned it is unlikely that the extracellular citrate increase is due to leakage across the cell membrane, because specific enrichment and depletion of metabolites was seen, suggesting the cell membrane was not "leaky". In almost all mammalian cells citrate is not transported out of the cell across the plasma membrane, but is transported into the cell if enough is not being produced in the mitochondria to sustain the TCA cycle and acetyl-CoA production. One exception to this is luminal prostate epithelial cells, which produce an increased amount of citrate due to inhibition of ACO2 by zinc (Costello and Franklin, 1981), sequestered to the mitochondria due to hormone levels (Costello and Franklin, 1994). The excess citrate is quickly exported across the plasma membrane before it can be broken down by cytosolic enzymes, via a plasma membrane isoform of the mitochondrial citrate transporter SLC25A1. This transporter is the same as the one found in the mitochondria of all cell types except for a modification at the N-terminus that causes it to be trafficked to the plasma membrane (Mazurek et al., 2010). It is not known what causes this isoform to be expressed in prostate luminal epithelial cells, but the possibility exists that the same isoform may be expressed in senescent cells too, representing one potential mechanism behind citrate transport across the plasma membrane. Transporters that normally exist in the plasma membrane are unlikely to be the method of citrate export, as they are sodium linked and the gradient of sodium is such that it always favours movement of citrate into the cell (Pajor, 1999, 2014) and do not transport citrate against the concentration gradient (Wolffram et al., 1994).

5.3.3 Limitations of this work

The key to finding a robust biomarker of senescence is to ensure that the marker is present/significantly elevated only as a result of senescence and not other similar condi-

tions which could lead to false positives. In this thesis efforts were made to ensure that the candidate biomarker was generic across different tissue types *in vitro* and across two well characterised modes of senescence induction; IrrDSBsen and PEsen. However, it was discovered that $p16^{INK4A}$ elevation was not required in either of these models of senescence so the validity of the marker in a senescence state sustained by $p16^{INK4A}$ still remains to be tested, along with oncogene induced senescence, to ensure that citrate is indeed a marker of senescence growth arrest and not of some other related condition specific to the IrrDSBsen and PEsen models tested here. While this study did cover several tissue types, all cells used were fibroblasts so it is not yet known whether extracellular citrate is also elevated in other cell types such as blood cells and keratinocytes, and what effect differentiation would have on citrate levels. In addition, *in vivo* validation is required.

Work has been started to address the mechanism behind the elevation of citrate, however the data are preliminary. The observation that the telomere lengthening activities of telomerase alone, and not the non-canonical activities possessed by TERT HA, are able to prevent senescence and elevation of extracellular citrate strongly supports the conclusion that the citrate elevation seen in the PEsen model is a result of telomere shortening and not just sustained time in culture however this needs to be verified with repeats. The $p16^{INK4A-/-}$cells used in this thesis did not have an isogenic $p16^{INK4A+/+}$ control, instead other fibroblasts of the same tissue type were used and that was not ideal so should be repeated using matched controls to ensure relative citrate levels are accurately measured. Also as p53 is involved in so many aspects of cell biology, complete knockout of p53 may have caused the cells to adapt and compensate its loss, so results from these cells should be verified using a transient knockdown as well.

5.3.4 Future work

As is usually the case, in undertaking to answer just a few questions about the senescence phenotype, many more questions have been raised and there are still some loose

ends to tie up.

5.3.4.1 Addressing the remaining questions

To move forward on the question of the source of citrate in senescent fibroblasts it will be useful to quantify the intracellular citrate in a normal population of young, growing cells and compare it to the amount of extracellular citrate produced by a similar sized population of senescent cells, to ascertain if the net amount is similar. The activity of citrate synthase, ACO1, ACO2 and ACLY should also be measured in the relevant cell fractions of senescent cells compared to controls. Further insight into the flux through these enzymes should be attainable by using stable carbon isotope labelled substrates, and monitoring the way in which the labelled carbons are incorporated into citrate, isocitrate, acetyl-CoA, aconitate and other related metabolites to elucidate which reactions must have occurred and therefore which enzymes are more active or inactive than in controls cells under the same conditions. The next challenge, assuming an altered enzyme activity will be identified, is to understand what is affecting the enzyme(s). Depending on the affected enzymes, the degree of mitochondrial function and ROS may be of interest, both of which could be assessed using fluorescent assays.

The role played by p53 (or lack of p53 activity on a background of other cellular events specific to senescence) may be related to some or all of the above, so developing transient knockdown of p53 or manipulating its activation could give important insights into the connection between extracellular citrate elevation and the senescence state.

In terms of the question of citrate transport out of the cell the possibility that a plasma membrane isoform of the mitochondrial citrate transporter SLC25A1 is expressed in senescence as in prostate epithelium and potentially gut luminal epithelium should not be ruled out. If present, the protein should be detectable in the plasma membrane using immunofluorescence microscopy and the mRNA identified using qPCR using primers described for the isoform found in prostate. Other transporters should also be investigated including NaDC1 and NaCT, which usually function as importers of

citrate. Questions about their function in senescent cells could potentially be answered using electrophysiological techniques; using pharmacological blocking agents to assess how specific molecules are moving through the channels and in which direction.

As already mentioned, it is also important that other modes of senescence namely OIS and $p16^{INK4A}$ dependent senescence are included in future investigations along with other cell types such as keratinocytes. This information will inform whether citrate can be used as a generic marker of senescence growth arrest or whether it is only useful for monitoring senescent fibroblasts induced to senesce via PEsen and IrrDSBsen.

A measure of the sensitivity of citrate as a biomarker *in vivo* would also need to be assessed to ensure its usefulness in detecting relevant changes in overall senescent cell population in response to interventions.

5.3.4.2 Wider future applications of this work

In the event that further robust testing confirms that citrate is a specific biomarker of senescence, across different cell types and induction methods, then finding the source of the elevated citrate and mechanism for its transport would lead to a greater understanding of the fundamental molecular processes that underpin the senescence growth arrest. This information would be extremely valuable for our understanding of cell biology and facilitate the manipulation of the senescent state.

In addition, validity in animal models of senescence and ageing could be tested by measuring serum levels of citrate in young and aged transgenic INK-ATTAC mice (Baker et al., 2011) before and after selective removal of senescent cells; if senescent cell accumulation in aged mice (which has already been shown (Baker et al., 2011, 2016)) was causing an elevation in extracellular citrate, the level of citrate should be reduced in the aged mice to a level similar to that found in young mice, and the serum level of citrate in young mice with few senescent cells should be largely unaffected. If shown to be valid, the use of citrate as a marker of senescence could enable more efficient animal use in studies designed to track the effects of senescent cell accumulation on

physiological processes with other known readouts such as cognitive decline or muscle wasting in ageing, or mobility in the case of fibrosis. Instead of sacrificing an animal at each time point or after interventions to assess traditional senescence markers, multiple serum citrate level measurements could be taken from the same animal as a readout of senescence which would afford higher statistical power to the work in addition to reducing the number of animals required.

Ultimately, having a biomarker of senescence that can be detected in human blood would be extremely useful for the senescence field, and any other fields that are directly affected by senescence including ageing, cancer and fibrosis. Some pathologies and processes that had previously not had a known association with senescence may also be identified by screening patients for elevated extracellular citrate. Using one clear marker would facilitate much larger multi-site and even global studies to monitor large groups of people throughout their lives, to see if there are any particular lifestyle, genetic or environmental factors that influence the rate of accumulation of senescent cells and any correlations to disease incidence or life span. The effects of interventions such as "anti-ageing" products or specific diets could also be measured over long periods of time. The effects of senescence- inducing cancer treatments could also be monitored for success non-invasively, providing serum citrate levels are sensitive to localised changes in senescent cell numbers.

5.3.5 Conclusions

To conclude, this thesis has made considerable progress towards identification of a robust and specific secreted biomarker of senescent cells, which has the potential to facilitate the long term study of the impact of senescence on human health, as well as in animal models. While there is still work to do to ensure the robustness of citrate as a marker of senescence, and questions still remain around the mechanism behind its elevation, the data gathered so far on these points represents a novel contribution to the field of senescence. The metabolic profiles of senescent fibroblasts along with matched

growth arrested and growing controls will be particularly useful for the field in general, as they represent information on many complex biological metabolic processes.

References

Bibliography

Abbas, T. and Dutta, A. (2009). p21 in cancer: intricate networks and multiple activities. *Nature Reviews Cancer*, 9(6):400–14.

Abbot, E. L., McCormack, J. G., Reynet, C., Hassall, D. G., Buchan, K. W., and Yeaman, S. J. (2005). Diverging regulation of pyruvate dehydrogenase kinase isoform gene expression in cultured human muscle cells. *The FEBS Journal*, 272(12):3004–14.

Acosta, J. C., Banito, A., Wuestefeld, T., Georgilis, A., Janich, P., Morton, J. P., Athineos, D., Kang, T.-W., Lasitschka, F., Andrulis, M., Pascual, G., Morris, K. J., Khan, S., Jin, H., Dharmalingam, G., Snijders, A. P., Carroll, T., Capper, D., Pritchard, C., Inman, G. J., Longerich, T., Sansom, O. J., Benitah, S. A., Zender, L., and Gil, J. (2013). A complex secretory program orchestrated by the inflammasome controls paracrine senescence. *Nature Cell Biology*, 15(8):978–990.

Acosta, J. C., O'Loghlen, A., Banito, A., Guijarro, M. V., Augert, A., Raguz, S., Fumagalli, M., Da Costa, M., Brown, C., Popov, N., Takatsu, Y., Melamed, J., d'Adda di Fagagna, F., Bernard, D., Hernando, E., and Gil, J. (2008). Chemokine Signaling via the CXCR2 Receptor Reinforces Senescence. *Cell*, 133(6):1006–1018.

Ahmed, S., Passos, J. F., Birket, M. J., Beckmann, T., Brings, S., Peters, H., Birch-Machin, M. A., von Zglinicki, T., and Saretzki, G. (2008). Telomerase does not counteract telomere shortening but protects mitochondrial function under oxidative stress. *Journal of Cell Science*, 121(Pt 7):1046–53.

Aird, K. M. and Zhang, R. (2013). Detection of senescence-associated heterochromatin foci (SAHF). *Methods in Molecular Biology (Clifton, N.J.)*, 965:185–96.

Alcorta, D. A., Xiong, Y., Phelps, D., Hannon, G., Beach, D., and Barrett, J. C. (1996). Involvement of the cyclin-dependent kinase inhibitor p16 (INK4a) in replicative senescence of normal human fibroblasts. *Proceedings of the National Academy of Sciences of the United States of America*, 93(24):13742–13747.

Ameziane-El-Hassani, R., Talbot, M., de Souza Dos Santos, M. C., Al Ghuzlan, A., Hartl, D., Bidart, J.-M., De Deken, X., Miot, F., Diallo, I., de Vathaire, F., Schlumberger, M., and Dupuy, C. (2015). NADPH oxidase DUOX1 promotes long-term persistence of oxidative stress after an exposure to irradiation. *Proceedings of the National Academy of Sciences of the United States of America*, 112(16):5051–6.

Angello, J., Pendergrass, W., Norwood, T., and Prothero, J. (1989). Cell enlargement: one possible mechanism underlying cellular senescence. *J. Cell. Physiol.*, 140(2):288–294.

Atlas, T. C. G. (2015). Gene Ranker: TCGA GBM 6000.

Baker, D. J., Childs, B. G., Durik, M., Wijers, M. E., Sieben, C. J., Zhong, J., A. Saltness, R., Jeganathan, K. B., Verzosa, G. C., Pezeshki, A., Khazaie, K., Miller, J. D., and van Deursen, J. M. (2016). Naturally occurring p16Ink4a-positive cells shorten healthy lifespan. *Nature*, 530(7589):184–189.

Baker, D. J., Wijshake, T., Tchkonia, T., LeBrasseur, N. K., Childs, B. G., van de Sluis, B., Kirkland, J. L., and van Deursen, J. M. (2011). Clearance of p16Ink4a-positive senescent cells delays ageing-associated disorders. *Nature*, 479(7372):232–236.

Baker, G. T. and Sprott, R. L. (1988). Biomarkers of aging. *Experimental Gerontology*, 23(4):223–239.

Balaban, R. S., Nemoto, S., and Finkel, T. (2005). Mitochondria, oxidants, and aging. *Cell*, 120(4):483–95.

Banin, S., Moyal, L., Shieh, S.-Y., Taya, Y., Anderson, C. W., Chessa, L., Smorodinsky, N. I., Prives, C., Reiss, Y., Shiloh, Y., and Ziv, Y. (1998). Enhanced Phosphorylation of p53 by ATM in Response to DNA Damage. *Science*, 281(5383):1674–1677.

Banumathy, G., Somaiah, N., Zhang, R., Tang, Y., Hoffmann, J., Andrake, M., Ceulemans, H., Schultz, D., Marmorstein, R., and Adams, P. D. (2008). Human UBN1 Is an Ortholog of Yeast Hpc2p and Has an Essential Role in the HIRA/ASF1a Chromatin-Remodeling Pathway in Senescent Cells. *Molecular and Cellular Biology*, 29(3):758–770.

Barradas, M., Anderton, E., Acosta, J. C., Li, S., Banito, A., Rodriguez-Niedenfuhr, M., Maertens, G., Banck, M., Zhou, M. M., Walsh, M. J., Peters, G., and Gil, J. (2009). Histone demethylase JMJD3 contributes to epigenetic control of INK4a/ARF by oncogenic RAS. *Genes & Development*, 23(10):1177–1182.

Belsky, D. W., Caspi, A., Houts, R., Cohen, H. J., Corcoran, D. L., Danese, A., Harrington, H., Israel, S., Levine, M. E., Schaefer, J. D., Sugden, K., Williams, B., Yashin, A. I., Poulton, R., and Moffitt, T. E. (2015). Quantification of biological aging in young adults. *Proceedings of the National Academy of Sciences of the United States of America*, 112(30):E4104–10.

Benanti, J. A. and Galloway, D. A. (2004). Normal human fibroblasts are resistant to RAS-induced senescence. *Molecular and Cellular Biology*, 24(7):2842–52.

Benarroch, E. E. (2005). Neuron-astrocyte interactions: partnership for normal function and disease in the central nervous system. *Mayo Clinic Proceedings*, 80(10):1326–38.

Bennett, D. C. (2016). Genetics of melanoma progression: the rise and fall of cell senescence. *Pigment Cell & Melanoma Research*, 29(2):122–40.

Bensaad, K., Tsuruta, A., Selak, M. A., Vidal, M. N. C., Nakano, K., Bartrons, R., Gottlieb, E., and Vousden, K. H. (2006). TIGAR, a p53-Inducible Regulator of Glycolysis and Apoptosis. *Cell*, 126(1):107–120.

Bhat, R., Crowe, E. P., Bitto, A., Moh, M., Katsetos, C. D., Garcia, F. U., Johnson, F. B., Trojanowski, J. Q., Sell, C., and Torres, C. (2012). Astrocyte senescence as a component of Alzheimer's disease. *PloS One*, 7(9):e45069.

Blagosklonny, M. V. (2012). Cell cycle arrest is not yet senescence, which is not just cell cycle arrest: terminology for TOR-driven aging. *Aging*, 4(3):159–65.

Boidot, R., Vegran, F., Meulle, A., Le Breton, A., Dessy, C., Sonveaux, P., Lizard-Nacol, S., and Feron, O. (2011). Regulation of Monocarboxylate Transporter MCT1 Expression by p53 Mediates Inward and Outward Lactate Fluxes in Tumors. *Cancer Research*, 72(4):939–948.

Bonuccelli, G., Tsirigos, A., Whitaker-Menezes, D., Pavlides, S., Pestell, R. G., Chiavarina, B., Frank, P. G., Flomenberg, N., Howell, A., Martinez-Outschoorn, U. E., Sotgia, F., and Lisanti, M. P. (2010). Ketones and lactate fuel tumor growth and metastasis: Evidence that epithelial cancer cells use oxidative mitochondrial metabolism. *Cell Cycle*, 9(17):3506–3514.

Bracken, A. P., Kleine-Kohlbrecher, D., Dietrich, N., Pasini, D., Gargiulo, G., Beekman, C., Theilgaard-Monch, K., Minucci, S., Porse, B. T., Marine, J. C., Hansen, K. H., and Helin, K. (2007). The Polycomb group proteins bind throughout the INK4A-ARF locus and are disassociated in senescent cells. *Genes & Development*, 21(5):525–530.

Braig, M., Lee, S., Loddenkemper, C., Rudolph, C., Peters, A. H. F. M., Schlegelberger, B., Stein, H., Dörken, B., Jenuwein, T., and Schmitt, C. A. (2005). Oncogene-induced senescence as an initial barrier in lymphoma development. *Nature*, 436(7051):660–5.

Brand, M. D. and Nicholls, D. G. (2011). Assessing mitochondrial dysfunction in cells. *The Biochemical Journal*, 435(2):297–312.

Brookes, S., Rowe, J., Gutierrez del Arroyo, A., Bond, J., and Peters, G. (2004). Contribution of p16INK4a to replicative senescence of human fibroblasts. *Experimental Cell Research*, 298(2):549–559.

Burd, C., Sorrentino, J., Clark, K., Darr, D., Krishnamurthy, J., Deal, A. M., Bardeesy, N., Castrillon, D. H., Beach, D. H., and Sharpless, N. E. (2013). Monitoring Tumorigenesis and Senescence In Vivo with a p16INK4a-Luciferase Model. *Cell*, 152(1-2):340–351.

Burtner, C. R. and Kennedy, B. K. (2010). Progeria syndromes and ageing: what is the connection? *Nature Reviews Molecular Cell Biology*, 11(8):567–578.

Buzzai, M., Jones, R. G., Amaravadi, R. K., Lum, J. J., DeBerardinis, R. J., Zhao, F., Viollet, B., and Thompson, C. B. (2007). Systemic Treatment with the Antidiabetic Drug Metformin Selectively Impairs p53-Deficient Tumor Cell Growth. *Cancer Research*, 67(14):6745–6752.

Capell, B. C., Drake, A. M., Zhu, J., Shah, P. P., Dou, Z., Dorsey, J., Simola, D. F., Donahue, G., Sammons, M., Rai, T. S., Natale, C., Ridky, T. W., Adams, P. D., and Berger, S. L. (2016). MLL1 is essential for the senescence-associated secretory phenotype. *Genes & Development*, 30(3):321–36.

Capparelli, C., Guido, C., Whitaker-Menezes, D., Bonuccelli, G., Balliet, R., Pestell, T. G., Goldberg, A. F., Pestell, R. G., Howell, A., Sneddon, S., Birbe, R., Tsirigos, A., Martinez-Outschoorn, U., Sotgia, F., and Lisanti, M. P. (2012). Autophagy and senescence in cancer-associated fibroblasts metabolically supports tumor growth and metastasis, via glycolysis and ketone production. *Cell Cycle*, 11(12):2285–2302.

Carrel, A. (1921). Age and multiplication of fibroblasts. *Journal of Experimental Medicine*, 34(6):599–623.

Cesare, A. J. and Reddel, R. R. (2010). Alternative lengthening of telomeres: models, mechanisms and implications. *Nature Reviews Genetics*, 11(5):319–30.

Chace, D. H., Kalas, T. A., and Naylor, E. W. (2002). The application of tandem mass spectrometry to neonatal screening for inherited disorders of intermediary metabolism. *Annual Review of Genomics and Human Genetics*, 3:17–45.

Chang, E. and Harley, C. B. (1995). Telomere length and replicative aging in human vascular tissues. *Proceedings of the National Academy of Sciences*, 92(24):11190–11194.

Chang, J., Wang, Y., Shao, L., Laberge, R.-M., Demaria, M., Campisi, J., Janakiraman, K., Sharpless, N. E., Ding, S., Feng, W., Luo, Y., Wang, X., Aykin-Burns, N., Krager, K., Ponnappan, U., Hauer-Jensen, M., Meng, A., and Zhou, D. (2015). Clearance of senescent cells by ABT263 rejuvenates aged hematopoietic stem cells in mice. *Nature Medicine*, 22(1):78–83.

Chehab, N. H., Malikzay, A., Stavridi, E. S., and Halazonetis, T. D. (1999). Phosphorylation of Ser-20 mediates stabilization of human p53 in response to DNA damage. *Proceedings of the National Academy of Sciences of the United States of America*, 96(24):13777–13782.

Chen, Z., Trotman, L. C., Shaffer, D., Lin, H.-K., Dotan, Z. A., Niki, M., Koutcher, J. A., Scher, H. I., Ludwig, T., Gerald, W., Cordon-Cardo, C., and Pandolfi, P. P. (2005). Crucial role of p53-dependent cellular senescence in suppression of Pten-deficient tumorigenesis. *Nature*, 436(7051):725–30.

Chinta, S. J., Woods, G., Rane, A., Demaria, M., Campisi, J., and Andersen, J. K. (2015). Cellular senescence and the aging brain. *Experimental Gerontology*, 68:3–7.

Chong, J. P. J., Mahbubani, H. M., Khoo, C.-Y., and Blow, J. J. (1995). Purification of an MCM-containing complex as a component of the DNA replication licensing system. *Nature*, 375(6530):418–421.

Choudhary, C., Weinert, B. T., Nishida, Y., Verdin, E., and Mann, M. (2014). The growing landscape of lysine acetylation links metabolism and cell signalling. *Nature Reviews Molecular Cell Biology*, 15(8):536–50.

Contractor, T. and Harris, C. R. (2011). p53 Negatively Regulates Transcription of the Pyruvate Dehydrogenase Kinase Pdk2. *Cancer Research*, 72(2):560–567.

Coppé, J.-P., Desprez, P.-Y., Krtolica, A., and Campisi, J. (2010a). The senescence-associated secretory phenotype: the dark side of tumor suppression. *Annual Review of Pathology*, 5:99–118.

Coppé, J.-P., Patil, C. K., Rodier, F., Krtolica, A., Beauséjour, C. M., Parrinello, S., Hodgson, J. G., Chin, K., Desprez, P.-Y., and Campisi, J. (2010b). A Human-Like Senescence-Associated Secretory Phenotype Is Conserved in Mouse Cells Dependent on Physiological Oxygen. *PLoS ONE*, 5(2):e9188.

Coppé, J.-P., Rodier, F., Patil, C. K., Freund, A., Desprez, P.-Y., and Campisi, J. (2011). Tumor suppressor and aging biomarker p16(INK4a) induces cellular senescence without the associated inflammatory secretory phenotype. *The Journal of Biological Chemistry*, 286(42):36396–403.

Correia-Melo, C., Marques, F. D., Anderson, R., Hewitt, G., Hewitt, R., Cole, J., Carroll, B. M., Miwa, S., Birch, J., Merz, A., Rushton, M. D., Charles, M., Jurk, D., Tait, S. W., Czapiewski, R., Greaves, L., Nelson, G., Bohlooly-Y, M., Rodriguez-Cuenca, S., Vidal-Puig, A., Mann, D., Saretzki, G., Quarato, G., Green, D. R., Adams, P. D., von Zglinicki, T., Korolchuk, V. I., and Passos, J. F. (2016). Mitochondria are required for pro-ageing features of the senescent phenotype. *The EMBO Journal*, page e201592862.

Correia-Melo, C. and Passos, J. F. (2015). Mitochondria: Are they causal players in cellular senescence? *Biochimica et biophysica acta*, 1847(11):1373–9.

Cortez, D., Wang, Y., Qin, J., and Elledge, S. J. (1999). Requirement of ATM-Dependent Phosphorylation of Brca1 in the DNA Damage Response to Double-Strand Breaks. *Science*, 286(5442):1162–1166.

Costello, L. C. and Franklin, R. B. (1981). Aconitase activity, citrate oxidation, and zinc inhibition in rat ventral prostate. *Enzyme*, 26(6):281–7.

Costello, L. C. and Franklin, R. B. (1991). Concepts of citrate production and secretion by prostate 1. Metabolic relationships. *The Prostate*, 18(1):25–46.

Costello, L. C. and Franklin, R. B. (1994). Effect of prolactin on the prostate. *The Prostate*, 24(3):162–6.

Counter, C. M., Hahn, W. C., Wei, W., Caddle, S. D., Beijersbergen, R. L., Lansdorp, P. M., Sedivy, J. M., and Weinberg, R. A. (1998). Dissociation among in vitro telomerase activity, telomere maintenance, and cellular immortalization. *Proceedings of the National Academy of Sciences of the United States of America*, 95(25):14723–8.

d'Adda di Fagagna, F., Reaper, P. M., Clay-Farrace, L., Fiegler, H., Carr, P., von Zglinicki, T., Saretzki, G., Carter, N. P., and Jackson, S. P. (2003). A DNA damage checkpoint response in telomere-initiated senescence. *Nature*, 426(6963):4.

de Ruijter, A. J. M., van Gennip, A. H., Caron, H. N., Kemp, S., and van Kuilenburg, A. B. P. (2003). Histone deacetylases (HDACs): characterization of the classical HDAC family. *The Biochemical journal*, 370(Pt 3):737–49.

Debacq-Chainiaux, F., Erusalimsky, J. D., Campisi, J., and Toussaint, O. (2009). Protocols to detect senescence-associated beta-galactosidase (SA-βgal) activity, a biomarker of senescent cells in culture and in vivo. *Nature Protocols*, 4(12):1798–1806.

Demidenko, Z. N. and Blagosklonny, M. V. (2008). Growth stimulation leads to cellular senescence when the cell cycle is blocked. *Cell cycle (Georgetown, Tex.)*, 7(21):3355–61.

Dempster, A. J. (1918). A new Method of Positive Ray Analysis. *Physical Review*, 11(4):316–325.

Deng, Q. (2003). High Intensity ras Signaling Induces Premature Senescence by Activating p38 Pathway in Primary Human Fibroblasts. *Journal of Biological Chemistry*, 279(2):1050–1059.

Dimri, G. P., Lee, X., Basile, G., Acosta, M., Scott, G., Roskelley, C., Medrano, E. E., Linskens, M., Rubelj, I., and Pereira-Smith, O. (1995). A biomarker that identifies senescent human cells in culture and in aging skin in vivo. *Proceedings of the National Academy of Sciences of the United States of America*, 92(20):9363–7.

Dörr, J. R., Yu, Y., Milanovic, M., Beuster, G., Zasada, C., Däbritz, J. H. M., Lisec, J., Lenze, D., Gerhardt, A., Schleicher, K., Kratzat, S., Purfürst, B., Walenta, S., Mueller-Klieser, W., Gräler, M., Hummel, M., Keller, U., Buck, A. K., Dörken, B., Willmitzer, L., Reimann, M., Kempa, S., Lee, S., and Schmitt, C. A. (2013). Synthetic lethal metabolic targeting of cellular senescence in cancer therapy. *Nature*, 501(7467):421–425.

Downward, J., Coppé, J.-P., Patil, C. K., Rodier, F., Sun, Y., Muñoz, D. P., Goldstein, J., Nelson, P. S., Desprez, P.-Y., and Campisi, J. (2008). Senescence-Associated Secretory Phenotypes Reveal Cell-Nonautonomous Functions of Oncogenic RAS and the p53 Tumor Suppressor. *PLoS Biology*, 6(12):e301.

Drane, P., Bravard, A., Bouvard, V., and May, E. (2001). Reciprocal down-regulation of p53 and SOD2 gene expression-implication in p53 mediated apoptosis. *Oncogene*, 20(4):430–9.

Dunn, W. B., Lin, W., Broadhurst, D., Begley, P., Brown, M., Zelena, E., Vaughan, A. A., Halsall, A., Harding, N., Knowles, J. D., Francis-McIntyre, S., Tseng, A., Ellis, D. I., O'Hagan, S., Aarons, G., Benjamin, B., Chew-Graham, S., Moseley, C., Potter, P., Winder, C. L., Potts, C., Thornton, P., McWhirter, C., Zubair, M., Pan, M., Burns, A., Cruickshank, J. K., Jayson, G. C., Purandare, N., Wu, F. C. W., Finn, J. D., Haselden, J. N., Nicholls, A. W., Wilson, I. D., Goodacre, R., and Kell, D. B. (2014). Molecular phenotyping of a UK population: defining the human serum metabolome. *Metabolomics*, 11(1):9–26.

Feng, J., Funk, S. S., Weinrich, S. L., Avilion, A. A., Chiu, C. P., Adams, R. R., Chang,

E., Allsopp, R. C., and Yu, J. (1995). The RNA component of human telomerase. *Science*, 269(5228):1236–1241.

Forsburg, S. L. (2004). Eukaryotic MCM Proteins: Beyond Replication Initiation.

Fransen, M., Nordgren, M., Wang, B., Apanasets, O., and Van Veldhoven, P. P. (2013). Aging, age-related diseases and peroxisomes. *Sub-cellular Biochemistry*, 69:45–65.

Fulton, D. J. (2009). Nox5 and the regulation of cellular function. *Antioxid Redox Signal*, 11(10):2443–2452.

Funayama, R., Saito, M., Tanobe, H., and Ishikawa, F. (2006). Loss of linker histone H1 in cellular senescence. *The Journal of Cell Biology*, 175(6):869–880.

Gannon, H. S. and Jones, S. N. (2012). Using Mouse Models to Explore MDM-p53 Signaling in Development, Cell Growth, and Tumorigenesis. *Genes & Cancer*, 3(3-4):209–18.

Gems, D. and Partridge, L. (2013). Genetics of Longevity in Model Organisms: Debates and Paradigm Shifts. *Annual Review of Physiology*, 75(1):621–644.

Gey, C. and Seeger, K. (2013). Metabolic changes during cellular senescence investigated by proton NMR-spectroscopy. *Mechanisms of Ageing and Development*, 134(3-4):130–8.

Ghneim, H. K. and Al-Sheikh, Y. A. (2010). The effect of aging and increasing ascorbate concentrations on respiratory chain activity in cultured human fibroblasts. *Cell Biochemistry and Function*, 28(4):283–92.

Giorgi, C., Bonora, M., Sorrentino, G., Missiroli, S., Poletti, F., Suski, J. M., Galindo Ramirez, F., Rizzuto, R., Di Virgilio, F., Zito, E., Pandolfi, P. P., Wieckowski, M. R., Mammano, F., Del Sal, G., and Pinton, P. (2015). p53 at the endoplasmic reticulum regulates apoptosis in a Ca2+-dependent manner. *Proceedings of the National Academy of Sciences of the United States of America*, 112(6):1779–84.

Goldstein, S., Ballantyne, S. R., Robson, A. L., and Moerman, E. J. (1982). Energy metabolism in cultured human fibroblasts during aging in vitro. *Journal of Cellular Physiology*, 112(3):419–424.

Gopal, E., Miyauchi, S., Martin, P. M., Ananth, S., Srinivas, S. R., Smith, S. B., Prasad, P. D., and Ganapathy, V. (2007). Expression and functional features of NaCT, a sodium-coupled citrate transporter, in human and rat livers and cell lines. *American Journal of Physiology. Gastrointestinal and lLver Physiology*, 292(1):G402–8.

Gottlieb, E. and Vousden, K. H. (2010). p53 regulation of metabolic pathways. *Cold Spring Harbor Perspectives in Biology*, 2(4):a001040.

Greer, E. L. and Shi, Y. (2012). Histone methylation: a dynamic mark in health, disease and inheritance. *Nature Reviews Genetics*, 13(5):343–357.

Griffith, J. D., Comeau, L., Rosenfield, S., Stansel, R. M., Bianchi, A., Moss, H., and de Lange, T. (1999). Mammalian Telomeres End in a Large Duplex Loop. *Cell*, 97(4):503–514.

Grotewiel, M. S., Martin, I., Bhandari, P., and Cook-Wiens, E. (2005). Functional senescence in Drosophila melanogaster. *Ageing Research Reviews*, 4(3):372–397.

Group, B. D. W. (2001). Biomarkers and surrogate endpoints: preferred definitions and conceptual framework. *Clinical Pharmacology and Therapeutics*, 69(3):89–95.

Halestrap, A. P. and Price, N. T. (1999). The proton-linked monocarboxylate transporter (MCT) family: structure, function and regulation. *Biochemical Journal*, 343(Pt 2):281–299.

Hara, E., Smith, R., Parry, D., Tahara, H., Stone, S., and Peters, G. (1996). Regulation of p16CDKN2 expression and its implications for cell immortalization and senescence. *Molecular and Cellular Biology*, 16(3):859–67.

Harman, D. (1992). Free radical theory of aging. *Mutation Research/DNAging*, 275(3-6):257–266.

Harper, J. W., Adami, G. R., Wei, N., Keyomarsi, K., and Elledge, S. J. (1993). The p21 Cdk-interacting protein Cip1 is a potent inhibitor of G1 cyclin-dependent kinases. *Cell*, 75(4):805–16.

Hassona, Y., Cirillo, N., Lim, K. P., Herman, A., Mellone, M., Thomas, G. J., Pitiyage, G. N., Parkinson, E. K., and Prime, S. S. (2013). Progression of genotype-specific oral cancer leads to senescence of cancer-associated fibroblasts and is mediated by oxidative stress and TGF beta. *Carcinogenesis*.

Haug, K., Salek, R. M., Conesa, P., Hastings, J., de Matos, P., Rijnbeek, M., Mahendraker, T., Williams, M., Neumann, S., Rocca-Serra, P., Maguire, E., González-Beltrán, A., Sansone, S.-A., Griffin, J. L., and Steinbeck, C. (2013). MetaboLights–an open-access general-purpose repository for metabolomics studies and associated meta-data. *Nucleic Acids Research*, 41(Database issue):D781–6.

Hayflick, L. and Moorhead, P. S. (1961). The serial cultivation of human diploid cell strains. *Experimental Cell Research*, 25(3):585–621.

He, L., He, X., Lim, L. P., de Stanchina, E., Xuan, Z., Liang, Y., Xue, W., Zender, L., Magnus, J., Ridzon, D., Jackson, A. L., Linsley, P. S., Chen, C., Lowe, S. W., Cleary, M. A., and Hannon, G. J. (2007). A microRNA component of the p53 tumour suppressor network. *Nature*, 447(7148):1130–4.

Herbig, U., Ferreira, M., Condel, L., Carey, D., and Sedivy, J. M. (2006). Cellular Senescence in Aging Primates. *Science*, 311(5765):1257.

Herranz, N., Gallage, S., Mellone, M., Wuestefeld, T., Klotz, S., Hanley, C. J., Raguz, S., Acosta, J. C., Innes, A., Banito, A., Georgilis, A., Montoya, A., Wolter, K., Dharmalingam, G., Faull, P., Carroll, T., Martínez-Barbera, J. P., Cutillas, P., Reisinger, F., Heikenwalder, M., Miller, R., Withers, D., Zender, L., Thomas, G. J., and

Gil, J. (2015). mTOR regulates MAPKAPK2 translation to control the senescence-associated secretory phenotype. *Nature Cell Biology*, 17(9):1205–1217.

Hiebert, S. W., Chellappan, S. P., Horowitz, J. M., and Nevins, J. R. (1992). The interaction of RB with E2F coincides with an inhibition of the transcriptional activity of E2F. *Genes & Development*, 6(2):177–185.

Hoenicke, L. and Zender, L. (2012). Immune surveillance of senescent cells–biological significance in cancer- and non-cancer pathologies. *Carcinogenesis*, 33(6):1123–6.

Hornebeck, W. (2003). Down-regulation of tissue inhibitor of matrix metalloprotease-1 (TIMP-1) in aged human skin contributes to matrix degradation and impaired cell growth and survival. *Pathologie-Biologie*, 51(10):569–73.

Hubackova, S., Bartek, J., Hodny, Z., and Krejcikova, K. (2012). IL1- and TGFβ-Nox4 signaling, oxidative stress and DNA damage response are shared features of replicative, oncogene-induced, and drug-induced paracrine âĂŸBystander senescence'. *Aging*, 4(12):932–951.

Huen, M. S. Y., Sy, S. M. H., and Chen, J. (2010). BRCA1 and its toolbox for the maintenance of genome integrity. *Nature Reviews. Molecular Cell Biology*, 11(2):138–48.

Hutter, E., Renner, K., Pfister, G., Stöckl, P., Jansen-Dürr, P., and Gnaiger, E. (2004). Senescence-associated changes in respiration and oxidative phosphorylation in primary human fibroblasts. *The Biochemical Journal*, 380(Pt 3):919–928.

Iannetti, A., Ledoux, A. C., Tudhope, S. J., Sellier, H., Zhao, B., Mowla, S., Moore, A., Hummerich, H., Gewurz, B. E., Cockell, S. J., Jat, P. S., Willmore, E., and Perkins, N. D. (2014). Regulation of p53 and Rb links the alternative NF-κB pathway to EZH2 expression and cell senescence. *PLoS Genetics*, 10(9):e1004642.

James, E. L., Michalek, R. D., Pitiyage, G. N., de Castro, A. M., Vignola, K. S., Jones, J., Mohney, R. P., Karoly, E. D., Prime, S. S., and Parkinson, E. K. (2015).

Senescent Human Fibroblasts Show Increased Glycolysis and Redox Homeostasis with Extracellular Metabolomes That Overlap with Those of Irreparable DNA Damage, Aging, and Disease. *Journal of Proteome Research*, 14(4):1854–1871.

James, E. L. and Parkinson, E. K. (2015). Serum metabolomics in animal models and human disease. *Current Opinion in Clinical Nutrition and Metabolic Care*, 18(5):478–483.

Jascur, T., Brickner, H., Salles-Passador, I., Barbier, V., El Khissiin, A., Smith, B., Fotedar, R., and Fotedar, A. (2005). Regulation of p21(WAF1/CIP1) stability by WISp39, a Hsp90 binding TPR protein. *Molecular Cell*, 17(2):237–49.

Jeyapalan, J. C., Ferreira, M., Sedivy, J. M., and Herbig, U. (2007). Accumulation of senescent cells in mitotic tissue of aging primates. *Mechanisms of Ageing and Development*, 128(1):36–44.

Jiang, P., Du, W., Mancuso, A., Wellen, K. E., and Yang, X. (2013). Reciprocal regulation of p53 and malic enzymes modulates metabolism and senescence. *Nature*, 493(7434):689–693.

Jones, R. G., Plas, D. R., Kubek, S., Buzzai, M., Mu, J., Xu, Y., Birnbaum, M. J., and Thompson, C. B. (2005). AMP-activated protein kinase induces a p53-dependent metabolic checkpoint. *Molecular Cell*, 18(3):283–93.

Jun, J. I. and Lau, L. F. (2010). Cellular senescence controls fibrosis in wound healing. *Aging*, 2(9):627–631.

Kato, Y., Ozawa, S., Miyamoto, C., Maehata, Y., Suzuki, A., Maeda, T., and Baba, Y. (2013). Acidic extracellular microenvironment and cancer. *Cancer Cell International*, 13(1):89.

Kavanagh, J. P. (1994). Isocitric and citric acid in human prostatic and seminal fluid: implications for prostatic metabolism and secretion. *The Prostate*, 24(3):139–42.

Kawauchi, K., Araki, K., Tobiume, K., and Tanaka, N. (2008). p53 regulates glucose metabolism through an IKK-NF-kappaB pathway and inhibits cell transformation. *Nature Cell Biology*, 10(5):611–8.

Kia, S. K., Gorski, M. M., Giannakopoulos, S., and Verrijzer, C. P. (2008). SWI/SNF Mediates Polycomb Eviction and Epigenetic Reprogramming of the INK4b-ARF-INK4a Locus. *Molecular and Cellular Biology*, 28(10):3457–3464.

Killela, P. J., Reitman, Z. J., Jiao, Y., Bettegowda, C., Agrawal, N., Diaz, L. A., Friedman, A. H., Friedman, H., Gallia, G. L., Giovanella, B. C., Grollman, A. P., He, T. C., He, Y., Hruban, R. H., Jallo, G. I., Mandahl, N., Meeker, A. K., Mertens, F., Netto, G. J., Rasheed, B. A., Riggins, G. J., Rosenquist, T. A., Schiffman, M., Shih, I. M., Theodorescu, D., Torbenson, M. S., Velculescu, V. E., Wang, T. L., Wentzensen, N., Wood, L. D., Zhang, M., McLendon, R. E., Bigner, D. D., Kinzler, K. W., Vogelstein, B., Papadopoulos, N., and Yan, H. (2013). TERT promoter mutations occur frequently in gliomas and a subset of tumors derived from cells with low rates of self-renewal. *Proceedings of the National Academy of Sciences of the United States of America*, 110(15):6021–6026.

Kim, N., Piatyszek, K. R., Harley, C. B., West, M. D., Ho, P. L., Coviello, G. M., Wright, W. E., Weinrich, S. L., Shay, J. W., and Prowse, M. (1994). Specific association of human telomerase activity with immortal cells and cancer. *Science*, 226(5193):2011–2015.

Kim, R. H., Kang, M. K., Kim, T., Yang, P., Bae, S., Williams, D. W., Phung, S., Shin, K.-H., Hong, C., and Park, N.-H. (2015). Regulation of p53 during senescence in normal human keratinocytes. *Aging Cell*, 14(5):838–46.

Kondoh, H., Lleonart, M. E., Gil, J., Wang, J., Degan, P., Peters, G., Martinez, D., Carnero, A., and Beach, D. (2005). Glycolytic enzymes can modulate cellular life span. *Cancer Research*, 65(1):177–185.

Krishnamurthy, J., Torrice, C., Ramsey, M. R., Kovalev, G. I., Al-Regaiey, K., Su, L., and Sharpless, N. E. (2004). Ink4a/Arf expression is a biomarker of aging. *The Journal of clinical investigation*, 114(9):1299–307.

Krizhanovsky, V., Yon, M., Dickins, R. A., Hearn, S., Simon, J., Miething, C., Yee, H., Zender, L., and Lowe, S. W. (2008). Senescence of activated stellate cells limits liver fibrosis. *Cell*, 134(4):657–67.

Krtolica, A., Parrinello, S., Lockett, S., Desprez, P.-Y., and Campisi, J. (2001). Senescent fibroblasts promote epithelial cell growth and tumorigenesis: A link between cancer and aging. *Proceedings of the National Academy of Sciences of the United States of America*, 98(21):12072–12077.

Kuilman, T., Michaloglou, C., Mooi, W. J., and Peeper, D. S. (2010). The essence of senescence. *Genes & Development*, 24(22):2463–79.

Kuilman, T., Michaloglou, C., Vredeveld, L. C. W., Douma, S., van Doorn, R., Desmet, C. J., Aarden, L. A., Mooi, W. J., and Peeper, D. S. (2008). Oncogene-induced senescence relayed by an interleukin-dependent inflammatory network. *Cell*, 133(6):1019–31.

Kumagai, A., Lee, J., Yoo, H. Y., and Dunphy, W. G. (2006). TopBP1 activates the ATR-ATRIP complex. *Cell*, 124(5):943–55.

Kurz, D., Decary, S., Hong, Y., and Erusalimsky, J. (2000). Senescence-associated (beta)-galactosidase reflects an increase in lysosomal mass during replicative ageing of human endothelial cells. *Journal of Cell Science*, 113(20):3613–3622.

Lane, D. and Levine, A. (2010). p53 Research: the past thirty years and the next thirty years. *Cold Spring Harbor Perspectives in Biology*, 2(12):a000893.

Langley, E., Pearson, M., Faretta, M., Bauer, U.-M., Frye, R. A., Minucci, S., Pelicci, P. G., and Kouzarides, T. (2002). Human SIR2 deacetylates p53 and antagonizes PML/p53-induced cellular senescence. *The EMBO Journal*, 21(10):2383–96.

Laplante, M. and Sabatini, D. M. (2012). mTOR signaling in growth control and disease. *Cell*, 149(2):274–93.

Latorre-Pellicer, A., Moreno-Loshuertos, R., Lechuga-Vieco, A. V., Sánchez-Cabo, F., Torroja, C., Acín-Pérez, R., Calvo, E., Aix, E., González-Guerra, A., Logan, A., Bernad-Miana, M. L., Romanos, E., Cruz, R., Cogliati, S., Sobrino, B., Carracedo, Á., Pérez-Martos, A., Fernández-Silva, P., Ruíz-Cabello, J., Murphy, M. P., Flores, I., Vázquez, J., and Enríquez, J. A. (2016). Mitochondrial and nuclear DNA matching shapes metabolism and healthy ageing. *Nature*, 535(7613):561–5.

Lee, A. C., Fenster, B. E., Ito, H., Takeda, K., Bae, N. S., Hirai, T., Yu, Z.-X., Ferrans, V. J., Howard, B. H., and Finkel, T. (1999). Ras Proteins Induce Senescence by Altering the Intracellular Levels of Reactive Oxygen Species. *Journal of Biological Chemistry*, 274(12):7936–7940.

Lee, B. Y., Han, J. A., Im, J. S., Morrone, A., Johung, K., Goodwin, E. C., Kleijer, W. J., DiMaio, D., and Hwang, E. S. (2006). Senescence-associated β-galactosidase is lysosomal β-galactosidase. *Aging Cell*, 5(2):187–195.

Lee, J.-H., Jang, H., Lee, S.-M., Lee, J.-E., Choi, J., Kim, T. W., Cho, E.-J., and Youn, H.-D. (2015). ATP-citrate lyase regulates cellular senescence via an AMPK- and p53-dependent pathway. *The FEBS Journal*, 282(2):361–71.

Lewis, B. D. (1990). Determination of citrate in urine by simple direct photometry. *Clinical Chemistry*, 36(3):578.

Li, H. and Jogl, G. (2008). Structural and Biochemical Studies of TP53-induced Glycolysis and Apoptosis Regulator. *Journal of Biological Chemistry*, 284(3):1748–1754.

Li, J., Poi, M. J., and Tsai, M.-D. (2011). Regulatory mechanisms of tumor suppressor P16(INK4A) and their relevance to cancer. *Biochemistry*, 50(25):5566–82.

Lin, A. W., Barradas, M., Stone, J. C., van Aelst, L., Serrano, M., and Lowe, S. W.

(1998). Premature senescence involving p53 and p16 is activated in response to constitutive MEK/MAPK mitogenic signaling. *Genes & Development*, 12(19):3008–19.

Lin, W.-C., Lin, F.-T., and Nevins, J. R. (2001). Selective induction of E2F1 in response to DNA damage, mediated by ATM-dependent phosphorylation. *Genes & Development*, 15(14):1833–1844.

Litovchick, L., Sadasivam, S., Florens, L., Zhu, X., Swanson, S. K., Velmurugan, S., Chen, R., Washburn, M. P., Liu, X. S., and DeCaprio, J. A. (2007). Evolutionarily Conserved Multisubunit RBL2/p130 and E2F4 Protein Complex Represses Human Cell Cycle-Dependent Genes in Quiescence. *Molecular Cell*, 26(4):539–551.

Liu, B., Chen, Y., and St. Clair, D. K. (2008). ROS and p53: A versatile partnership. *Free Radical Biology and Medicine*, 44(8):1529–1535.

Liu, D. and Hornsby, P. J. (2007). Senescent human fibroblasts increase the early growth of xenograft tumors via matrix metalloproteinase secretion. *Cancer Research*, 67(7):3117–26.

Liu, Y., Sanoff, H. K., Cho, H., Burd, C. E., Torrice, C., Ibrahim, J. G., Thomas, N. E., and Sharpless, N. E. (2009). Expression of p16(INK4a) in peripheral blood T-cells is a biomarker of human aging. *Aging Cell*, 8(4):439–48.

Lundblad, D., Landberg, G., Roos, G., and Lundgren, E. (1991). Ki-67 as a marker for cell cycle regulation by interferon. *Anticancer Research*, 11(6):2131–6.

Macleod, K. F., Sherry, N., Hannon, G., Beach, D., Tokino, T., Kinzler, K., Vogelstein, B., and Jacks, T. (1995). p53-dependent and independent expression of p21 during cell growth, differentiation, and DNA damage. *Genes & Development*, 9(8):935–944.

Makrides, S. C. (1983). Protein synthesis and degradation during aging and senescence. *Biological reviews of the Cambridge Philosophical Society*, 58(3):343–422.

Marechal, A. and Zou, L. (2013). DNA Damage Sensing by the ATM and ATR Kinases. *Cold Spring Harbor Perspectives in Biology*, 5(9):a012716–a012716.

Martinez-Outschoorn, U. E., Whitaker-Menezes, D., Pavlides, S., Chiavarina, B., Bonuccelli, G., Casey, T., Tsirigos, A., Migneco, G., Witkiewicz, A., Balliet, R., Mercier, I., Wang, C., Flomenberg, N., Howell, A., Lin, Z., Caro, J., Pestell, R. G., Sotgia, F., and Lisanti, M. P. (2010). The autophagic tumor stroma model of cancer or âĂIJbattery-operated tumor growthâĂİ: A simple solution to the autophagy paradox. *Cell Cycle*, 9(21):4297–4306.

Masutomi, K., Possemato, R., Wong, J. M. Y., Currier, J. L., Tothova, Z., Manola, J. B., Ganesan, S., Lansdorp, P. M., Collins, K., and Hahn, W. C. (2005). The telomerase reverse transcriptase regulates chromatin state and DNA damage responses. *Proceedings of the National Academy of Sciences of the United States of America*, 102(23):8222–7.

Matoba, S., Kang, J.-G., Patino, W. D., Wragg, A., Boehm, M., Gavrilova, O., Hurley, P. J., Bunz, F., and Hwang, P. M. (2006). p53 regulates mitochondrial respiration. *Science*, 312(5780):1650–3.

Mauro, C., Leow, S. C., Anso, E., Rocha, S., Thotakura, A. K., Tornatore, L., Moretti, M., De Smaele, E., Beg, A. A., Tergaonkar, V., Chandel, N. S., and Franzoso, G. (2011). NF-κB controls energy homeostasis and metabolic adaptation by upregulating mitochondrial respiration. *Nature Cell Biology*, 13(10):1272–1279.

Mazurek, M. P., Prasad, P. D., Gopal, E., Fraser, S. P., Bolt, L., Rizaner, N., Palmer, C. P., Foster, C. S., Palmieri, F., Ganapathy, V., Stühmer, W., Djamgoz, M. B. A., and Mycielska, M. E. (2010). Molecular origin of plasma membrane citrate transporter in human prostate epithelial cells. *EMBO Reports*, 11(6):431–437.

McAnulty, R. J. (2007). Fibroblasts and myofibroblasts: Their source, function and role in disease. *The International Journal of Biochemistry & Cell Biology*, 39(4):666–671.

McAnulty, R. J., Campa, J. S., Cambrey, A. D., and Laurent, G. J. (1991). The effect of transforming growth factor β on rates of procollagen synthesis and degradation in vitro. *Biochimica et Biophysica Acta (BBA) - Molecular Cell Research*, 1091(2):231–235.

McCool, K. W. and Miyamoto, S. (2012). DNA damage-dependent NF-κB activation: NEMO turns nuclear signaling inside out. *Immunological Reviews*, 246(1):311–26.

McFarland, G. A. and Holliday, R. (1994). Retardation of the senescence of cultured human diploid fibroblasts by carnosine. *Experimental Cell Research*, 212(2):167–75.

Medrano, A., Fernández-Novell, J. M., Ramió, L., Alvarez, J., Goldberg, E., Montserrat Rivera, M., Guinovart, J. J., Rigau, T., and Rodríguez-Gil, J. E. (2006). Utilization of citrate and lactate through a lactate dehydrogenase and ATP-regulated pathway in boar spermatozoa. *Molecular Reproduction and Development*, 73(3):369–78.

Melk, A., Ramassar, V., Helms, L. M., Moore, R., Rayner, D., Solez, K., and Halloran, P. F. (2000). Telomere shortening in kidneys with age. *Journal of the American Society of Nephrology : JASN*, 11(3):444–53.

Menni, C., Kastenmüller, G., Petersen, A. K., Bell, J. T., Psatha, M., Tsai, P.-C., Gieger, C., Schulz, H., Erte, I., John, S., Brosnan, M. J., Wilson, S. G., Tsaprouni, L., Lim, E. M., Stuckey, B., Deloukas, P., Mohney, R., Suhre, K., Spector, T. D., and Valdes, A. M. (2013). Metabolomic markers reveal novel pathways of ageing and early development in human populations. *International Journal of Epidemiology*, 42(4):1111–1119.

Metallo, C. M. and VanderHeiden, M. G. (2013). Understanding Metabolic Regulation and Its Influence on Cell Physiology. *Molecular Cell*, 49(3):388–398.

Michaloglou, C., Vredeveld, L. C. W., Soengas, M. S., Denoyelle, C., Kuilman, T., van der Horst, C. M. A. M., Majoor, D. M., Shay, J. W., Mooi, W. J., and Peeper,

D. S. (2005). BRAFE600-associated senescence-like cell cycle arrest of human naevi. *Nature*, 436(7051):720–724.

Mikawa, T., Maruyama, T., Okamoto, K., Nakagama, H., Lleonart, M. E., Tsusaka, T., Hori, K., Murakami, I., Izumi, T., Takaori-Kondo, A., Yokode, M., Peters, G., Beach, D., and Kondoh, H. (2014). Senescence-inducing stress promotes proteolysis of phosphoglycerate mutase via ubiquitin ligase Mdm2. *The Journal of Cell Biology*, 204(5):729–45.

Moiseeva, O., Bourdeau, V., Roux, A., Deschênes-Simard, X., and Ferbeyre, G. (2009). Mitochondrial dysfunction contributes to oncogene-induced senescence. *Molecular and Cellular Biology*, 29(16):4495–507.

Moyzis, R. K., Buckingham, J. M., Cram, L. S., Dani, M., Deaven, L. L., Jones, M. D., Meyne, J., Ratliff, R. L., and Wu, J. R. (1988). A highly conserved repetitive DNA sequence, (TTAGGG)n, present at the telomeres of human chromosomes. *Proceedings of the National Academy of Sciences of the United States of America*, 85(18):6622–6626.

Muller, A. J., Teresky, A. K., and Levine, A. J. (2000). A male germ cell tumor-susceptibility-determining locus, pgct1, identified on murine chromosome 13. *Proceedings of the National Academy of Sciences of the United States of America*, 97(15):8421–6.

Muñoz-Espín, D., Cañamero, M., Maraver, A., Gómez-López, G., Contreras, J., Murillo-Cuesta, S., Rodríguez-Baeza, A., Varela-Nieto, I., Ruberte, J., Collado, M., and Serrano, M. (2013). Programmed Cell Senescence during Mammalian Embryonic Development. *Cell*, 155(5):1104–1118.

Munro, J., Barr, N. I., Ireland, H., Morrison, V., and Parkinson, E. K. (2004). Histone deacetylase inhibitors induce a senescence-like state in human cells by a p16-

dependent mechanism that is independent of a mitotic clock. *Experimental Cell Research*, 295(2):525–538.

Munro, J., Steeghs, K., Morrison, V., Ireland, H., and Parkinson, E. K. (2001). Human fibroblast replicative senescence can occur in the absence of extensive cell division and short telomeres. *Oncogene*, 20(27):3541–52.

Muraki, K., Han, L., Miller, D., and Murnane, J. P. (2013). The role of ATM in the deficiency in nonhomologous end-joining near telomeres in a human cancer cell line. *PLoS Genetics*, 9(3):e1003386.

Murphy, M. (2009). How mitochondria produce reactive oxygen species. *Biochemical Journal*, 417(1):1.

Mycielska, M. E., Patel, A., Rizaner, N., Mazurek, M. P., Keun, H., Patel, A., Ganapathy, V., and Djamgoz, M. B. A. (2009). Citrate transport and metabolism in mammalian cells. *BioEssays*, 31(1):10–20.

Nahlé, Z., Hsieh, M., Pietka, T., Coburn, C. T., Grimaldi, P. A., Zhang, M. Q., Das, D., and Abumrad, N. A. (2008). CD36-dependent regulation of muscle FoxO1 and PDK4 in the PPAR delta/beta-mediated adaptation to metabolic stress. *The Journal of Biological Chemistry*, 283(21):14317–26.

Nakatsuru, S., Sudo, K., and Nakamura, Y. (1995). Isolation and mapping of a human gene (MCM2) encoding a product homologous to yeast proteins involved in DNA replication. *Cytogenet.Cell Genet.*, 68(3-4):226–230.

Narita, M., Nuñez, S., Heard, E., Narita, M., Lin, A. W., Hearn, S. A., Spector, D. L., Hannon, G. J., and Lowe, S. W. (2003a). Rb-Mediated Heterochromatin Formation and Silencing of E2F Target Genes during Cellular Senescence. *Cell*, 113(6):703–716.

Narita, M., Nuñez, S., Heard, E., Narita, M., Lin, A. W., Hearn, S. A., Spector, D. L., Hannon, G. J., and Lowe, S. W. (2003b). Rb-Mediated Heterochromatin Formation and Silencing of E2F Target Genes during Cellular Senescence. *Cell*, 113(6):703–716.

Newsholme, E. A., Sugden, P. H., and Williams, T. (1977). Effect of citrate on the activities of 6-phosphofructokinase from nervous and muscle tissues from different animals and its relationships to the regulation of glycolysis. *The Biochemical Journal*, 166(1):123–9.

Noda, A., Ning, Y., Venable, S. F., Pereira-Smith, O. M., and Smith, J. R. (1994). Cloning of senescent cell-derived inhibitors of DNA synthesis using an expression screen. *Experimental Cell Research*, 211(1):90–8.

Nowakowski, R. S., Lewin, S. B., and Miller, M. W. (1989). Bromodeoxyuridine immunohistochemical determination of the lengths of the cell cycle and the DNA-synthetic phase for an anatomically defined population. *Journal of Neurocytology*, 18(3):311–8.

Olivier, M., Hollstein, M., and Hainaut, P. (2010). TP53 mutations in human cancers: origins, consequences, and clinical use. *Cold Spring Harbor Perspectives in Biology*, 2(1):a001008.

Olovnikov, A. M. (1971). Principle of marginotomy in template synthesis of polynucleotides. *Doklady Akademii nauk SSSR*, 201(6):1496–9.

O'Neill, P. and Fielden, E. M. (2013). *DNA and Chromatin Damage Caused by Radiation*. Elsevier Science.

Pajor, A. M. (1999). Sodium-coupled transporters for Krebs cycle intermediates. *Annual Review of Physiology*, 61(1):663–682.

Pajor, A. M. (2014). Sodium-coupled dicarboxylate and citrate transporters from the SLC13 family. *Pflügers Archiv - European Journal of Physiology*, 466(1):119–130.

Paradis, V., Youssef, N., Dargère, D., Bâ, N., Bonvoust, F., Deschatrette, J., and Bedossa, P. (2001). Replicative senescence in normal liver, chronic hepatitis C, and hepatocellular carcinomas. *Human Pathology*, 32(3):327–32.

Parkinson, E. K., Fitchett, C., and Cereser, B. (2008). Dissecting the non-canonical functions of telomerase. *Cytogenetic and Genome Research*, 122(3-4):273–80.

Pasmant, E., Laurendeau, I., Héron, D., Vidaud, M., Vidaud, D., and Bièche, I. (2007). Characterization of a germ-line deletion, including the entire INK4/ARF locus, in a melanoma-neural system tumor family: identification of ANRIL, an antisense non-coding RNA whose expression coclusters with ARF. *Cancer research*, 67(8):3963–9.

Passos, J. F., Saretzki, G., Ahmed, S., Nelson, G., Richter, T., Peters, H., Wappler, I., Birket, M. J., Harold, G., Schaeuble, K., Birch-Machin, M. A., Kirkwood, T. B. L., and von Zglinicki, T. (2007). Mitochondrial Dysfunction Accounts for the Stochastic Heterogeneity in Telomere-Dependent Senescence. *PLoS Biology*, 5(5):e110.

Pauling, L., Robinson, A. B., Teranishi, R., and Cary, P. (1971). Quantitative analysis of urine vapor and breath by gas-liquid partition chromatography. *Proceedings of the National Academy of Sciences of the United States of America*, 68(10):2374–6.

Pazolli, E., Alspach, E., Milczarek, A., Prior, J., Piwnica-Worms, D., and Stewart, S. A. (2012). Chromatin Remodeling Underlies the Senescence-Associated Secretory Phenotype of Tumor Stromal Fibroblasts That Supports Cancer Progression. *Cancer Research*, 72(9):2251–2261.

Peng, C. Y., Graves, P. R., Thoma, R. S., Wu, Z., Shaw, A. S., and Piwnica-Worms, H. (1997). Mitotic and G2 checkpoint control: regulation of 14-3-3 protein binding by phosphorylation of Cdc25C on serine-216. *Science*, 277(5331):1501–5.

Pertusa, M., García-Matas, S., Rodríguez-Farré, E., Sanfeliu, C., and Cristòfol, R. (2007). Astrocytes aged in vitro show a decreased neuroprotective capacity. *Journal of Neurochemistry*, 101(3):794–805.

Ping, B., He, X., Xia, W., Lee, D.-F., Wei, Y., Yu, D., Mills, G., Shi, D., and Hung, M.-C. (2006). Cytoplasmic expression of p21CIP1/WAF1 is correlated with

IKKbeta overexpression in human breast cancers. *International Journal of Oncology*, 29(5):1103–10.

Pitiyage, G. N., Lim, K. P., Gemenitzidis, E., Teh, M.-T., Waseem, A., Prime, S. S., Tilakaratne, W. M., Fortune, F., and Parkinson, E. K. (2012). Increased secretion of tissue inhibitors of metalloproteinases 1 and 2 (TIMPs -1 and -2) in fibroblasts are early indicators of oral sub-mucous fibrosis and ageing. *Journal of Oral Pathology & Medicine : Official Publication of the International Association of Oral Pathologists and the American Academy of Oral Pathology*, 41(6):454–62.

Pitiyage, G. N., Slijepcevic, P., Gabrani, A., Chianea, Y. G., Lim, K. P., Prime, S. S., Tilakaratne, W. M., Fortune, F., and Parkinson, E. K. (2011). Senescent mesenchymal cells accumulate in human fibrosis by a telomere-independent mechanism and ameliorate fibrosis through matrix metalloproteinases. *The Journal of Pathology*, 223(5):604–617.

Polyak, K., Xia, Y., Zweier, J. L., Kinzler, K. W., and Vogelstein, B. (1997). A model for p53-induced apoptosis. *Nature*, 389(6648):300–5.

Prieur, A., Besnard, E., Babled, A., and Lemaitre, J.-M. (2011). p53 and p16(INK4A) independent induction of senescence by chromatin-dependent alteration of S-phase progression. *Nature Communications*, 2:473.

Qian, Y. and Chen, X. (2013). Senescence regulation by the p53 protein family. *Methods in Molecular bBology (Clifton, N.J.)*, 965:37–61.

Quijano, C., Cao, L., Fergusson, M. M., Romero, H., Liu, J., Gutkind, S., Rovira, I. I., Mohney, R. P., Karoly, E. D., and Finkel, T. (2012). Oncogene-induced senescence results in marked metabolic and bioenergetic alterations. *Cell Cycle*, 11(7):1383–1392.

Rasband, W. (1997). ImageJ.

Rinehart, C. A. and Torti, V. R. (1997). Aging and cancer: The role of stromal interactions with epithelial cells. *Molecular Carcinogenesis*, 18(4):187–192.

Robles, S. J. and Adami, G. R. (1998). Agents that cause DNA double strand breaks lead to p16INK4a enrichment and the premature senescence of normal fibroblasts. *Oncogene*, 16(9):1113–23.

Rodier, F., Coppé, J.-P., Patil, C. K., Hoeijmakers, W. A. M., Muñoz, D. P., Raza, S. R., Freund, A., Campeau, E., Davalos, A. R., and Campisi, J. (2009). Persistent DNA damage signalling triggers senescence-associated inflammatory cytokine secretion. *Nature Cell Biology*, 11(8):973–979.

Rodier, F., Muñoz, D. P., Teachenor, R., Chu, V., Le, O., Bhaumik, D., Coppé, J.-P., Campeau, E., Beauséjour, C. M., Kim, S.-H., Davalos, A. R., and Campisi, J. (2011). DNA-SCARS: distinct nuclear structures that sustain damage-induced senescence growth arrest and inflammatory cytokine secretion. *Journal of Cell Science*, 124(Pt 1):68–81.

Rosner, M., Schipany, K., and Hengstschläger, M. (2013). Merging high-quality biochemical fractionation with a refined flow cytometry approach to monitor nucleocytoplasmic protein expression throughout the unperturbed mammalian cell cycle. *Nature Protocols*, 8(3):602–26.

Rovillain, E., Mansfield, L., Caetano, C., Alvarez-Fernandez, M., Caballero, O. L., Medema, R. H., Hummerich, H., and Jat, P. S. (2011). Activation of nuclear factor-kappa B signalling promotes cellular senescence. *Oncogene*, 30(20):2356–66.

Sablina, A. A., Budanov, A. V., Ilyinskaya, G. V., Agapova, L. S., Kravchenko, J. E., and Chumakov, P. M. (2005). The antioxidant function of the p53 tumor suppressor. *Nature Medicine*, 11(12):1306–1313.

Sadasivam, S. and DeCaprio, J. A. (2013). The DREAM complex: master coordinator of cell cycle-dependent gene expression. *Nature reviews. Cancer*, 13(8):585–95.

Salama, R., Sadaie, M., Hoare, M., and Narita, M. (2014). Cellular senescence and its effector programs. *Genes & Development*, 28(2):99–114.

Salminen, A. and Kaarniranta, K. (2012). AMP-activated protein kinase (AMPK) controls the aging process via an integrated signaling network. *Ageing Research Reviews*, 11(2):230–41.

Schneider, C. A., Rasband, W. S., and Eliceiri, K. W. (2012). NIH Image to ImageJ: 25 years of image analysis. *Nature Methods*, 9(7):671–675.

Scholzen, T. and Gerdes, J. (2000). The Ki-67 protein: from the known and the unknown. *Journal of Cellular Physiology*, 182(3):311–22.

Schultz, L. B., Chehab, N. H., Malikzay, A., and Halazonetis, T. D. (2000). p53 binding protein 1 (53BP1) is an early participant in the cellular response to DNA double-strand breaks. *The Journal of Cell Biology*, 151(7):1381–90.

Schwarcz, R., Bruno, J. P., Muchowski, P. J., and Wu, H.-Q. (2012). Kynurenines in the mammalian brain: when physiology meets pathology. *Nature Reviews. Neuroscience*, 13(7):465–77.

Schwartzenberg-Bar-Yoseph, F., Armoni, M., and Karnieli, E. (2004). The Tumor Suppressor p53 Down-Regulates Glucose Transporters GLUT1 and GLUT4 Gene Expression. *Cancer Research*, 64(7):2627–2633.

Seltzer, J. L., Lee, A.-Y., Akers, K. T., Sudbreck, B., Southon, E. A., Wayner, E. A., and Eisen, A. Z. (1994). Activation of 72-kDa Type IV Collagenase/Gelatinase by Normal Fibroblasts in Collagen Lattices Is Mediated by Integrin Receptors but Is Not Related to Lattice Contraction. *Experimental Cell Research*, 213(2):365–374.

Serra, V., von Zglinicki, T., Lorenz, M., and Saretzki, G. (2003). Extracellular superoxide dismutase is a major antioxidant in human fibroblasts and slows telomere shortening. *The Journal of Biological Chemistry*, 278(9):6824–30.

Serrano, M., Hannon, G. J., and Beach, D. (1993). A new regulatory motif in cell-cycle control causing specific inhibition of cyclin D/CDK4. *Nature*, 366(6456):704–7.

Serrano, M., Lin, A. W., McCurrach, M. E., Beach, D., and Lowe, S. W. (1997). Oncogenic ras Provokes Premature Cell Senescence Associated with Accumulation of p53 and p16INK4a. *Cell*, 88(5):593–602.

Sheikh, M. S., Rochefort, H., and Garcia, M. (1995). Overexpression of p21WAF1/CIP1 induces growth arrest, giant cell formation and apoptosis in human breast carcinoma cell lines. *Oncogene*, 11(9):1899–905.

Sitte, N., Merker, K., Von Zglinicki, T., Grune, T., and Davies, K. J. (2000). Protein oxidation and degradation during cellular senescence of human BJ fibroblasts: part I–effects of proliferative senescence. *FASEB Journal : Official Publication of the Federation of American Societies for Experimental Biology*, 14(15):2495–502.

Speakman, J. R. and Selman, C. (2011). The free-radical damage theory: Accumulating evidence against a simple link of oxidative stress to ageing and lifespan. *BioEssays*, 33(4):255–259.

Sreekumar, A., Poisson, L. M., Rajendiran, T. M., Khan, A. P., Cao, Q., Yu, J., Laxman, B., Mehra, R., Lonigro, R. J., Li, Y., Nyati, M. K., Ahsan, A., Kalyana-Sundaram, S., Han, B., Cao, X., Byun, J., Omenn, G. S., Ghosh, D., Pennathur, S., Alexander, D. C., Berger, A., Shuster, J. R., Wei, J. T., Varambally, S., Beecher, C., and Chinnaiyan, A. M. (2009). Metabolomic profiles delineate potential role for sarcosine in prostate cancer progression. *Nature*, 457(7231):910–4.

Srere, P. A. (1959). The citrate cleavage enzyme. I. Distribution and purification. *The Journal of Biological Chemistry*, 234:2544–7.

Stein, G. H., Drullinger, L. F., Soulard, A., and Dulić, V. (1999). Differential roles for cyclin-dependent kinase inhibitors p21 and p16 in the mechanisms of senescence and differentiation in human fibroblasts. *Molecular and Cellular Biology*, 19(3):2109–17.

Sterner, J. M., Dew-Knight, S., Musahl, C., Kornbluth, S., and Horowitz, J. M. (1998).

Negative regulation of DNA replication by the retinoblastoma protein is mediated by its association with MCM7. *Molecular and Cellular Biology*, 18(5):2748–57.

Storer, M., Mas, A., Robert-Moreno, A., Pecoraro, M., Ortells, M., DiÂăGiacomo, V., Yosef, R., Pilpel, N., Krizhanovsky, V., Sharpe, J., and Keyes, W. (2013). Senescence Is a Developmental Mechanism that Contributes to Embryonic Growth and Patterning. *Cell*, 155(5):1119–1130.

Stott, F. J., Bates, S., James, M. C., McConnell, B. B., Starborg, M., Brookes, S., Palmero, I., Ryan, K., Hara, E., Vousden, K. H., and Peters, G. (1998). The alternative product from the human CDKN2A locus, p14(ARF), participates in a regulatory feedback loop with p53 and MDM2. *The EMBO Journal*, 17(17):5001–14.

Sugden, M. C. and Holness, M. J. (2003). Recent advances in mechanisms regulating glucose oxidation at the level of the pyruvate dehydrogenase complex by PDKs. *American Journal of Physiology. Endocrinology and Metabolism*, 284(5):E855–62.

Sulli, G., Di Micco, R., and d'Adda di Fagagna, F. (2012). Crosstalk between chromatin state and DNA damage response in cellular senescence and cancer. *Nature Reviews Cancer*, 12(10):709–720.

Suram, A., Kaplunov, J., Patel, P. L., Ruan, H., Cerutti, A., Boccardi, V., Fumagalli, M., Di Micco, R., Mirani, N., Gurung, R. L., Hande, M. P., d'Adda di Fagagna, F., and Herbig, U. (2012). Oncogene-induced telomere dysfunction enforces cellular senescence in human cancer precursor lesions. *The EMBO Journal*, 31(13):2839–51.

Takahashi, S., Seifter, S., and Davidson, A. (1978). Enzymes of the gamma-glutamyl cycle in 'aging' WI-38 fibroblasts and in HeLa S3 cells. *Biochimica et Biophysica Acta*, 522(1):63–73.

Takai, H., Smogorzewska, A., and de Lange, T. (2003). DNA Damage Foci at Dysfunctional Telomeres. *Current Biology*, 13(17):1549–1556.

Takeda, T., Hosokawa, M., and Higuchi, K. (1997). Senescence-Accelerated Mouse (SAM): A novel murine model of senescence. In *Experimental Gerontology*, volume 32, pages 105–109.

Ternette, N., Yang, M., Laroyia, M., Kitagawa, M., O'Flaherty, L., Wolhulter, K., Igarashi, K., Saito, K., Kato, K., Fischer, R., Berquand, A., Kessler, B. M., Lappin, T., Frizzell, N., Soga, T., Adam, J., and Pollard, P. J. (2013). Inhibition of mitochondrial aconitase by succination in fumarate hydratase deficiency. *Cell Reports*, 3(3):689–700.

Thomson, J. (1913). Rays of positive electricity.

Tomás-Loba, A., Bernardes de Jesus, B., Mato, J. M., and Blasco, M. A. (2013). A metabolic signature predicts biological age in mice. *Aging Cell*, 12(1):93–101.

Uchida, K. and Stadtman, E. R. (1992). Modification of histidine residues in proteins by reaction with 4-hydroxynonenal. *Proceedings of the National Academy of Sciences of the United States of America*, 89(10):4544–8.

Vaziri, H. and Benchimol, S. (1998). Reconstitution of telomerase activity in normal human cells leads to elongation of telomeres and extended replicative life span. *Current Biology*, 8(5):279–282.

Velarde, M. C., Flynn, J. M., Day, N. U., Melov, S., and Campisi, J. (2012). Mitochondrial oxidative stress caused by Sod2 deficiency promotes cellular senescence and aging phenotypes in the skin. *Aging*, 4(1):3–12.

von Sonntag, C. (2006). *Free-Radical-Induced DNA Damage and Its Repair: A Chemical Perspective*. Springer Science & Business Media.

Voncken, J. W., Niessen, H., Neufeld, B., Rennefahrt, U., Dahlmans, V., Kubben, N., Holzer, B., Ludwig, S., and Rapp, U. R. (2004). MAPKAP Kinase 3pK Phosphorylates and Regulates Chromatin Association of the Polycomb Group Protein Bmi1. *Journal of Biological Chemistry*, 280(7):5178–5187.

Vousden, K. H. and Ryan, K. M. (2009). p53 and metabolism. *Nature Reviews Cancer*, 9(10):691–700.

Wang, C.-H., Wu, S.-B., Wu, Y.-T., and Wei, Y.-H. (2013). Oxidative stress response elicited by mitochondrial dysfunction: implication in the pathophysiology of aging. *Experimental biology and medicine (Maywood, N.J.)*, 238(5):450–60.

Wang, J., Geiger, H., and Rudolph, K. (2011a). Immunoaging induced by hematopoietic stem cell aging. *Current Opinion in Immunology*, 23(4):532–6.

Wang, W., Chen, J. X., Liao, R., Deng, Q., Zhou, J. J., Huang, S., and Sun, P. (2002). Sequential activation of the MEK-extracellular signal-regulated kinase and MKK3/6-p38 mitogen-activated protein kinase pathways mediates oncogenic ras-induced premature senescence. *Molecular and Cellular Biology*, 22(10):3389–403.

Wang, W., Yang, X., Cristofalo, V. J., Holbrook, N. J., and Gorospe, M. (2001). Loss of HuR Is Linked to Reduced Expression of Proliferative Genes during Replicative Senescence. *Molecular and Cellular Biology*, 21(17):5889–5898.

Wang, W., Yang, X., López de Silanes, I., Carling, D., and Gorospe, M. (2003). Increased AMP:ATP ratio and AMP-activated protein kinase activity during cellular senescence linked to reduced HuR function. *The Journal of Biological Chemistry*, 278(29):27016–23.

Wang, Z., Klipfell, E., Bennett, B. J., Koeth, R., Levison, B. S., Dugar, B., Feldstein, A. E., Britt, E. B., Fu, X., Chung, Y.-M., Wu, Y., Schauer, P., Smith, J. D., Allayee, H., Tang, W. H. W., DiDonato, J. A., Lusis, A. J., and Hazen, S. L. (2011b). Gut flora metabolism of phosphatidylcholine promotes cardiovascular disease. *Nature*, 472(7341):57–63.

Warburg, O., Posener, K., and Negelein, E. (1924). Uber den Stoffwechsel der Tumoren (On metabolism of tumors). *Biochem Z*, 152:319–344.

Webley, K., Bond, J. A., Jones, C. J., Blaydes, J. P., Craig, A., Hupp, T., and Wynford-Thomas, D. (2000). Posttranslational Modifications of p53 in Replicative Senescence Overlapping but Distinct from Those Induced by DNA Damage. *Molecular and Cellular Biology*, 20(8):2803–2808.

Wei S.; Sedivy, J. M., S. W. (1999). Expression of catalytically active telomerase does not prevent premature senescence caused by overexpression of oncogenic Ha-Ras in normal human fibroblasts. *Cancer Research*, 59(7):1539–1543.

Whitaker-Menezes, D., Martinez-Outschoorn, U. E., Lin, Z., Ertel, A., Flomenberg, N., Witkiewicz, A. K., Birbe, R. C., Howell, A., Pavlides, S., Gandara, R., Pestell, R. G., Sotgia, F., Philp, N. J., and Lisanti, M. P. (2011). Evidence for a stromal-epithelial âĂIJlactate shuttleâĂİ in human tumors: MCT4 is a marker of oxidative stress in cancer-associated fibroblasts. *Cell Cycle*, 10(11):1772–1783.

Wieser, R. J., Renauer, D., Schäfer, A., Heck, R., Engel, R., Schütz, S., and Oesch, F. (1990). Growth control in mammalian cells by cell-cell contacts. *Environmental Health Perspectives*, 88:251–3.

Wiley, C. D., Velarde, M. C., Lecot, P., Liu, S., Sarnoski, E. A., Freund, A., Shirakawa, K., Lim, H. W., Davis, S. S., Ramanathan, A., Gerencser, A. A., Verdin, E., and Campisi, J. (2016). Mitochondrial Dysfunction Induces Senescence with a Distinct Secretory Phenotype. *Cell Metabolism*, 23(2):303–14.

Williams, G. C. (1957). Pleiotropy, Natural Selection, and the Evolution of Senescence. *Evolution*, 11(4):398.

Winkler, B. S., DeSantis, N., and Solomon, F. (1986). Multiple NADPH-producing pathways control glutathione (GSH) content in retina. *Experimental Eye Research*, 43(5):829–47.

Wishart, D. S., Jewison, T., Guo, A. C., Wilson, M., Knox, C., Liu, Y., Djoumbou, Y., Mandal, R., Aziat, F., Dong, E., Bouatra, S., Sinelnikov, I., Arndt, D., Xia, J.,

Liu, P., Yallou, F., Bjorndahl, T., Perez-Pineiro, R., Eisner, R., Allen, F., Neveu, V., Greiner, R., and Scalbert, A. (2013). HMDB 3.0–The Human Metabolome Database in 2013. *Nucleic Acids Research*, 41(Database issue):D801–7.

Wolffram, S., Unternährer, R., Grenacher, B., and Scharrer, E. (1994). Transport of citrate across the brush border and basolateral membrane of rat small intestine. *Comparative Biochemistry and Physiology. Physiology*, 109(1):39–52.

Wu, C., Maiti, B., Saavedra, H. I., Sang, L., Chong, G. T., Nuckolls, F., Giangrande, P., Wright, F. A., Field, S. J., Greenberg, M. E., Orkin, S., Nevins, J. R., Robinson, M. L., Leone, G., and Lizhao, T. (2001). The E2F1-3 transcription factors are essential for cellular proliferation. *Nature*, 414(6862):457–462.

Wu, P., Blair, P. V., Sato, J., Jaskiewicz, J., Popov, K. M., and Harris, R. A. (2000). Starvation increases the amount of pyruvate dehydrogenase kinase in several mammalian tissues. *Archives of Biochemistry and Biophysics*, 381(1):1–7.

Xu, Y., Li, N., Xiang, R., and Sun, P. (2014). Emerging roles of the p38 MAPK and PI3K/AKT/mTOR pathways in oncogene-induced senescence. *Trends in Biochemical Sciences*, 39(6):268–76.

Yamakuchi, M., Ferlito, M., and Lowenstein, C. J. (2008). miR-34a repression of SIRT1 regulates apoptosis. *Proceedings of the National Academy of Sciences of the United States of America*, 105(36):13421–6.

Yan, L.-J., Levine, R. L., and Sohal, R. S. (1997). Oxidative damage during aging targets mitochondrial aconitase. *Proceedings of the National Academy of Sciences of the United States of America*, 94(21):11168–11172.

Yang, G., Rosen, D. G., Zhang, Z., Bast, R. C., Mills, G. B., Colacino, J. A., Mercado-Uribe, I., and Liu, J. (2006). The chemokine growth-regulated oncogene 1 (Gro-1) links RAS signaling to the senescence of stromal fibroblasts and ovarian tumorigenesis.

Proceedings of the National Academy of Sciences of the United States of America, 103(44):16472–7.

Yang, N.-C. and Hu, M.-L. (2005). The limitations and validities of senescence associated-beta-galactosidase activity as an aging marker for human foreskin fibroblast Hs68 cells. *Experimental Gerontology*, 40(10):813–9.

Yap, K. L., Li, S., Muñoz-Cabello, A. M., Raguz, S., Zeng, L., Mujtaba, S., Gil, J., Walsh, M. J., and Zhou, M.-M. (2010). Molecular interplay of the noncoding RNA ANRIL and methylated histone H3 lysine 27 by polycomb CBX7 in transcriptional silencing of INK4a. *Molecular cell*, 38(5):662–74.

Young, A. R. J. and Narita, M. (2009). SASP reflects senescence. *EMBO Reports*, 10(3):228–230.

Zhang, H. S., Gavin, M., Dahiya, A., Postigo, A. A., Ma, D., Luo, R. X., Harbour, J. W., and Dean, D. C. (2000). Exit from G1 and S Phase of the Cell Cycle Is Regulated by Repressor Complexes Containing HDAC-Rb-hSWI/SNF and Rb-hSWI/SNF. *Cell*, 101(1):79–89.

Zhang, R., Poustovoitov, M. V., Ye, X., Santos, H. A., Chen, W., Daganzo, S. M., Erzberger, J. P., Serebriiskii, I. G., Canutescu, A. A., and Dunbrack, R. L. (2005). Formation of MacroH2A-Containing Senescence-Associated Heterochromatin Foci and Senescence Driven by ASF1a and HIRA. *Developmental Cell*, 8(1):19–30.

Zhu, J., Woods, D., McMahon, M., and Bishop, J. M. (1998). Senescence of human fibroblasts induced by oncogenic Raf. *Genes & Development*, 12(19):2997–3007.

Zwerschke, W., Stöckl, P., Hütter, E., Eigenbrodt, E., Jansen-Dürr, P., and Mazurek, S. (2003). Metabolic analysis of senescent human fibroblasts reveals a role for AMP in cellular senescence. *Biochemical Journal*.

Appendix A

Appendix: Table of genes present on qPCR array for glucose metabolism

Gene	IrrDSBsen/growing fold up/down regulation		PEsen/growing fold up/down regulation		Alternative name: Function
	IMR90	NHOF1	IMR90	NHOF1	
ACLY	1.43	1.59	-1.51	-1.03	**ATP citrate lyase**: primary enzyme responsible for catalysing the conversion of citrate and CoA-Acetyl to CoA and oxaloacetate producing ADP and phosphate from ATP.
ACO1	-1.11	-1.23	1.13	1.11	**Aconitase 1, soluble**: Binds a 4Fe-4S cluster and functions as aconitase when cellular iron levels are high. Functions as mRNA binding protein that regulates uptake, sequestration and utilization of iron when cellular iron levels are low. Binds to iron-responsive elements (IRES) in target mRNA species when iron levels are low. Catalyses the isomerization of citrate to isocitrate via cis-aconitate
ACO2	1.20	2.24	-1.03	1.05	**Aconitate hydratase, mitochondrial**: catalyses the interconversion of citrate to isocitrate via cis-aconitate in the second step of the TCA cycle. It was found to be one of the mitochondrial matrix proteins that are preferentially degraded by the serine protease 15(PRSS15), also known as Lon protease, after oxidative modification.
AGL	1.50	1.34	1.61	1.14	**Amylo-alpha-1, 6-glucosidase, 4-alpha-glucanotransferase**: the glycogen debrancher enzyme which is involved in glycogen degradation. This enzyme has two independent catalytic activities which occur at different sites on the protein: a 4-alpha-glucotransferase activity and a amylo-1,6-glucosidase activity
ALDOA	2.27	2.19	-1.20	1.18	**Aldolase A, fructose-bisphosphate**: glycolytic enzyme that catalyses the reversible conversion of fructose-1,6-bisphosphate to glyceraldehyde 3-phosphate and dihydroxyacetone phosphate.
ALDOB	1.98	7.07	-1.36	1.79	**Aldolase B, fructose-bisphosphate**: glycolytic enzyme that catalyses the reversible conversion of fructose-1,6-bisphosphate to glyceraldehyde 3-phosphate and dihydroxyacetone phosphate
ALDOC	1.78	1.19	1.65	-1.38	**Aldolase C, fructose-bisphosphate**: Expressed specifically in the hippocampus and Purkinje cells of the brain, the encoded protein is a glycolytic enzyme that catalyses the reversible aldol cleavage of fructose-1,6-biphosphate and fructose 1-phosphate to dihydroxyacetone phosphate and either glyceraldehyde-3-phosphate or glyceraldehyde, respectively.
BPGM	3.71	1.33	2.23	1.86	**2,3-bisphosphoglycerate mutase**: a multifunctional enzyme that catalyses 2,3-DPG synthesis via its

Gene	IrrDSBsen/growing fold up/down regulation		PEsen/growing fold up/down regulation		Alternative name: Function
	IMR90	NHOF1	IMR90	NHOF1	
					synthetase activity, and 2,3-DPG degradation via its phosphatase activity. The enzyme also has phosphoglycerate phosphomutase activity. Deficiency of this enzyme increases the affinity of cells for oxygen.
CS	-1.62	1.04	-1.29	1.12	**Citrate synthase, mitochondrial**: a Krebs tricarboxylic acid cycle enzyme that catalyses the synthesis of citrate from oxaloacetate and acetyl coenzyme A. The enzyme is found in nearly all cells capable of oxidative metabolism.
DLAT	1.14	1.39	-1.18	1.03	**Dihydrolipoamide S-acetyltransferase**: component E2 of the multi-enzyme pyruvate dehydrogenase complex (PDC). PDC resides in the inner mitochondrial membrane and catalyses the conversion of pyruvate to acetyl coenzyme A. The protein product of this gene, dihydrolipoamide acetyltransferase, accepts acetyl groups formed by the oxidative decarboxylation of pyruvate and transfers them to coenzyme A. Mutations in this gene are also a cause of pyruvate dehydrogenase E2 deficiency which causes primary lactic acidosis in infancy and early childhood.
DLD	1.43	-1.10	1.15	1.35	**Dihydrolipoamide dehydrogenase**: the L protein of the mitochondrial glycine cleavage system. The L protein, also named dihydrolipoamide dehydrogenase, is also a component of the pyruvate dehydrogenase complex, the alpha-ketoglutarate dehydrogenase complex, and the branched-chain alpha-keto acid dehydrogenase complex.
DLST	1.59	1.63	1.14	1.12	**Dihydrolipoyllysine-residue succinyltransferase component of 2-oxoglutaratedehydrogenase complex, mitochondrial**: a mitochondrial protein that belongs to the 2-oxoacid dehydrogenase family. This protein is one of the three components (the E2 component) of the 2-oxoglutarate dehydrogenase complex that catalyses the overall conversion of 2-oxoglutarate to succinyl-CoA and CO_2
ENO1	1.17	1.30	-1.42	-1.14	**Enolase 1, (alpha)**: one of three enolase isoenzymes found in mammals. Each isoenzyme is a homodimer composed of 2 alpha, 2 gamma, or 2 beta subunits, and functions as a glycolytic enzyme. Alpha-enolase in addition, functions as a structural lens protein (tau-crystallin) in the monomeric form.

Gene	IrrDSBsen/growing fold up/down regulation		PEsen/growing fold up/down regulation		Alternative name: Function
	IMR90	NHOF1	IMR90	NHOF1	
					Plays a part in various processes such as growth control, hypoxia tolerance and allergic responses. May also function in the intravascular and pericellular fibrinolytic system due to its ability to serve as a receptor and activator of plasminogen on the cell surface of several cell-types such as leukocytes and neurons. Stimulates immunoglobulin production. Binds to the myc promoter and acts as a transcriptional repressor.
ENO2	4.12	2.28	-1.26	-1.24	**Enolase 2 (gamma, neuronal)**: Has neurotrophic and neuroprotective properties on a broad spectrum of central nervous system (CNS) neurons.
ENO3	1.50	3.34	1.22	-1.19	**Enolase 3 (beta, muscle)**: proposed role in glycolysis, gluconeogenesis and RNA degradation pathways as well as aging and skeletal muscle tissue regeneration processes. Expected to have lyase activity, magnesium ion binding, phosphopyruvate hydratase activity, hetero and homo-dimerisation activity.
FBP1	1.98	3.08	3.01	2.03	**Fructose-1,6-bisphosphatase**: gluconeogenesis regulatory enzyme, catalyses the hydrolysis of fructose1,6-bisphosphate to fructose 6-phosphate and inorganic phosphate. Fructose-1,6-diphosphatase deficiency is associated with hypoglycemia and metabolic acidosis.
FBP2	1.98	2.99	-1.36	4.75	**Fructose-1,6-bisphosphatase 2**: catalyses the hydrolysis of fructose 1,6-bisphosphate to fructose 6-phosphate and inorganic phosphate.
FH	-2.46	1.02	1.03	1.30	**Fumarate hydratase**: component of the tricarboxylic acid (TCA) cycle, catalyses the formation of L-malate from fumarate. It exists in both a cytosolic form and an N-terminal extended form, differing only in the translation start site used. The N-terminal extended form is targeted to the mitochondrion, where the removal of the extension generates the same form as in the cytoplasm.
G6PC	3.98	3.10	-2.43	1.73	**Glucose-6-phosphatase:** integral membrane protein of the endoplasmic reticulum that catalyses the hydrolysis of D-glucose 6-phosphate to D-glucose and orthophosphate. It is a key enzyme in glucose homeostasis, functioning in gluconeogenesis and glycogenolysis
G6PC3	2.00	1.78	1.09	1.40	**Glucose-6-phosphatase 3:** catalytic subunit of glucose 6-phosphatase (G6Pase). G6Pase is

Gene	IrrDSBsen/growing fold up/down regulation		PEsen/growing fold up/down regulation		Alternative name: Function
	IMR90	NHOF1	IMR90	NHOF1	
					located in the endoplasmic reticulum and catalyses the hydrolysis of glucose 6-phosphate to glucose and phosphate in the last step of the gluconeogenic and glycogenolytic pathways
G6PD	-2.26	-1.78	-1.51	1.66	**Glucose-6-phosphate dehydrogenase**: a cytosolic enzyme encoded by a housekeeping X-linked gene whose main function is to produce NADPH, a key electron donor in the defence against oxidizing agents and in reductive biosynthetic reactions.
GALM	1.86	1.81	1.49	2.04	**Galactose mutarotase (aldose 1-epimerase):** catalyses the epimerisation of hexose sugars such as glucose and galactose. The encoded protein is expressed in the cytoplasm and has a preference for galactose. The encoded protein may be required for normal galactose metabolism by maintaining the equilibrium of alpha and beta anomers of galactose. Mutarotase converts alpha-aldose to the beta-anomer. It is active on D-glucose, L-arabinose, D-xylose, D-galactose, maltose and lactose.
GBE1	3.14	1.91	1.41	1.81	**Glucan (1,4-alpha-) branching enzyme 1**: glycogen branching enzyme that catalyses the transfer of alpha-1,4-linked glucosyl units from the outer end of a glycogen chain to an alpha-1,6 position on the same or a neighbouring glycogen chain. Branching of the chains is essential to increase the solubility of the glycogen molecule and reducing the osmotic pressure within cells.
GCK	3.21	5.82	-1.36	4.99	**Glucokinase (hexokinase 4):** phosphorylates glucose to produce glucose-6-phosphate, the first step in glycolysis. Alternative splicing of this gene results in three tissue-specific forms of glucokinase, one found in pancreatic islet beta cells and two found in liver. Localised to the outer membrane of mitochondria, unlike other forms of hexokinase, this enzyme is not inhibited by its product glucose-6-phosphate but remains active while glucose is abundant.
GPI	1.34	2.85	-1.40	1.19	**Glucose-6-phosphate isomerase**: Catalyses the reversible isomerisation of glucose-6-phosphate and fructose-6-phosphate in glycolysis and gluconeogenesis. Localised to the cytoplasm.
GSK3A	1.29	1.38	-1.13	1.33	**Glycogen synthase kinase 3 alpha**: Constitutively active protein kinase that acts as a negative regulator in the hormonal control of glucose

Gene	IrrDSBsen/growing fold up/down regulation		PEsen/growing fold up/down regulation		Alternative name: Function
	IMR90	NHOF1	IMR90	NHOF1	
					homeostasis, Wnt signalling and regulation of transcription factors and microtubules, by phosphorylating and inactivating glycogen synthase (GYS1 or GYS2), CTNNB1/beta-catenin, APC and AXIN1. Requires primed phosphorylation of the majority of its substrates. Contributes to insulin regulation of glycogen synthesis by phosphorylating and inhibiting GYS1 activity and hence glycogen synthesis. Regulates glycogen metabolism in liver, but not in muscle. May also mediate the development of insulin resistance by regulating activation of transcription factors. In Wnt signalling, regulates the level and transcriptional activity of nuclear CTNNB1/beta-catenin. Facilitates amyloid precursor protein (APP) processing and the generation of APP-derived amyloid plaques found in Alzheimer disease. May be involved in the regulation of replication in pancreatic beta-cells.
GSK3B	1.77	2.50	1.75	1.31	**Glycogen synthase kinase 3 beta**: Similar to GSK3A however this isoform is more abundant in the brain where it is involved in synaptic plasticity, possibly via regulation of NMDA receptor trafficking.
GYS1	3.08	2.81	-1.09	1.42	**Glycogen synthase 1**: catalyses the addition of glucose monomers to the growing glycogen molecule through the formation of alpha-1,4-glycoside linkages. Transfers the glycosyl residue from UDP-Glc to the non-reducing end of alpha-1,4-glucan.
GYS2	2.57	5.74	1.21	1.90	**Glycogen synthase 2**: liver glycogen synthase, catalyses the rate-limiting step in the synthesis of glycogen - the transfer of a glucose molecule from UDP-glucose to a terminal branch of the glycogen molecule.
H6PD	1.52	-1.01	1.27	1.55	**Hexose-6-phosphate dehydrogenase (glucose 1-dehydrogenase)**: There are 2 forms of glucose-6-phosphate dehydrogenase. G form is X-linked and H form, encoded by this gene, is autosomally linked. The H form shows activity with other hexose-6-phosphates, especially galactose-6-phosphate, whereas the G form is specific for glucose-6-phosphate. Both forms are present in most tissues, but H form is not found in red cells.
HK2	4.01	6.03	-1.02	1.06	**Hexokinase 2**: the predominant form of glucose phosphorylating enzyme found in skeletal muscle.

Gene	IrrDSBsen/growing fold up/down regulation		PEsen/growing fold up/down regulation		Alternative name: Function
	IMR90	NHOF1	IMR90	NHOF1	
					It localizes to the outer membrane of mitochondria. Expression of this gene is insulin-responsive, and is probably involved in the increased rate of glycolysis seen in rapidly growing cancer cells. Activation of mitochondrial hexokinases is regulated by Akt/PKB-mediated phosphorylation and they are subject to inhibition by their end product, glucose-6-phosphate. In addition to glucose metabolism, mitochondrial hexokinases have been implicated in anti-apoptotic and cell survival signalling.
HK3	1.98	**8.01**	**-1.11**	1.79	**Hexokinase 3 (white cell)**: Similar to hexokinases 1 and 2, this enzyme is inhibited by its product glucose-6-phosphate
IDH1	1.06	1.29	-1.00	1.40	**Isocitrate dehydrogenase 1 (NADP+), soluble**: catalyses the oxidative decarboxylation of isocitrate to 2-oxoglutarate. IDH enzymes belong to two distinct subclasses, one of which utilises NAD(+) as the electron acceptor and the other NADP(+). Five IDH have been reported: three NAD(+)-dependent, which localize to the mitochondrial matrix, and two NADP(+)-dependent, one of which is mitochondrial and the other predominantly cytosolic. Each NADP(+)-dependent isozyme is a homodimer. The protein encoded by this gene is the NADP(+)-dependent IDH found in the cytoplasm and peroxisomes. It contains the PTS-1 peroxisomal targeting signal sequence. The presence of this enzyme in peroxisomes suggests roles in the regeneration of NADPH for intraperoxisomal reductions, such as the conversion of 2, 4-dienoyl-CoAs to 3-enoyl-CoAs, as well as in peroxisomal reactions that consume 2-oxoglutarate, namely the alpha-hydroxylation of phytanic acid. The cytoplasmic enzyme serves a significant role in cytoplasmic NADPH production.
IDH2	1.02	-1.60	1.31	2.01	**Isocitrate dehydrogenase 2:** NADP(+)-dependent isocitrate dehydrogenase found in the mitochondria. It plays a role in intermediary metabolism and energy production. This protein may tightly associate or interact with the pyruvate dehydrogenase complex.
IDH3A	1.02	1.81	-1.01	1.10	**Isocitrate dehydrogenase 3 (NAD+) alpha**: NAD(+)-dependent isocitrate

Gene	IrrDSBsen/growing fold up/down regulation		PEsen/growing fold up/down regulation		Alternative name: Function
	IMR90	NHOF1	IMR90	NHOF1	
					dehydrogenases catalyses the allosterically regulated rate-limiting step of the tricarboxylic acid cycle. Each isozyme is a heterotetramer that is composed of two alpha subunits, one beta subunit, and one gamma subunit. The protein encoded by this gene is the alpha subunit of one isozyme of NAD(+)-dependent IDH.
IDH3B	-1.03	1.25	1.06	1.31	**Isocitrate dehydrogenase 3 (NAD+) beta**: the beta subunit of one isozyme of NAD(+)-dependent IDH.
IDH3G	1.40	1.17	1.21	1.03	**Isocitrate dehydrogenase 3 (NAD+) gamma**: the gamma subunit of one isozyme of NAD(+)-dependent isocitrate dehydrogenase.
MDH1	1.08	-1.04	1.13	1.44	**Malate dehydrogenase 1, NAD (soluble)**: catalyses the reversible oxidation of malate to oxaloacetate, utilizing the NAD/NADH cofactor system in the TCA cycle. Localises to the cytoplasm and may play pivotal roles in the malate-aspartate shuttle that operates in the metabolic coordination between cytosol and mitochondria.
MDH1B	3.16	1.96	2.46	4.65	**Malate dehydrogenase 1B, NAD (soluble)**: Putative malate dehydrogenase.
MDH2	1.29	1.35	-1.30	1.20	**Malate dehydrogenase 2, NAD (mitochondrial)**: catalyses the reversible oxidation of malate to oxaloacetate, utilizing the NAD/NADH cofactor system in the TCA cycle. The protein encoded by this gene is localized to the mitochondria and may play pivotal roles in the malate-aspartate shuttle that operates in the metabolic coordination between cytosol and mitochondria.
OGDH	1.50	1.45	1.47	1.57	**Oxoglutarate (alpha-ketoglutarate) dehydrogenase (lipoamide):** one subunit of the 2-oxoglutarate dehydrogenase complex. This complex catalyses the overall conversion of 2-oxoglutarate (alpha-ketoglutarate) to succinyl-CoA and CO_2 during the Krebs cycle. Localised to the mitochondrial matrix and uses thiamine pyrophosphate as a cofactor.
PC	2.38	2.33	1.59	1.31	**Pyruvate carboxylase**: requires biotin and ATP to catalyse the carboxylation of pyruvate to oxaloacetate. The active enzyme is a homotetramer arranged in a tetrahedron which is located exclusively in the mitochondrial matrix. Involved in gluconeogenesis, lipogenesis, insulin secretion and synthesis of the neurotransmitter glutamate.

Gene	IrrDSBsen/growing fold up/down regulation		PEsen/growing fold up/down regulation		Alternative name: Function
	IMR90	NHOF1	IMR90	NHOF1	
PCK1	1.98	2.99	-1.36	1.79	**Phosphoenolpyruvate carboxykinase 1 (soluble):** a main control point for the regulation of gluconeogenesis. The cytosolic enzyme encoded by this gene, along with GTP, catalyses the formation of phosphoenolpyruvate from oxaloacetate, with the release of carbon dioxide and GDP. The expression of this gene can be regulated by insulin, glucocorticoids, glucagon and cAMP.
PCK2	-1.08	-4.46	2.87	-2.50	**Phosphoenolpyruvate carboxykinase 2 (mitochondrial)**: a mitochondrial enzyme that catalyses the conversion of oxaloacetate to phosphoenolpyruvate in the presence of GTP. Constitutively expressed and not modulated by hormones such as glucagon and insulin that regulate the cytosolic form.
PDHA 1	-1.01	1.48	-1.05	1.01	**Pyruvate dehydrogenase (lipoamide) alpha 1**: The pyruvate dehydrogenase (PDH) complex is a nuclear-encoded mitochondrial multienzyme complex that catalyses the overall conversion of pyruvate to acetyl-CoA and CO(2), and provides the primary link between glycolysis and the tricarboxylic acid (TCA) cycle. The PDH complex is composed of multiple copies of three enzymatic components: pyruvate dehydrogenase (E1), dihydrolipoamide acetyltransferase (E2) and lipoamide dehydrogenase (E3). The E1 enzyme is a heterotetramer of two alpha and two beta subunits. This gene encodes the E1 alpha 1 subunit containing the E1 active site, and plays a key role in the function of the PDH complex.
PDHB	1.02	-1.27	1.03	1.09	**Pyruvate dehydrogenase (lipoamide) beta**: the E1 beta subunit. Mutations in this gene are associated with pyruvate dehydrogenase E1-beta deficiency.
PDK1	2.24	2.89	-1.21	1.11	**Pyruvate dehydrogenase kinase, isozyme 1**: one of the three pyruvate dehydrogenase kinases that inhibits the PDH complex by phosphorylation of the E1 alpha subunit.
PDK2	4.57	1.64	2.20	1.35	**Pyruvate dehydrogenase kinase, isozyme 2**: one of the three pyruvate dehydrogenase kinases that inhibits the PDH complex by phosphorylation of the E1 alpha subunit.
PDK3	1.48	4.09	2.62	2.33	**Pyruvate dehydrogenase kinase, isozyme 3**: one of the three pyruvate dehydrogenase kinases that inhibits the PDH complex by phosphorylation of the E1 alpha subunit.

Gene	IrrDSBsen/growing fold up/down regulation		PEsen/growing fold up/down regulation		Alternative name: Function
	IMR90	NHOF1	IMR90	NHOF1	
PDK4	122.11	15.80	10.56	2.46	**Pyruvate dehydrogenase kinase, isozyme 4**: a member of the PDK/BCKDK protein kinase family and encodes a mitochondrial protein with a histidine kinase domain. This protein is located in the matrix of the mitochondria and inhibits the pyruvate dehydrogenase complex by phosphorylating one of its subunits. Expression of this gene is regulated by glucocorticoids, retinoic acid and insulin.
PDP2	-1.16	1.50	1.40	-1.05	**Pyruvate dehydrogenase phosphatase catalytic subunit 2**: Catalyses the de-phosphorylation and concomitant reactivation of the alpha subunit of the E1 component of the pyruvate dehydrogenase complex (By similarity)
PDPR	2.54	-1.57	4.03	1.40	**Pyruvate dehydrogenase phosphatase regulatory subunit**: Decreases the sensitivity of PDP1 to magnesium ions, and this inhibition is reversed by the polyamine spermine (By similarity)
PFKL	1.87	1.83	1.13	1.03	**Phosphofructokinase, liver**: tetrameric enzyme that catalyses the conversion of D-fructose 6-phosphate to D-fructose 1,6-bisphosphate. Separate genes encode a muscle subunit (M) and a liver subunit (L). PFK from muscle is a homotetramer of M subunits; PFK from liver is a homotetramer of L-subunits, while PFK from platelets can be composed of any tetrameric combination of M and L subunits. The protein encoded by this gene represents the L subunit
PGAM 2	6.07	6.42	1.52	2.39	**Phosphoglycerate mutase 2**: catalyses the reversible reaction of 3-phosphoglycerate (3-PGA) to 2-phosphoglycerate (2-PGA) in the glycolytic pathway. PGAM is a dimeric enzyme containing, in different tissues, different proportions of a slow-migrating muscle (MM) isozyme, a fast-migrating brain (BB) isozyme, and a hybrid form (MB). This gene encodes muscle-specific PGAM subunit.
PGK1	2.79	1.40	1.26	-1.10	**Phosphoglycerate kinase 1**: is a glycolytic enzyme that catalyses the conversion of 1,3-diphosphoglycerate to 3-phosphoglycerate. The encoded protein may also act as a cofactor for polymerase alpha.
PGK2	1.83	-1.62	2.62	2.34	**Phosphoglycerate kinase 2**: encoded by an autosomal gene, is unique to meiotic and post-meiotic spermatogenic cells
PGLS	1.31	-1.01	1.47	-777.12	**6-phosphogluconolactonase**: catalyses the

Gene	IrrDSBsen/growing fold up/down regulation		PEsen/growing fold up/down regulation		Alternative name: Function
	IMR90	NHOF1	IMR90	NHOF1	
					hydrolysis of 6-phosphogluconolactone to 6-phosphogluconate
PGM1	2.70	1.10	1.87	-1.01	**Phosphoglucomutase 1**: isozyme of phosphoglucomutase (PGM) and belongs to the phosphohexose mutase family. There are several PGM isozymes, which are encoded by different genes and catalyse the transfer of phosphate between the 1 and 6 positions of glucose. In most cell types, this PGM isozyme is predominant, representing about 90% of total PGM activity
PGM2	-1.39	1.17	1.38	1.20	**Phosphoglucomutase 2**: Catalyses the conversion of the nucleoside breakdown products ribose-1-phosphate and deoxyribose-1-phosphate to the corresponding 5-phosphopentoses. May also catalyse the interconversion of glucose-1-phosphate and glucose-6-phosphate. Has low glucose 1,6-bisphosphate synthase activity
PGM3	1.82	1.37	-1.17	1.12	**Phosphoglucomutase 3**: mediates both glycogen formation and utilisation by catalysing the interconversion of glucose-1-phosphate and glucose-6-phosphate.
PHKA 1	1.87	4.06	1.64	5.20	**Phosphorylase kinase, alpha 1 (muscle):** alpha 1 subunit of phosphorylase kinase, an enzymes that catalyses the phosphorylation of serine in various substrates including troponin I. The alpha chain may bind calmodulin.
PHKB	1.51	-1.08	1.30	1.15	**Phosphorylase b kinase:** beta chain of phosphorylase kinase. The beta chain acts as a regulatory unit and modulates the activity of the holoenzyme in response to phosphorylation
PHKG 1	-1.05	13.38	3.86	4.95	**Phosphorylase kinase, gamma 1 (muscle)**: a protein with one protein kinase domain and two calmodulin-binding domains. This protein is the catalytic member of a 16 subunit protein kinase complex which contains equimolar ratios of 4 subunit types. The complex is a crucial glycogenolytic regulatory enzyme.
PHKG 2	1.38	3.14	-1.25	1.17	**Phosphorylase kinase subunit gamma-2**: Catalytic subunit of the phosphorylase b kinase (PHK), which mediates the neural and hormonal regulation of glycogen breakdown (glycogenolysis) by phosphorylating and thereby activating glycogen phosphorylase (PYGB, PYGL or PYGM). May regulate glycogeneolysis in the testis. In vitro, phosphorylates TNNI3, TNNT2, MAPT/TAU, GAP43

Gene	IrrDSBsen/growing fold up/down regulation		PEsen/growing fold up/down regulation		Alternative name: Function
	IMR90	NHOF1	IMR90	NHOF1	
					and NRGN/RC3
PKLR	1.98	3.16	-1.36	1.79	**Pyruvate kinase**: catalyses the transphosphorylation of phohsphoenolpyruvate into pyruvate and ATP, which is the rate-limiting step of glycolysis
PRPS1	1.70	1.77	-2.45	1.62	**Phosphoribosyl pyrophosphate synthetase 1**: catalyses the phospho-ribosylation of ribose 5-phosphate to 5-phosphoribosyl-1 pyrophosphate, which is necessary for purine metabolism and nucleotide biosynthesis
PRPS1 L1	1.24	3.21	-1.71	2.16	**Phosphoribosyl pyrophosphate synthetase 1-like 1**: highly homologous to the two subunits of phosphoribosylpyrophosphate synthetase encoded by human X-linked genes, PRPS1 and PRPS2. These enzymes convert pyrimidine, purine or pyridine bases to the corresponding ribonucleoside monophosphates.
PRPS2	-1.80	1.93	1.13	1.26	**Phosphoribosyl pyrophosphate synthetase 2**: plays a central role in the synthesis of purines and pyrimidines. The encoded protein catalyses the synthesis of 5-phosphoribosyl 1-pyrophosphate from ATP and D-ribose 5-phosphate
PYGL	1.78	-1.17	1.64	1.51	**Phosphorylase, glycogen, liver**: homodimeric protein that catalyses the cleavage of alpha-1,4-glucosidic bonds to release glucose-1-phosphate from liver glycogen stores. This protein switches from inactive phosphorylase B to active phosphorylase A by phosphorylation of serine residue 15. Activity of this enzyme is further regulated by multiple allosteric effectors and hormonal controls. Humans have three glycogen phosphorylase genes that encode distinct isozymes that are primarily expressed in liver, brain and muscle, respectively. The liver isozyme serves the glycemic demands of the body in general while the brain and muscle isozymes supply just those tissues.
PYGM	2.13	58.57	1.36	1.39	**Phosphorylase, glycogen, muscle**: catalyses the cleavage of alpha-1,4-glucosidic bonds to release glucose-1-phosphate in muscle tissue.
RBKS	5.14	3.01	2.23	1.59	**Ribokinase**: belongs to the pfkB family of carbohydrate kinases. It phosphorylates ribose to form ribose-5-phosphate in the presence of ATP and magnesium as a first step in ribose metabolism.

Gene	IrrDSBsen/growing fold up/down regulation		PEsen/growing fold up/down regulation		Alternative name: Function
	IMR90	NHOF1	IMR90	NHOF1	
RPE	-1.01	1.32	-1.00	1.20	**Ribulose-5-phosphate-3-epimerase**: Catalyses the reversible epimerization of D-ribulose 5-phosphate to D-xylulose 5-phosphate.
RPIA	-1.35	1.98	-1.47	1.33	**Ribose 5-phosphate isomerase A**: catalyses the reversible conversion between ribose-5-phosphate and ribulose-5-phosphate in the pentose-phosphate pathway. This gene is highly conserved in most organisms.
SDHA	1.30	1.65	-1.25	1.38	**Succinate dehydrogenase complex, subunit A, flavoprotein**: a major catalytic subunit of succinate-ubiquinone oxidoreductase, involved complex of the mitochondrial respiratory chain. The complex is composed of four nuclear-encoded subunits and is localized in the mitochondrial inner membrane. SDHA is involved in complex II of the mitochondrial electron transport chain and is responsible for transferring electrons from succinate to ubiquinone (coenzyme Q).
SDHB	1.10	1.55	-1.12	1.12	**Succinate dehydrogenase complex, subunit B, iron sulphur**: Iron-sulphur protein (IP) subunit of succinate dehydrogenase (SDH) that is involved in complex II of the mitochondrial electron transport chain and is responsible for transferring electrons from succinate to ubiquinone (coenzyme Q)
SDHC	1.42	2.00	1.34	1.37	**Succinate dehydrogenase complex, subunit C, integral membrane protein**: Membrane-anchoring subunit of succinate dehydrogenase (SDH) that is involved in complex II of the mitochondrial electron transport chain and is responsible for transferring electrons from succinate to ubiquinone (coenzyme Q).
SDHD	1.58	1.33	1.15	1.38	**Succinate dehydrogenase complex, subunit D, integral membrane protein**: one of two integral membrane proteins anchoring the complex to the matrix side of the membrane
SUCLA 2	-1.08	1.65	1.37	1.26	**Succinate-CoA ligase, ADP-forming, beta subunit**: Succinyl-CoA synthetase (SCS) is a mitochondrial matrix enzyme that acts as a heterodimer, being composed of an invariant alpha subunit and a substrate-specific beta subunit. The protein encoded by this gene is an ATP-specific SCS beta subunit that dimerises with the SCS alpha subunit to form SCS-A, an essential component of the tricarboxylic acid cycle. SCS-A hydrolyses ATP to convert succinate to succinyl-CoA.

Gene	IrrDSBsen/growing fold up/down regulation		PEsen/growing fold up/down regulation		Alternative name: Function
	IMR90	NHOF1	IMR90	NHOF1	
SUCLG1	1.01	1.39	-1.20	1.05	**Succinate-CoA ligase, alpha subunit**: the alpha subunit of the heterodimeric enzyme succinate coenzyme A ligase. This enzyme is targeted to the mitochondria and catalyses the conversion of succinyl CoA and ADP or GDP to succinate and ATP or GTP.
SUCLG2	1.07	1.43	-1.02	1.10	**Succinate-CoA ligase, GDP-forming, beta subunit**: a GTP-specific beta subunit of succinyl-CoA synthetase.
TALDO1	1.27	1.65	-2.41	1.19	**Transaldolase 1**: a key enzyme of the non-oxidative pentose phosphate pathway providing ribose-5-phosphate for nucleic acid synthesis and NADPH for lipid biosynthesis. This pathway can also maintain glutathione at a reduced state and thus protect sulfhydryl groups and cellular integrity from oxygen radicals
TKT	-1.42	1.16	1.47	1.08	**Transketolase**: a thiamine-dependent enzyme which plays a role in the channelling of excess sugar phosphates to glycolysis in the pentose phosphate pathway. Catalyses the transfer of a two-carbon ketol group from a ketose donor to an aldose acceptor, via a covalent intermediate with the cofactor thiamine pyrophosphate.
TPI1	1.19	-1.49	-1.04	-1.13	**Triosephosphate isomerase 1**: catalyses the isomerization of glyceraldehydes 3-phosphate (G3P) and dihydroxy-acetone phosphate (DHAP) in glycolysis and gluconeogenesis.
UGP2	1.63	-1.62	1.56	1.23	**UDP-glucose pyrophosphorylase 2**: transfers a glucose moiety from glucose-1-phosphate to MgUTP and forms UDP-glucose and MgPPi. In liver and muscle tissue, UDP-glucose is a direct precursor of glycogen; in lactating mammary gland it is converted to UDP-galactose which is then converted to lactose.
ACTB	-1.79	-2.69	-1.83	-1.56	**Actin, beta**: This actin is a major constituent of the contractile apparatus and one of the two non-muscle cytoskeletal actins.
B2M	1.40	3.44	1.89	2.01	**Beta-2-microglobulin**: a serum protein found in association with the major histocompatibility complex (MHC) class I heavy chain on the surface of nearly all nucleated cells. The protein has a predominantly beta-pleated sheet structure that can form amyloid fibrils in some pathological conditions.
GAPD	2.45	1.56	1.14	-1.19	**Glyceraldehyde-3-phosphate dehydrogenase**:

Gene	IrrDSBsen/growing fold up/down regulation		PEsen/growing fold up/down regulation		Alternative name: Function
	IMR90	NHOF1	IMR90	NHOF1	
H					catalyses an important energy-yielding step in carbohydrate metabolism, the reversible oxidative phosphorylation of glyceraldehyde-3-phosphate in the presence of inorganic phosphate and nicotinamide adenine dinucleotide (NAD).
HPRT1	-1.60	1.17	-1.16	-1.02	**Hypoxanthine phosphoribosyl transferase 1**: catalyses the conversion of hypoxanthine to inosine monophosphate and guanine to guanosine monophosphate via transfer of the 5-phosphoribosyl group from 5-phosphoribosyl 1-pyrophosphate. This enzyme plays a central role in the generation of purine nucleotides through the purine salvage pathway
RPLP0	-1.20	-2.34	-1.01	-1.06	**Ribosomal protein, large, P0**: a neutral phosphoprotein with a C-terminal end that is nearly identical to the C-terminal ends of the acidic ribosomal phosphoproteins P1 and P2. The P0 protein can interact with P1 and P2 to form a pentameric complex consisting of P1 and P2 dimers, and a P0 monomer. The protein is located in the cytoplasm.

Appendix B

Appendix: Table of genes present on qPCR array for oxidative stress

Gene	IrrDSBsen/growing fold up/down regulation		PEsen/growing fold up/down regulation		Alternative name: Function
	IMR90	NHOF1	IMR90	NHOF1	
ALB	2.60	27.02	-1.11	2.36	**Albumin:** soluble, monomeric protein which comprises about one-half of the blood serum protein. Functions primarily as a carrier protein for steroids, fatty acids, and thyroid hormones and plays a role in stabilizing extracellular fluid volume.
ALOX12	-1.09	10.38	-4.13	1.96	**Arachidonate 12-lipoxygenase**: Non-heme iron-containing dioxygenase that catalyses the stereo-specific peroxidation of free and esterified polyunsaturated fatty acids generating a spectrum of bioactive lipid mediators. Mainly converts arachidonic acid to (12S)-hydroperoxyeicosatetraenoic acid/(12S)-HPETE but can also metabolise linoleic acid. Can also convert leukotriene A4/LTA4 into both the bioactive lipoxin A4/LXA4 and lipoxin B4/LXB4. Through the production of specific bioactive lipids like (12S)-HPETE it regulates different biological processes including platelet activation. Plays a role in apoptotic process, promoting the survival of vascular smooth muscle cells, and may also play a role in the control of cell migration and proliferation.
AOX1	1.09	2.61	-1.33	2.23	**Aldehyde oxidase 1**: produces hydrogen peroxide and, under certain conditions, can catalyse the formation of superoxide.
APOE	2.58	5.80	-1.39	1.26	**Apolipoprotein E**: Mediates the binding, internalisation, and catabolism of lipoprotein particles.
ATOX1	1.57	1.81	-1.03	1.34	**Antioxidant protein 1**: functions as an antioxidant against superoxide and hydrogen peroxide
BNIP3	4.05	2.08	-1.54	-1.45	**BCL2/adenovirus E1B 19kDa interacting protein 3**: Apoptosis-inducing protein that may play a role in repartitioning calcium between the two major intracellular calcium stores in association with BCL2. Involved in mitochondrial quality control via its interaction with SPATA18/MIEAP: in response to mitochondrial damage, participates to mitochondrial protein catabolic process (also named MALM) leading to the degradation of damaged proteins inside mitochondria.

Gene	IrrDSBsen/growing fold up/down regulation		PEsen/growing fold up/down regulation		Alternative name: Function
	IMR90	NHOF1	IMR90	NHOF1	
CAT	1.84	-1.36	1.58	1.67	**Catalase**: protects cells from the toxic effects of hydrogen peroxide by catalysing its conversion to water and oxygen. Promotes growth of cells including T-cells, B-cells, myeloid leukemia cells, melanoma cells, mastocytoma cells and normal and transformed fibroblast cells
CCL5	6.72	479.70	2.61	53.37	**Small inducible cytokine A5 (RANTES):** one of several CC cytokine genes clustered on the q-arm of chromosome 17. Cytokines are a family of secreted proteins involved in immunoregulatory and inflammatory processes. The CC cytokines are proteins characterized by two adjacent cysteines. The cytokine encoded by this gene functions as a chemoattractant for blood monocytes, memory T helper cells and eosinophils. It causes the release of histamine from basophils and activates eosinophils. This cytokine is one of the major HIV-suppressive factors produced by CD8+ cells. It functions as one of the natural ligands for the chemokine receptor CCR5 and it suppresses in vitro replication of the R5 strains of HIV-1.
CCS	3.01	2.31	-1.10	1.20	**Copper chaperone for superoxide dismutase1**: specifically delivers Cu to copper/zinc superoxide dismutase and may activate copper/zinc superoxide dismutase through direct insertion of the Cu cofactor and is specific for sod1 therefore doesn't deliver to nucleus, mitochondria or secretory pathways.
CYBB	1.37	1.85	-1.11	1.26	**Cytochrome b-245, beta polypeptide**: Critical component of the membrane-bound oxidase of phagocytes that generates superoxide. It is the terminal component of a respiratory chain that transfers single electrons from cytoplasmic NADPH across the plasma membrane to molecular oxygen on the exterior. Also functions as a voltage-gated proton channel that mediates the H(+) currents of resting phagocytes. It participates in the regulation of cellular pH and is blocked by zinc.
CYGB	7.88	6.39	-2.94	16.54	**Cytoglobin**: Hexacoordinate hemoglobin which binds ligand differently from the pentacoordinate hemoglobins involved in oxygen transport, and may

Gene	IrrDSBsen/growing fold up/down regulation		PEsen/growing fold up/down regulation		Alternative name: Function
	IMR90	NHOF1	IMR90	NHOF1	
					be involved in protection during oxidative stress.
DHCR 24	-1.13	1.16	-1.24	-2.18	**24-dehydrocholesterol reductase**: Flavin adenine dinucleotide (FAD)-dependent oxidoreductase which catalyses the reduction of the delta-24 double bond of sterol intermediates during cholesterol biosynthesis. Protects cells from oxidative stress by reducing caspase 3 activity during apoptosis induced by oxidative stress. Also protects against amyloid-beta peptide-induced apoptosis
DUOX 1	1.81	4.25	1.25	-1.04	**Dual oxidase 1**: Glycoprotein and a member of the NADPH oxidase family. Generates hydrogen peroxide which is required for the activity of thyroid peroxidase/TPO and lactoperoxidase/LPO dual oxidase because it has both a peroxidase homology domain and a gp91phox domain. This protein generates hydrogen peroxide and thereby plays a role in the activity of thyroid peroxidase, lactoperoxidase, and in lactoperoxidase-mediated antimicrobial defense at mucosal surfaces
DUOX 2	1.22	6.30	1.62	-1.07	**Dual oxidase 2**: Same as above
DUSP 1	1.10	3.15	1.14	1.15	**Dual specificity phosphatase 1:** Expression of DUSP1 gene is induced in human skin fibroblasts by oxidative/heat stress and growth factors. DUSP1 protein has intrinsic phosphatase activity and specifically inactivates MAP kinase in vitro by the concomitant dephosphorylation of both its phosphothreonine and phosphotyrosine residues. It also suppresses the activation of MAP kinase by oncogenic ras in extracts of Xenopus oocytes.
EPHX2	11.38	1.48	62.42	1.80	**Epoxide hydrolase 2, cytoplasmic**: Bifunctional enzyme. The C-terminal domain has epoxide hydrolase activity and acts on epoxides (alkene oxides, oxiranes) and arene oxides. Plays a role in xenobiotic metabolism by degrading potentially toxic epoxides. Also determines steady-state levels of physiological mediators. The N-terminal domain has lipid phosphatase activity
EPX	-1.58	1.55	1.29	1.86	**Eosinophil peroxidase**: The encoded precursor

Gene	IrrDSBsen/growing fold up/down regulation		PEsen/growing fold up/down regulation		Alternative name: Function
	IMR90	NHOF1	IMR90	NHOF1	
					protein is processed into covalently attached heavy and light chains to form the mature enzyme, which functions as an oxidant. The enzyme is released at sites of parasitic infection or allergen stimulation to mediate lysis of protozoa or parasitic worms.
FOXM1	-28.48	-1.66	1.07	-1.49	**Forkhead box M1**: Transcriptional activator involved in cell proliferation. The encoded protein is phosphorylated in M phase and regulates the expression of several cell cycle genes, such as cyclin B1 and cyclin D1. Plays also a role in DNA breaks repair participating in the DNA damage checkpoint response
FTH1	1.06	1.93	1.54	1.34	**Ferritin, heavy polypeptide 1**: Stores iron in a soluble, non-toxic, readily available form. Important for iron homeostasis. Has ferroxidase activity. Iron is taken up in the ferrous form and deposited as ferric hydroxides after oxidation. Also plays a role in delivery of iron to cells.
GCLC	2.79	3.11	1	-1.10	**Glutamate-cysteine ligase, catalytic subunit:** Also known as gamma-glutamylcysteine synthetase. The first rate-limiting enzyme of glutathione synthesis. The enzyme consists of two subunits, a heavy catalytic subunit and a light regulatory subunit. This locus encodes the catalytic subunit.
GCLM	1.18	1.41	-1.01	1.12	**Glutamate-cysteine ligase, modifier subunit:** As above, but regulatory subunit.
GPX1	1.20	2.05	1.01	1.22	**Glutathione peroxidase 1:** Detoxifies hydrogen peroxide, and is one of the most important antioxidant enzymes in humans.
GPX2	2.08	6.09	-1.63	-1.67	**Glutathione peroxidase 2 (gastrointestinal):** Selenium-dependent glutathione peroxidase that is one of two isoenzymes responsible for the majority of the glutathione-dependent hydrogen peroxide-reducing activity in the epithelium of the gastrointestinal tract. Could play a major role in protecting mammals from the toxicity of ingested organic hydroperoxides.

Gene	IrrDSBsen/growing fold up/down regulation		PEsen/growing fold up/down regulation		Alternative name: Function
	IMR90	NHOF1	IMR90	NHOF1	
GPX3	6.76	1.87	1.57	4.11	**Glutathione peroxidase 3 (plasma):** Protects cells and enzymes from oxidative damage, by catalyzing the reduction of hydrogen peroxide, lipidperoxides and organic hydroperoxide by glutathione
GPX4	-1.19	-1.05	-1.12	1.23	**Glutathione peroxidase 4**: Protects cells against membrane lipid peroxidation and cell death, caused by radiation and oxidative damage
GPX5	1.37	3.04	-1.11	1.26	**Glutathione peroxidase 5 (epididymal androgen-related protein):** specifically expressed in the epididymis in the mammalian male reproductive tract, and is androgen-regulated. Has been proposed to play a role in protecting the membranes of spermatozoa from the damaging effects of lipid peroxidation and/or preventing premature acrosome reaction.
GPX6	1.16	3.04	-1.58	1.26	**Glutathione peroxidase 6 (olfactory):** Expression of this gene is restricted to embryos and adult olfactory epithelium.
GPX7	-1.82	-1.21	7.43	1.10	**Glutathione peroxidase 7**: Protects oesophageal epithelia from hydrogen peroxide-induced oxidative stress. It suppresses bile acid-induced ROS.
GSR	1.01	2.49	-3.70	1.16	**Glutathione reductase**: Member of the class-I pyridine nucleotide-disulfide oxidoreductase family. Reduces GSSG to GSH and maintains high levels of GSH in the cytosol.
GSS	1.27	1.95	-1.07	-1.04	**Glutathione synthetase**: Homodimer that catalyses the second step of glutathione biosynthesis, which is the ATP-dependent conversion of gamma-L-glutamyl-L-cysteine to glutathione.
GSTP1	1.62	1.21	-1.01	1.12	**Glutathione S-transferase pi 1**: Glutathione S-transferases (GSTs) are a family of enzymes that play an important role in detoxification by catalysing the conjugation of many hydrophobic and electrophilic compounds with reduced glutathione. Based on their biochemical, immunologic, and structural properties, the soluble GSTs are categorized into 4 main classes: alpha, mu, pi, and

Gene	IrrDSBsen/growing fold up/down regulation		PEsen/growing fold up/down regulation		Alternative name: Function
	IMR90	NHOF1	IMR90	NHOF1	
					theta.
GSTZ1	1.44	1.09	2.45	1.24	**Glutathione S-transferase zeta 1**: Bifunctional enzyme showing minimal glutathione-conjugating activity with ethacrynic acid and 7-chloro-4-nitrobenz-2-oxa-1,3-diazole and maleylacetoacetate isomerase activity. Has also low glutathione peroxidasen activity with T-butyl and cumene hydroperoxides.
GTF2I	1.94	1.71	-1.46	1.27	**General transcription factor IIi**: Multifunctional phosphoprotein with roles in transcription and signal transduction
HMOX 1	-2.41	7.29	1.14	-1.10	**Haem oxygenase (decycling) 1:** Haem oxygenase (HO) catalyses the degradation of haem. This membrane-bound enzyme cleaves the haem ring at the alpha-methene bridge to produce bilverdin (which is metabolised further by bilirubin reductase to form bilirubin), iron and carbon monoxide. There are three isoforms of haem oxygenase; the inducible HO-1, which is active at high concentrations of haem and at times of physiological stress, the constitutively active HO-2 and the non-catalytic HO-3, which is thought to function as an oxygen sensor.
HSPA1 A	1.32	5.53	-2.18	1.22	**Heat shock 70kDa protein 1A**: In cooperation with other chaperones, Hsp70s stabilize pre-existent proteins against aggregation and mediate the folding of newly translated polypeptides in the cytosol as well as within organelles. These chaperones participate in all these processes through their ability to recognize non-native conformations of other proteins. They bind extended peptide segments with a net hydrophobic character exposed by polypeptides during translation and membrane translocation, or following stress-induced damage.
KRT1	1.37	3.04	-1.11	1.26	**Keratin 1:** he type II cytokeratins consist of basic or neutral proteins which are arranged in pairs of heterotypic keratin chains co-expressed during differentiation of simple and stratified epithelial tissues. May regulate the activity of kinases such as PKC and SRC via binding to integrin beta-1 (ITB1)

Gene	IrrDSBsen/growing fold up/down regulation		PEsen/growing fold up/down regulation		Alternative name: Function
	IMR90	NHOF1	IMR90	NHOF1	
					and the receptor of activated protein kinase C (RACK1/GNB2L1)
LPO	1.37	-6.61	-1.11	1.26	**Lactoperoxidase:** Oxidoreductase secreted from salivary, mammary, and other mucosal glands that functions as a natural antibacterial agent.
MB	1.59	8.85	-1.11	2.96	**Myoglobin**: member of the globin superfamily and is expressed in skeletal and cardiac muscles. The encoded protein is a haemoprotein contributing to intracellular oxygen storage and transcellular facilitated diffusion of oxygen.
MBL2	1.37	3.04	-1.11	1.26	**Mannose-binding lectin (protein C) 2, soluble**: Calcium-dependent lectin involved in innate immune defense. Binds mannose, fructose and N-acetylglucosamine on different microorganisms and activates the lectin complement pathway. Binds to late apoptotic cells, as well as to apoptotic blebs and to necrotic cells, but not to early apoptotic cells, facilitating their uptake by macrophages. May bind DNA.
MGST 3	1.52	1.24	1.31	1.12	**Glutathione S-transferase** 3: Enzyme that catalyses the conjugation of leukotriene A4 and reduced glutathione to produce leukotriene C4. This enzyme also demonstrates glutathione-dependent peroxidase activity towards lipid hydroperoxides
MPO	1.37	3.04	-1.11	1.26	**Myeloperoxidase:** Haem protein synthesised during myeloid differentiation that constitutes the major component of neutrophil azurophilic granules. Produced as a single chain precursor, myeloperoxidase is subsequently cleaved into a light and heavy chain. The mature myeloperoxidase is a tetramer composed of 2 light chains and 2 heavy chains. This enzyme produces hypohalous acids central to the microbicidal activity of neutrophils.
MPV17	1.25	1.49	1.36	1.23	**Mitochondrial inner membrane protein**: a mitochondrial inner membrane protein that is implicated in the metabolism of reactive oxygen species.

Gene	IrrDSBsen/growing fold up/down regulation		PEsen/growing fold up/down regulation		Alternative name: Function
	IMR90	NHOF1	IMR90	NHOF1	
MSRA	-1.0	1.98	-1.27	1.12	**Methionine sulfoxide reductase A:** ubiquitous and highly conserved. It carries out the enzymatic reduction of methionine sulfoxide to methionine. Its proposed function is the repair of oxidative damage to proteins to restore biological activity.
MT3	6.86	3.04	-1.24	1.26	**Metallothionein 3**: Binds heavy metals. Contains three zinc and three copper atoms per polypeptide chain and a negligible amount of cadmium.
NCF1	1.64	4.25	-1.37	1.34	**Neutrophil cytosolic factor 1**: Cytosolic subunit of neutrophil NADPH oxidase. This oxidase is a multicomponent enzyme that is activated to produce superoxide anion.
NCF2	1.23	21.05	1.11	-1.58	**Neutrophil cytosolic factor 2**: NCF2, NCF1, and a membrane bound cytochrome b558 are required for activation of the latent NADPH oxidase (necessary for superoxide production).
NOS2	1.37	3.65	-1.11	1.26	**Nitric oxide synthase 2, inducible:** Nitric oxide synthase which is expressed in liver and is inducible by a combination of lipopolysaccharide and certain cytokines.
NOX4	2.17	13.51	-3.62	-1.13	**NADPH oxidase 4**: a member of the NOX-family of enzymes that functions as the catalytic subunit the NADPH oxidase complex. The encoded protein is localized to non-phagocytic cells where it acts as an oxygen sensor and catalyses the reduction of molecular oxygen to various ROS.
NOX5	23.72	8.79	8.31	23.88	**NADPH oxidase, EF-hand calcium binding domain 5:** Calcium-dependent NADPH oxidase that generates superoxide. Also functions as a calcium-dependent proton channel and may regulate redox-dependent processes in lymphocytes and spermatozoa.
NQO1	-2.7	-1.61	-1.77	-1.41	**NADPH dehydrogenase, quinone 1**: a cytoplasmic 2-electron reductase. This FAD-binding protein forms homodimers and reduces quinones to hydroquinones. This protein's enzymatic activity prevents the one electron reduction of quinones that results in the production of radical species.

Gene	IrrDSBsen/growing fold up/down regulation		PEsen/growing fold up/down regulation		Alternative name: Function
	IMR90	NHOF1	IMR90	NHOF1	
NUDT 1	-2.59	-1.39	-1.72	1.03	**Nudix (nucleoside diphosphate linked moiety X)-type motif 1**: Enzyme that hydrolyses oxidized purine nucleoside triphosphates, such as 8-oxo-dGTP, 8-oxo-dATP, 2-hydroxy-dATP, and 2-hydroxy rATP, to monophosphates, thereby preventing misincorporation. The encoded protein is localized mainly in the cytoplasm, with some in the mitochondria, suggesting that it is involved in both nuclear and mitochondrial genomes.
OXR1	1.52	-1.02	1.24	1.02	**Oxidation resistance 1**: Phosphorylated upon DNA damage, probably by ATM or ATR, and upregulates the expression of antioxidant genes via the p21 signalling pathway to suppress hydrogen peroxide-induced oxidative stress and maintain mitochondrial DNA integrity.
OXSR1	1.04	3.20	-1.00	1.02	**Oxidative-stress responsive 1**: belongs to the Ser/Thr protein kinase family of proteins. It regulates downstream kinases in response to environmental stress, and may play a role in regulating the actin cytoskeleton.
PDLIM 1	3.41	1.02	-2.63	-2.04	**PDZ and LIM domain 1:** Cytoskeletal protein that may act as an adapter that brings other proteins (like kinases) to the cytoskeleton.
PNKP	1.16	1.87	-1.24	-1.02	**Polynucleotide kinase 3'-phosphatase**: Involved in DNA repair. In response to ionizing radiation or oxidative damage, the protein encoded by this locus catalyses 5' phosphorylation and 3' dephosphorylation of nucleic acids functioning as part of both the non-homologous end-joining (NHEJ) and base excision repair (BER) pathways.
PRDX1	1.14	2.04	-1.46	1.01	**Peroxiredoxin 1**: Reduces peroxides with reducing equivalents provided through the thioredoxin system but not from glutaredoxin. Might participate in the signaling cascades of growth factors and tumor necrosis factor-alpha by regulating the intracellular concentrations of H_2O_2.
PRDX2	1.57	1.75	-1.24	1.16	**Peroxiredoxin 2**: Same as above.
PRDX3	1.43	-1.07	-1.37	1.06	**Peroxiredoxin 3:** As above, but localised in the

Gene	IrrDSBsen/growing fold up/down regulation		PEsen/growing fold up/down regulation		Alternative name: Function
	IMR90	NHOF1	IMR90	NHOF1	
					mitochondria.
PRDX4	2.36	1.26	-1.41	1.40	**Peroxiredoxin 4**: As above, but localised to the cytoplasm. Also plays a regulatory role in the activation of the transcription factor NF-KB.
PRDX5	2.31	1.03	1.82	1.23	**Peroxiredoxin 5:** As PRDX1, also this protein interacts with peroxisome receptor 1.
PRDX6	2.10	2.82	-1.53	-1.01	**Peroxiredoxin 6:** bifunctional enzyme with two distinct active sites. It is involved in redox regulation of the cell; it can reduce H_2O_2 and short chain organic, fatty acid, and phospholipid hydroperoxides.
PREX1	-4.44	3.02	-1.33	1.12	**Phosphatidylinositol-3,4,5-Trisphosphate-Dependent Rac Exchange Factor 1**: Acts as a guanine nucleotide exchange factor for the RHO family of small GTP-binding proteins (RACs). It has been shown to bind to and activate RAC1 by exchanging bound GDP for free GTP.
PRNP	2.60	2.82	2.01	1.85	**Prion Protein**: The protein encoded by this gene is a membrane glycosylphosphatidylinositol-anchored glycoprotein that tends to aggregate into rod-like structures.
PTGS1	3.34	1.19	1.43	2.11	**Prostaglandin-Endoperoxide Synthase 1 (Prostaglandin G/H Synthase And Cyclooxygenase)/ COX1 (constitutive)**: one of two genes encoding similar enzymes that catalyse the conversion of arachidonate to prostaglandin.
PTGS2	7.45	144.61	34.39	1.01	**Prostaglandin-Endoperoxide Synthase 2 (Prostaglandin G/H Synthase And Cyclooxygenase)/ COX2 (inducible):** As above, but inducible isozyme.
PXDN	1.85	1.28	-1.84	-1.16	**Peroxidasin Homolog (Drosophila):** Displays low peroxidase activity and is likely to participate in H_2O_2 metabolism and peroxidative reactions in the cardiovascular system.
RNF7	1.58	1.23	1.35	1.27	**Ring Finger Protein 7**: essential subunit of SKP1-cullin/CDC53-F box protein ubiquitin ligases, which are a part of the protein degradation machinery

Gene	IrrDSBsen/growing fold up/down regulation		PEsen/growing fold up/down regulation		Alternative name: Function
	IMR90	NHOF1	IMR90	NHOF1	
					important for cell cycle progression and signal transduction. May play a role in protecting cells from apoptosis induced by redox agents.
SCARA 3	-2.83	-1.11	-11.28	1.28	**Scavenger Receptor Class A, Member 3:** Macrophage scavenger receptor-like protein. This protein has been shown to deplete reactive oxygen species, and is induced by oxidative stress.
SELS	1.09	1.46	-1.55	-1.13	**VIMP:** a selenoprotein, which may regulate cytokine production, and thus play a key role in the control of the inflammatory response. Involved in the degradation process of misfolded endoplasmic reticulum (ER) luminal proteins. Participates in the transfer of misfolded proteins from the ER to the cytosol, where they are destroyed by the proteasome in a ubiquitin-dependent manner.
SEPP1	1.23	1.48	5.22	2.99	**Selenoprotein P, Plasma, 1**: Heparin-binding protein that appears to be associated with endothelial cells, and has been implicated to function as an antioxidant in the extracellular space.
SFTPD	2.20	6.09	3.35	1.83	**Surfactant Protein D**: Contributes to the lung's defence against inhaled microorganisms. Binds strongly maltose residues and to a lesser extent other alpha-glucosyl moieties.
SIRT2	1.39	1.27	-1.29	1.48	**Silent information regulator (Sir2)-like family deacetylases (Sirtuin) 2**: Catalyses the removal of acetyl groups from lysine residues in histones and non-histone proteins, which is coupled to NAD+ hydrolysis. In general, sirtuins do not act autonomously but as components of large multiprotein complexes, such as pRb-E2F.
SOD1	1.51	1.81	1.02	2.00	**Superoxide Dismutase 1, Soluble:** Binds copper and zinc ions and is one of two isozymes responsible for destroying free superoxide radicals in the body. The encoded isozyme is a soluble cytoplasmic protein, acting as a homodimer to convert naturally-occuring but harmful superoxide radicals to O_2 and H_2O_2.
SOD2	3.89	11.13	-2.17	1.58	**Superoxide Dismutase 2, Mitochondrial**: As

Gene	IrrDSBsen/growing fold up/down regulation		PEsen/growing fold up/down regulation		Alternative name: Function
	IMR90	NHOF1	IMR90	NHOF1	
					above but the mitochondrial isozyme.
SOD3	1.63	8.98	21.77	2.55	**Superoxide Dismutase 3, Extracellular**: This protein is secreted into the extracellular space and forms a glycosylated homotetramer that is anchored to the extracellular matrix (ECM) and cell surfaces through an interaction with heparan sulfate proteoglycan and collagen. A fraction of the protein is cleaved near the C-terminus before secretion to generate circulating tetramers that do not interact with the ECM. Protects the extracellular space from toxic effect of reactive oxygen intermediates by converting superoxide radicals to O_2 and H_2O_2.
SQSTM1	2.05	6.13	-1.16	1.33	**Sequestosome 1**: Multifunctional protein that binds ubiquitin and regulates activation of the NF-kB signaling pathway. The protein functions as a scaffolding/adaptor protein in concert with TNF receptor-associated factor 6 to mediate activation of NF-kB in response to upstream signals.
SRXN1	1.26	4.91	-1.63	1.04	**Sulfiredoxin 1:** Contributes to oxidative stress resistance by reducing cysteine-sulfinic acid formed under exposure to oxidants in the peroxiredoxins PRDX1, PRDX2, PRDX3 and PRDX4. Does not act on PRDX5 or PRDX6. May catalyse the reduction in a multi-step process by acting both as a specific phosphotransferase and a thioltransferase.
STK25	1.40	1.26	1.49	1.05	**Serine/Threonine Kinase 25**: Oxidant stress-activated serine/threonine kinase that may play a role in the response to environmental stress. Targets to the Golgi apparatus where it appears to regulate protein transport events, cell adhesion, and polarity complexes important for cell migration.
TPO	3.65	23.20	-1.11	1.26	**Thyroid Peroxidase:** Iodination and coupling of the hormonogenic tyrosines in thyroglobulin to yield the thyroid hormones T3 and T4.
TTN	1.37	4.49	-1.11	1.26	**Titin**: In non-muscle cells seems to play a role in chromosome condensation and chromosome segregation during mitosis.

Gene	IrrDSBsen/growing fold up/down regulation		PEsen/growing fold up/down regulation		Alternative name: Function
	IMR90	NHOF1	IMR90	NHOF1	
TXN	1.23	1.79	-1.58	1.49	**Thioredoxin:** Participates in various redox reactions through the reversible oxidation of its active center dithiol to a disulfide and catalyses dithiol-disulfide exchange reactions. Plays a role in the reversible S-nitrosylation of cysteine residues in target proteins, and thereby contributes to the response to intracellular nitric oxide. Nitrosylates the active site Cys of CASP3 in response to nitric oxide, and thereby inhibits caspase-3 activity.
TXNRD1	1.39	2.31	-1.58	1.09	**Thioredoxin Reductase 1:** Isoform 1 may possess glutaredoxin activity as well as thioredoxin reductase activity and induces actin and tubulin polymerization, leading to formation of cell membrane protrusions.
TXNRD2	2.29	1.38	-1.11	1.20	**Thioredoxin Reductase 2:** Maintains thioredoxin in a reduced state.
UCP2	-1.34	1.20	-2.23	-4.76	**Uncoupling Protein 2 (Mitochondrial, Proton Carrier):** Separates oxidative phosphorylation from ATP synthesis with energy dissipated as heat, also referred to as the mitochondrial proton leak. UCPs facilitate the transfer of anions from the inner to the outer mitochondrial membrane and the return transfer of protons from the outer to the inner mitochondrial membrane. They also reduce the mitochondrial membrane potential in mammalian cells although the exact methods of how UCPs transfer H+/OH- are not known.
ACTB	-1.46	-2.78	-1.94	-1.27	**Actin, Beta:** Cytoskeletal protein.
B2M	1.60	3.4	1.45	1.69	**Beta-2-Microglobulin:** Component of MHC class I molecules, which are present on all nucleated cells.
GAPDH	1.98	1.71	1.49	-1.06	**Glyceraldehyde-3-Phosphate Dehydrogenase:** Has both glyceraldehyde-3-phosphate dehydrogenase and nitrosylase activities, thereby playing a role in glycolysis and nuclear functions, respectively.
HPRT1	-1.76	1.01	-1.36	-1.13	**Hypoxanthine Phosphoribosyltransferase 1:** Catalyses conversion of hypoxanthine to inosine

Gene	IrrDSBsen/growing fold up/down regulation		PEsen/growing fold up/down regulation		Alternative name: Function
	IMR90	NHOF1	IMR90	NHOF1	
					monophosphate and guanine to guanosine.
RPLP0	-1.24	-2.12	1.23	-1.11	**Ribosomal Protein, Large, P0**: Encodes a ribosomal protein that is a component of the 60S subunit.